Characterisation of de-structured starch and its interactions in whey protein isolate gels

A thesis submitted in partial fulfilment of the requirements for the degree of

Doctor of Philosophy

in

Food Technology

At Massey University, Palmerston North, New Zealand

Cai Ling Ang

2022

Abstract

Starch serves as an important additive to enhance the physico-chemical properties of many food products. With the increased pursuit of natural products, there is an increasing demand for "clean-label" starches. In this study, waxy potato starch was physically-modified at elevated temperatures of 120–150 °C for 30 min at 300 rpm, in a pressurised reactor. The treatment converted native starch granules into their macromolecular chains (denoted as de-structured waxy potato starch, DWPS). This doctoral thesis presents the: (i) method of modifying starch (*i.e.*, the de-structuring process), (ii) the mechanism of starch de-structuring, (iii) the rheological changes in DWPS samples and the shear-thickening mechanism, and (iv) the interactions of these DWPS ingredients with whey protein isolate (WPI) in a protein-based gel system, at different pH and ionic strength.

The molar mass (M_w), particle size, rheological properties, degree of branching (DB) and side-chain length distribution of DWPS samples were characterised to elucidate the starch de-structuring mechanism. DWPS treated at 120 °C DWPS showed similar M_w (~3.6×10^8 Da) as its native form (~3.7×10^8 Da) indicating that the treatment at 120 °C resulted in the disassembly of starch granules into their macromolecular chains. Reduction in viscosity, M_w and particle size was observed with an increase in temperature from 120 to 150 °C, suggesting a cleavage in amylopectin chains. The DB and side-chain distribution data suggest that the reduction in M_w is likely due to the cleavage at α-1,4 linkages near the middle of the main amylopectin backbone. Particle size analysis by laser diffraction measurements revealed the presence of large fragment particles (> 1 μm) in DWPS samples, indicating that the starch de-structuring process into its macromolecules was incomplete even at 150 °C for 30 min.

The DWPS (5% w/w) samples were found to exhibit a wide range of rheological properties—Newtonian, shear-thinning, shear-thickening and anti-thixotropy behaviours—depending on their treatment temperature (120–150 °C). In particular, 120 °C DWPS exhibited interesting shear-thickening, anti-thixotropy and shear-induced gelation. These rheological properties are different from the shear-thinning and thixotropy behaviours observed in most conventionally gelatinised waxy potato starches treated at 95 °C. The complex shear-induced structures of 120 °C DWPS were attributed to a two-step process: (i) upon shear at the critical shear rate (~10–20 s^{-1}), the shear stress caused a size reduction in the starch fragments and (ii) the increased number of small fragments together with the amylopectin chains in very close proximity could lead to the formation of a complex network probably consisting of amylopectin chains and a large number of fragments (2–20 μm). Shear

thickening properties were attributed largely to these soft fragment particles colliding and sliding past each other during shear. The data from this study has also shown that the hydrogen bonding, electrostatic, hydrophobic interactions, or the combination of these interactions did not cause the shear-thickening behaviour.

The influence of 4% w/w DWPS on 13% w/w WPI gels was studied by characterising the phase stability of the liquid mixtures, and mechanical properties, microstructure, and water-immersion stability of fine-stranded polymeric and coarse-stranded particulate protein gels at pH 7 and pH 5, respectively. At neutral pH, synergistic gel hardness of WPI was obtained with the incorporation of 140 °C DWPS. The increased gel strength was attributed to the enhanced density of a very fine-stranded gel network. The ability of the gel to retain its shape when immersed in water for 40 h was most noticeable for the composite gels containing either gelatinised starch or DWPS samples (swollen gels but with intact shape). In contrast, pure WPI gel and composite gel containing maltodextrin turned into very weak fluid-like and disintegrated gels, respectively. At pH 5, WPI formed particulate gels. The addition of gelatinised starch or DWPS weakened the particulate protein gels, likely due to phase separation and interrupted protein network with starch polymers acting as inactive fillers.

The effects of NaCl and $CaCl_2$ (*i.e.*, type of salts and ionic strength) on the mechanical and microstructural properties of composite gels containing 13% w/w WPI and 4% w/w 140 °C DWPS were also evaluated. Thermodynamic incompatibility between WPI and 140 °C DWPS was observed upon the addition of NaCl (~75 mM) or $CaCl_2$ (10–75 mM). The combined effects of such thermodynamic incompatibility with the changes in protein connectivity induced by varied ionic strength led to the formation of distinctive gel structures (inhomogeneous self-supporting gels with a liquid centre and weak gels with paste-like consistency) that were different from thermodynamic compatible homogeneous self-supporting gels (pure WPI and WPI + maltodextrin gels). At ≥ 250 mM NaCl, instead of a paste-like texture, a recovered soft self-supporting gel structure was observed when using 140 °C DWPS. The ability to generate a range of textures in WPI gelation-based foods by using 140 °C DWPS under different ionic conditions, is a feasible strategy for structuring high-protein foods for dysphagia—aimed to be either thickened fluids or soft solids. Additionally, this acquired knowledge is also relevant when formulating food gels for 3-D printing.

The desirable rheological properties of DWPS samples and their ability to alter WPI gel structure signify the potential of DWPS as a clean-label ingredient to structure foods of specific needs (*e.g.*, whipping cream for enhanced structure upon shear and high-protein foods for dysphagia sufferers).

Acknowledgements

I like to express my most heartfelt thank you to Kelvin Goh, my chief supervisor in Singapore, without your encouragement and reminders, I would not have begun this PhD journey. Thank you for being such a patient mentor that puts up with my struggles with English language (yes, I will remember to write shorter sentences) and my "occasion" stubbornness. I am grateful to you for shaping me into a better writer and researcher.

A big, big thank you to Lara Matia-Merino, my co-supervisor in New Zealand, who is always there for her students. Thank you for all the encouragement and positivity that you ~~whipped into~~ instilled in me whenever I started to doubt myself. Thank you for all that you have done for me, from the valuable and constructive feedback for my studies to ensuring that I have a life outside work. I cannot thank you enough for being such a great supervisor, I am really lucky to have you.

A special thank you to Kaiyang Lim, my co-supervisor in Singapore. Thank you for being patient and understanding of my circumstances when I was at the Singapore Institute of Technology (SIT). I am grateful for the overtime hours that you had put in, so I could get my lab work done. Also, thank you for freeze-drying my precious de-structured starch. Without your help, I would not have enough samples to complete this project.

I also like to acknowledge the College of Sciences for the PhD scholarship and Riddet Institute for funding my tuition fees.

I am also thankful for the technical help provided by Ian Sims, Cara Luiten, Liam Sargison and Simon Hinley (for accommodating me at Ferrier Institute and their assistance on starch side-chain distribution analysis), Patrick Edwards (on the ^{1}H-NMR analysis), Collins Bjork and Richard Love (for advice on language), Raoul Solomon, Matthew Savoian, Yanyu He from Manawatu Microscopy Imaging Centre (for the microscopic training and sample preparation).

Thank you to all the extremely helpful lab managers and technicians—Michelle Tamehana (our lab mum), Steve Glasgow, Garry Radford, Warwick Johnson, Maggie Zou, Kylie Evans and Haoran Wang—that have made my lab work possible and manageable.

I like to thank SIT for allowing me to use their laboratory during the first nine months of my studies. Thank you to all the professional officers and technicians in SIT that had provided me with

administrative help, training and advice: Sherlyn Tan, Xin Ying Chua, Yen Yen Liew, Serene Siew, Hwee Khim Chang, and Andy Long.

A big thank you and hug to my family, especially my parents for their understanding and willingness to let me fulfil my PhD studies. Thank you for believing that I could do this. To my brothers, thank you for taking care of our parents, so that I can focus on my studies, I know it has been hard, especially during Covid times. Thank you to my friends in Singapore: Jamie, Kai Zhi, Chi Siong, Andy, Xinying and Sherlyn who frequently check on me to ensure that I am doing well.

A special thank you to my close friends in New Zealand whom I call them my NZ family: Feng Ming, Hazwani, Akshay and Neville. Thank you for a life outside my PhD hours and for having to put up with my complaints and occasion craziness. I would also like to thank Wang Che and Chih Chein for inviting me over to their place during festival seasons (the food is always so yum!). I am thankful to my lab buddies: Hazwani, Akshay (Again!) and Teck Ann (the unofficial 4th supervisor that I appointed) for making my lab hours more manageable and ~~louder at times due to heated debates~~ lively. To my dear officemates: Hazwani, Akshay, Teck Ann (you guys just keep popping up), Emmanuel, Dong, Jiuk, Jolin and Marzieh, thank you for all the gatherings outside the university (and having to endure the disturbance due to my presence in the office, as I been told that the office is noisier when I am around… Am I correct, Akshay?).

Table of contents

Abstract i

Acknowledgements iii

Table of contents v

List of figures xiii

List of tables xxi

List of publications and conference proceedings xxiii

Chapter 1 Introduction 1

Chapter 2 Literature review 4

2.1. Starch 4

2.1.1. Components of starch granules 4

2.1.1.1. Amylopectin 4

2.1.1.2. Amylose 7

2.1.1.3. Minor components 8

2.1.2. Structural organisation 9

2.1.3. Physical and rheological properties 12

2.1.3.1. Gelatinisation 12

2.1.3.2. Pasting 13

2.1.3.3. Retrogradation 14

2.1.3.4. Shear-induced behaviour 15

2.1.3.4.1. Association of polymers 16

2.1.3.4.2. Hydrogen bonding 17

2.1.3.4.3. Hydrophobic interactions 18

2.1.3.4.4. Electrostatic interactions 18

2.1.4. Physical modification 19

2.1.4.1. Heat-moisture treatment 19

2.1.4.2. Annealing 23

2.1.4.3. Autoclaving 25

2.2. Whey proteins 28

2.2.1. β-Lactoglobulin 30

2.2.2. α-Lactalbumin 31

2.2.3. Heat-induced denaturation and gelation of whey protein 31

2.3. Interactions between starch and proteins 33

2.3.1. Types of polymer interactions 33

2.3.2. Whey protein and starch 34

2.3.2.1. Effect of sodium ions 38

2.3.2.2. Effect of calcium ions 38

2.4. Gaps in the literature 39

Chapter 3 Experimental techniques 40

3.1. De-structured starch sample preparation 40

3.2. Molecular characterisation 44

3.2.1. Proton nuclear magnetic resonance (^{1}H-NMR) 44

3.2.2. High-performance size-exclusion chromatography (HP-SEC) 45

3.2.3. Size-exclusion chromatography coupled with multi-angle laser light scattering (SEC-MALLS) 48

3.3. Particle sizing 50

3.3.1. Dynamic light scattering 50

3.3.2. Laser diffraction 51

3.4. Mechanical characterisation 52

3.4.1. Rheology 52

3.4.1.1. Shear-dependency viscosity 53

3.4.1.2. Time-dependency viscosity 54

3.4.1.3. Oscillatory shear rheology 54

3.4.2. Texture profile analysis 57

3.5. Microstructural characterisation 58

3.5.1. Scanning electron microscopy (SEM) 59

3.5.2. Transmission electron microscopy (TEM) 61

3.5.3. Confocal scanning laser microscopy (CSLM) 61

3.6. Conclusions 65

Chapter 4 Characterisation of de-structured starch and its de-structuring mechanism[1,2] 66

4.1. Introduction 66

4.2. Materials and Methods 68

4.2.1. Sample preparation 68

4.2.2. Laser diffraction 68

4.2.3. Dynamic light scattering 68

4.2.4. Zeta potential measurements 68

4.2.5. Size-exclusion chromatography coupled with multi-angle laser light scattering (SEC-MALLS) 69

4.2.6. High-performance size-exclusion chromatography 69

4.2.7. ^{1}H-NMR Spectroscopy 70

4.2.8. Rheological measurements 70

4.2.9. Statistical analysis 70

4.3. Results and discussion 71

4.3.1. Particle size, viscosity and zeta-potential of DWPS samples 71

4.3.2. Molar mass, size, and conformation of DWPS samples 73

4.3.3. Side-chain length distributions and degree of branching of DWPS samples 75

4.3.4. Proposed mechanism of starch de-structuring 77

4.4. Conclusions 80

Chapter 5 Rheological characterisation of de-structured starch[1,2,3] 81

5.1. Introduction 81

5.2. Materials and Methods 82

5.2.1. Sample preparation 82

5.2.2. Rheological measurements 82

5.2.2.1. Rotational test 82

5.2.2.2. Oscillatory test 83

5.3. Results and discussion 84

5.3.1. Shear-dependent viscosity of DWPS samples 84

5.3.2. Time-dependent shear behaviour of DWPS samples 85

5.3.3. Viscoelasticity of sheared and unsheared DWPS samples 88

5.3.4. Factors affecting shear-thickening behaviours of 120 °C DWPS 89

5.3.4.1. Effect of shear rate 89

5.3.4.2. Effect of shear-history 91

5.3.4.3. Effect of concentration 95

5.3.5. General remarks 96

5.4. Conclusions 97

Chapter 6 Mechanism of shear-thickening, anti-thixotropy and shear-induced gelation of de-structured starch[1,2] 98

6.1. Introduction 98

6.2. Materials and Methods 100

6.2.1. Sample preparation 100

6.2.1.1. Addition of urea to 120 °C DWPS 100

6.2.1.2. Addition of NaCl to 120 °C DWPS 100

6.2.1.3. Addition of urea and NaCl to 120 °C DWPS 100

6.2.2. Rheological measurements 100

6.2.2.1. Rotational test 100

6.2.2.2. Oscillatory test 100

6.2.3. Size-exclusion chromatography coupled with multi-angle laser light scattering (SEC-MALLS) 101

6.2.4. Laser diffraction 101

6.2.5. Dynamic light scattering 101

6.2.6. Starch content determination 102

6.2.7. Turbidity measurements 102

6.2.8. Statistical analysis 102

6.3. Results and discussion 103

6.3.1. Turbidity of unsheared and sheared DWPS samples 103

6.3.2. Molecular parameters of unsheared and sheared DWPS samples 104

6.3.3. Particle size of unsheared and sheared DWPS samples 106

6.3.4. Effect of environmental conditions on the shear-thickening behaviour of 120 °C DWPS 109

6.3.4.1. Effect of urea 109

6.3.4.2. Effect of ionic strength 110

6.3.4.3. Effect of temperature 111

6.3.4.4. Combined effects of urea, ionic strength and temperature 115

6.3.5. Proposed mechanism for shear-thickening, anti-thixotropy and shear-induced gelation of DWPS 115

6.4. Conclusions 118

Chapter 7 The influence of de-structured starch on the mechanical properties, microstructure, and water immersion stability of polymeric and particulate whey protein isolate gels[1] 119

7.1. Introduction 119

7.2. Materials and Methods 121

7.2.1. Sample preparation of whey protein + starch mixtures at pH 7 and pH 5 121

7.2.2. Phase stability 121
7.2.3. Rheological measurements 121
7.2.4. Zeta-potential measurements 122
7.2.5. Textural measurements 122
7.2.5.1. Gel preparation 122
7.2.5.2. Gel hardness 122
7.2.6. Syneresis measurements 122
7.2.6.1. Protein leaching 123
7.2.6.2. Carbohydrate leaching 123
7.2.7. Gel water-immersion test 124
7.2.8. Microscopy analysis 124
7.2.8.1. Transmission electron microscopy (TEM) 124
7.2.8.2. Confocal scanning laser microscopy (CSLM) 125
7.2.9. Statistical analysis 125
7.3. Results and discussion 126
7.3.1. Phase stability of WPI + 140 °C DWPS mixtures at pH 7 and 5 126
7.3.2. Influence of 140 °C DWPS on fine-stranded WPI polymeric gels (pH 7) 127
7.3.2.1. Rheological, textural and microstructural properties 127
7.3.2.2. Gel immersion in water 130
7.3.3. Influence of 140 °C DWPS on coarse-stranded WPI particulate gels (pH 5) 133
7.3.3.1. Rheological, textural and microstructural properties 133
7.3.3.2. Water-holding capacity 136
7.3.3.3. Gel immersion in water 139
7.3.4. General remarks 141
7.4. Conclusions 142
Chapter 8 Manipulation of mechanical properties and microstructure of whey protein gels using DWPS and salts 143

8.1. Introduction 143

8.2. Materials and Methods 144

8.2.1. Sample preparation of whey protein + starch mixtures at varied NaCl and $CaCl_2$ concentrations 144

8.2.2. Phase stability 144

8.2.3. Rheological measurements 144

8.2.4. Textural hardness measurements 144

8.2.5. Microscopy analysis 144

8.2.5.1. Scanning electron microscopy (SEM) 144

8.2.5.2. Confocal scanning microscopy (CSLM) 145

8.2.6. Statistical analysis 145

8.3. Results and discussion 146

8.3.1. Effect of ionic strength on phase stability of WPI + DWPS mixtures 146

8.3.2. Effect of ionic strength on gelation temperature of WPI + DWPS mixtures 148

8.3.3. Effect of ionic strength on the rheological, textural and microstructural properties of WPI + DWPS gels 150

8.3.3.1. Effect of NaCl 150

8.3.3.2. Effect of $CaCl_2$ 155

8.4. General remarks 158

8.5. Conclusions 159

Chapter 9 Overall conclusions and recommendations 160

9.1. Overall conclusions 160

9.1.1. How does the de-structuring process disassemble the waxy potato starch granules? (Chapter 4) 161

9.1.2. How do the structural changes of DWPS during the de-structuring process alter its rheological properties? (Chapter 5 and 6) 162

9.1.3. How does DWPS affect the mechanical properties, microstructure and water-immersion stability of polymeric and particulate whey protein isolate gels (Chapter 7)? 163

9.1.4. What are the effects of NaCl and $CaCl_2$ on the interaction between WPI and DWPS (Chapter 8)? 164

9.1.5. Potential applications of de-structured starch 165

9.2. Recommendations 167

References 170

Appendices I

List of figures

Figure 1-1 Overview of the research chapters. 3

Figure 2-1 Schematic illustration of amylopectin with its A-, B1-, B2- and B3-chains represented by blue, green, grey and yellow, with α-1,4 and α-(1,6)-linkages denoted as — and → symbols, respectively. The reducing end of the C-chain is represented by Ø. 5

Figure 2-2 Average side-chain distributions for A-, B- and C-type starch. Reprinted from Ai & Jane (2018b), with permission from Elsevier. 6

Figure 2-3 Schematic illustration of a starch granule at multi-levels: (A) at the lowest magnification level of starch granule organisation, the alternating crystalline and semicrystalline shells/growth rings are represented by dark and light colours respectively, (B) at the higher magnification level of starch structure, the blocklet structure is shown together with the amorphous radial channels. Noting that the size of blocklets in the semicrystalline shells is smaller than that of blockets in the crystalline shells, (C) blocklet containing alternating amorphous and crystalline lamellae, (D) organisation of amylopectin chains in the crystalline and amorphous lamellae. Reprinted from Cornejo-Ramírez *et al.* (2018). 9

Figure 2-4 Schematic illustration of packing arrangements of amylopectin double-helices and water molecules in A- and B-type starch at a plane projection. Reprinted from Tester *et al.* (2004), with permission from Elsevier. 11

Figure 2-5 Typical DSC thermogram of a starch. Republished with permission of Royal Society of Chemistry, from Wang & Copeland (2013); permission conveyed through Copyright Clearance Centre, Inc. 12

Figure 2-6 Typical pasting curve of a starch. Reprinted from Rincón-Londoño, Vega-Rojas, Contreras-Padilla, Acosta-Osorio, & Rodríguez-García (2016), with permission from Elsevier. 13

Figure 2-7 Schematic representation of amylose retrogradation with the formation of intra- and intermolecular hydrogen bonds within and between amylose chains. Reprinted from Tako et al. (2014). 15

Figure 2-8 Schematic illustration of polymer association for polymers with (A) single associative block, (B) two associative ends and (C) many associative groups at increasing polymer concentration. Associative and solvophilic blocks are represented in red and blue, respectively. Reprinted from Chassenieux *et al.* (2011), with permission from Elsevier. 16

Figure 2-9 Effect of concentration of urea on shear-thickening behaviour of 5% w/w Mamaku gum. Reprinted from Jaishankar *et al.* (2015), with permission from Elsevier. 18
Figure 2-10 Egg-box model showing calcium bridges formed between two non-esterified galacturonic acid units. Reprinted from Gawkowska *et al.* (2018)..... 18
Figure 2-11 Production of WPC and WPI. 29
Figure 2-12 Schematic illustration of the molecular structure of β-LG showing five of its cysteine residuals. Reprinted from Wijayanti, Brodkorb, Hogan, & Murphy (2019), with permission from Elsevier. 31
Figure 2-13 Possible thermodynamic interactions between protein and starch. 33
Figure 2-14 Phase behaviours of amylopectin-β-LG mixtures: (a) initial appearance of 5.64% w/w amylopectin and 16.44% w/w β-LG, (b) appearance of 5.90% w/w amylopectin and 17.43% w/w β-LG after 24 h, appearance of mixtures stored for 24 h and centrifuged at 40 000 rpm for 3 h at (c) 5.90% w/w amylopectin and 17.43% w/w β-LG, (d) 2.79% w/w amylopectin and 22.29% w/w β-LG, (e) 10.80% w/w amylopectin and 5.80% w/w β-LG. The layer boundaries are denoted with the bracket "}". Reprinted from Quiroga & Bergenståhl (2008), with permission from Elsevier..... 34
Figure 2-15 Schematic illustration of fracture structure of composite gels made with WPI and tapioca or potato starch in fine-stranded and particulate networks at pH 6.8 and 5.8, respectively (Fu & Nakamura, 2017). 36
Figure 2-16 Effect of starch concentration on the compressive stress of WPI-cassava starch composite gel at total solids of 10, 12, 15 and 18% w/w. Reprinted from Aguilera (2000), with permission from Food Technology. 37
Figure 3-1 Schematic illustration of centrifuged samples of waxy potato starch samples (5% w/w, 24,408 *g* for 2 h) treated at 120 °C for 30 min under continuous stirring of 100 and 300 rpm. 41
Figure 3-2 Visual appearance of 5% w/w native starch and de-structured starch samples treated at 150, 160 and 170 °C for 30 min under continuous stirring at 300 rpm. 41
Figure 3-3 Effect of temperature on the z-average hydrodynamic diameter of DWPS samples treated at 120, 130, 140, and 150 °C for 30 and 120 min under continuous stirring at 300 rpm. Values are plotted with mean ± standard error obtained at 20 °C. 42
Figure 3-4 Effect of treatment duration on the viscosity of DWPS samples treated at 120, 130, 140, and 150 °C for (A) 30 and (B) 120 min under continuous stirring at 300 rpm. Values are plotted with mean ± standard error obtained at 20 °C. 43
Figure 3-5 A ^{1}H-NMR spectrum of DWPS solubilised in d_6-DMSO. The integration limits of the signals corresponding to α-1,4 and α-1,6 signals are shown by the black and grey dotted lines, respectively.

The inset graph shows the exchangeable proton shifted by the addition of d_1-TFA at 11.79 ppm, and * is from the residual signal from the d_6-DMSO. 45
Figure 3-6 Schematic illustration of size-exclusion chromatography of polymers of different molecular sizes. 46
Figure 3-7 Calibration curves of polymers with different shape conformations (spherical, random coil and rod-like). Reprinted with permission from Striegel, Yau, Kirkland, & Bly (2009). Copyright 2009 John Wiley & Sons, Inc. 47
Figure 3-8 Size-exclusion chromatographs of debranched corn starch eluted with mobile phase of (A) 0.1 and (B) 0.3 M sodium nitrate. Reprinted with permission from Lin *et al.* (2011). Copyright 2011 American Chemical Society. 48
Figure 3-9 Chromatograph of a mixture containing maltohexaose (DP 6), acetate buffer and isoamylase, (A) without and (B) with the addition of barium acetate to remove sulphate ions from the chromatograph. Reprinted with permission from Lin *et al.* (2011). Copyright 2011 American Chemical Society. 48
Figure 3-10 Double log plot of radius of gyration against molar mass for polymers of different conformations. 50
Figure 3-11 Measurable size ranges for dynamic light scattering and laser diffraction. 50
Figure 3-12 Schematic illustration of the influence of particle size on the angle of light scattering. .. 52
Figure 3-13 Two-plates-model illustrating the generation of the flow velocity of a fluid caused by the applied force. 53
Figure 3-14 Viscosity curves of Newtonian, shear-thinning and shear-thickening fluids. 54
Figure 3-15 Viscosity curves of fluids that exhibit anti-thixotropic and thixotropic behaviour under shear at a fixed shear rate over time. 54
Figure 3-16 Linear and non-linear viscoelastic regions (LVR and non-LVR) with increasing amplitude strain. 55
Figure 3-17 Stress response of elastic solid, viscous liquid and viscoelastic material under applied stress. 57
Figure 3-18 A typical TPA force-displacement curve. 58
Figure 3-19 Scanning electron micrograph of (A) 20% w/w tapioca starch, (B) WPI and tapioca starch (1:1 ratio) at 15% w/w total solids, (C) 20% w/w corn starch and (D) WPI and corn starch (1:1 ratio) at 15% w/w total solid. Reprinted with permission from Carvalho, Onwulata, & Tomasula (2007). Copyright 2007 SAGE Publications. 60
Figure 3-20 Transmission electron micrographs of whey protein isolate paste (60% w/w) (A) before and (B) extrusion at 100 °C. Reprinted from Onwulata *et al.* (2003), with permission from Elsevier. 61

Figure 3-21 Schematic diagram of the principle of CSLM. 62
Figure 3-22 Confocal scanning laser micrographs of 13% w/w WPI gels with increasing concentration of k-carrageenan from 0–0.6% w/w at 50 mM NaCl. The scale bar is 50 µm. Reprinted from Çakır & Foegeding (2011), with permission from Elsevier. 63
Figure 3-23 Confocal scanning laser micrographs of native waxy potato starch granules stained with (A) APTS, (B) Rhodamine B, (C) fast green, and 13% w/w whey protein gel with 500 mM NaCl stained with APTS and fast green with emissions under (D) APTS and I fast green channels and (F) their overlay. The scale bar is 20 µm 64
Figure 4-1 Effect of temperature on the z-average hydrodynamic diameter and viscosity at 10 s^{-1} of DWPS samples treated at 120, 130, 140, and 150 °C. Values are plotted with means ± standard error, with measurements taken at 20 °C. 72
Figure 4-2 Particle-size distribution of gelatinised waxy potato starch (95 °C) and DWPS samples treated at 120, 140 and 150 °C determined by laser diffraction. 72
Figure 4-3 Light scattering (LS) signal, differential refractive index (dRI) signal and M_w distribution of native waxy potato starch, amylopectin (potato), and DWPS samples treated at 120, 140, and 150 °C eluted with 0.1 M sodium nitrate containing 0.02% sodium azide. 75
Figure 4-4 Starch side-chain length distribution of debranched native waxy potato starch and DWPS samples treated at 120, 140 and 150 °C, with the degree of polymerisation denoted as DP. Values are plotted as means ± standard error. Values in the same DP group denoted with the same superscripts are not significantly different ($p \leqslant 0.05$). 76
Figure 4-5 Schematic illustrations of (A) starch degradation during the de-structuring process from 120 to 150 °C and (B) dRI chromatograms of 120, 140 and 150 °C DWPS becoming more mono-modal due to amylopectin chains being cleaved near the middle. 79
Figure 5-1 Shear-dependent viscosity of 5% w/w gelatinised waxy potato starch (95 °C) and DWPS samples treated at 120, 130, 140, and 150 °C. Values are plotted as means ± standard error with measurements taken at 20 °C. 84
Figure 5-2 Hysteresis area between upward and downward flow curves of 5% w/w (A) gelatinised starch (95 °C) and DWPS samples treated at (B) 120, (C) 130, (D) 140, aI(E) 150 °C DWPS. Values are plotted as means ± standard error with measurements taken at 20 °C. 86
Figure 5-3 Effect of shear (1000 s^{-1} for 5 min) on the storage and loss moduli (*G'* and *G"*) of 5% w/w DWPS samples treated at 120, 140 and 150 °C. Measurements were taken at 20 °C. Note that the *G"* of 150 °C DWPS upon shear was outside of the detectable range of the rheometer. 89

Figure 5-4 Effect of shear rate on the viscosity of 5% w/w 120 °C DWPS, at 1, 5, 10, 15, 30, 45, 60, 120, 300 and 1000 s^{-1} for 12 min, with an inset graph at 10, 15, 30, 45, and 60 s^{-1} during the first 4 min of the measurement. Measurements were taken at 20 °C. 91
Figure 5-5 Hysteresis behaviour of 5% w/w 120 °C DWPS upon increasing or decreasing shear rate at 20 °C: (A) 0.1 to 5 s^{-1}, (B) 0.1 to 60 s^{-1}, and (C) 0.1 to 1000 s^{-1}. Measurements were taken at 20 °C. .. 92
Figure 5-6 Effect of shear history on the *G'* and *G"* of 5% w/w 120 °C DWPS: (A) in-shear structural recovery with a step increase of pre-shear from 1, 10, 100 to 1000 s^{-1} for 5 min; and (B) long-term structural recovery over 72 h at 12 h intervals (measurement were only taken during the first 2 h) after shear-induced gelation at one shear cycle (0.1 to 1000 s^{-1}) and 1000 s^{-1} for 5 min, with an inset graph of viscosity of the same sample before and after shear-induced gelation. Measurements were taken at 20 °C. 94
Figure 5-7 Effect of concentration on the: (A) viscosity of 0.5, 1.0, 2.5, 5.0, 7.5, and 10.0% w/w 120 °C treated waxy potato starch, and (B) visual appearance of 2.5, 5.0, 7.5, and 10.0% w/w 120 °C treated waxy potato starch before and after rheological measurements. Measurements were taken at 20 °C. 96
Figure 6-1 Turbidity of 5% w/w unsheared and sheared DWPS samples treated at 120, 140 and 150 °C. Values are plotted as means ± standard error, with measurements taken at 20 °C. 103
Figure 6-2 Light scattering (LS) signal, differential refractive index (dRI) signal and weight-average molar mass (M_w) of unsheared and sheared DWPS samples treated at (A) 120, (B) 140 and (C) 150 °C eluted with 0.1 M sodium nitrate containing 0.02% sodium azide. 105
Figure 6-3 Particle-size distribution of unsheared and sheared DWPS samples treated at: (A) 120, (B) 140 and (C) 150 °C determined using dynamic light scattering (DLS; with measurable region coloured in grey) and laser diffraction (LD; with measurable region shaded in grey) 108
Figure 6-4 DWPS samples treated at 120, 140 and 150 °C that remained (% w/w, with respect to the original unsheared sample) after passing through a 5 µm filter or sheared at 1000 s^{-1} for 5 min or sheared at 1000 s^{-1} for 5 min and then passed through a 5 µm filter. Note that unsheared-120 °C DWPS cannot be filtered through a 5 µm filter. Values are plotted as means ± standard error, with measurements taken at 20 °C. 109
Figure 6-5 Effect of urea on the viscosity of 5% w/w 120 °C DWPS at 0, 0.5, 1.5, 2.5, and 3.0 M urea. Measurements were taken at 20 °C. 110
Figure 6-6 Effect of NaCl on the viscosity of 5% w/w 120 °C DWPS, at 0, 0.001, 0.005, 0.01, 0.05, 0.1, 0.25, and 0.5 M NaCl. Measurements were taken at 20 °C. 111
Figure 6-7 The effect of temperature on 5% w/w 120 °C DWPS: (A) viscosity at varied temperatures of 20, 35, 50, 65, 80, and 90 °C, (B) Arrhenius plots of critical shear rate ($\gamma crit$) and critical viscosity

($\eta crit$), and (C) maximum viscosity (ηmax) and characteristic time scale (1/γmax), and D) viscoelastic moduli of shear-induced structure heated at 90 °C for 20 min. The viscoelasticity was measured at 1% strain and 1 Hz frequency. 114

Figure 6-8 Combined effects of urea (3 M) and NaCl (0.1 M) with and without temperature (20 or 95 °C) on the viscosity of 5% w/w 120 °C DWPS. 115

Figure 6-9 Schematic illustration of shear-thickening and anti-thixotropy mechanism of 120 °C DWPS. 117

Figure 7-1 Phase stability of 13% w/w WPI solutions and mixtures of 13% w/w WPI + 4% maltodextrin or gelatinised starch or DWPS (120–150 °C) at (A) pH 7 and (B) pH 5, after 24 h storage at 20 °C. .. 127

Figure 7-2 Influence of DWPS on fine-stranded polymeric protein gels (13 % w/w WPI, 13% w/w + 4% w/w maltodextrin or gelatinised starch or DWPS (120–150 °C) at pH 7): (A) *G'* from frequency sweep at 1% strain and 1 Hz frequency at 20 °C and gel hardness at room temperature, and (B) TEM micrographs (60 000×) with a scale bar of 200 nm. Values are presented as means ± standard error. Values denoted with the same superscript/number are not significantly different ($p \leqslant 0.05$). 129

Figure 7-3 *G'* from frequency sweep at 1% strain and 1 Hz frequency at 20 °C and textural hardness at room temperature of 13–17% w/w WPI and 13% w/w WPI + 4% w/w 140 °C DWPS at pH 7. Values are presented as means ± standard error. Values denoted with the same superscript/number are not significantly different ($p \leqslant 0.05$). 130

Figure 7-4 Influence of DWPS on the water-immersion stability of fine-stranded polymeric protein gels (13% w/w WPI and 13% w/w WPI + 4% w/w maltodextrin or gelatinised starch or DWPS (120–150 °C) at pH 7) over 40 h: (A) degree of water absorption, (B) appearance of drained gels (13 % w/w WPI gels after 2, 6, 12 and 20 h, and all gel samples at 40 h), (C) degree of protein leaching, with an inset graph showing 0–3% w/w of protein leaching, and (D) degree of carbohydrate leaching with an inset graph showing 0–3.9% w/w of carbohydrate leaching. Values are plotted as means ± standard error with measurements taken at room temperature. The red marker indicates fluid gel. 132

Figure 7-5 Effect of the molar mass of added carbohydrates on the degree of carbohydrate leaching from fine-stranded polymeric protein gels (at pH 7) containing maltodextrin or gelatinised starch or DWPS (120–150 °C) at 40 h water-immersion. Values are plotted as means ± standard error. 133

Figure 7-6 Influence of DWPS on the *G'* (from frequency sweep at 1% strain and 1 Hz frequency) at 20 °C and gel hardness at room temperature of coarse-stranded particulate protein gels (13% w/w WPI and 13% w/w + 4% w/w maltodextrin or gelatinised starch or DWPS (120–150 °C) at pH 5. Values denoted with the same superscript/number are not significantly different ($p \leqslant 0.05$). 135

Figure 7-7 Effect of molar mass of carbohydrates on the gel hardness and microstructure of coarse-stranded particulate protein gels (13% w/w WPI + 4% w/w maltodextrin or gelatinised starch or DWPS

(120–150 °C)) at pH 5. Values are plotted with means ± standard error. Confocal scanning laser micrographs were taken at 630× magnification, with a scale bar of 20 µm. 135
Figure 7-8 Appearance of serum released from coarse-stranded particulate protein gels at pH 5 during compression test: (A) 13% w/w WPI or 13% w/w WPI + 4% w/w maltodextrin (B) 13% w/w WPI + 4% w/w gelatinised starch or DWPS (120–150 °C), and (C) visual appearance of deformed particulate protein gels of 13% w/w WPI and 13% w/w WPI + 4% w/w maltodextrin or gelatinised starch or DWPS (120–150 °C) after compression test. 137
Figure 7-9 Effect of molar mass of carbohydrates on the degree of carbohydrate leaching of centrifuged coarse-stranded particulate protein gels containing maltodextrin or gelatinised starch or DWPS (120–150 °C) at pH 5. Values are plotted as means ± standard error. 139
Figure 7-10 Influence of DWPS on the water-immersion stability of coarse-stranded particulate protein gels (13 % w/w WPI and 13% w/w + 4% w/w maltodextrin or gelatinised starch or DWPS (120–150 °C) at pH 5) over 40 h: (A) degree of water absorption, (B) appearance of drained gels at 40 h, (C) degree of protein leaching, and (D) degree of carbohydrate leaching. Values are plotted as means ± standard error with measurements taken at room temperature. 140
Figure 8-1 Effect of NaCl (0, 25, 50, 75, 100, 250 and 500 mM) and $CaCl_2$ (0, 2.5, 5, 7.5, 10, 25, 50, 75, 100, 250 and 500 mM) on the phase stability of 13% w/w WPI solutions and mixtures of 13% w/w WPI + 4% w/w maltodextrin or gelatinised starch or 140 °C DWPS after 24 h storage at 20 °C. 147
Figure 8-2 Effect of salts on the gelation temperature of 13 % w/w WPI and 13 % w/w WPI + 4% w/w maltodextrin or gelatinised starch or 140 °C DWPS at varied: (A) NaCl concentrations of 0, 12.5, 25, 50, 75, 100, 250 and 500 mM, and (B) $CaCl_2$ concentrations of 0, 2.5, 5, 7.5, 10, 25, 50, 75, 100, 250 and 500 mM, and (C) effect of NaCl and $CaCl_2$ on gelation temperature at equivalent ionic strengths (lines serve as visual aids). The gelation temperatures were obtained from temperature sweep when *G'* crossed over *G"* (tan δ = 1, at 1% strain and 1 Hz frequency) during the heat-induced gelation. Values are plotted as means ± standard error. 149
Figure 8-3 Effect of NaCl on the: (A) *G'* from frequency sweep at 1% strain and 1 Hz frequency of 13% w/w WPI and 13% w/w WPI + 4% w/w maltodextrin or gelatinised starch or 140 °C DWPS with 0–500 mM NaCl at 20 °C. Lines in the graphs serve as visual aids, (B) visual appearance of 13% w/w WPI and 13% w/w WPI + 4% w/w gelatinised starch or 140 °C DWPS at 50, 75, 100 and 250 mM NaCl, (C) textural hardness of 13% w/w WPI and 13% w/w WPI + 4% w/w gelatinised starch or DWPS with 0–500 mM NaCl at room temperature. Values are plotted as means ± standard error. Note that compression test was not performed on inhomogeneous/paste-like gels (denoted with *). 153
Figure 8-4 Effect of NaCl on the microstructure of 13% w/w WPI and 13% w/w WPI + 4% w/w gelatinised starch or 140 °C DWPS gels at 0, 25, 75 and 500 mM NaCl: CSLM micrographs (630×) and

SEM micrographs (2500×). Note that SEM was not done on paste-like samples. The scale bars are 20 µm. 154

Figure 8-5 Effect of $CaCl_2$ on the: (A) *G'* from frequency sweep at 1% strain and 1 Hz frequency of 13% w/w WPI and 13% w/w WPI + 4% w/w maltodextrin or gelatinised starch or 140 °C DWPS with 0–500 mM $CaCl_2$ at 20 °C. Lines in the graphs serve as visual aids, (B) visual appearance of 13% w/w WPI and 13% w/w WPI + 4% w/w gelatinised starch or 140 °C DWPS at 25, 50, 75 and 500 mM $CaCl_2$, (C) textural hardness of 13 % w/w WPI and 13% w/w + 4% w/w gelatinised starch or 140 °C DWPS with 0–500 mM $CaCl_2$ at room temperature. Values are plotted as means ± standard error. Note that compression test was not performed on inhomogeneous/paste-like gels (denoted with *). 156

Figure 8-6 Effect of $CaCl_2$ on the microstructure of 13% w/w WPI and 13% w/w WPI + 4% w/w gelatinised starch or 140 °C DWPS gels at 0, 10, 75 and 500 mM $CaCl_2$: CSLM micrographs (630×) and SEM micrographs (2500×). Note that SEM was not done for paste-like samples. The scale bars are 20 µm. 157

Figure 9-1 General overview of the DWPS characteristics and its interactions under investigation in this thesis. 160

Figure 9-2 Schematic illustration of amylopectin degradation during the de-structuring process from 120 to 150 °C. 161

Figure 9-3 Rheological profiles of gelatinised starch (95 °C) and DWPS treated at 120, 140 and 150 °C upon increasing (unfilled markers, 1) or decreasing shear rate (filled markers, 2). Measurements were taken at 20 °C. 162

Figure 9-4 Varied gel textures of 13% w/w WPI + 4% w/w 140 °C DWPS at different NaCl concentrations (0 – 500 mM). 164

Figure A-1: Scanning electron micrograph (8000× magnification) of (A) 13% w/w WPI + 4% w/w maltodextrin, (B) 13% w/w WPI + 4% w/w gelatinised starch, and (C) 13% w/w WPI + 4% w/w 140 °C DWPS. The scale bars are 5 µm. I

List of tables

Table 2-1 Weight-average molecular weight (M_w) and z-average radius of gyration (R_z) of amylopectin from different botanical origins. 6

Table 2-2 Molar fraction of branched and unbranched amylose molecules from different botanical sources. Table modified from Takeda *et al.* (1987). 7

Table 2-3 Number-average degree of polymerisation and number-average chain length of amylose from different botanical sources. 7

Table 2-4 Blocket length from different botanical sources. 10

Table 2-5 Definition of DSC parameters (Wang & Copeland, 2013). 13

Table 2-6 Definition of pasting curve parameters (Rincón-Londoño *et al.*, 2016). 14

Table 2-7 Altered physico-chemical properties in starches modified by heat-moisture treatment (HMT). 21

Table 2-8 Altered physico-chemical properties in annealed starches. 24

Table 2-9 Modification conditions for resistant starch. 26

Table 2-10 Composition of sweet and acid whey from cheddar cheese and cottage cheese production respectively (Morr & Ha, 1993). 28

Table 2-11 Composition of Fonterra SureProtein^{TM} WPI 895 and WPI 8855. 29

Table 2-12 Chemical and physical properties of β-lactoglobulin and α-lactalbumin (Guo & Wang, 2019a). 30

Table 3-1 Parameters studied for the starch de-structuring process. 40

Table 3-2 Common food microscopy techniques (Auty, 2019). 59

Table 3-3 Details of fluorescence dyes (rhodamine B, fast green and APTS) used in the study. 63

Table 4-1 Weight-average molar mass (M_w), root-mean-square radius (R_z), and slope from the plot of M_w against the root-mean-square radius of DMSO-solubilised native waxy potato starch, amylopectin (from potato), and DWPS samples treated at 120, 140, and 150 °C. 74

Table 4-2 Degree of branching of native waxy potato starch and DWPS samples treated at 120, 140 and 150 °C. 77

Table 5-1 Hysteresis areas of the 5% w/w gelatinised starch (95 °C) and DWPS samples treated at 120, 130, 140, and 150 °C. 87

Table 5-2 Power-law model parameters for 5% w/w gelatinised starch (95 °C) and DWPS samples treated at 120, 130, 140, and 150 °C. 88

Table 6-1 Weight-average molar mass (M_w) and root-mean-square radius (R_z) of unsheared and sheared DWPS samples treated at 120, 140 and 150 °C. 106

Table 7-1 Degree of syneresis, protein leaching, and carbohydrate leaching from coarse-stranded particulate protein gels (13 % w/w WPI and 13% w/w + 4% w/w maltodextrin or gelatinised starch or DWPS (120–150 °C) at pH 5). 138

List of publications and conference proceedings

1. Ang, C. L., Matia-Merino, L., Lim, K., & Goh, K. K. T. (2019, 1st–3rd October). Formation and characterisation of de-structured starch. [Poster presentation]. 5th International Conference on Food Structures, Digestion and Health, Rotorua, New Zealand.
2. Ang, C. L., Matia-Merino, L., Lim, K., & Goh, K. K. T. (2021b). Molecular and physico-chemical characterisation of de-structured waxy potato starch. *Food Hydrocolloids, 117*, 106667.
3. Ang, C. L., Matia-Merino, L., Lim, K., & Goh, K. K. T. (2021, 7th–9th April). Molecular and rheological characterisation of de-structured waxy potato starch. [Poster presentation]. Riddet Institute Student Colloquium 2021 Wellington, New Zealand.
4. Ang, C. L., Goh, K. K. T., Lim, K., & Matia-Merino, L. (2021a). Rheological characterisation of a physically-modified waxy potato starch: Investigation of its shear-thickening mechanism. *Food Hydrocolloids, 120*, 106908.
5. Ang, C. L., Matia-Merino, L., Lim, K., & Goh, K. K. T. (2021, 6th–8th July). De-structured starch as a "clean-label" ingredient and its potential in food applications. [Poster presentation]. New Zealand Institute of Food Science and Technology Conference 2021, Palmerston North, New Zealand.
6. Ang, C. L., Matia-Merino, L., Lim, K., & Goh, K. K. T. (2021, 19th–20th October). De-structured starch as a "clean-label" ingredient and its potential in food applications. [Poster presentation]. 4th Food Structure and Functionality Symposium, Online live and on-demand.
7. Ang, C. L., Matia-Merino, L., Sims, I. M., Sargison, L., Edwards, P. J. B., Lim, K., & Goh, K. K. T. (2022b). Characterisation of de-structured starch and its shear-thickening mechanism. *Food Hydrocolloids, 132*, 107864.
8. Ang, C. L., Goh, K. K. T., Lim, K., & Matia-Merino, L. (2022a). High-Protein Foods for Dysphagia: Manipulation of Mechanical and Microstructural Properties of Whey Protein Gels Using De-Structured Starch and Salts. *Gels, 8*(7), 399.
9. Ang, C. L., Matia-Merino, L., Lim, K., & Goh, K. K. T. (2023). Influence of de-structured starch on fine-stranded polymeric and coarse-stranded particulate whey protein gels. *Food Hydrocolloids, 135*, 108201.

Chapter 1 Introduction

Starch is a naturally occurring polysaccharide that is found in abundance in plant parts including leaves, fruits, stems, roots, and tubers. Due to its gelling, stabilising, film-forming, and thickening properties, starch is widely used as an ingredient in food products. However, native starch tends to retrograde and has poor processing stability. Such undesirable properties limit the use of native starch. To overcome these shortcomings of native starch, starch is traditionally chemically-modified. However, due to the rising trend in pursuing "clean-label" food products, there has been increasing pressure on starch manufacturers to modify starch without using chemicals. This has led to increasing research being conducted on physical modification methods of starch. Some such examples include heat-moisture treatment, annealing and high-pressure processing, where the modified starch retains the starch granular structure after modification. Up till now, there has been limited research on modifying starch to intentionally release starch macromolecules from its granule and use these macromolecules as an ingredient to structure food systems. Thus, this gap in the literature prompted the research questions in this thesis.

In fact, the idea of using starch macromolecules as an ingredient to structure foods came from how starch is being used in papermaking. In order to be an efficient binder, starch macromolecules have to be completely solubilised. Complete solubilisation of starch in papermaking can be achieved by using a high temperature at 120 °C under pressure with high shear (*i.e.*, jet cooking) or by adding a strong base under atmospheric conditions (Maurer, 2009). Other applications that use high temperature include solubilisation of starch granules for starch fractionation and production of resistant starch. Traditionally, a starch paste containing butanol or isoamyl alcohol is autoclaved to fractionate starch into its macromolecules (amylose and amylopectin) for molecular weight analysis and other research studies (Hopkins & Jelinek, 1948). Autoclaving is used to increase the solubility of gelatinised starch (at 121–148 °C for 60 min) before retrogradation at low temperature (*e.g.*, 4 °C for overnight) to produce resistant starch (Sievert & Pomeranz, 1989). There are limited studies that use starch as an individual macromolecule (as an ingredient) to structure foods. It is hypothesised that the combination of physical treatments including thermal, pressure, shear, and duration (*i.e.*, starch de-structuring process) can be used to solubilise waxy potato starch granules into their macromolecular chains. These macromolecules are expected to exhibit physico-chemical properties that are different from gelatinised starch and other conventional physical-modified starches and can potentially be used with other biopolymers to create new food structures to confer the desired health and sensory

benefits. As such, in Chapter 3, screening of treatment parameters (*i.e.*, temperature from 120–170 °C with corresponding pressure of 1.2–6.9 barg, stirring speed of 100 and 300 rpm, and duration of 30 and 120 min) were carried out to obtain waxy potato starch samples with different degrees of disassembly. The treated starch is denoted as de-structured waxy potato starch (DWPS). To the best of this author's knowledge, the DWPS samples obtained by such physical treatment regimes are not well-characterised and understood. Therefore, the objective of Chapter 4 is to study the disassembly of waxy potato starch granules during the de-structuring process, using various molecular and physico-chemical characterisation techniques on the respective DWPS samples. The data obtained from this study not only provided insights into the mechanism of the de-structuring process, but the knowledge acquired also provided useful avenues in exploring potential applications for DWPS as a clean-label food ingredient.

The rheological properties of DWPS were studied in Chapter 5. Interesting shear-induced behaviours such as shear-thickening, anti-thixotropy and shear-induced gelation, particularly for 120 °C DWPS samples, were observed. Although shear-thickening behaviour has been reported in some starch systems, the exact mechanism is still not well-understood. Thus, an attempt was made to elucidate the mechanism of shear-thickening, anti-thixotropy and shear-induced gelation of DWPS (Chapter 6).

Binary polysaccharide-protein systems have been a popular topic for food research over the past decades. Mixtures of polysaccharides and proteins can be used to generate novel gel structures that possess different physico-chemical properties as compared to the individual gel properties (Yang, Li, Li, Guo, & Sun, 2021). The introduction of DWPS to other food proteins such as whey protein isolate (WPI) could open new possibilities to create novel food structures. In Chapter 7, the influence of various DWPS samples was evaluated in fine-stranded polymeric and coarse-stranded particulate WPI gels, at pH 7 and pH 5, respectively. The functionalities studied include phase stability of liquid mixtures, mechanical properties, microstructure, and water immersion stability of the WPI + DWPS gels. Ionic strength is another factor that heavily affects the WPI gel properties. Thus, the effects of salts (NaCl and $CaCl_2$) were also evaluated on WPI + 140 °C DWPS gel (Chapter 8). The parameters examined in this ionic strength study include phase stability, gelation temperature, mechanical properties, and microstructure of the composite gels.

The thesis follows a methodical flow to meet the project objectives, where the relevant literature background and theories of the characterisation techniques used are presented in Chapter 2 and Chapter 3, respectively. The key objectives and hypotheses for the thesis have been addressed in Chapter 4 to 8 (research chapters). An overview of the organisation of the thesis is illustrated in Figure 1-1 for ease of reference.

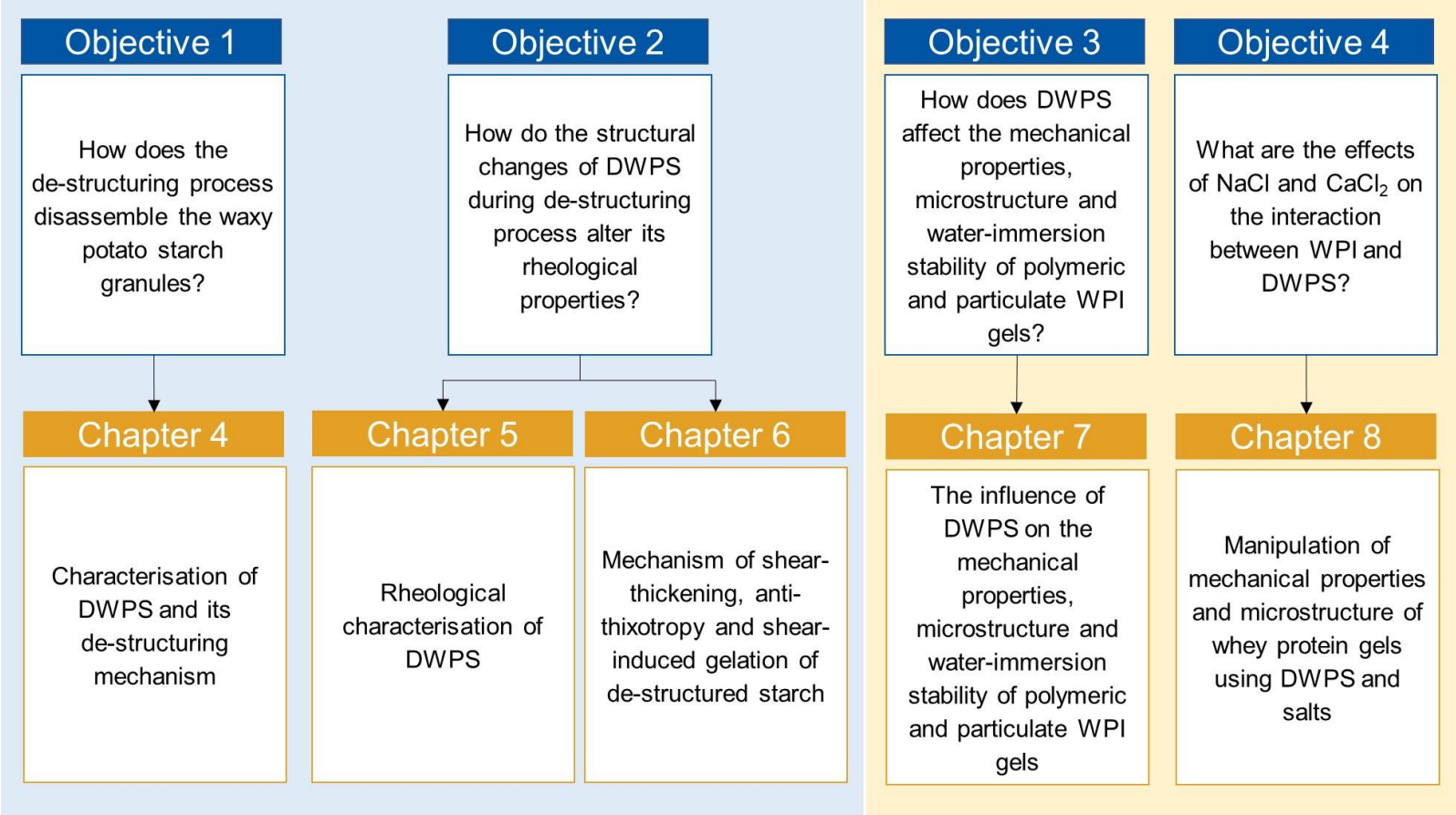

Figure 1-1 Overview of the research chapters.

Chapter 2 Literature review

2.1. Starch

Starch is a biopolymer that is mainly composed of two polymers, namely amylopectin and amylose molecules. Normal/regular starches from maize, rice, wheat, and potato contain 70–80% w/w amylopectin and 20–30% w/w amylose (Fredriksson, Silverio, Andersson, Eliasson, & Åman, 1998; Pérez & Bertoft, 2010). Waxy starches generally contain a very small amount of amylose, usually less than 1% w/w. On the other hand, high-amylose variety starches can contain up to 80% w/w apparent amylose content (Pérez & Bertoft, 2010). Other minor components in starch granules include proteins, lipids and phosphorous. These components are reported to have a profound effect on the physio-chemical properties of starches (Debet & Gidley, 2006; Morrison, 1988).

2.1.1. Components of starch granules

2.1.1.1. Amylopectin

Amylopectin is a highly branched molecule that has its branching points (4–5% w/w) connected by α-1,6 linkages and the rest of the anhydroglucose monomers are linked by α-1,4 linkages. The branching occurs periodically at about every 20–30 anhydroglucose monomers (Tiefenbacher, 2019). A 2-D schematic illustration of amylopectin is presented in Figure 2-1. The A-chains are the outermost chains that are unsubstituted, which are connected to either B-chains or C-chain. C-chain is the backbone of an amylopectin chain, which carries the reducing end of the molecule. B-chains can be further classified into B1-, B2-, B3- and B4-chains depending on the extent of cluster substitution; *i.e.*, B1-, B2-, B3- and B4-chains stretch across one, two, three and four or more clusters, respectively (Hizukuri, 1986). It is also found that the respective side-chains of an amylopectin molecule can be identified using their degree of polymerisation (DP) through high-performance size-exclusion chromatography (HP-SEC). For the analysis, debranched linear side-chains will be produced first by subjecting the amylopectin molecules to enzymatic debranching using isoamylase. The resulting linear side-chains will then be grouped into A-, B1-, B2- and B3-chains using their DP, where their DP is believed to corresponds with side-chains of DP 6–12, DP 13–24, DP 25–36 and DP > 36, respectively (Pedrosa Silva Clerici, Sampaio, & Schmiele, 2019).

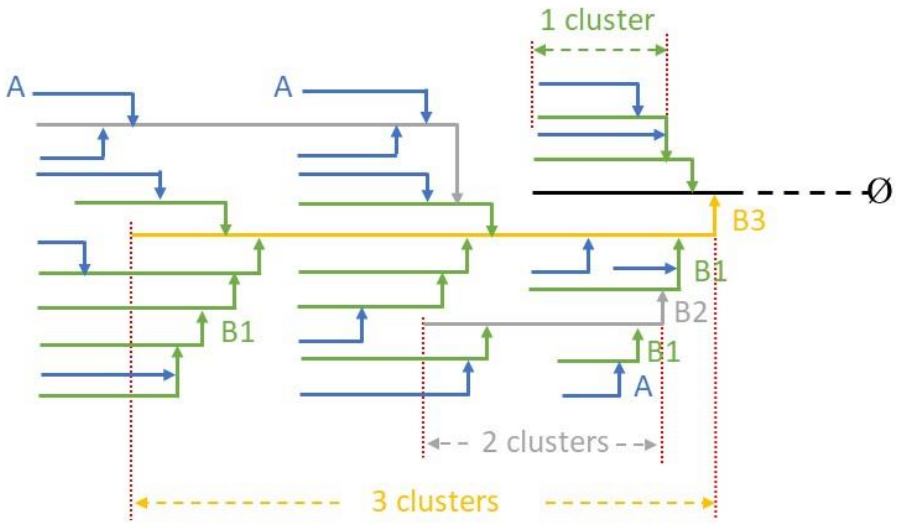

Figure 2-1 Schematic illustration of amylopectin with its A-, B1-, B2- and B3-chains represented by blue, green, grey and yellow, with α-1,4 and α-(1,6)-linkages denoted as —and → symbols, respectively. The reducing end of the C-chain is represented by Ø.

Starches can be categorised into A-, B- and C-type depending on their crystal polymorph. A-, B- and C-type starches are generally associated with starches from cereal, tubers and legumes, respectively (Cornejo-Ramírez *et al.*, 2018). Starches from different origins are observed to have different side-chain distributions (Figure 2-2), which can range from DP 6 to ~100. The side-chain distribution results in Figure 2-2 show that A-type starch is made up of a larger fraction of short A-chains and smaller fractions of longer B-chains (side-chains that stretch across ≥ 1 cluster). In contrast, B-type starch has a larger fraction of longer B-chains and smaller fractions of the short A-chains. C-type has a combined crystal polymorph of A- and B-type starch, thus consisting of large fractions of both very long B-chains and short A-chains (Ai & Jane, 2018b). The observations from Ai & Jane (2018b) are in agreement with the hypothesis from Hizukuri (1986) where the A-chains are presented in a higher ratio in A-type amylopectin (waxy rice) than that of B-type (potato) and C-type (tapioca and kuzu) starch. The A-chain: B-chains ratio for waxy rice, tapioca, kudzu, and potato amylopectin chains was reported to be 2.2, 0.89, 0.89 and 0.79, respectively.

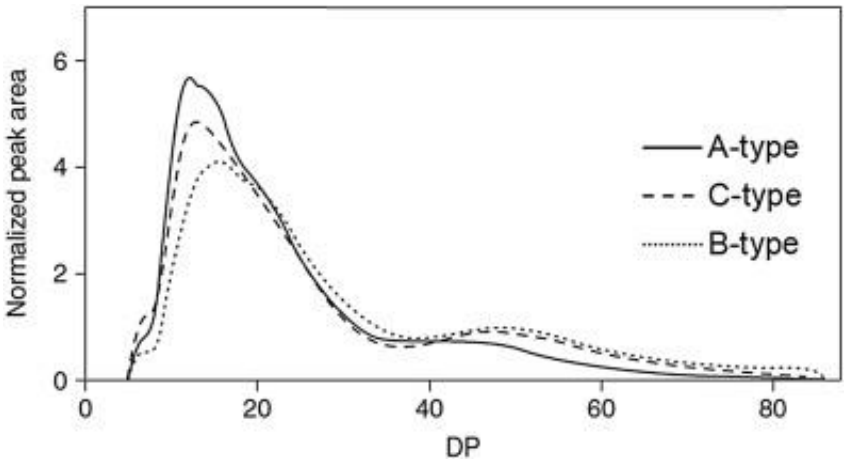

Figure 2-2 Average side-chain distributions for A-, B- and C-type starch. Reprinted from Ai & Jane (2018b), with permission from Elsevier.

Amylopectin has a high molar mass (M_w) ranging from 0.7 to 56.8 × 10^8 mol/g, the M_w and gyration radius of amylopectin from different botanical origins are presented in Table 2-1. The high M_w of amylopectin contributes to its high swelling power and viscosity development during gelatinisation (Kumar & Khatkar, 2017; Tester & Morrison, 1990).

Table 2-1 Weight-average molecular weight (M_w) and z-average radius of gyration (R_z) of amylopectin from different botanical origins.

Polymorph	Source	Weight-average M_w (× 10^8 g/mol)	z-average radius of gyration, R_z (nm)
Type A	Normal maize[a]	4.9 ± 0.8	312 ± 23
	Waxy maize[a]	8.3 ± 0.2	372 ± 11
	Normal rice[a]	26.8 ± 2.9	581 ± 41
	Waxy rice[a]	56.8 ± 9.3	782 ± 36
	Normal wheat[a]	3.1 ± 0.3	302 ± 3
	Waxy wheat[a]	5.2 ± 0.4	328 ± 6
Type B	Potato[a]	1.7 ± 0.2	356 ± 36
	Waxy potato[a]	2.0 ± 0.2	344 ± 37
Type C	Tapioca[a]	0.7 ± 0.1	191 ± 25
	Water chestnut[a]	7.1 ± 1.5	230 ± 25
	Pea[b]	7.7 ± 0.2	135 ± 1
	Mung bean[b]	10.6 ± 0.4	227 ± 3

Values are presented as means ± standard deviation.
[a]Taken from Yoo & Jane (2002).
[b]Taken from Yang et al. (2019b).

2.1.1.2. Amylose

In contrast to its branched counterpart, amylose is a linear polysaccharide connected by α-1,4 linkages. The weight-average M_w and radius of gyration of amylose can range from 0.2 to 2 × 10^7 g/mol and 19 to 60 nm, respectively (Aberle, Burchard, Vorwerg, & Radosta, 1994). Although amylose chains are generally considered linear, amylose can be lightly branched—containing up to ten branches— where the average number of chains in one branched amylose molecule can vary from 2.9 in corn to 9.8 in sweet potato (Takeda, Hizukuri, Takeda, & Suzuki, 1987). The molar fraction of branched and unbranched amylose molecules in starches from different botanical sources are summarised in Table 2-2, and the DP and chain length of amylose from maize, wheat, potato and rice are presented in Table 2-3.

Table 2-2 Molar fraction of branched and unbranched amylose molecules from different botanical sources. Table modified from Takeda *et al.* (1987).

	Molar fraction					
Amylose type	**Corn**	**Rice**	**Wheat**	**Chestnut**	**Tapioca**	**Sweet potato**
Unbranched	0.56	0.69	0.73	0.66	0.58	0.30
Branched	0.44	0.31	0.27	0.34	0.42	0.70

Table 2-3 Number-average degree of polymerisation and number-average chain length of amylose from different botanical sources.

Source	**Number-average degree of polymerisation, DP_n (g/mol)**	**Number-average chain length, CL_n**
Maize	930–990[a]	305–340[a]
Wheat	830–1570[b]	135–270[a]
Potato	4920–6340[a]	520–670[a]
Rice	920–1110[a]	200–380[c]

[a]Taken from Bertoft (2017).
[b]Taken from Pérez & Bertoft (2010).
[c]Taken from Hanashiro et al. (2008).

When the amylose chain is reduced to its individual chain, it adopts a random coil conformation in an aqueous solution (Kong & Ziegler, 2014). Such conformation is unstable for amylose due to the presence of both hydrophobic hydrocarbon groups and hydrophilic hydroxyl groups in the amylose chain (Ai & Jane, 2018a; Pérez & Bertoft, 2010). Thus, amylose adopts a double-helix conformation when it is cooled to room temperature—with its hydrophobic arrays of the chain folded inside of the double-helix—allowing minimal contact of its hydrophobic regions with the water phase. In contrast, when a guest molecule (*e.g.*, lipid, emulsifier, alcohol and flavour compound) is presented, amylose

chain forms a single helical structure with six to eight glucose units per turn depending on the size of the guest molecule with the non-polar molecule located inside the hydrophobic moiety of amylose (Kim, Kim, & Baik, 2012; Yamashita & Hirai, 1966). This complex exhibits a V-type X-ray diffraction pattern and is amorphous, which can be melted at 100–125 °C (Le Bail *et al.*, 1999).

2.1.1.3. Minor components

Besides the major components found in starch granules, starch contains a small amount of lipids, proteins and phosphorous, which have profound effects on the starch properties. Lipid content found in starch granules is usually < 1.5% w/w. The amount of lipid present is usually tied to the amylose content with a positive correlation between them, *i.e.,* waxy starch contains a minimal amount of amylose, thus, a small amount of lipids was found (Morrison, 1988). Starches from tuber, root, and legumes contain a negligible amount of lipids, up to 0.6 w/w% (Debet & Gidley, 2006). While cereal starches contain lipids such as triglyceride, free fatty acids, glycolipids, and phospholipids, which are found on the surface of the starch granules. In contrast, monoacyl lipids such as lysophospholipids and free fatty acids are found in the interior of cereal starch granules (Vasanthan & Hoover, 1992). As mentioned earlier, the lipid forms an inclusion complex with amylose in native starch granules (Le Bail *et al.*, 1999). The presence of such an amylose-lipid complex tends to restrict the swelling of starches (Tester & Morrison, 1990).

Protein content in starch granules ranges from 0.1–0.6% w/w. Proteins can be found both in the interior and on the surface of the granules. Most of these proteins function as enzymes, catalysing certain bioreactions within the starch granules. Amylolytic enzymes and granule-bound starch synthase represent two enzymes that are commonly found in starches. Amylolytic enzymes (*e.g.,* in sorghum starch) create interior channels (0.07–0.10 µm) by enlarging the pores on the granules during germination (Debet & Gidley, 2006). In contrast to amylolytic enzymes, granule-bound starch synthase—responsible for amylose synthesis—is found in the central cavity and internal concentric sphere of normal maize and wheat starch granules. These locations are believed to be the regions where amylose synthesis occurs (Han & Hamaker, 2002).

Phosphorous in starches are found in the form of phospholipids and phosphate monoesters. Phospholipids found in cereal starches reduced the clarity of gelatinised starch. In native starch, phosphate monoesters are mainly found in amylopectin; mostly substituted on the C-6 and C-3 of glucose residues (Bertoft, 2018; Lim, Kasemsuwan, & Jane, 1994). Among the common native starches, potato starch contains the largest concentration of phosphate monoester (~0.5% w/w), one phosphate monoester is found at about every 317 anhydroglucose monomers; one phosphate per 13 branch chains (Ai & Jane, 2018b; Pérez & Bertoft, 2010; Xu, Huang, Visser, & Trindade, 2017). Each of

these phosphate-monoester derivatives carries two negative charges, resulting in electrostatic repulsion with its neighbouring negatively charged amylopectin chains (BeMiller, 2019a). The electrostatic repulsion gives potato starch its unique properties, such as good paste clarity and high viscosity (Jane *et al.*, 1999).

2.1.2. Structural organisation

Starch granule is known to exhibit a birefringent pattern when viewed under a polarised light microscope. The phenomenon is caused by the radial arrangement of amylose and amylopectin molecules centred at the hilum and perpendicular to the granule surface (Conde-Petit, 2003; French, 1972). Starch molecules are organised at various levels into a granule as shown in Figure 2-3.

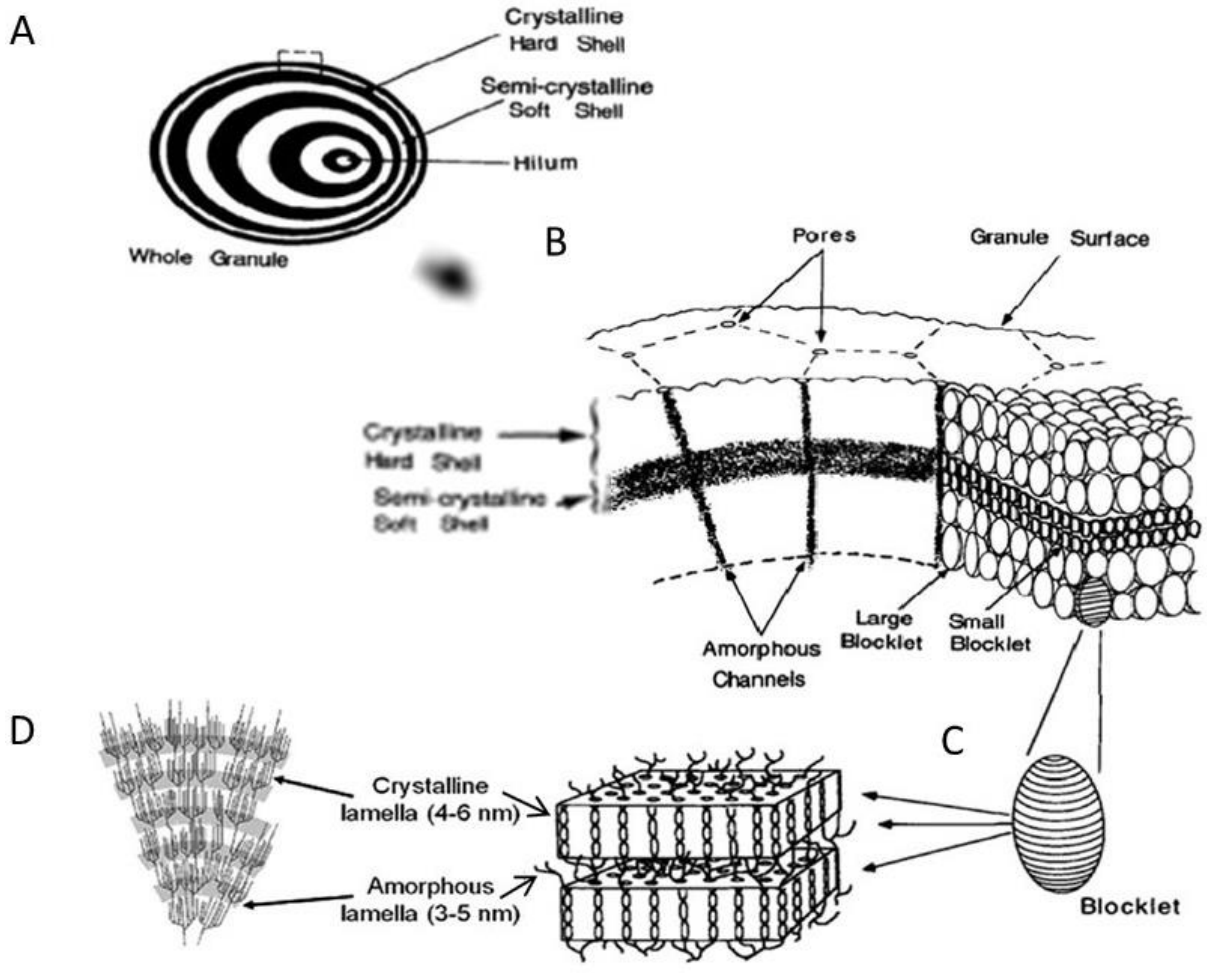

Figure 2-3 Schematic illustration of a starch granule at multi-levels: (A) at the lowest magnification level of starch granule organisation, the alternating crystalline and semicrystalline shells/growth rings are represented by dark and light colours respectively, (B) at the higher magnification level of starch structure, the blocklet structure is shown together with the amorphous radial channels. Noting that the size of blocklets in the semicrystalline shells is smaller than that of blockets in the crystalline shells, (C) blocklet containing alternating amorphous and crystalline lamellae, (D) organisation of amylopectin chains in the crystalline and amorphous lamellae. Reprinted from Cornejo-Ramírez *et al.* (2018).

At the lowest magnification level of starch granule organisation, the starch granule is made up of alternating semi-crystalline and amorphous growth rings (Figure 2-3A). Semi-crystalline growth rings have a thickness ranging from 120–400 nm, depending on the origin of the starch (Conde-Petit, 2003). The size of growth rings is believed to increase with amylose content (Yuryev *et al.*, 2004). The semi-crystalline and amorphous growth rings are made up of continuous bundles of crystalline and amorphous lamellae of amylopectin, known as "blockets" (Figure 2-3B and C). Blocklets from the different botanical sources have similar spherical shapes but are varied in dimensions. The length of blocklet from different botanical origins is presented in Table 2-4. Semi-crystalline growth ring is suggested to be made up of stacks of alternating crystalline and amorphous lamellae (Figure 2-3D), with a total lamellae unit of ~9 nm. The amorphous lamella of blocklet is made up of the branching point of amylopectin chains and amylose chains. In contrast, the crystalline lamella of blocklet is made up of the branches of amylopectin chain clusters, where the amylopectin chains interact with their adjacent chains to form ordered double-helices clusters (Atkin, Cheng, Abeysekera, & Robards, 1999; Beck, Jekle, & Becker, 2011; Yuryev *et al.*, 2004). It is also believed that the A- and B1-chains are responsible for this intermolecular double-helices association among amylopectin chains (Tester, Karkalas, & Qi, 2004).

Table 2-4 Blocket length from different botanical sources.

Botanical sources	Maximum blocklet length (nm)
Corn	30[a]
Peas	130 – 250[b]
Potato	200 – 500[c]
Wheat	80 – 120[c]

[a]Taken from Becker, Hill, & Mitchell (2001)
[b]Taken from Ridout, Parker, Hedley, Bogracheva, & Morris (2003)
[c]Taken from Gallant, Bouchet, & Baldwin (1997)

The packing of these double-helices can exist as an A- and/or B-polymorph, which allows the starch to be categorised into A-, B- or C-type depending on this specific packing arrangement of amylopectin double-helices within the starch granules (Ai & Jane, 2018a). The packing arrangements of A- and B-type starches are shown in Figure 2-4.

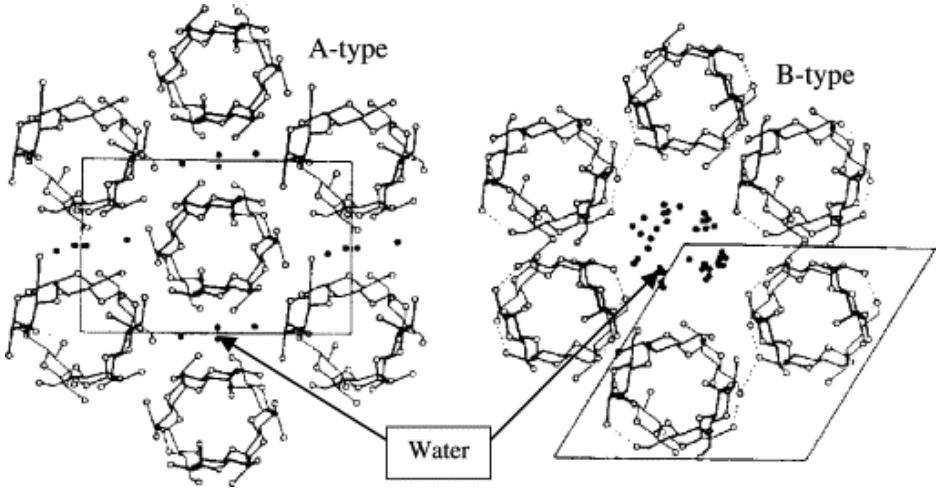

Figure 2-4 Schematic illustration of packing arrangements of amylopectin double-helices and water molecules in A- and B-type starch at a plane projection. Reprinted from Tester *et al.* (2004), with permission from Elsevier.

The main differences between the crystal polymorphs are: (i) A-type polymorph has a denser packing arrangement than B-type polymorph, and (ii) the water molecules are presented randomly in the A-type polymorph, whereas water molecules exist as a helical column and are surrounded by the amylopectin double helices in B-type polymorph (Figure 2-4) (Kim *et al.*, 2012). The formation of these crystalline polymorphs is highly dependent upon the environmental conditions where the plant is cultivated. Under warm and dry conditions, *e.g.*, cereal grains, an A-type starch crystal polymorph is preferred. In contrast, under cool and wet conditions, *e.g.*, potato tuber, a B-type starch crystal polymorph is adopted. Legume and rhizome starches are C-type starch, where a combination of A- and B-type polymorphs exists within a single starch source. One such example is pea starch, where both A- and B-type polymorphs are found dominating in the peripheral regions and at the centre of a pea starch granule, respectively (Tester *et al.*, 2004). The specific packing arrangement of its semi-crystalline region of granules can be determined by X-ray diffraction. Depending on the botanical sources, the crystallinity of starch ranges from 15 to 45% based on the total starch in its granules (Kim *et al.*, 2012).

2.1.3. Physical and rheological properties

2.1.3.1. Gelatinisation

When starch is suspended in excess water, the native granules can absorb up to ~35% w/w moisture, which causes reversible swelling and plasticisation. The absorbed water mainly exists in the amorphous region of the granules. When the starch suspension is heated above a specific temperature (*i.e.*, gelatinisation temperature, T_{gel}), the molecular organisation of starch granules is disrupted, where irreversible swelling and melting of crystalline regions occur (Ai & Jane, 2018b; Allan, Chamberlain, & Mauer, 2020). These changes result in the loss of birefringent pattern and cause an increase in viscosity where starch polymers interact with water molecules through hydrogen bonding (Jackson, 2003; Schmiele, Sampaio, & Pedrosa Silva Clerici, 2019). The length of amylopectin side-chains has been found to influence the T_{gel}. Starch with larger fractions of A-chains (short chains) has lower T_{gel}, whereas starch with larger fractions of longer amylopectin chains (DP 14–25) has higher T_{gel} (Allan et al., 2020). The gelatinisation properties of starch can be characterised using differential scanning calorimetry (DSC). A typical DSC thermogram of starch heated from 30 to 100 °C is shown in Figure 2-5 and its respective parameters are defined in Table 2-5.

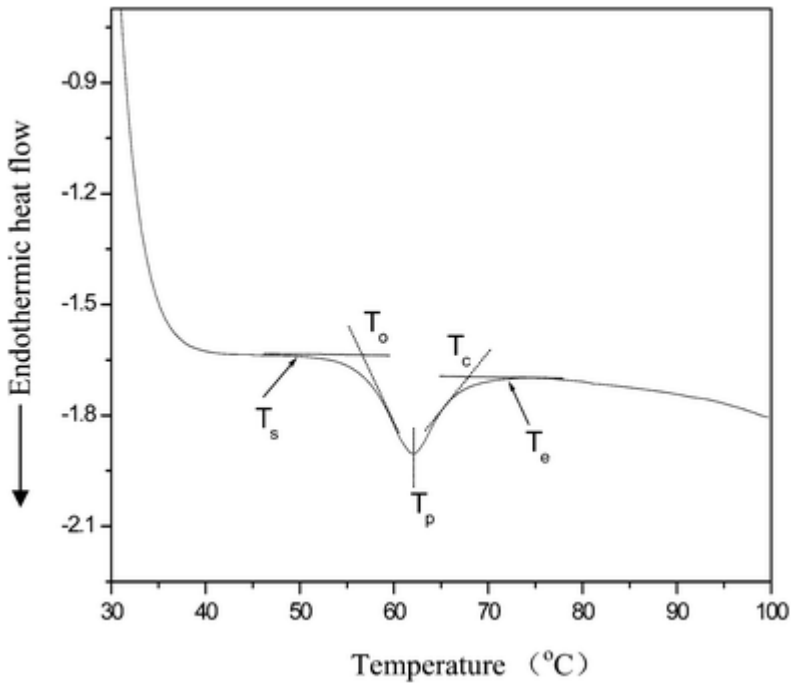

Figure 2-5 Typical DSC thermogram of a starch. Republished with permission of Royal Society of Chemistry, from Wang & Copeland (2013); permission conveyed through Copyright Clearance Centre, Inc.

Table 2-5 Definition of DSC parameters (Wang & Copeland, 2013).

DSC parameters	Definition
Start temperature (T_s)	Inflexion point where endothermic heat flow starts to drift from a flat baseline.
Onset temperature (T_o)	The temperature at which the tangents to the thermogram at T_s and the decreasing slope of the heat flow intersect.
Peak temperature (T_p)	The temperature where maximum heat flow is observed.
Conclusion temperature (T_c)	The temperature at which the tangents to the trace at the ascending slope after T_p and an estimated baseline intersect.
End temperature (T_e)	Inflexion point where the endothermic heat flow stops drifting from a flat baseline.
Gelatinisation enthalpy (ΔH_{gel})	The area under the line drawn from T_s to T_e. The energy needed for gelatinisation to take place.

2.1.3.2. Pasting

Pasting follows after gelatinisation where starch granules swell and leaching of amylose molecules are involved. During pasting—at temperature higher than gelatinisation—a total disruption of starch granules takes place under continuous shear. The pasting profile can also be measured using a Brabender Amylograph or Rapid Visco-Analyser (RVA). A typical pasting profile of starch is presented in Figure 2-6 and its respective parameters are defined in Table 2-6.

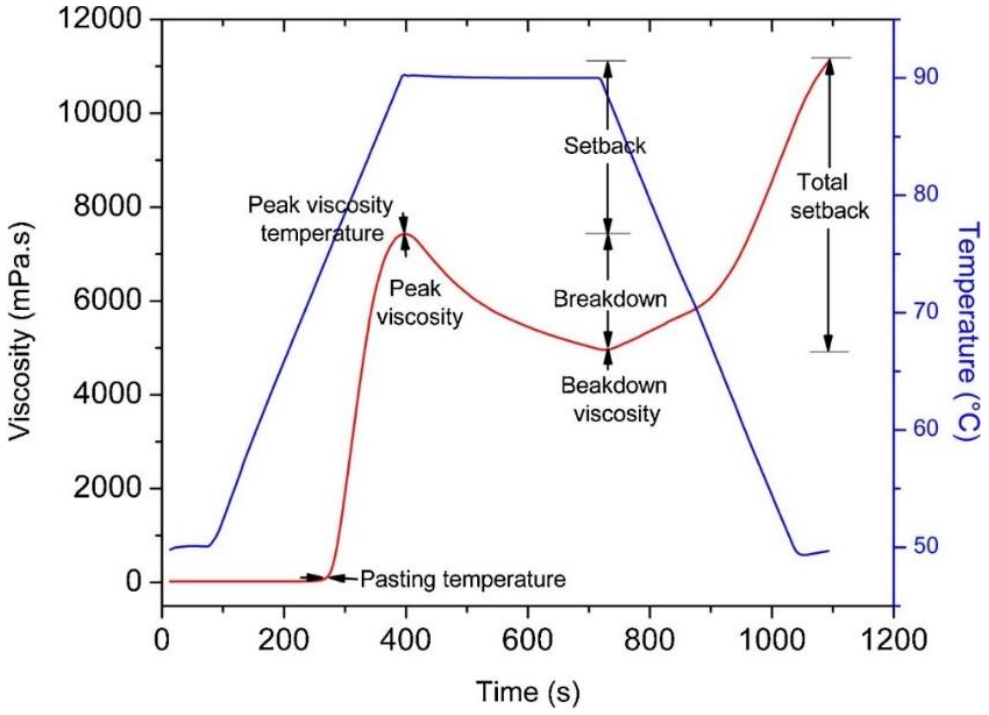

Figure 2-6 Typical pasting curve of a starch. Reprinted from Rincón-Londoño, Vega-Rojas, Contreras-Padilla, Acosta-Osorio, & Rodríguez-García (2016), with permission from Elsevier.

Table 2-6 Definition of pasting curve parameters (Rincón-Londoño *et al.*, 2016).

Pasting parameters	Definition
Pasting temperature	Minimum temperature needed to cook the starch dispersion.
Peak viscosity	Maximum viscosity before the cessation of granular swelling. Reflects on the capacity and ability of water absorption of starch granules.
Breakdown viscosity	Viscosity drop caused by shear. Reflects on the paste stability.
Setback viscosity	The increase in viscosity between peak viscosity and final viscosity of the cooled paste. Reflects on the degree of retrogradation from starch polymers reassociation.

The swelling power and subsequent viscosity development of starch are generally attributed to the amylopectin molecules. This explains why a waxy starch variety often has higher peak viscosity than normal and high-amylose starch varieties. In contrast, amylose molecules—especially in the presence of lipids form amylose-lipid complexes—tend to prevent starch swelling during pasting, due to enhanced interactions between amylose and amylopectin molecules promoted by amylose-lipid complexation. The setback viscosity is also highly influenced by amylose content, where amylose reassociates better than amylopectin causing a higher setback viscosity for starch with higher amylose content (Ai & Jane, 2018b).

2.1.3.3. Retrogradation

Retrogradation occurs when a gelatinised starch paste is cooled down, where amorphous amylopectin and amylose molecules recrystallise to form double-helical orientation which results in syneresis. The retrogradation process can be enhanced by: (i) increasing the concentration of starch or amylose, (ii) increasing the branch chain length of amylopectin, and (iii) refrigerating the starch paste at 0–5 °C (Ai & Jane, 2018b).

Retrograded amylose and amylopectin exhibit different rheological properties. Waxy starches (containing a minimal amount of amylose) tend to form a soft paste, whereas normal starches (containing amylose) tend to form rigid gels when cooled (Tiefenbacher, 2019). The behaviour of retrograded waxy starches can be attributed to the steric hindrance caused by the highly branched amylopectin molecules, resulting in lesser intermolecular hydrogen bonding among amylopectin chains (Cornejo-Ramírez *et al.*, 2018). In contrast, gelation or precipitation is observed for a pure amylose solution during retrogradation due to intermolecular hydrogen bonding between the neighbouring amylose chains, as illustrated in Figure 2-7 (Sievert & Wüsch, 1993; Tako, Tamaki, Teruya, & Takeda, 2014). This double-helical association of amylose can only be reversed at high heating

temperature of 170 °C (Kalichevsky & Ring, 1987). Thus, the gel hardness is generally associated with the amylose content, whereas the viscosity of the starch paste is determined by the amylopectin content, including the presence of ghost structure (Li & Wei, 2020). It has also been reported that the swollen starch granules reinforce the network of a starch gel, where the amylose interacts with amylopectin to form a 3-D gel network to trap the swollen starch granules in the matrix (Ai & Jane, 2018b).

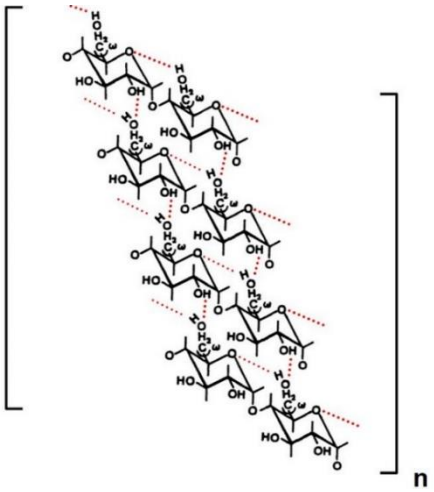

Figure 2-7 Schematic representation of amylose retrogradation with the formation of intra- and intermolecular hydrogen bonds within and between amylose chains. Reprinted from Tako et al. (2014).

2.1.3.4. Shear-induced behaviour

Even though gelatinised starch has been commonly reported as a shear-thinning material, shear-thickening behaviour has also been observed by some researchers (Fang *et al.*, 2019). A research group reported that shear-thickening was found only in the waxy variety of starches (maize, rice, barley and potato) at diluted concentrations between 2–8% w/w, and such shear-thickening behaviour was not noted in normal maize starch (27% w/w amylose and 73% w/w amylopectin) at similar starch concentration. Thus, the authors attributed the occurrence of shear-thickening to the amylopectin structure (Dintzis & Bagley, 1995; Dintzis, Bagley, & Felker, 1995; Dintzis, Berhow, Bagley, Wu, & Felker, 1996). However, in a later study by Kim, Willett, Carriere, & Felker (2002), the authors demonstrated that shear-thickening behaviour in normal maize starch (1.5% w/w) can be achieved using a gentle sample preparation method (gently shaken sample vial). Thus, this led the authors to conclude that starch clusters are presented in the gently prepared normal maize starch sample, which are destroyed in the sample preparation method followed by Dintzis *et al.* (1996). The authors also believe that the clusters in waxy starch samples are more stable than those presented in normal starch samples. Kim *et al.* (2002) conclude that shear-thickening behaviour is likely due to a cluster-breaking process caused by the shear in the rotational tests, which leads to an increase in the overall effective starch

concentration. More recently, Fang, Martinez, Campanella, & Hamaker (2020b) also observed a shear-thickening behaviour in waxy potato starch (10% w/w) gelatinised at 95 °C for 15 min. The shear-thickening behaviour is attributed to the intermolecular double-helical aggregation of the waxy potato amylopectin (proven using ^{13}C CP/MAS NMR), instead of a structure-breaking process proposed by Kim *et al.* (2002). Interestingly, when a complete shear cycle (shear-up and shear-down) was applied, anti-thixotropy behaviours were also noted in these starch samples, indicating a formation of a network due to shear (Dintzis *et al.*, 1996; Fang *et al.*, 2019; Kim *et al.*, 2002).

Other plausible mechanisms for shear-thickening behaviour in gelatinised starch dispersion may include polymer association and jamming of starch polymers when the material is subjected to shear above a certain critical shear rate.

2.1.3.4.1. Association of polymers

The association of polymers leading to shear-thickening behaviour can be attributed to regions on the polymer that result in an overall net attractive force for associations to take place. Such regions can exist in polymer chains as one associative block, two associative ends or many associative groups, as presented in Figure 2-8A, B and C, respectively. In addition, jamming or cross-linking of associated particles could eventually form a soft solid (Chassenieux, Nicolai, & Benyahia, 2011).

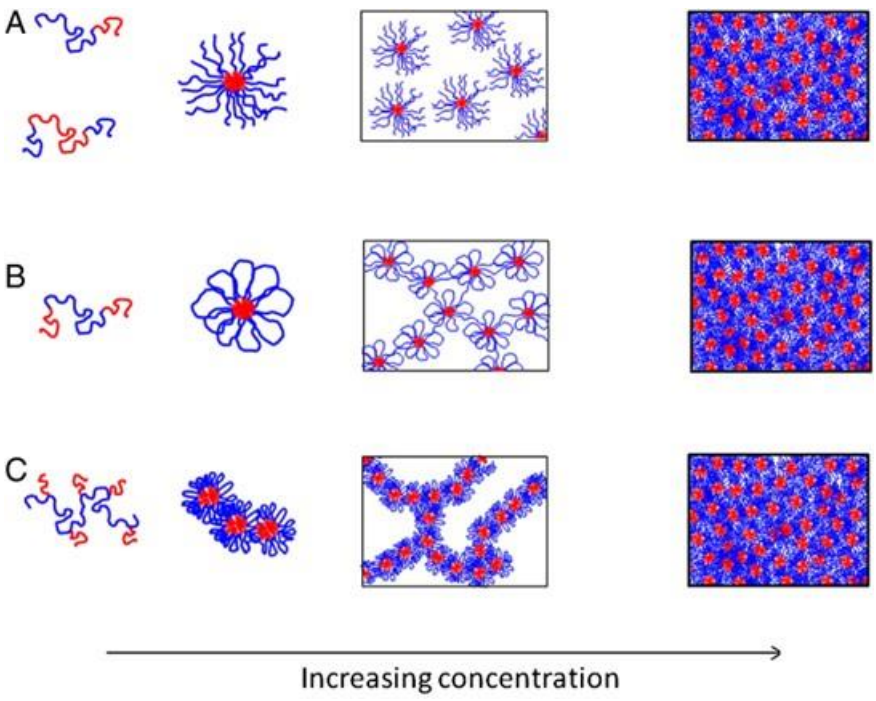

Figure 2-8 Schematic illustration of polymer association for polymers with (A) single associative block, (B) two associative ends and (C) many associative groups at increasing polymer concentration. Associative and solvophilic blocks are represented in red and blue, respectively. Reprinted from Chassenieux *et al.* (2011), with permission from Elsevier.

Polymers with a single associative block are usually associated with particles that have star-like conformation (Figure 2-8A). The interactions between individual particles in such an association are usually repulsive. Thus, at high concentrations, jamming occurs due to increased viscosity of solution, which may stop the flow of the sample. For polymers with more than one associative end, the blocks can associate into the same or different cores by forming loops or bridges between the particles respectively (Figure 2-8B). Such interactions are usually noted in spherical colloids with short-range attraction forces and a soft excluded volume. Finally, for polymers with several associative groups, the polymers associate through intra- and intermolecular interactions, where one polymer can bridge with several particles simultaneously (Figure 2-8C) (Chassenieux *et al.*, 2011). It is also important to note that for shear-thickening to happen, the associations among polymers should occur during shear. If the association occurred prior to shear, no shear-thickening will be observed during the rheological measurement. Interactions leading to the associations among polymers could be due to hydrogen bonding, hydrophobic interactions, and/or electrostatic attraction.

2.1.3.4.2. Hydrogen bonding

A hydrogen bond is a result of dipole-dipole interaction between an electronegative donor atom (–$X^{-}\cdots H^{+}$–) and a positively polarised (electron-depleted) hydrogen atom acceptor. The strength of hydrogen bonding weakens with increasing temperature (Sun, Shi, Zhang, Zhao, & Liu, 2011). This can be illustrated by the study done by Fang (2017), where the thermo-reversibility of a shear-induced waxy potato starch gel is noted at 65 °C, where the shear-induced structure is stabilised by hydrogen bonding. A similar observation is also noted in retrograded amylopectin starch where a DSC melting endotherm peak is observed between 45 and 60 °C by Huang & Perdon (2020). Other than the use of temperature, chaotropic agents such as urea and guanidium hydrochloride can be also used to probe hydrogen bonding interaction in polymers (Sun *et al.*, 2011). Jaishankar, Wee, Matia-Merino, Goh, & McKinley (2015) observed a reduction in the extent of shear-thickening behaviour in Mamaku gum (isolated from the fronds of the black tree fern found in New Zealand) at increasing concentrations of urea (Figure 2-9). The authors attributed the reduced shear-thickening behaviour to the competition from urea for hydrogen bonding sites, thus, lowering the formation of intermolecular hydrogen bonding with neighbouring Mamaku polymer chains.

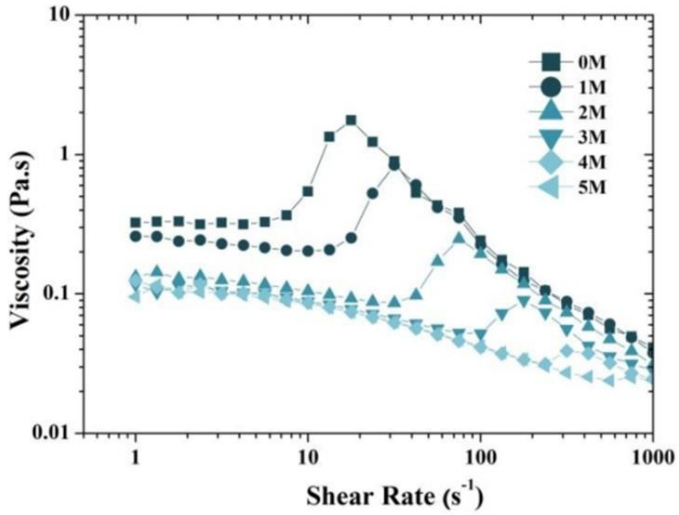

Figure 2-9 Effect of concentration of urea on shear-thickening behaviour of 5% w/w Mamaku gum. Reprinted from Jaishankar *et al.* (2015), with permission from Elsevier.

2.1.3.4.3. Hydrophobic interactions

Hydrophobic interaction is the strong attraction force between two hydrophobic entities to minimise the Gibbs energy of the system caused by the unfavourable interaction of hydrophobic entities with water molecules. Hydrophobic interactions can be enhanced with increased temperature (Sun *et al.*, 2011). Hydrophobic interactions are not commonly observed in a naturally-occurring polysaccharide, but gelation of high-methoxyl (HM) pectin is one such example. The gel network of HM pectin is stabilised by the combination of hydrophobic interactions (between the non-polar methoxyl groups) and hydrogen bonding (between functional oxygen atoms) between pectin molecules (Freitas, Coimbra, Souza, & Sousa, 2021; Thakur, Singh, Handa, & Rao, 1997).

2.1.3.4.4. Electrostatic interactions

Electrostatic interaction and/or cross-linking (*e.g.*, calcium bridging) can occur for charged polysaccharides. Low-methoxyl pectin and alginate are examples of charged anionic polysaccharides that form junction zones by calcium-bridging between two non-esterified galacturonic acid units as shown in Figure 2-10 (Gawkowska, Cybulska, & Zdunek, 2018). Such cross-linking between polysaccharide chains can give rise to shear-thickening behaviour if chain-chain interaction occurs during an applied shear.

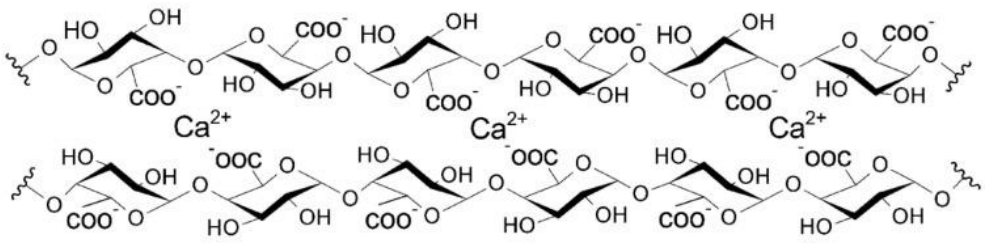

Figure 2-10 Egg-box model showing calcium bridges formed between two non-esterified galacturonic acid units. Reprinted from Gawkowska *et al.* (2018).

2.1.4. Physical modification

In recent years, more attention has been placed on the development of "clean-label" food products. The market for clean-label ingredients is valued at ~US $10.35 billion in 2022 and is forecasted to increase to ~US$ 17.15 billion by 2026 (MarketWatch, 2022). Starch is a common ingredient used in food formulation and is usually chemically-modified to improve its physico-chemical properties (*e.g.*, gelatinisation, swelling, and retrogradation) under certain processing and environmental conditions (*e.g.*, freezing, high temperature, high shear, and low pH) (BeMiller, 2019b). Since chemically-modified starch cannot be considered as clean-label, there is a need for clean-label starch to be developed.

Clean-label modified starch can be achieved through either physical or enzymatic modification. Under physical modification, some commonly studied methods include hydrothermal treatment, high-pressure processing, pulsed-electric field, and ultrasound processing. Among these methods, hydrothermal and high-pressure treatments stand out as the more promising methods for starch modification. In addition, hydrothermal treatments such as heat-moisture treatment, annealing and autoclaving are of more relevance to the starch modification conducted in this thesis. Thus, heat-moisture treatment, annealing and autoclaving will be discussed in the following sections.

2.1.4.1. Heat-moisture treatment

Heat-moisture treatment (HMT) has been widely applied as a physical-based method to alter the physico-chemical properties of starches while preserving their granular structure. Such modification strategy involves: (i) limited moisture content between 10 – 30% w/w, (ii) a treatment temperature above the glass transitional temperature of starch (usually 90 – 120 °C), and (iii) a treatment duration between 15 min and 16 h (Maache-Rezzoug, Zarguili, Loisel, Queveau, & Buléon, 2008). There seems to be a proportional relationship between processing conditions and HMT modification elicited. Various studies have demonstrated that increasing moisture content and treatment temperature can result in the modification of the starch to a larger extent (Brumovsky & Thompson, 2001; Lee, Kim, Choi, & Moon, 2012; Wu *et al.*, 2021). In a study by Vermeylen, Goderis, & Delcour (2006), the authors studied the influence of temperature (90–130 °C) on HMT-modified potato starch at a moisture content of 26% w/w. A similar side-chain distribution was observed in native starch and HMT-treated starches at 90–120 °C exhibited similar side-chain distribution when compared to that of the native starch. However, at 130 °C, an increased proportion of polymer chains with DP 6–12 (short A-chains) was observed. The results indicate that starch is thermally degraded during the HMT at 130 °C. Concurrently, a higher crystallinity of 54% was also noted in 130 °C-treated HMT-starch as compared to that of other samples treated at lower temperatures between 90 and 120 °C (35–42%). Thus, their

results suggest that the thermal degradation of amylopectin during HMT enhances the recrystallisation process.

The combined effects of temperature, moisture, and duration during the HMT process cause significant disruption to the starch crystalline structure and dissociation of double-helical structures in the amorphous region. As a result, there is increased mobility of polymer chains, enabling interaction among polymer chains (Yeh & Lai, 2021). At a macromolecular level, higher degrees of ordered crystalline and amorphous structures are noted due to the reorientation of the disrupted crystals (Sandhu, Siroha, Punia, & Nehra, 2020).

In the crystalline regions, a partial or complete transformation of B- to A-type polymorph is likely to occur due to enhanced stability of the A-type polymorph (Ambigaipalan, Hoover, Donner, & Liu, 2014; Gunaratne & Hoover, 2002; Huang, Zhou, Jin, Xu, & Chen, 2016; Jacobs & Delcour, 1998; Lee *et al.*, 2012; Vermeylen *et al.*, 2006). Due to the transformation from B- to A-type polymorph, it has been commonly reported that the starch type has a strong influence on the extent of HMT modification, with B-type starch being the most susceptible to HMT, followed by C-type and A-type starches (Yeh & Lai, 2021). Such observation is also made by Wu *et al.* (2021) where no or minimal modification is reported in A-type starches (sand-rich starch) with HMT at 110 °C for 8 h over varied moisture contents from 15–30 % w/w. In addition, the growth and perfection of double-helices in the native crystalline region are also noted (Jacobs & Delcour, 1998). Even though there is minimal crystal transformation in A-type starch, an increased content in the V-type polymorph is found in HMT-treated A-type starch, due to the formation of amylose-lipid complexes in the amorphous region (Chen, He, Fu, & Huang, 2015). Other reported molecular changes in the amorphous region of the starch granules include: (i) disruption of helical structure, (ii) formation of a higher-ordered structure due to more interactions from amylose-amylose, amylose-amylopectin, and/or amylopectin-amylopectin chains (Varatharajan *et al.*, 2011). In general, the HMT of starches can lead to various changes in the physico-chemical properties of starches (Table 2-7).

Table 2-7 Altered physico-chemical properties in starches modified by heat-moisture treatment (HMT).

Physico-chemical properties	**Remarks**
Crystallinity	Enhanced crystallinity is commonly observed at low moisture contents (15–25% w/w), due to increased interactions between amylose-amylose, amylose-amylopectin, and amylopectin-amylopectin chains after HMT (Chen *et al.*, 2015; Huang *et al.*, 2016; Varatharajan *et al.*, 2011). However, in the system with a high moisture content of 35% w/w, decreased crystallinity was noted due to enhanced amylopectin double-helices movement and partial gelatinisation of wheat starch (Chen *et al.*, 2015).
Solubility, swelling power and amylose leaching	Reduced solubility, swelling power and amylose leaching due to newly formed amylose-lipid complexes and enhanced interactions between amylose-amylose, amylose-amylopectin, and amylopectin-amylopectin chains after HMT (Gunaratne & Hoover, 2002; Olayinka, Adebowale, & Olu-Owolabi, 2008).
Pasting behaviour	Modifications in pasting behaviour with an increase in pasting temperature and a decrease in peak viscosity, final viscosity, and breakdown were noted. Such altered behaviours are attributed to strengthened intramolecular interaction between amylose and amylopectin chains. Thus, more energy is needed for structural disintegration and paste formation (Jacobs & Delcour, 1998; Maache-Rezzoug *et al.*, 2008; Olayinka *et al.*, 2008).
Thermal property	In general, an increase in T_o, T_p and T_c and lower ΔH_{gel} is noted with increasing HMT (Gunaratne & Hoover, 2002; Huang *et al.*, 2016; Lee *et al.*, 2012; Wu *et al.*, 2021). The increase in T_o, T_p and T_c is attributed to enhanced interactions between amylose-amylose, amylose-amylopectin, and amylopectin-amylopectin chain, whereas the reduction of ΔH_{gel} is likely to be caused by partial gelatinisation of starch during HMT (Sharma, Yadav, Singh, & Tomar, 2015). Furthermore, Hoover & Manuel (1996) observed that amylose content in starches did not influence the ΔH_{gel} of HMT starches, with similar ΔH_{gel} values noted among the different types of HMT-maize starch samples (normal maize, waxy maize, dull waxy maize and amylomaize V).

Granule morphology	Slight changes in granule surface morphology were observed. Kawabata *et al.* (1994) reported the formation of cracks on the surface of HMT-maize and HMT-potato starches, together with a hole inside the granules. A similar observation was made by Vermeylen *et al.* (2006). Ambigaipalan *et al.* (2014) also observed cracked surfaces with weakened birefringence for HMT-faba bean starch.
Enzyme susceptibility	Conflicting results on the enzymatic susceptibility of HMT starches have been reported. Starch can be classified based on its digestibility, namely rapidly digestible starch (RDS, easiest to digest), slowly digestible starch (SDS), and resistant starch (RS, most difficult to digest) (Englyst, Kingman, & Cummings, 1992). Chung, Liu, & Hoover (2009b) found an increased content of slowly digestible starch (SDS) and resistant starch (RS) in HMT-maize, HMT-pea, and HMT-lentil starches treated at 120° C for 2 h (30% w/w moisture). The SDS and RS increased by 2.5 and 7.7% w/v in HMT-maize, 2.8 and 11.2% w/v in HMT-pea, and 4.7 and 10.4 % w/v in HMT-lentil starches, respectively. The increment in SDS and RS is attributed to the enhanced starch polymer interactions during HMT, which subsequently reduce the accessibility of enzymes to starch chains during digestion. However, the same group of authors reported an increase in RDS and reduced SDS and RS contents in HMT-maize starch treated at the same temperature (120 °C) but for a longer treatment duration of 24 h. The increased digestibility is attributed to exposure of α-1,4 linkages that are hidden in native and shorter duration treated starches (Chung, Hoover, & Liu, 2009a). Such enhanced enzymatic digestibility was also observed by other authors, where the disruption of crystalline structure near the surface of HMT treated starch granule resulted in greater accessibility of α-amylase into the interior part of starch granule (Ambigaipalan *et al.*, 2014; Gunaratne & Hoover, 2002). In addition, BeMiller (2019b) suggests that starch treated in the presence of fatty acids (especially lauric acid) during HMT shows a notable increase in SDS and RS, due to amylose-lipid complex formation, which lowers the digestibility of HMT starch.

HMT-starches are used in a broad range of food products including noodles, dressing, baked goods, and retort products, due to their tolerance to pH, thermal and mechanical shear (Hoover, 2010; Sui & Kong, 2018). HMT-starch is a good candidate to be used in normal and gluten-free noodle

manufacturing as a clean-label ingredient due to its reduced amylose leaching and swelling power. Gluten-free noodles (starch-based) tend to be stickier, which hinder the smooth extrusion of noodles. However, HMT lowers the stickiness of the starch and thus improves the processability. Noodles made with HMT-sago starch (110 °C for 16 h, 25% w/w moisture) showed enhanced firmness and lower stickiness. Improvement in cooking loss and rehydration weight were also observed in noodles made with HMT-sago starch as compared to that of the noodles made with native sago starch (Purwani, Widaningrum, Thahir, & Muslich, 2006). Similar observations in such textural improvement were also noted in noodles made with HMT-amaranth starch (110 °C for 2.5 h, 28% w/w moisture) and HMT-sweet potato starch (110 °C for 3 h, 27-30% w/w moisture) (Chandla, Saxena, & Singh, 2017; Collado, Mabesa, Oates, & Corke, 2001). HMT-potato starch (110 °C for 16 h, 27% w/w moisture) also showed better viscosity retention in retorted tomato sauce application at a use level of 1.5% w/w, where the reduction of viscosity in retorted tomato sauce with HMT-starch and native potato starch was 33% and 61%, respectively. Fathi, Aalami, Kashaninejad, & Sadeghi Mahoonak (2016) found that 75% w/w replacement of proso millet flour with HMT-proso millet flour (100 °C for 3 h, 30% w/w moisture) aided in the improvement of cake volume, colour and texture without compromising on the sensory attributes. In addition, owing to its reduced digestibility (higher level of SDS and RS), HMT-starches are suitable to be used for the development of low GI functional foods targeted at diabetic patients.

2.1.4.2. Annealing

Annealing is another hydrothermal-based modification strategy commonly adopted to modify starch without disrupting its granular integrity (Jacobs & Delcour, 1998; Zavareze & Dias, 2011). Contrary to HMT where high temperature and low moisture content are implemented, annealing involves treating starch granules at a moderate temperature (higher than its glass transitional temperature but lower than gelatinisation temperature, typically < 55 °C), in an excessive amount of moisture (≥ 40 % w/w) for up to 72 h (Chung *et al.*, 2009b; Jacobs & Delcour, 1998).

Detailed analysis shows that the annealed starch crystalline structure is enhanced by an increased interaction between the starch polymer chains. The reorganisation of starch molecules and amylopectin double helices results in a higher-ordered crystalline structure through enhanced amylose-amylose, amylose-amylopectin, and amylopectin-amylopectin interactions (Yeh & Lai, 2021). As opposed to HMT, the use of low temperatures in annealing does not cause hydrolysis of native starch (Rocha, Felizardo, Jane, & Franco, 2012). In addition, the mild conditions applied in annealing meant that transformation of B-type to A-type crystal polymorph is unlikely (Rocha *et al.*, 2012; Vermeylen *et al.*, 2006). Table 2-8 highlights some of the physico-chemical changes that are commonly observed in annealed starches.

Table 2-8 Altered physico-chemical properties in annealed starches.

Physico-chemical properties	**Remarks**
Crystallinity and gel strength	An increase in starch crystallinity and gel strength is typically noted with a reduction in swelling power and starch solubility. These changes are attributed to increased interactions between amylose and amylopectin molecules (Adebowale, Henle, Schwarzenbolz, & Doert, 2009; Dias, da Rosa Zavareze, Spier, de Castro, & Gutkoski, 2010; Lan *et al.*, 2008; Zavareze & Dias, 2011).
Swelling power	
Solubility	
Pasting behaviour	Altered pasting behaviours—an increase in pasting temperature and final viscosity coupled with a reduction in peak viscosity—are observed. These changes are attributed to strengthened intramolecular bonds. Thus, more heat is needed for structural disintegration and paste formation (Lan *et al.*, 2008; Waduge, Hoover, Vasanthan, Gao, & Li, 2006).
Thermal property	Due to the perfection of crystalline areas, an increase in the transition temperatures (T_o, T_p and T_c) is observed in annealed starch. A slight increase in ΔH_{gel} is observed in the annealed starch for the same reason (Lan *et al.*, 2008).
Granule morphology	Typically no change in granule morphology upon annealing of wheat, oat, lentil, potato, finger millet, and yam starches is observed (Zavareze & Dias, 2011). However, some researchers observed otherwise. Adebowale *et al.* (2009) reported indentation and groves formation on the surface and centre of starch granules, respectively. Formation of pores and indentations was also found on the surface of normal and waxy barley starches upon annealing (Lan *et al.*, 2008). Dias *et al.* (2010) observed the presence of pores on annealed high-amylose rice starch granule surface as compared to that of its native rice starch which had a smooth surface.
Enzyme susceptibility	A decrease in enzyme susceptibility was noted in annealed legume starches. The reduced susceptibility is attributed to crystallite perfection and amylose–amylose and/or amylose–amylopectin interactions (Chung *et al.*, 2009a; Hoover & Zhou, 2003). However, an increase in enzymatic activity has also been reported for annealed starches, due to the presence of indentations on the starch surface upon annealing (Dias *et al.*, 2010; Lan *et al.*, 2008).

Annealing can be used as a single or dual modification, before or after HMT to produce clean-label starch (Chung *et al.*, 2009a). The application of annealed starch is less studied as compared to HMT starch. However, owing to its similar reduced swelling power and improved thermal stability, annealed starch is also suitable for noodle application (Wang *et al.*, 2018). Hormdok & Noomhorm (2007) reported that noodles made with annealed rice starch (55 °C for 24 h, 75% w/w moisture) exhibited more similar textural qualities (in terms of hardness, adhesiveness, chewiness, and tensile strength) to commercial noodles, where its properties were more superior than noodles made with conventional aged rice flour (noting that aged rice flour has lower swelling power) (Zhou, Robards, Helliwell, & Blanchard, 2002). With the altered physio-chemical properties of reduced retrogradation and improved thermal stability, annealed starches also show potential in bakery and retorted products. More recently, Werlang *et al.* (2021) reported that annealed oat starch (50 °C for 24 h, 75% w/w moisture) can acts as a fat replacer (up to 75% w/w of oil) in mayonnaise. The annealed oat starch improved the overall product stability and imparted a smooth texture, which is desirable in mayonnaise.

2.1.4.3. Autoclaving

The autoclave has been used to produce resistant starch for a long time, the modification can be elicited by using the autoclave system alone or in tandem with other processing strategies such as HMT, enzymatic debranching and acid hydrolysis (Arp, Correa, & Ferrero, 2020; Rahayu, Praseptiangga, Samanhudi, & Hariyanto, 2020; Zheng *et al.*, 2020). The principle for the formation of resistant starch lies in the retrogradation process, which is heavily dependent on the extent of gelatinisation. Retrograded starch (a type of resistant starch) is produced through the ageing of the gelatinised starch, where the retrograded starch gains a higher-ordered structure, which is more difficult to digest (Escarpa, González, Mañas, García-Diz, & Saura-Calixto, 1996). Some of the modification conditions used by researchers to produce resistant starch are summarised in Table 2-9. While it can be presented as a method to modify starch, autoclaving has not been widely used for such a purpose. Autoclave is used mostly for the production of retrograded starch and solubilisation of starch.

Table 2-9 Modification conditions for resistant starch.

Modification(s)	Starch	Conditions	Reference
Autoclaving	Wheat, pea, potato, normal maize, waxy maize, high amylose maize starches	121, 134, 148 °C for 60 min (67, 78 and 91% moisture). Stored at 4 °C overnight. The heating-cooling cycles were repeated up to 20 times.	Sievert & Pomeranz (1989)
	Potato starch, potato amylose and potato amylopectin	≥ 115 °C for 20 min (95% moisture). Stored at -20 °C for 12 h.	Escarpa *et al.* (1996)
	Rice grain	120 °C for 20, 40, 60, 80 and 100 min with 0, 10, 20, 30, 40,50, 60 and 70% of water added based on total weight of sample). Stored at 4 °C for 3, 6, 12, 24, 36 and 48 h. The heating-cooling cycles were repeated up to 5 times.	Zheng *et al.* (2020)
Autoclaving and acid hydrolysis	High amylose maize starch Hylon VII	140 and 145 °C for 30 min (20% moisture). Stored at 4 °C for 24, 48 and 72 h.	Dundar & Gocmen (2013)
	Breadfruit starch	100 °C, 121 °C, 140 °C for 30 min	Rahayu *et al.* (2020)

		(20% moisture). Stored at 4 °C for 24 and 48 h.	
Autoclaved and debranching	Cassava starch	121 °C for 15 min then treated with isoamylase (89% moisture). Stored at 5–7 °C for 24 and 48 h.	Abioye, Adeyemi, Akinwande, Kulakow, & Maziya-Dixon (2017)
Debranched starch and autoclaving	Wheat starch	Treated with pullulanase and subjected to 121 °C for 30 min (90% moisture). Stored at 0 and 4 °C for 24 h.	Arp *et al.* (2020)

2.2. Whey proteins

Whey, also known as milk serum, is a yellowish-green clear solution obtained from straining of milk curd (coagulated by either rennet or acid). The physico-chemical properties of whey protein depend heavily on the source of whey, *i.e.*, sweet or acid whey. Sweet whey is the by-product of cheese coagulated by rennet, *e.g.*, Cheddar and Mozzarella cheese. In contrast, acid whey comes from a process that involves acidification, *e.g.*, in cottage cheese and Greek yoghurt where the coagulation is induced by lactic acid, or in acidified casein production where a mineral acid is added. Due to the differences in the processing of sweet whey and acid whey, the pH and minerals content of these whey products are different (Table 2-10).

Table 2-10 Composition of sweet and acid whey from cheddar cheese and cottage cheese production respectively (Morr & Ha, 1993).

	Sweet whey from cheddar	**Acid whey from cottage**
pH	6.3	4.6
Ash (% w/w)	0.53	0.69
Lactose (% w/w)	4.77	4.71
Protein (% w/w)	0.82	0.75
Fat (% w/w)	0.07	0.03
Lactic acid (% w/w)	0.15	0.55
Calcium (% w/w)	0.05	0.13
Sodium (% w/w)	0.07	0.06
Potassium (% w/w)	0.13	0.15
Phosphorous (% w/w)	0.06	0.09

Commercially available whey is processed into high-protein products such as whey protein concentrate (WPC) and whey protein isolate (WPI) with a protein content of ≤ 80% w/w and ≥ 90% w/w, respectively (Guo & Wang, 2019b). The processing of WPC and WPI is outlined in Figure 2-11. A neutral WPI (Fonterra SureProtein™ WPI 895, > 90% w/w) is used for this study, as it has a higher protein content than WPC (≤ 80% w/w). The product specification is presented in Table 2-11. Note that the WPI 895 used in Chapters 7 and 8 is likely to be from a sweet whey as it is a neutral product with low mineral content, whereas Fonterra SureProtein™ WPI 8855 (WPI used in Appendix H) is likely to be an acidified WPI, as it is a low pH product (Table 2-11).

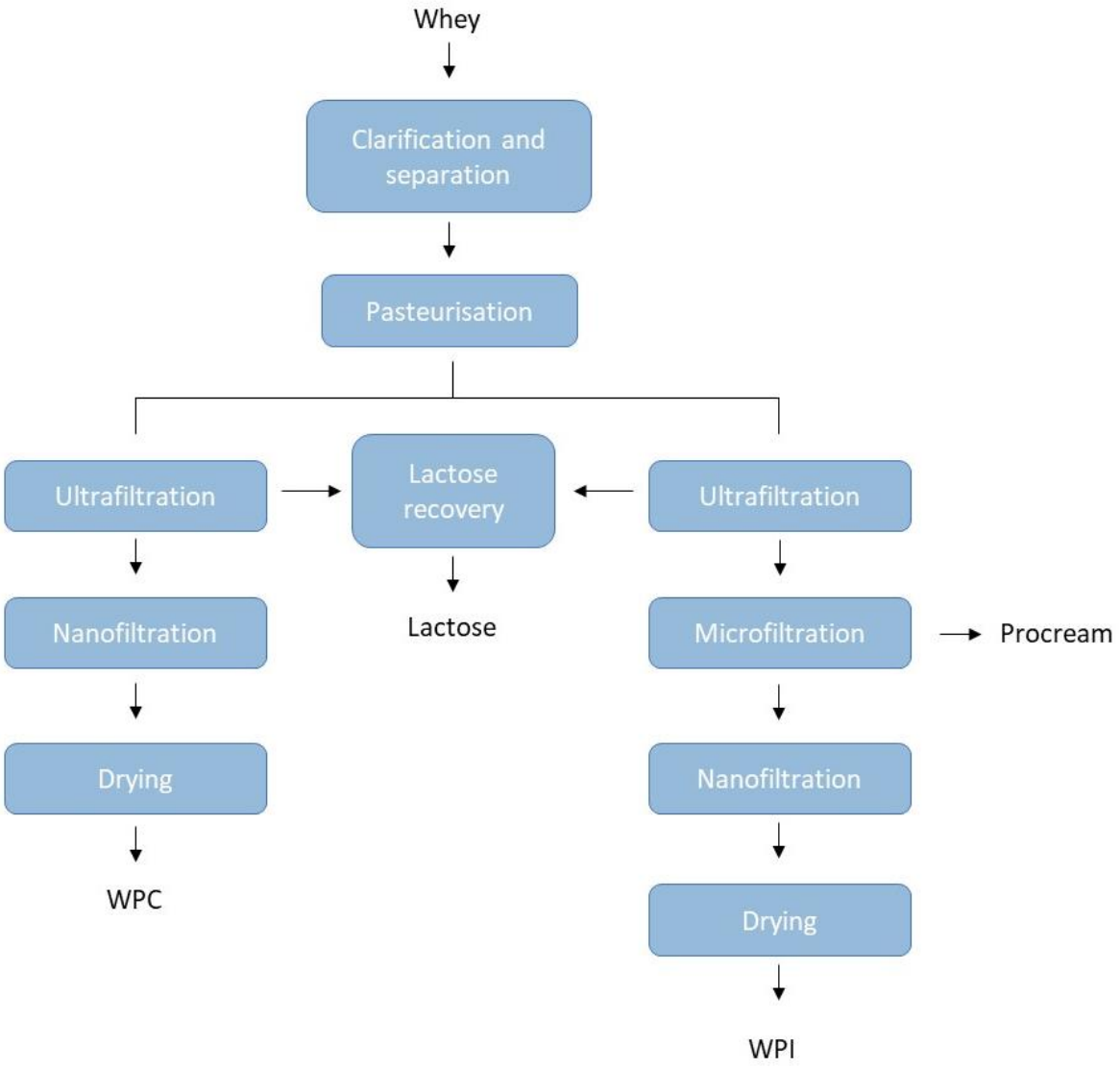

Figure 2-11 Production of WPC and WPI.

Table 2-11 Composition of Fonterra SureProtein™ WPI 895 and WPI 8855.

	WPI 895	**WPI 8855**
Protein (% w/w)	93.9	93.5
Moisture (% w/w)	4.7	4.7
Fat (% w/w)	0.3	0.3
Total carbohydrate (% w/w)	0.4	0.4
Ash (% w/w)	1.5	0.3
pH (5% w/w at 20 °C)	6.8	3.8
Inhibitory substances	< 0.005	Not detected

Whey proteins are made up mainly of β-lactoglobulin (β-LG, 50–55% w/w) and α-lactalbumin (α-LA, 20–25% w/w). The remaining portion is made up of bovine serum albumin (BSA, 5–10% w/w), glycomacropeptide (10–15% w/w, only found in sweet whey), immunoglobulin (10–15% w/w), lactoferrin (1–2% w/w) and other minor proteins (*e.g.*, lactoperoxidase and lysozyme) at < 1% w/w (Wang & Guo, 2019b). Some of the common chemical and physical properties of the major whey proteins (*i.e.*, β-LB and α-LA) are summarised in Table 2-12.

Table 2-12 Chemical and physical properties of β-lactoglobulin and α-lactalbumin (Guo & Wang, 2019a).

Whey components	p*I*	Molecular weight (kDa)	Denaturation temperature (°C)	Number of thiol group/disulphide bond	Number of subunits
β-LG	5.2	18.4	70–73	1/2	2
α-LA	4.5–4.8	14.2	64	0/4	1

2.2.1. β-Lactoglobulin

β-LG is a highly structured globular protein that plays a dominant role in the functionality of whey proteins. At the neutral pH of milk, the protein exists as a dimer. The protein is held together strongly by hydrophobic interactions. β-LG dissociates into monomers when heated > 40 °C or at extreme pH conditions. Each native β-LG contains five cysteine residuals on site of 66, 106, 119, 121 and 160, which are located at the interior of the folded molecules (Figure 2-12). Four of the cysteine residuals make up two disulphide bonds (S-S), *i.e.*, Cys66–Cys160 and Cys106–Cys119, which stabilise the β-LG structure. When heated > 60 °C, the protein unfolds and the free thiol group (-SH, *i.e.*, Cys121) will be exposed. Note that between 65 and 70 °C, denaturation of β-LG is a first-order process, and the conformational change is reversible. However, irreversible polymerisation of β-LG occurs at ≥ 70 °C due to a series of -SH/S-S interchange reactions or -SH/-SH oxidation reactions (Guo & Wang, 2019a; Wang & Guo, 2019a).

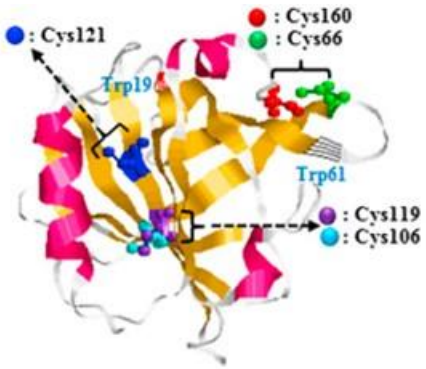

Figure 2-12 Schematic illustration of the molecular structure of β-LG showing five of its cysteine residuals. Reprinted from Wijayanti, Brodkorb, Hogan, & Murphy (2019), with permission from Elsevier.

2.2.2. α-Lactalbumin

α-LA is a calcium metalloprotein, which is a small globular protein, where calcium is crucial for the proper folding and S-S bond formation of a native α-lactalbumin molecule. Among the whey proteins, α-LA has the highest resistance to heat. During indirect UHT heating, only 50–80% of α-LA is denatured as compared to < 90% denaturation for β-LG. The heat-stability of α-LA is attributed to the presence of S-S bonds, the absence of -SH group and its strong binding with a calcium ion (Deeth & Bansal, 2019).

2.2.3. Heat-induced denaturation and gelation of whey protein

Whey proteins are a mixture of globular whey proteins with β-LG predominating the thermal denaturation process. Due to the structural differences of whey proteins, the molecular properties and denaturation kinetics of an individual protein are altered in the presence of other proteins. For example, when β-LG was mixed with α-LA at a 1:1 ratio, the denaturation temperature of β-LG decreased from 71.9 to 69.1 °C, which indicates lower thermal stability of β-LG when heated in the presence of α-LA. The authors attribute this lower thermal stability to the cross-linking interactions between unfolded α-LA and β-LG, which are believed to be initiated by the unfolding of α-LA (Boye & Alli, 2000). In addition, the size of β-LG aggregates increased when heated together with α-LA. When α-LA was heated alone, no aggregation of α-LA can occur due to the lack of active -SH group. When heated together, β-LG was able to deprive α-LA of one -SH group, which allowed α-LA to form a S-S bond. Thus, the authors conclude that such interactions lead to a resultant solution containing a mixture of β-LG aggregates, α-LA aggregates, and β-LG/α-LA aggregates (Wang & Guo, 2019a). Schokker, Singh, & Creamer (2000) suggest that the aggregation of the protein mixture is similar to that of β-LG, which indicates that the aggregation mechanism of β-LG and α-LA is influenced solely by β-LG.

Gelation of whey proteins occurs in a two-step process: (i) denaturation and (ii) polymerisation. Both the -SH group and S-S bonds play a vital role in the whey protein gel network, especially for the S-S bond where strong intermolecular interactions are needed for the polymerisation of whey protein. A high concentration of β-LG of ≥ 4% w/w (heated at 80 °C for 30 min in 0.1 M potassium phosphate buffer at pH 6.8) is needed for the formation of a self-supporting gel. The addition of other whey proteins such as α-LA and BSA increases the strength of the resulting gel due to stabilisation of the gel network through -SH/S-S interaction reactions and formation of S-S bonded complexes between β-LG and BSA, respectively (Wang & Guo, 2019a). The gelation process is heavily dependent on the balance of attractive and repulsion forces among protein molecules during aggregation, which is affected by the pH and presence of ionic salt. When the pH of the protein solution is far from its p*I* and contains low salt concentration, a strong intermolecular electrostatic repulsion among proteins is expected. Such conditions result in a fine-stranded polymeric gel that is clear, rubbery, and deformable. In cases where the pH of the protein is close to its p*I* or at high ionic strength, there is a drastic reduction in the intermolecular electrostatic repulsion resulting in the attractive forces being predominant, which causes a random aggregation with a final particulate gel structure. The particulate gel has a turbid appearance, coarser microstructure and is less deformable (Picone, Takeuchi, & Cunha, 2011; Tobitani & Ross-Murphy, 1997). In addition, Wijayanti *et al.* (2019) reported that at neutral pH (~pH 6.9), small aggregates of ~40 nm were formed when heated due to the reactive nature of the available -SH groups. When pH was dropped to 6.4, whey proteins formed secondary aggregates of much larger size (~100 nm) through non-covalent cross-linking (electrostatic and hydrophobic interactions) of the smaller aggregates.

Contrasting to sodium ion—where the sodium ion is believed to shield the electrostatic repulsion on whey proteins which facilitates aggregation—calcium ion is known to cause extensive aggregation through cross-linking of whey proteins where calcium bridges are formed between two β-LG and by reducing intramolecular electrostatic interactions among negatively charged groups (Wijayanti *et al.*, 2019). However, some authors disagree with the above and have reported that the calcium ion enhances the aggregation of β-LG solely by reducing the overall negative charge of the protein, rather than through inter- or intra-molecular interactions (Hongsprabhas, Barbut, & Marangoni, 1999; Xiong, Dawson, & Wan, 1993).

2.3. Interactions between starch and proteins

2.3.1. Types of polymer interactions

When starch is mixed with protein, the resulting mixture dispersion can be thermodynamically compatible or incompatible as presented in Figure 2-13. In the case of thermodynamic compatibility, the mixture can exist as: (i) a single-phase system with a homogeneous concentration of polymers throughout the mixture and (ii) a two-phase system where associative phase separation occurs due to complex coacervation because of electrostatic attraction between two oppositely charged polymers. As for thermodynamic incompatibility, segregative phase separation occurs, which results in a two-phase system where each phase contains one polymer that is separated from the other (Fang, Li, Inoue, Lundin, & Appelqvist, 2006; Wang & Guo, 2019a). Phase separation threshold has been reported to be > 4% w/w and > 12% w/w for globular protein-polysaccharide and globular protein-protein mixtures, respectively. In general, thermodynamic incompatibility is enhanced with the increase in protein denaturation, M_w, ionic salt and temperature. In contrast, the compatibility of the system can be enhanced when one of the polymers is gelled (Tolstoguzov, 2000). The nature of the polymer compatibility between starch and whey protein during heat-induced gelation defines the final characteristics of the composite gel.

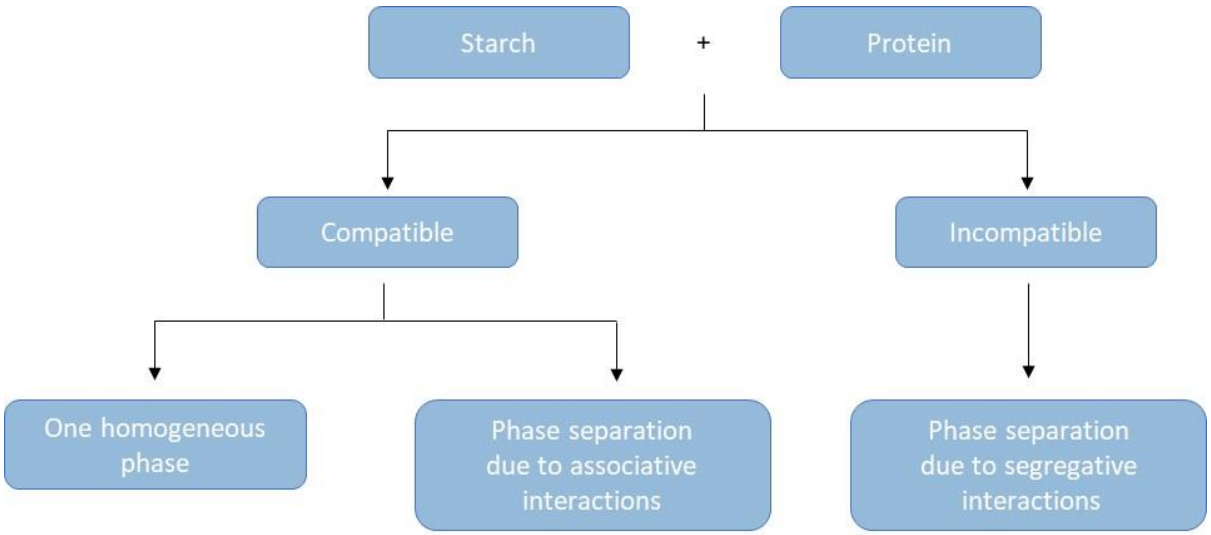

Figure 2-13 Possible thermodynamic interactions between protein and starch.

2.3.2. Whey protein and starch

Quiroga & Bergenståhl (2008) studied the phase stability of waxy maize amylopectin and β-LG mixture at different concentrations. At low polymer concentrations (< 10% w/w), the samples had a clear appearance, which became more turbid and viscous with increasing amylopectin concentrations. No immediate separation was noted in all the samples after mixing (Figure 2-14A). Phase segregation was noted after 24 h of storage and the samples were centrifuged to enhance the phase boundaries of the systems (Figure 2-14B and C). Most of the samples contained two- (Figure 2-14D and E) or three-separated layers (Figure 2-14C). The Fourier transform infrared spectroscopy (FTIR) analysis revealed that the upper, middle and lower layers were β-LG-rich (21% w/w β-LG and 2% w/w amylopectin), a mixture of β-LG and amylopectin (15% and 6% respectively), and amylopectin-rich (26% w/w amylopectin and 3% w/w β-LG), respectively. The authors also concluded that the amylopectin and β-LG mixture solution had a high phase separation threshold of > 20% w/w, where the high threshold was attributed to the native state of the polymers (based on lack of heating, pH and ionic strength adjustments). In another study by the same group of authors, Quiroga & Bergenståhl (2007), the microstructure of phase-segregated amylopectin and β-LG dry mixtures was examined. A continuous phase of β-LG was observed at amylopectin to β-LG ratio < 1:6, when the ratio was adjusted to > 1:3, amylopectin was found to be the continuous phase. Between these ratios, a bi-continuous microstructure was noted.

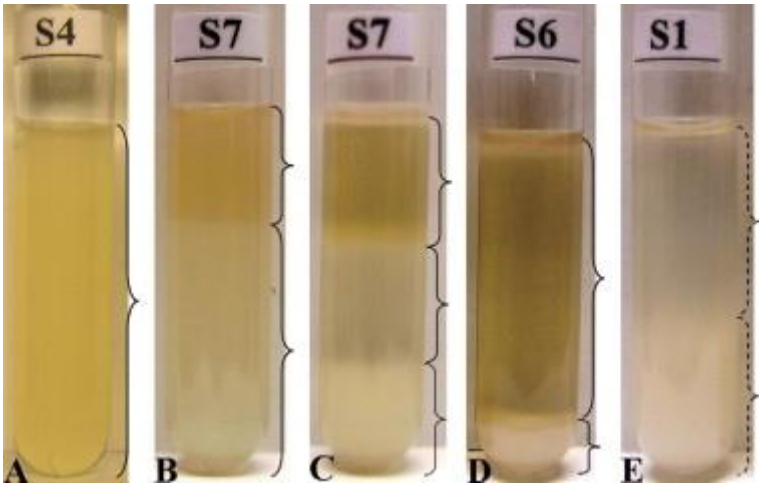

Figure 2-14 Phase behaviours of amylopectin-β-LG mixtures: (a) initial appearance of 5.64% w/w amylopectin and 16.44% w/w β-LG, (b) appearance of 5.90% w/w amylopectin and 17.43% w/w β-LG after 24 h, appearance of mixtures stored for 24 h and centrifuged at 40 000 rpm for 3 h at (c) 5.90% w/w amylopectin and 17.43% w/w β-LG, (d) 2.79% w/w amylopectin and 22.29% w/w β-LG, (e) 10.80% w/w amylopectin and 5.80% w/w β-LG. The layer boundaries are denoted with the bracket "}". Reprinted from Quiroga & Bergenståhl (2008), with permission from Elsevier.

In order to make a heat-induced WPI + starch composite gel, the WPI is hydrated first before mixing with the starch dispersion, the mixture is then incubated at high temperature (*e.g.*, 80–95 °C) to induce gelation. The WPI + starch composite gel network has been reported to have its network contributed primarily by WPI, a secondary gel network may be formed dependent on the gelling capability of participating starch polymers under the same incubation conditions (Yang *et al.*, 2021). Several studies have shown that WPI and starch do not have any associative interactions, by which the gelatinised starch generally acts as an inactive filler in the continuous protein network (Fitzsimons, Mulvihill, & Morris, 2008a; Yang, Luan, Ashton, Gorczyca, & Kasapis, 2014). Similar observations were made by Lavoisier & Aguilera (2019) at low potato starch concentrations (> 5% w/v), where the swollen granules weakened the gel network. However, at a high starch concentration of 9% w/v, an interpenetrating network was formed between WPI and starch, which resulted in the strengthening of the binary network.

The type of starch is found to affect the microstructural and textural properties of composite gels. Ren & Wang (2019) studied the effect of modified tapioca starches (*i.e.*, cross-linked, acetylated and hydroxypropylated) on composite gels containing 10% w/w WPI and 5% w/w starch. The authors found that heat treatment at 85 °C for 20 min resulted in a continuous protein network with intact swollen cross-linked starch granules, as the granular integrity of cross-linked starch is enhanced through its starch modification. However, different microstructures were reported for composite gels containing acetylated starch or hydroxypropylated starch where these modified starches appeared as swollen starch fragments that were embedded in the WPI networks. In another study by Fu & Nakamura (2017), the authors evaluated the effect of tapioca and potato starches on the textural properties of fine-stranded polymeric (pH 6.8) and coarse-stranded particulate (pH 5.8) WPI + starch composite gels containing 15% w/w WPI and 2.5% w/w starch, where the gels were heat-set at 95 °C for 10 min. The fracture behaviours of these composite gels are presented in Figure 2-15. For composite gel samples containing tapioca starch, fracture occurred in the continuous phase of the polymeric protein network at pH 6.8, whereas for the particulate gel—formed from random aggregation of WPI at pH 5.8—the break occurred within tapioca starch. As for samples containing potato starch, the breakage point was noted on the interface between the continuous protein phase and dispersed potato starch of the polymeric composite gel. In contrast, for particulate gels containing potato starch, the fracture occurred in the continuous phase of the randomly aggregated protein network with deformed potato starch trapped in the gel matrix (Figure 2-15). The results demonstrate that the textural behaviour of composite gels can be manipulated through the type of starch and pH adjustment.

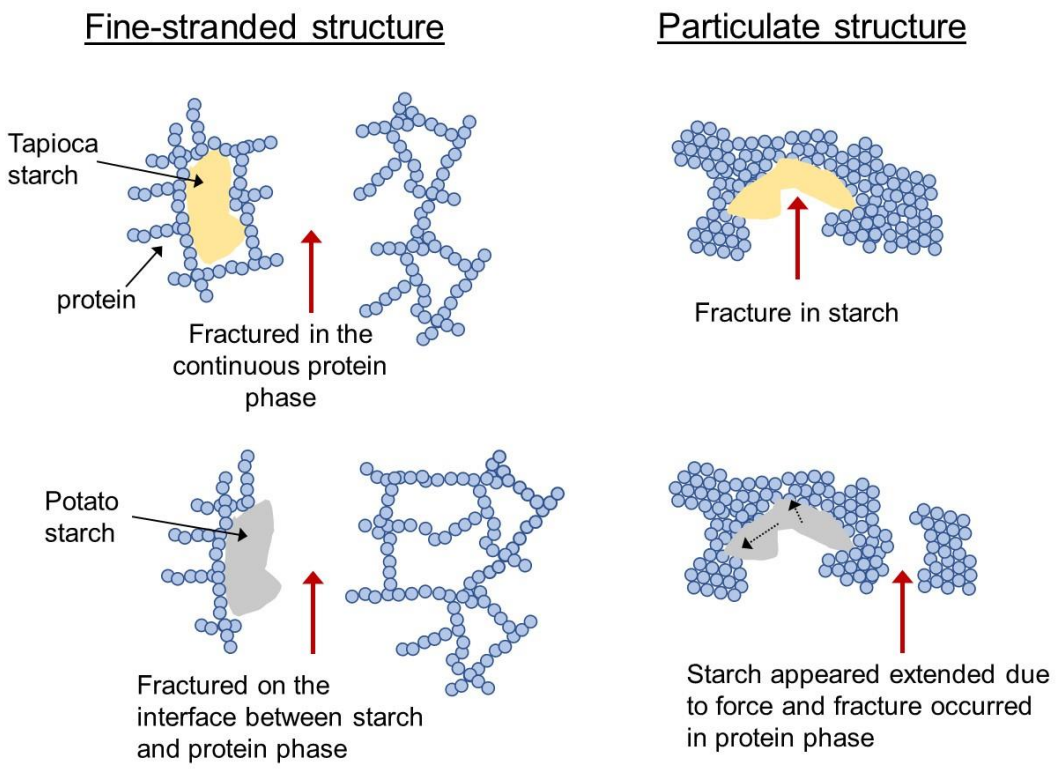

Figure 2-15 Schematic illustration of fracture structure of composite gels made with WPI and tapioca or potato starch in fine-stranded and particulate networks at pH 6.8 and 5.8, respectively (Fu & Nakamura, 2017).

The continuous phase of the composite gel network could be determined by the volume fraction of starch and protein components. Aguilera & Baffico (1997) studied WPI and corn cassava starch gels (pH 5.75) at different total solid contents of 10, 12, 15 and 18% w/w with varied starch volume fractions from 0–0.6%. At low starch fractions of < 0.2, the elastic moduli of the composite gels were higher than pure whey protein gels. When the starch fraction was increased to > 0.3, the protein network was disrupted extensively by the gelatinisation of starch. Furthermore, in a follow-up study by Aguilera (2000), the authors observed a phase inversion of the gel network where the original continuous protein network (filled with gelatinised starch) transitioned to a continuous gelatinised starch network (embedded with aggregated protein) at the higher starch fraction (Figure 2-16). The authors also noticed that a self-supporting gel could not be formed at a starch fraction of > 0.7 due to the weakened gel network caused by phase inversion (Hongsprabhas, 2010).

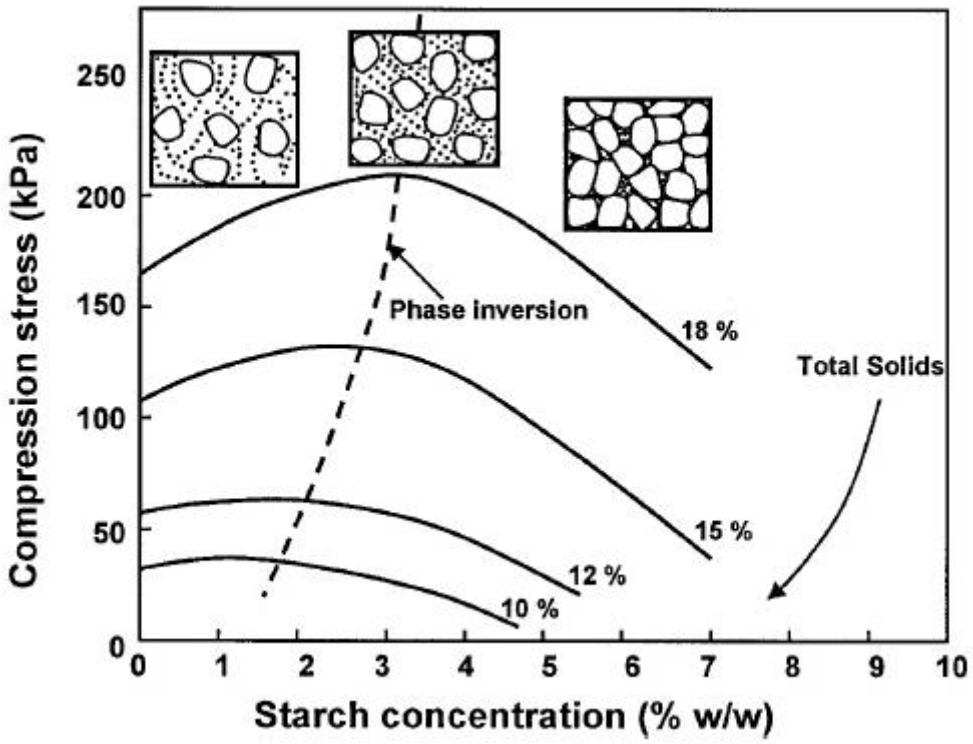

Figure 2-16 Effect of starch concentration on the compressive stress of WPI-cassava starch composite gel at total solids of 10, 12, 15 and 18% w/w. Reprinted from Aguilera (2000), with permission from Food Technology.

Contrasting to starch acting as an inactive starch filler in the WPI network, Yang, Zhong, Goff, & Li (2019a) reported associative interactions between protein and starch polymers *via* hydrogen bonding during the cooling of a heat-induced composite gel containing 10% w/w corn starch and 4.5% w/w WPI. The authors also confirmed through FTIR that no covalent bonding was involved in the interaction of corn starch and WPI in the gel. A similar FTIR result was also reported by Liu *et al.* (2017a), where no new covalent bond was generated in the composite gel made with 10% w/v WPI w/v and 1% w/v lotus root amylopectin. Lotus root amylopectin was found to enhance the gel network of composite gel at increasing amylopectin concentrations from 0 to 1% w/v. The authors attributed the enhanced network to the increased concentration of -SH group, C-N bond and /or N-H bond in the composite gels.

It has been reported that an increase in M_w (from 3.2×10^5 to 2.7×10^7 Da) of potato and barley amylopectin affected the aggregation of 6.0% w/w β-LG at pH 5.4. A higher storage modulus was noted with composite gels containing amylopectin of higher M_w. Such gels had a more porous structure with thicker strands of densely packed β-LG clusters. In addition, the TEM micrograph of composite gels showed that amylopectin with higher M_w was located outside of the protein cluster, whereas amylopectin of lower M_w was embedded inside the protein clusters (Olsson, Frigård, Andersson, & Hermansson, 2003; Olsson, Langton, & Hermansson, 2002). Lopes, Alviano, Torres,

Gonçalves, & Andrade (2006) used light microscopy to confirm phase segregation between WPC (10% w/v) and partially hydrolysed non-gelling waxy corn starch (10 w/v and 15% w/v) at pH 7.5. A denser protein network with starch-enriched regions was noted at increased starch concentrations from 10 to 15% w/v. Furthermore, a more homogeneous microstructure was also observed with the addition of 0.5% w/v urea, which suggests that urea enhances the thermodynamic compatibility between starch and WPC.

2.3.2.1. Effect of sodium ions

Contrasting to its pure systems (*i.e.*, WPI and starch), limited research has been carried out on the effect of salt on WPI + starch composite gel system. Liu *et al.* (2019) evaluated the effect of sodium ions (0 to 200 mM NaCl) on WPI + lotus root amylopectin composite gel. Maximum gel strength, storage modulus and water-holding capacity of composite gels were noted at 50 mM NaCl. These maximum parameters were also found to coincide with the increased in -SH group, C-N bond and /or N-H bond in the composite gels at 50 mM NaCl, which resulted in a more compact microstructure.

2.3.2.2. Effect of calcium ions

Yang *et al.* (2014) studied the effect of $CaCl_2$ (0, 30, 64 and 120 mM) on the gel hardness of heat-induced WPI + wheat starch composite gels (15% w/v WPI with 6 and 12% w/v of starch). The authors showed that there was a drop in the composite gel hardness when $CaCl_2$ concentration was increased from 0 to 30 mM (from ~92 to ~55 N and ~143 to ~73 N for gels containing 6 and 12% w/v of starch, respectively). With a further increase in $CaCl_2$ concentration to 64 mM, no change in hardness was found in composite gels containing 6% w/v starch, whereas the hardness increased (from ~73 to ~85 N) in gels containing 12% w/v starch. A recovery in hardness values—similar to those without $CaCl_2$—was noted when the $CaCl_2$ was further increased to 120 mM. The authors attributed the initial drop in gel hardness in the mixed system to the suppressed starch swelling, which is likely contributed by the interactions between calcium ions and water molecules. At a higher $CaCl_2$ concentration of 120 mM, the interactions between calcium ions and WPI dominated, resulting in the recovery of gel hardness.

2.4. Gaps in the literature

As summarised earlier in Section 2.1.4, the vast majority of the research on physical modification of starches focuses on hydrothermal treatments (heat-moisture treatment and annealing) and high-pressure processing. These techniques modify the physico-chemical properties of starch while preserving its granule integrity. With that, the gaps in the current literature are as follows:

- Limited research has been carried out on modifying starch intentionally to release its macromolecules and use these macromolecules as an ingredient to structure food systems. Thus, there is a need for a systematic study that follows through how starch is being de-structured into its macromolecular form. In addition, this research aimed to study the physico-chemical properties and functionality of de-structured starch so this starch can potentially be used as a functional clean-label food ingredient.
- Since 1995, there are two proposed mechanisms (*i.e.*, increase in effective starch concentration and hydrogen bonding) for shear-thickening behaviour. However, the exact shear-thickening mechanism is still not well-understood. Understanding the underlying mechanism for shear thickening will allow manufacturers to have better consistency in managing the processing conditions and find relevant applications in different food systems.
- In the current literature, numerous studies have been conducted on starch + WPI composite gels, which tend to focus on the starch being the primary structuring dominating ingredient. Hence, there is a need to better understand the WPI-dominating systems to better structure high-protein food products.
- The effects of salts have been widely studied for pure starch and WPI systems, but only a limited amount of research has been done on the mixed system. Thus, further studies on the interaction of de-structured starch in a WPI gel system at varied NaCl and $CaCl_2$ concentrations are needed to better understand the influence of salts on the mixed system.

Chapter 3 Experimental techniques

This chapter justifies the chosen parameters for starch de-structuring process as well as provides the theoretical background on the principles of the main characterisation techniques used in this thesis.

3.1. De-structured starch sample preparation

A combination of physical treatments including thermal, pressure, shear, and duration was used to modify starch physically in this study. It is hypothesised that subjecting the native starch to such treatments would result in the granules undergoing disassembly into their macromolecular chains, forming de-structured starch. These de-structured starch samples could exhibit physico-chemical properties that are different from conventional physical-modified starch. The detailed method of producing the de-structured starch is described in the next paragraph.

Waxy potato starch (Eliane 100, Avebe, Netherlands) dispersion was prepared with Milli-Q water (5% w/w, 400 ml) and transferred to a 600 ml stirred high-pressure reactor (4563, Paar Instrument Company, USA). The reactor was carefully secured before the operation. The suspension was continuously stirred with a turbine impeller. Treatments were carried out at the respective heating temperature, process shear rate and duration summarised in Table 3-1. The samples were then cooled to 90 °C in the reactor and transferred to a 15 °C water bath to be further cooled to room temperature before centrifugation at 28,408 g for 2 h (Rotina 380R, Hettich, Germany). The liquid phase of the centrifuged samples—denoted as de-structured waxy potato starch (DWPS) in the study—was either subjected to rheological or dynamic light scattering analysis. Additional samples were lyophilised using a freeze-dryer (BenchTop Pro with Omnitronics, SP Scientific, England) for storage and further analysis.

Table 3-1 Parameters studied for the starch de-structuring process.

Stirring speed	Heating temperature	Duration
100 and 300 rpm	120, 130, 140, 150, 160 and 170 °C (corresponded to pressure at ~1.2, 1.8, 2.7, 3.7, 5.4 and 6.9 barg respectively)	30 and 120 min

In order to better understand how the process parameters affect the de-structuring of starch, the effects of (i) process stirring speed, (ii) temperature and (iii) heating duration on the de-structuring of 5% w/w waxy potato starch were investigated.

For stirring speed, the samples were treated at 120 °C under continuous shear at either 100 or 300 rpm. Samples treated at 100 rpm resulted in a substantial amount of gel observed at the bottom of the tubes after centrifugation, as illustrated in Figure 3-1. However, no visible gel was observed when the stirring speed was increased to 300 rpm. At 300 rpm, the centrifuged sample consisted of a bulk liquid phase with a small amount of pellet (Figure 3-1). The observation suggests that a low stirring rate at 100 rpm was insufficient to reduce the majority of the gelatinised starch into its disassembled starch polymers. Hence, 300 rpm was selected at this speed, as the shear rate generated was adequate.

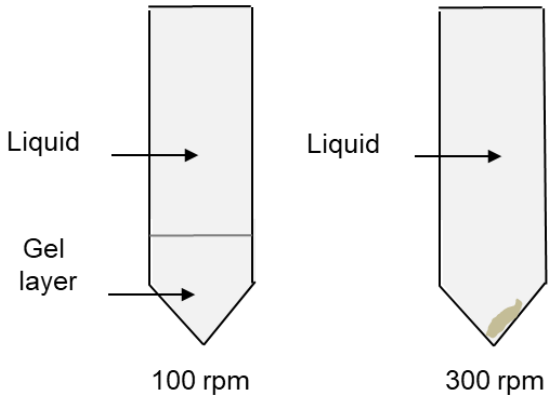

Figure 3-1 Schematic illustration of centrifuged samples of waxy potato starch samples (5% w/w, 24,408 *g* for 2 h) treated at 120 °C for 30 min under continuous stirring of 100 and 300 rpm.

The second studied parameter was the treatment temperature. The effect of temperature was studied from 120 to 170 °C. A gradual darkening of the starch samples was observed with increasing treatment temperature (Figure 3-2). At 170 °C, a dark brown solution was obtained. It has been reported that during high heat treatment, starch undergoes thermal hydrolysis producing oligosaccharides and monosaccharides. Subsequent fragmentation of these materials will lead to the formation of brown furfural-like compounds (Falco, Baccile, & Titirici, 2011). Thus, to avoid the colourisation and extreme hydrolysis of samples, the upper limit of temperature for this study was set to 150 °C.

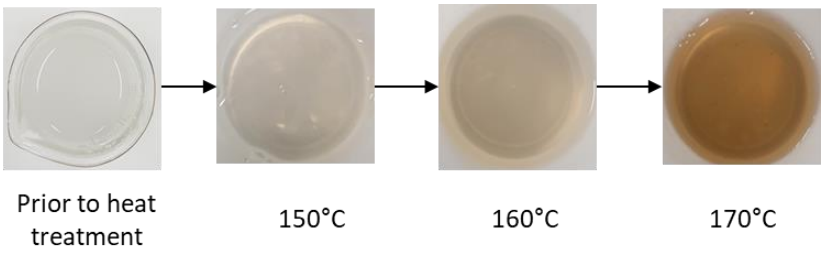

Figure 3-2 Visual appearance of 5% w/w native starch and de-structured starch samples treated at 150, 160 and 170 °C for 30 min under continuous stirring at 300 rpm.

The last studied factor was the heating duration. The hydrodynamic (z-average) diameter of treated starch and viscosity were used as indicators to monitor the starch de-structuring process. The hydrodynamic diameter and viscosity profile of DWPS samples treated from 120 to 150 °C for a heating duration of 30 and 120 min are presented in Figure 3-3 and Figure 3-4, respectively. A similar reducing

trend in the hydrodynamic diameter was observed at both treatment durations, with greater size reduction at 120 min. As for the viscosity profile of DWPS samples, changes in rheological profiles from shear-thickening, shear-thinning to near-Newtonian behaviours were noted at 120–130, 140 and 150 °C for 30 min, respectively (Figure 3-4A). Similar changes in rheological profiles were also noted in samples treated at 120 min, at a lower temperature (*i.e.*, near-Newtonian behaviour was noted in DWPS treated at 140 °C for 120 min rather than in DWPS treated at 150 °C for 30 min, in Figure 3-4B and A respectively). To answer the research question on the mechanism of starch de-structuring, DWPS samples with different degrees of disassembly (*i.e.*, different rheological properties and diameters) were needed. Since the treatment at 120–150 °C for 30 min was able to achieve that, the shorter duration of 30 min was selected instead of 120 min.

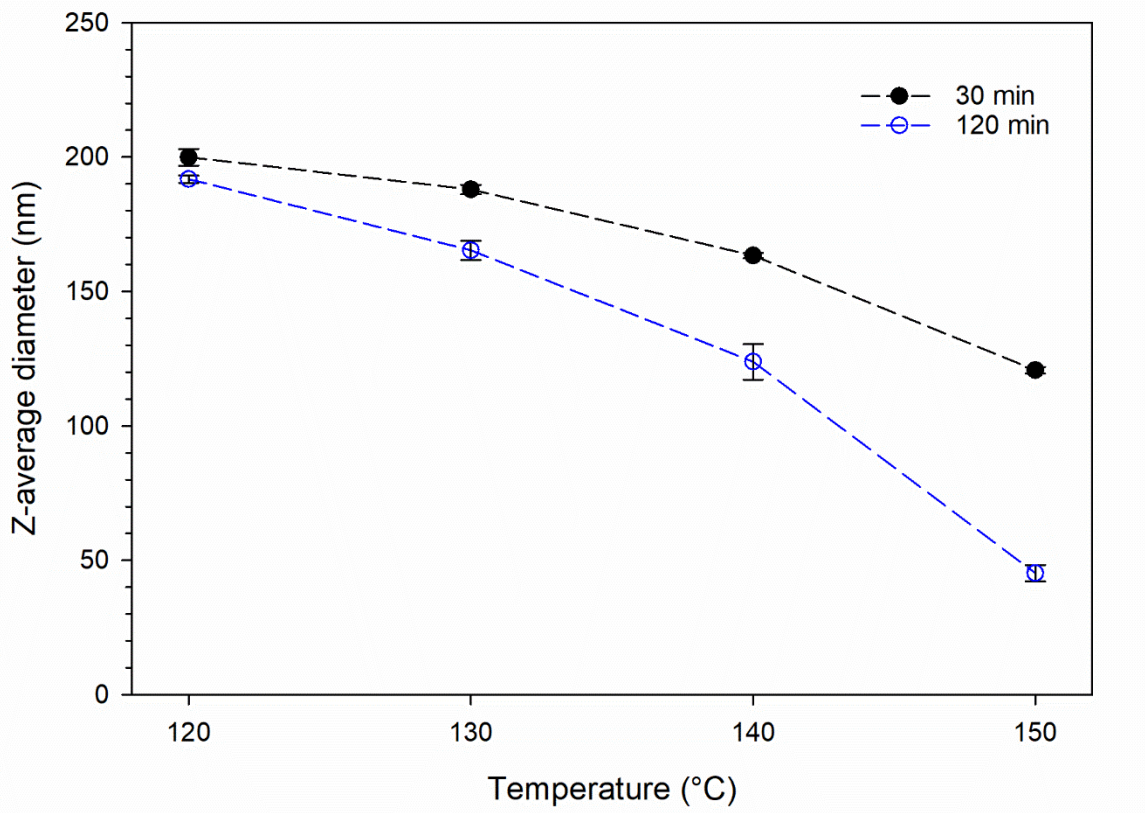

Figure 3-3 Effect of temperature on the z-average hydrodynamic diameter of DWPS samples treated at 120, 130, 140, and 150 °C for 30 and 120 min under continuous stirring at 300 rpm. Values are plotted with mean ± standard error obtained at 20 °C.

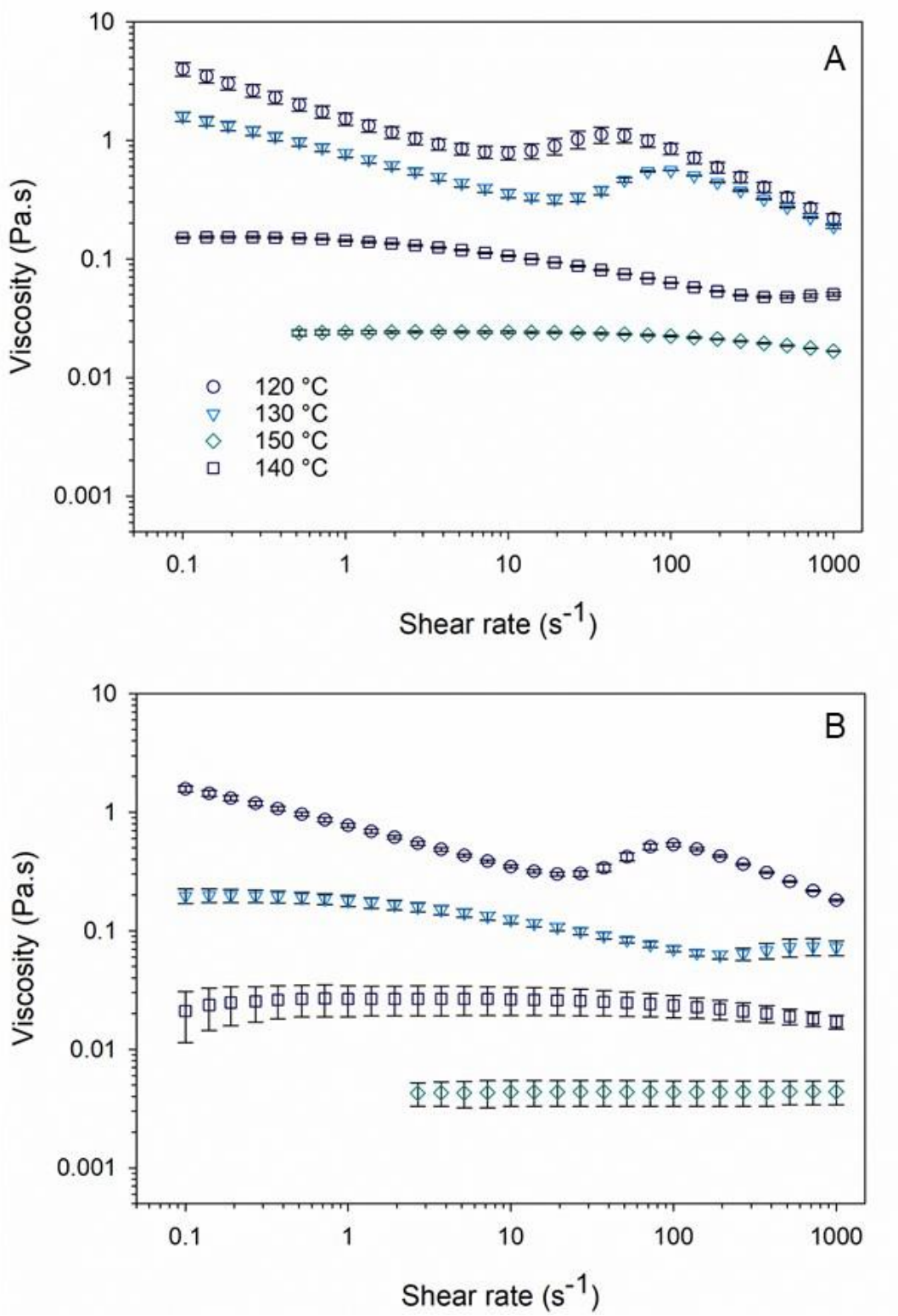

Figure 3-4 Effect of treatment duration on the viscosity of DWPS samples treated at 120, 130, 140, and 150 °C for (A) 30 and (B) 120 min under continuous stirring at 300 rpm. Values are plotted with mean ± standard error obtained at 20 °C.

Thus, the de-structuring process for this study was fixed at 120, 130, 140 and 150 °C for 30 min under continuously stirring at 300 rpm, the overall yields for the freeze-dried DWPS samples were 88.5 ± 3.5, 88.0 ± 5.7, 91.2 ± 2.6, and 91.6 ± 5.2% w/w, respectively.

3.2. Molecular characterisation

Characterisation techniques such as proton nuclear magnetic resonance (^{1}H-NMR), size-exclusion chromatography together with or without multi-angle laser light scattering (SEC or SEC-MALLS), particle sizing and rheology are common characterisation methodologies adopted to study the polymers, as they provide valuable information on their molecular and physico-chemical properties.

3.2.1. Proton nuclear magnetic resonance (^{1}H-NMR)

The waxy potato starch used in this study contains mainly amylopectin, which is a highly branched polymer, and its degree of branching (DB) can be determined *via* ^{1}H-NMR (Hernández *et al.*, 2008; Nilsson, Gorton, Bergquist, & Nilsson, 1996). The principle of NMR is based on the spinning of atomic nuclei when placed in an external magnetic field (B_0) to produce two (low and high energy) spin states (Atta-ur-Rahman, 1986). The common spinning nuclei used in NMR include ^{1}H, ^{13}C, ^{19}F, ^{15}N, ^{29}Si and ^{31}P. In NMR, absorption spectroscopy is generated by the atomic nucleus in an external magnetic field absorbing electromagnetic waves from one spin state to another. The collected data contains information on the individual nucleus and its environment. This information is then expressed as a chemical shift (δ, ppm), which can be used to identify the anomeric signals corresponding to α-1,4 and α-1,6 linkages of a starch molecule to determine its DB (Yao, Wang, Yin, Nie, & Xie, 2021). The DB of native starch and DWPS samples in the experiment (Section 4.2.7) were determined using the method from Tizzotti, Sweedman, Tang, Schaefer, & Gilbert (2011) *via* ^{1}H-NMR, DB is calculated using Equation 3-1:

$$DB(\%) = \frac{I_{\alpha-(1,6)}}{I_{\alpha-(1,6)} + I_{\alpha-(1,4)}} \qquad \text{(Equation 3-1)}$$

where $I_{\alpha-1,4}$ and $I_{\alpha-1,6}$ are the integrals of the anomeric signals corresponding to the α-1,4 and α-1,6 linkages, centred at 5.10 and 4.78 ppm (Figure 3-5).

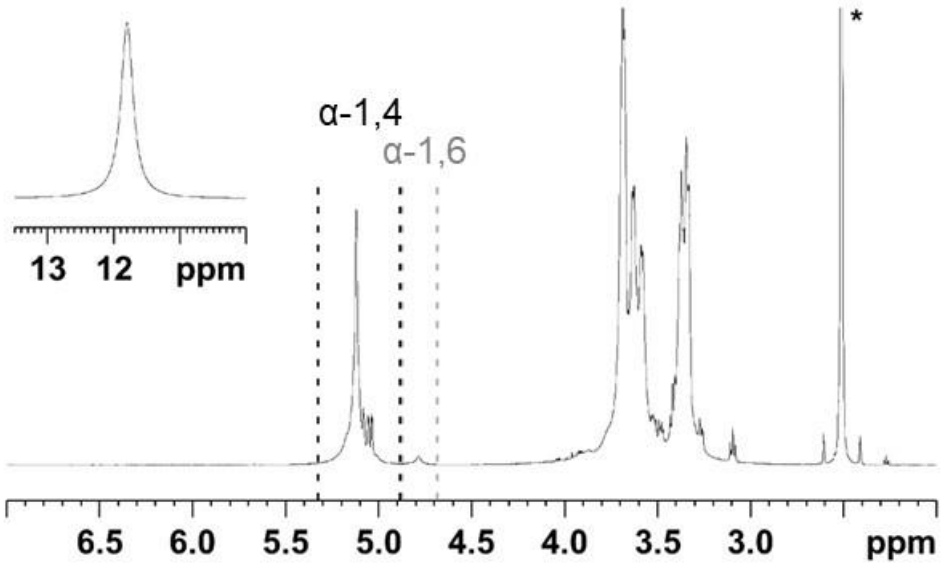

Figure 3-5 A ^{1}H-NMR spectrum of DWPS solubilised in d_6-DMSO. The integration limits of the signals corresponding to α-1,4 and α-1,6 signals are shown by the black and grey dotted lines, respectively. The inset graph shows the exchangeable proton shifted by the addition of d_1-TFA at 11.79 ppm, and * is from the residual signal from the d_6-DMSO.

Full solubilisation of polymer is critical in NMR. Solubilisation of starch can be achieved through a repeated cycle of boiling the starch in D_2O and subsequently freeze-drying (Nilsson *et al.*, 1996). However, this method is slow and tedious. Alternatively, DMSO-d_6 has been used to ensure proper solubilisation of starch. However, due to the hygroscopic nature of DMSO, DMSO-d_6 has a water signal at 3.35 ppm, which may interfere with the peak of interest in the ^{1}H-NMR spectrum (Ross & Lowe, 2000). Deuterated trifluoroacetic acid (d_1-TFA) was added to shift the water signal to high frequency as shown in the inset of Figure 3-5. This shift yielded an area free of other signals for easier identification of peaks corresponding to α-1,4 and α-1,6 linkages. It is also noted that since the quantity of added TFA is small, no significant degradation to starch chains was observed after 24 h (Tizzotti *et al.*, 2011).

3.2.2. High-performance size-exclusion chromatography (HP-SEC)

The starch side-chain distribution of native and de-structured starch samples was determined using HP-SEC. Size-exclusion chromatography (SEC) is a technique that separates molecules by size (hydrodynamic radius) *via* the use of column packed with porous particles. In this study (Section 4.2.6), three aqueous SEC columns (TSK-Gel G5000$_{PWXL}$, G4000$_{PWXL}$, and G3000$_{PWXL}$, 300 × 7.8 mm, Tosoh Corp., Tokyo, Japan) were used. These columns are packed with polymeric methacrylate resin that allow molar mass separation ranging from 4 x 10^3 to 1 x 10^6, 2 x 10^3 to 3 x 10^5 and up to 5 x 10^4, respectively. The separation process is illustrated in Figure 3-6, whereby a sample containing different polymers sizes will be passed through the column, and polymers that are too large to penetrate the column

pores will be eluted first. This is called the void volume or exclusion limit of a column (V_i). The polymers will elute in descending order of their molecular size. This order is attributed to the penetration of polymers into the pores of the column. The smallest polymers will have access to all the pore volume (V_p), they will be eluted last. In contrast, polymers that have sizes in between these two extremes will have partial access to the V_p and be eluted at an elution volume (V_e), which is defined by Equation 3-2:

$$V_e = V_i + K_{SEC}V_p \qquad \text{(Equation 3-2)}$$

Where K_{SEC} is the equilibrium constant of a sample in a column, which ranges from 0 to 1 (Mori & Barth, 1999; Pasch & Trathnigg, 1999).

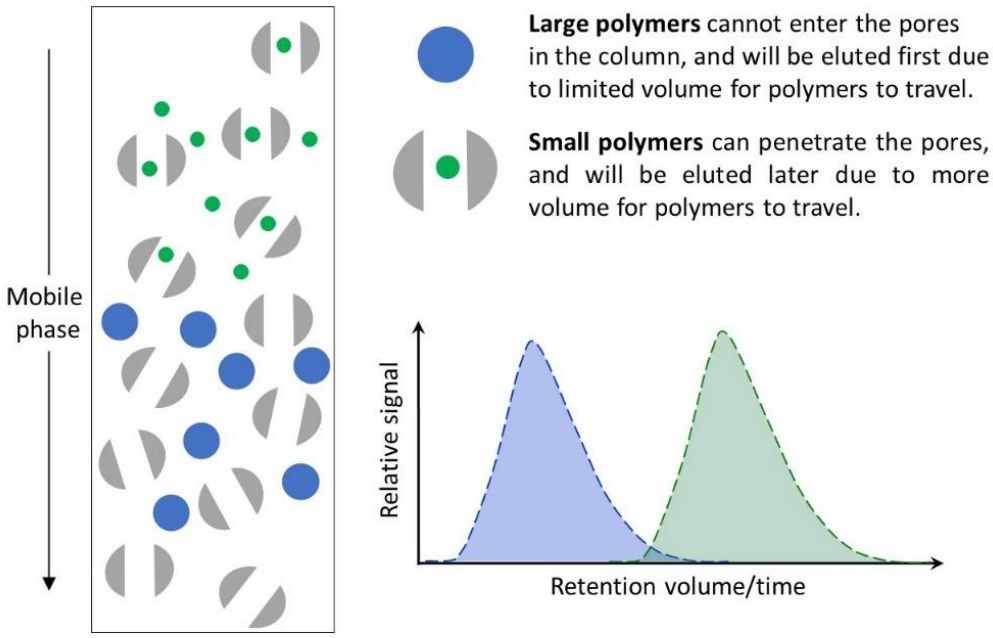

Figure 3-6 Schematic illustration of size-exclusion chromatography of polymers of different molecular sizes.

The molecular weight of molecules is obtained using a calibration curve from polymer standards, where polymers having the same retention volume are regarded as having the same molecular size. However, it is noted that polymers of similar molecular size can also have a different molecular weight if they are not having the same molecular conformation (*i.e.*, highly branched versus random coil conformation). The effect of conformation of molecules on the retention volume is presented in Figure 3-7. This highlights the importance of using appropriate standards of similar conformation to obtain a reliable calibration curve to avoid erroneous results.

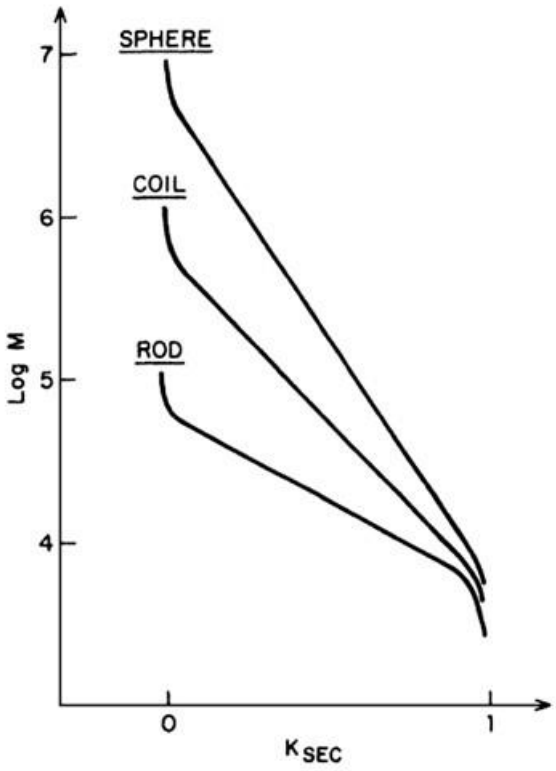

Figure 3-7 Calibration curves of polymers with different shape conformations (spherical, random coil and rod-like). Reprinted with permission from Striegel, Yau, Kirkland, & Bly (2009). Copyright 2009 John Wiley & Sons, Inc.

The acetate buffer and ammonium sulphate (from added isoamylase) used in the preparation of debranched starch chains are known to cause interferences that result in overestimation in molecular species. In order to ensure accurate quantification of different starch chain lengths, these interferences must be removed. A baseline-to-baseline separation between acetate buffer and debranched starch polymers was not found at the usual mobile phase (sodium nitrate) concentration of 0.1 M (Figure 3-8A). This interference can be overcome by using a mobile phase with higher sodium nitrate concentrations of 0.15–0.3 M as presented in Figure 3-8B (Han *et al.*, 2017; Lin, Chang, Chou, & Lu, 2011; Yasui, Ashida, & Sasaki, 2009).

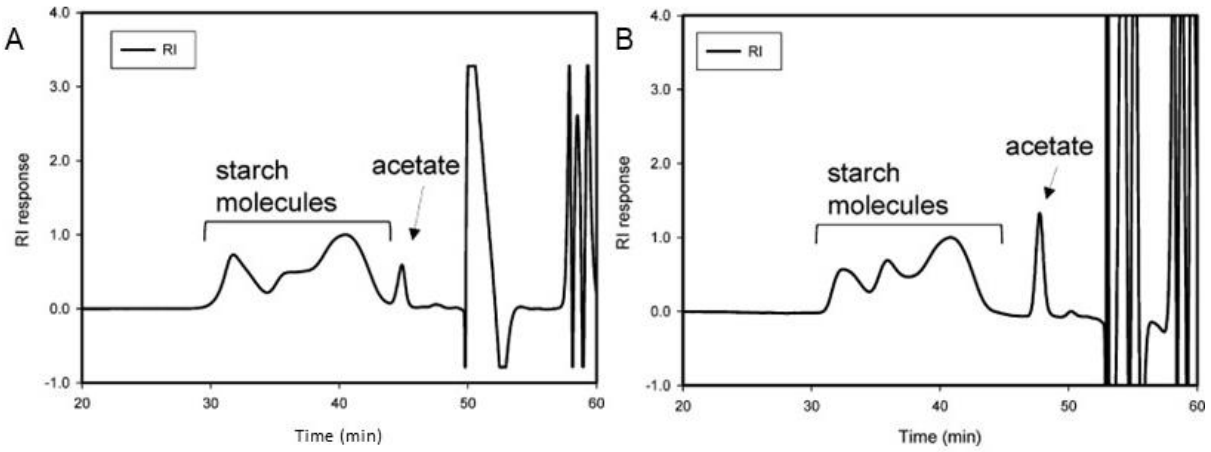

Figure 3-8 Size-exclusion chromatographs of debranched corn starch eluted with mobile phase of (A) 0.1 and (B) 0.3 M sodium nitrate. Reprinted with permission from Lin *et al.* (2011). Copyright 2011 American Chemical Society.

The second interference in the SEC chromatograph was due to the overlapping peak of sulphate ion with the peak of debranched starch polymers (note that the M_w of debranched starch polymers is larger than the molar mass of maltohexaose), as presented in Figure 3-9A. This interference can be resolved by adding barium acetate to precipitate the sulphate ions from samples as barium sulphate, where barium sulphate was subsequently removed through filtration (Figure 3-9B).

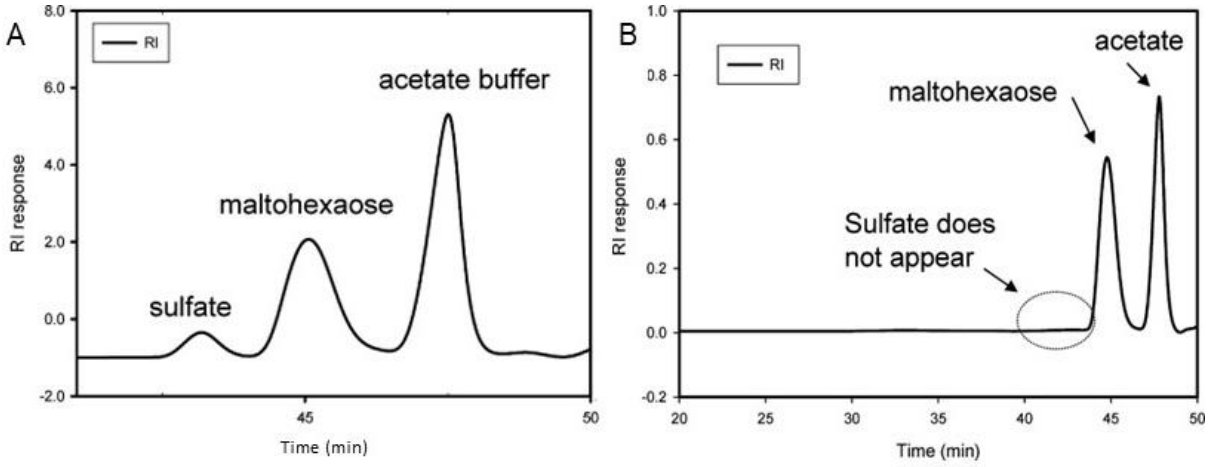

Figure 3-9 Chromatograph of a mixture containing maltohexaose (DP 6), acetate buffer and isoamylase, (A) without and (B) with the addition of barium acetate to remove sulphate ions from the chromatograph. Reprinted with permission from Lin *et al.* (2011). Copyright 2011 American Chemical Society.

3.2.3. Size-exclusion chromatography coupled with multi-angle laser light scattering (SEC-MALLS)

The combination of SEC with multi-angle laser light scattering (MALLS) enables the characterisation of macromolecules in terms of M_w, size and conformation. Unlike the SEC technique mentioned in Section 3.2.2, the M_w is not determined by the retention volume/time (Wyatt Technology, 2021). In

SEC-MALLS, the SEC columns are first used to separate the polymers based on their hydrodynamic volume. The polymers then subsequently enter the MALLS detector where their molar masses are determined through online MALLS and its concentration detector (*i.e.*, refractive index or UV detector). MALLS measures the light scattered by the polymers at different angles and extrapolates back to the y-intercept at zero degree (Nobbmann, 2014). The data allows the calculation of molar mass (M_i) and radius of gyration ($R_i = \langle r_g^2 \rangle_i^{1/2}$), using the Equation 3-3:

$$\left(\frac{Kc}{R_\theta}\right) = \frac{1}{M_i}\left(1 + \frac{16\pi^2}{3\lambda^2}\langle r_g^2\rangle_i \sin^2(\theta/2) - 2A_2 M_i c_i\right) \quad \text{(Equation 3-3)}$$

Where K is the optical constant, R_θ is the excess Rayleigh ratio of the solute or excess intensity of scattered light at angle θ, λ is the wavelength of the incident laser beam (632.8 nm), A_2 is the second viral coefficient (assumes to be 0, usually negligible due to the small concentration in SEC separation), and c_i is the sample concentration (Bello-Pérez, Roger, Baud, & Colonna, 1998).

Various fitting methods (i.*e.*, Zimm, Debye and Berry) have been used to determine M_i and R_i from the intercept and the slope by extrapolating the multi-angle signal to zero degrees. These models are based on the above equation, where $\sin^2(\theta/2)$ is plotted against $\frac{Kc}{R_\theta}$, $\frac{R_\theta}{Kc}$ and $\sqrt{\frac{Kc}{R_\theta}}$ for Zimm, Debye and Berry models, respectively (Yokoyama, Renner-Nantz, & Shoemaker, 1998). A second-order Berry model was selected to determine the M_w and R_z values in this study (Section 0), which is the model commonly used to analyse starch samples (Roger, Bello-Pérez, & Colonna, 1999; Yoo & Jane, 2002). In an earlier paper by Yokoyama *et al.* (1998), the authors compared the calculated values of M_w by Zimm, Berry, and Debye models. The M_w of starch samples determined with Zimm model yielded ~50 % higher M_w than that of those determined using Berry and Debye models. Such trends can be attributed to the Zimm model being highly dependent on detectors and the fit order used in the calculation, which resulted in lower accuracy for determining samples with a molecular size lower than 100 nm. In addition, poor experimental data fit with the Debye model ($R^2 < 0.89$) compared to the Berry model ($R^2 > 0.99$) was noted in this study.

The gross macromolecular conformation of a polymer can be deduced from the M_w dependency of a number of hydrodynamic parameters, where R_g is one of such parameters. The power law relation of M_w and R_g is listed in Equation 3-4:

$$R_g = k_r M_w{}^c \quad \text{(Equation 3-4)}$$

Where k_r and c are the intercept and slope of the double log-plot of R_g and M_w, respectively. The slope values of 0.33, 0.5–0.6, and 1 correspond to macromolecules having sphere, random coil and stiff rod conformations respectively, as illustrated in Figure 3-10 (Morris, Adams, & Harding, 2014).

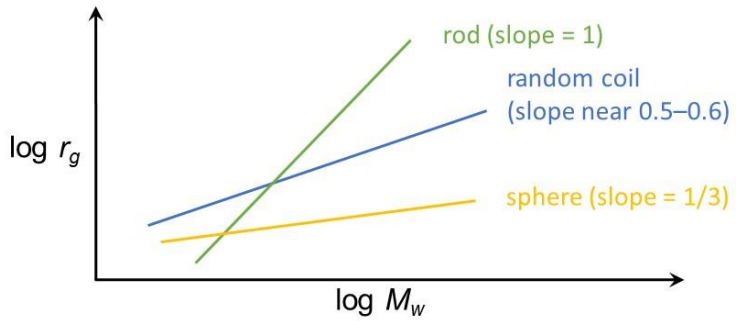

Figure 3-10 Double log plot of radius of gyration against molar mass for polymers of different conformations.

3.3. Particle sizing

Dynamic light scattering (DLS) and laser diffraction (LD) are techniques that are used commonly to characterise the particle size of polymers. The selection of technique mainly relies on the expected size range of the sample, the measurable size ranges for DLS and LD are shown in Figure 3-11. Both DLS and LD were used to measure the particle size of DWPS samples, as the samples contained both nano- and micro-size particles.

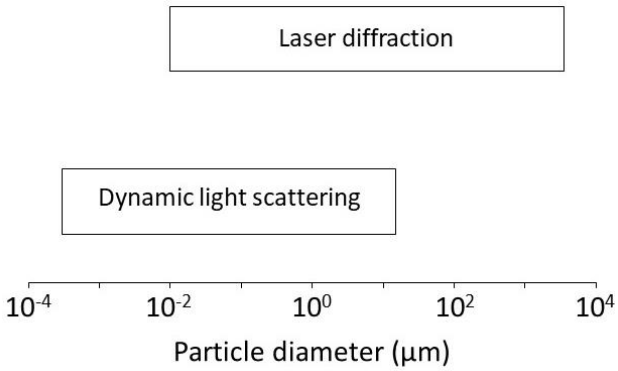

Figure 3-11 Measurable size ranges for dynamic light scattering and laser diffraction.

3.3.1. Dynamic light scattering

In DLS (also known as photon correlation spectroscopy or quasi-elastic light scattering), the sample has to be in the form of a liquid dispersion or solution (liquid/liquid or powder/liquid) (Anton Paar, 2022; Tekade, 2018). The theory of DLS is based on the Brownian motion of particles/molecules, which results in the incident laser light being scattered at different intensities. The fluctuations in the intensity of the dispersed light generate the velocity of Brownian motion which is then used to

determine the particle size (hydrodynamic radius, R_H) *via* the Stokes-Einstein relationship using Equation 3-5:

$$R_H = \frac{k_B \mathrm{T}}{6\pi\eta \mathrm{D_t}} \quad \text{(Equation 3-5)}$$

Where k_B is the Boltzmann constant (1.38064852 × 10^{-23} J/K), T is temperature, η is the absolute temperature and D_t is the translational diffusion coefficient (Bhattacharjee, 2016).

3.3.2. Laser diffraction

In LD, the particle size is determined by the scattering angle of light, based on the Mie theory of light scattering. The equipment (MasterSizer Hydro 2000MU, Malvern Panalytical Ltd., Malvern, UK) consisted of a laser beam light source, a measurement cell connected to a dispersion unit and fixed detectors. The principle of the technique is based on the scattering of light, where particles of smaller sizes scatter light at a lower intensity at wider angles. In contrast, larger particles scatter light more intensely at smaller angles, as shown in Figure 3-12 (Tekade, 2018). The scattered light is then captured by the detector, which is then used to determine the particle size.

Four assumptions are made in Mie theory: (i) particles are spherical, (ii) only one particle is scattering the light, thus a dilute sample is needed, (iii) particles have varying opacity and will scatter light at unequal efficiencies, and (iv) particles are homogeneous. Mie theory considers the differences in refractive indices of particles and their dispersing medium to calculate the intensity of the scattered light. Mie theory also covers how the transmitted light through the particle is either reflected or refracted, this capability is significant for transparent particles and/or particles with a diameter < 50 µm. This capability is contrasting with the simpler Fraunhofer theory (also known as static light scattering), which is the earlier diffraction technique for LD. The Fraunhofer theory assumes that (i) particles are opaque discs, (ii) light is scattered at narrow angles only, (iii) all particles scatter with equal efficiency and (iv) the difference in refractive indices of particle and dispersing medium is infinite. Due to the assumption made in the theories, the Mie theory is recommended for analysis across a wide measurement range of 0.1 to 3000 µm. In contrast, the Franunhefer theory is good for systems with particles of ≥ 50 um and opaque particles (Malvern Panalytical, 2010).

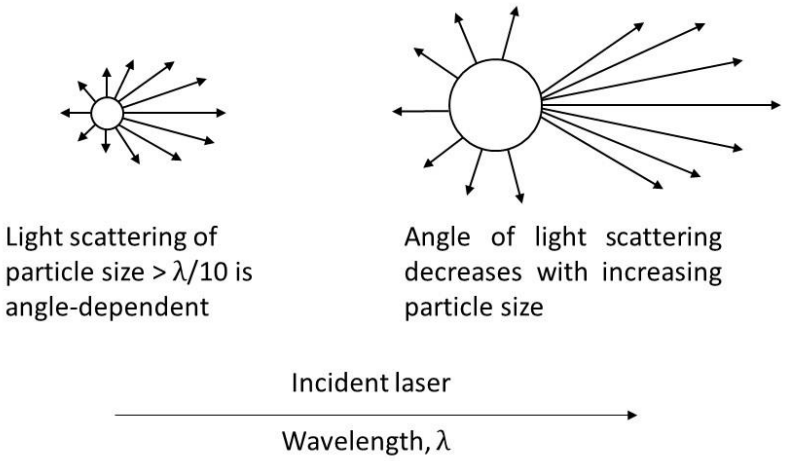

Figure 3-12 Schematic illustration of the influence of particle size on the angle of light scattering.

The size of the measured particles is usually expressed in either volume-weighted-mean-diameter, D(4,3), or surface-weighted-mean-diameter, D(3,2). A D(4,3) is used to evaluate the changes in the distribution of particle size range. In contrast, a D(3,2) computes the surface area of particles in equivalent spheres. The mean diameters are defined by the following equations:

$$D(4,3) = \frac{\sum_i n_i d_i^4}{\sum_i n_i d_i^3} \quad \text{(Equation 3-6)}$$

$$D(3,2) = \frac{\sum_i n_i d_i^3}{\sum_i n_i d_i^2} \quad \text{(Equation 3-7)}$$

Where n_i is the number of particles with diameter d_i (Rawle & Sagar, 2017). It is also worth noting that D(4,3) is also more sensitive to changes in size distribution containing larger particles than that of D(3,2) (Risi, Sante, & Colangelo, 2005).

3.4. Mechanical characterisation

Mechanical characterisation techniques such as rheology and texture profile analysis (TPA) are used widely to characterise polymeric gels. For the study of whey protein + starch composite gels, the oscillatory test was used together with TPA (first compression to determine hardness) and microscopy techniques to obtain data needed for the deduction of possible interaction mechanisms between the polymers of interest.

3.4.1. Rheology

Rheology is the study of the flow and deformation of materials under stress. Rheological properties of a material such as viscosity, viscoelasticity and flow behaviour can be measured using the appropriate tests. These rheological properties are intrinsic characteristics that can reveal molecular information about the tested materials. Materials can be categorised into ideally viscous liquids, ideally elastic-like

solids, or viscoelastic materials, for which viscoelastic materials exhibit both viscous and elastic behaviour. Most polymers have complex flow behaviour, the understanding of their rheology enables us to better utilise the material in food formulation and production.

3.4.1.1. Shear-dependency viscosity

For flowing fluids, the movement between molecules in a system creates an internal frictional force, where the resistance force to the flow of the material is defined as viscosity. Viscosity (η) is also defined as the ratio of shear stress (τ) to its corresponding shear rate ($\dot{\gamma}$) (Equation 3-8):

$$\eta = \frac{\tau}{\dot{\gamma}} \qquad \text{(Equation 3-8)}$$

The two-plates-model can be used to further explain the fundamental rheological parameters (*i.e.*, τ and $\dot{\gamma}$). Shear stress is defined by Equation 3-9:

$$\tau = \frac{F}{A} \qquad \text{(Equation 3-9)}$$

Where F is the shear force that causes the shear area (A) on the top plate to move, while the bottom plate stays stationary (Figure 3-13). This motion produces a velocity (v) over the distance between plates (h), which is defined as shear rate ($\dot{\gamma}$) presented in Equation 3-10 (Mezger, 2011a):

$$\dot{\gamma} = \frac{v}{h} = \frac{dv}{dh} \qquad \text{(Equation 3-10)}$$

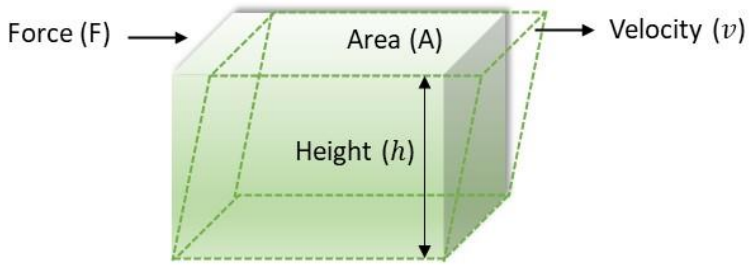

Figure 3-13 Two-plates-model illustrating the generation of the flow velocity of a fluid caused by the applied force.

The viscosity of a Newtonian fluid is unaffected by the shear rate. In contrast, the viscosity of non-Newtonian fluids changes with varying shear rates, *i.e.*, shear-thinning or shear-thickening as shown in Figure 3-14. Most starch dispersions usually exhibit shear-thinning behaviour after gelatinisation. However, shear-thickening behaviour in starches has also been reported in a few reports (Bagley & Dintzis, 1999; Fang *et al.*, 2019; Kim *et al.*, 2002). The flow behaviour of a material is attributed to its molecular structure and the interactions among molecules/particles. For instance, if a system contains particle agglomerates, these agglomerates may break down under shear, causing the viscosity to drop, thus, leading to shear-thinning behaviour. On the other hand, shear-thickening behaviour is usually

associated with structural agglomeration upon shear, *e.g.*, physical entanglements between polymer chains (Mezger, 2011a).

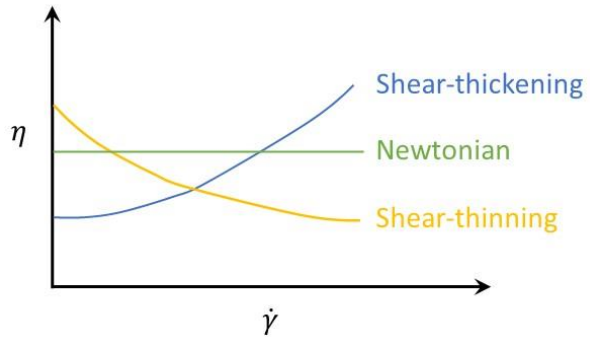

Figure 3-14 Viscosity curves of Newtonian, shear-thinning and shear-thickening fluids.

3.4.1.2. Time-dependency viscosity

The viscosity of a material can also be time-dependent (Figure 3-15). If the material breakdown over time at a fixed shear rate, this will result in a decrease in viscosity, and the material is said to exhibit thixotropic behaviour. In contrast, if the viscosity or structure of a material increases with time at a fixed shear rate, the material is known to be anti-thixotropic (Carreau, De, & Chhabra, 2021).

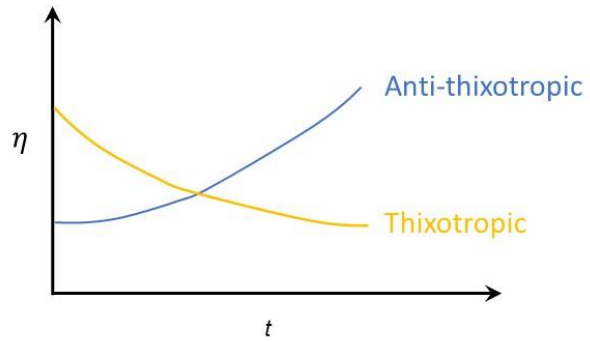

Figure 3-15 Viscosity curves of fluids that exhibit anti-thixotropic and thixotropic behaviour under shear at a fixed shear rate over time.

3.4.1.3. Oscillatory shear rheology

Viscoelastic materials are often characterised using an oscillatory test. The oscillatory test provides useful information on the viscoelasticity of a material. This information can be useful in characterising the gelation process (*e.g.*, determination of gelation temperature and duration) and ageing of gels (retrogradation of starch gels). Different from a rotational test, an oscillatory test is conducted by applying a small sinusoidal small-amplitude deformation to a viscoelastic material to determine its storage (*G'*) and loss (*G"*) moduli. The *G'* represents the elastic portion of a material which reflects the amount of stored energy stored during the deformation. The *G"* represents the viscous portion and

reflects on the energy that is lost. The predominant behaviour of the material will be determined by the higher value moduli, *i.e.*, if *G"* value is higher than *G'*, the material behaves as a viscoelastic liquid. The oscillatory tests conducted in this study were done within the linear viscoelastic region (LVR) to ensure the viscoelastic moduli were measured accurately. Within the LVR, the strain response of a material is proportional to the applied stress, *i.e.*, the viscoelastic moduli are not affected by the magnitude of stress, deforming strain or the rate of strain. The LVR can be determined using a large deformation amplitude sweep—the viscoelastic moduli are measured with increasing amplitude strain (γ_0)—by which LVR is defined as the region where the constant moduli values were observed. Beyond the LVR, the measured viscoelastic moduli are no longer linear, which usually signify a structural or configurational change in the sample (Figure 3-17) (Mezger, 2011a).

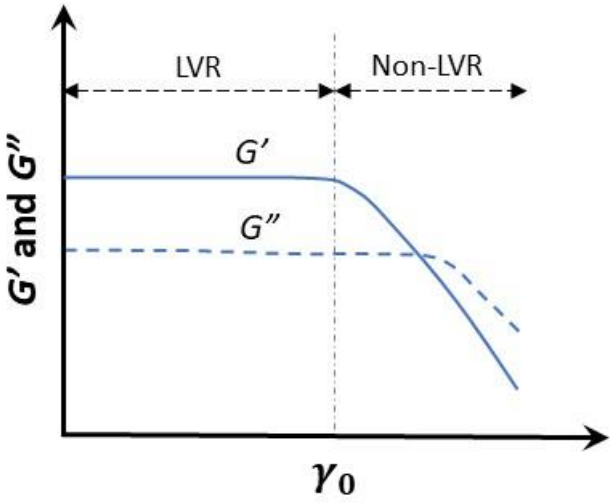

Figure 3-16 Linear and non-linear viscoelastic regions (LVR and non-LVR) with increasing amplitude strain.

The two-plates-model can be used again to explain how an oscillatory test works. Sinusoidal stress will be applied to the top plate at an angular frequency (ω), while the bottom plate remains stationary. This motion creates a sinusoidal strain (γ) that is defined by Equation 3-11:

$$\gamma = \gamma_0 \sin \omega t \qquad \text{(Equation 3-11)}$$

Where γ_0 is the amplitude strain and t is the time. Within the LVR, a corresponding out-of-phase sinusoidal stress response (σ) is created by the applied strain, *i.e.*, defined by Equation 3-12:

$$\sigma = \sigma_0 \sin(\omega t + \delta) \qquad \text{(Equation 3-12)}$$

Where σ_0 is the shear stress amplitude and δ is the shift angle (also known as phase lag). For an ideal elastic solid, the application of sinusoidal stress produces a strain response that is in phase with the strain input, *i.e.*, δ = 0°. In contrast, the strain response of a viscous liquid has a 90° out of phase with

the applied stress. Since viscoelastic material has both elastic and viscous properties, this results in a δ between 0–90° (Figure 3-17). This allows *G′* and *G″* to be expressed as the ratio of stress and strain amplitude in Equation 3-13 and Equation 3-14, respectively (Miri, 2011):

$$G' = \frac{\tau_0}{\gamma_0}\cos\delta \qquad \text{(Equation 3-13)}$$

$$G'' = \frac{\tau_0}{\gamma_0}\sin\delta \qquad \text{(Equation 3-14)}$$

The ratio between these viscoelastic moduli (*G″*/*G′*) is known as loss tangent ($\tan\delta$), which is a useful parameter in determining the nature of the materials, *i.e.*, predominately elastic or viscous. The $\tan\delta$ is also used to identify the gelation point of a material, as $\tan\delta$ = 1 when a crossover of *G′* and *G″* occurs (Miri, 2011).

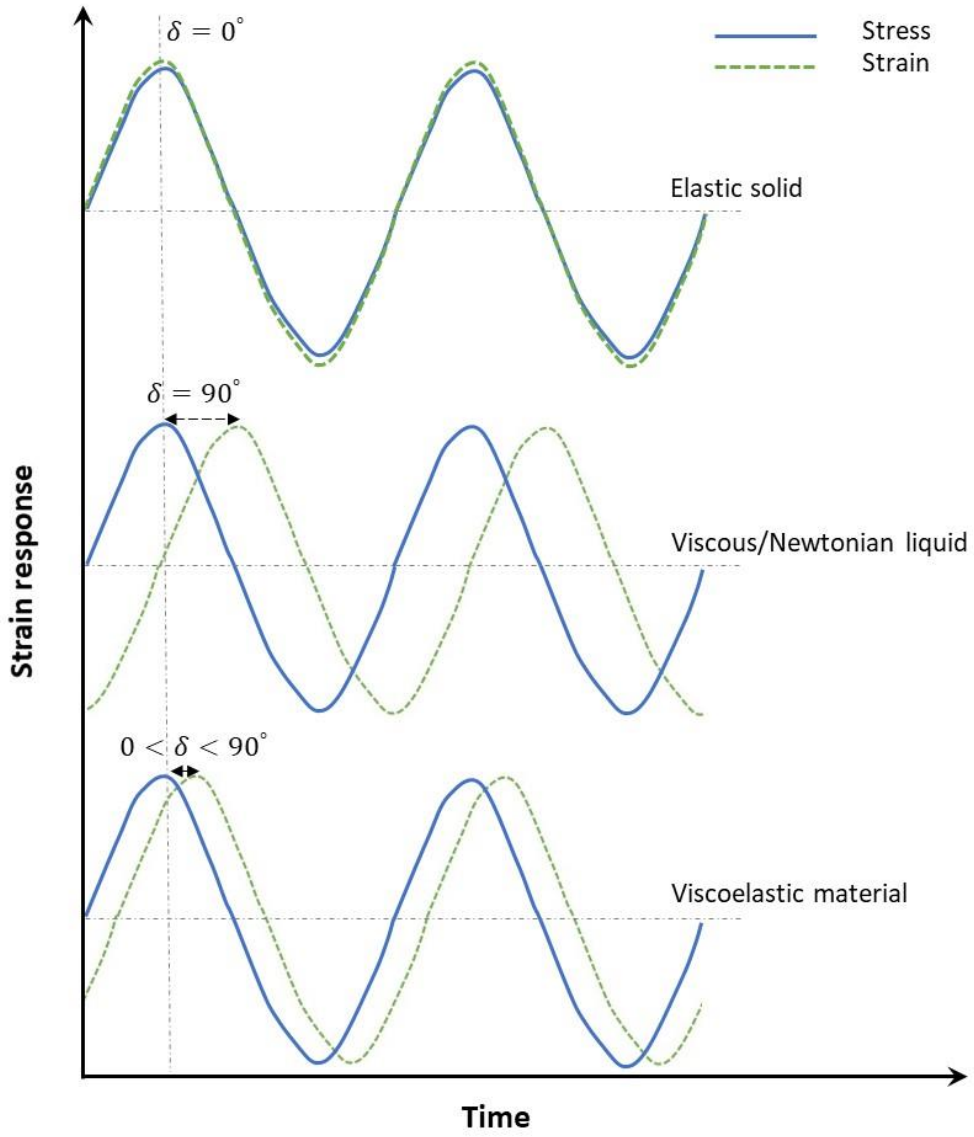

Figure 3-17 Stress response of elastic solid, viscous liquid and viscoelastic material under applied stress.

3.4.2. Texture profile analysis

The TPA technique is a useful standardised method that is used to quantify the textural properties of solid/semi-solid food and gel systems. In TPA, a double compression is being conducted to mimic the process of mastication. It is important to note that since mastication is a complex process, the structural change of food/gel during mastication cannot be replicated fully by the double-compression in TPA (Wee, Goh, Stieger, & Forde, 2018). TPA parameters such as fracturability, hardness, adhesiveness, cohesiveness, springiness, gumminess and chewiness are generated from the force-displacement curve from TPA as shown in Figure 3-18. In general, TPA parameters are found to have a good correlation with their sensory counterparts (Meullenet, Lyon, Carpenter, & Lyon, 1998; Szcesniak, Brandt, & Friedman, 1963).

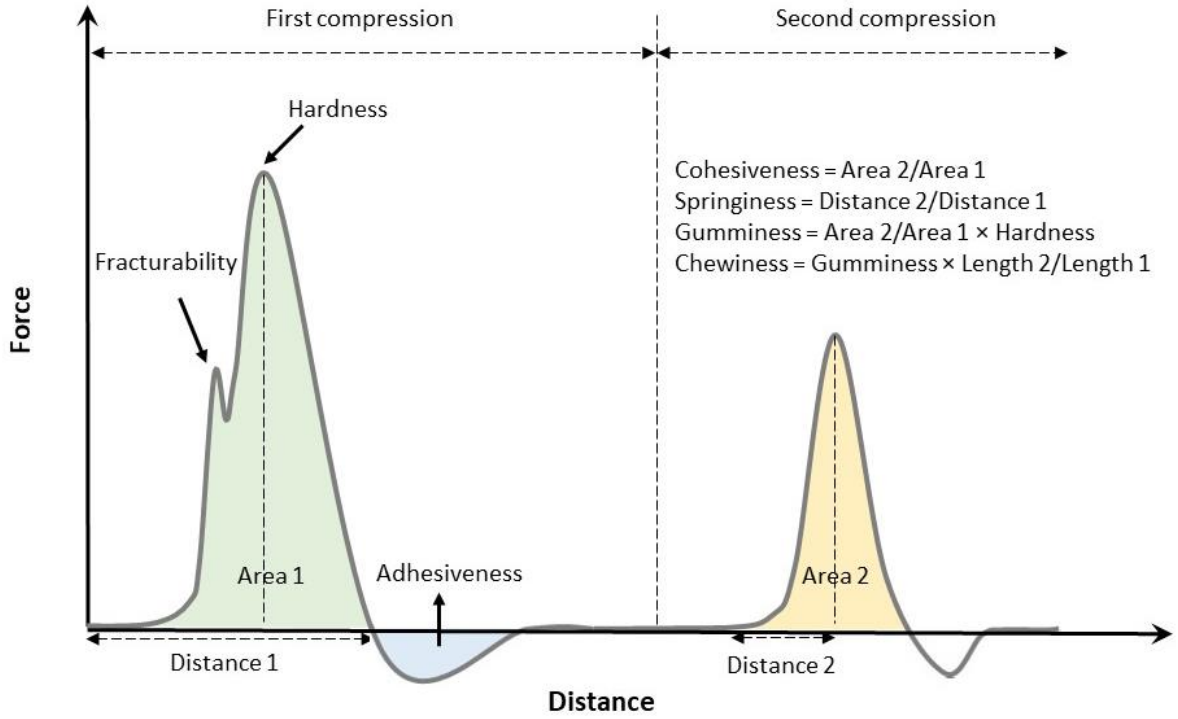

Figure 3-18 A typical TPA force-displacement curve.

It is also worthy to note that in this study, the compression was done at large deformation of 75% which caused the less elastic (or more brittle) gel samples to break, which is different from the *G'* obtained in an oscillatory test where small deformation was applied within their LVR. In addition, the *G'* and *G"* are intrinsic parameters of a material that reflect on the strength of bonding or other interactions among polymers. In contrast, the hardness determined from TPA is a measure of the sample's resistance to its compression forces by surface indentation Thus, this explains why the hardness and *G'* of the same sample may not always be in good agreement (Nanoscience Instruments, 2022). It is noteworthy that hardness is the only TPA parameter that is presented in Chapter 7 and Chapter 8, as the hardness parameter was the most consistent and meaningful among the investigated characteristics.

3.5. Microstructural characterisation

The use of microscopy techniques to study food microstructure has born great significance in understanding the physicochemical properties of food ingredients and systems. The microstructure of binary (whey protein + starch) systems in this thesis was studied using the respective microscopy techniques shown in Table 3-2.

Table 3-2 Common food microscopy techniques (Auty, 2019).

Technique	**Radiation type**	**Theoretical resolution**	**Applications**
Scanning electron microscopy (SEM)	Electrons	~4 nm	Large depth of field – simulated 3-D view and morphology
Transmission electron microscopy (TEM)	Electrons	~1 nm	Fine structural detail and macromolecular interactions
Confocal scanning laser microscopy (CSLM)	Photons	~200 nm	Material identification and 3-D information

3.5.1. Scanning electron microscopy (SEM)

Scanning electron microscopy (SEM) is a technique that utilises the behaviour of electrons to create 3-D images of the respective surface, providing topology and morphology information of a sample. The scanning electron microscope is a piece of powerful equipment that produces high-resolution micrographs. The microscope consists of an electron column (to create a beam of electrons), a sample chamber (location for the electron beam to interact with the sample), electron detectors (to collect a range of signals from beam-sample interaction) and a viewing system (to build an image from the received signals). A beam of electrons is created and accelerated by the electron gun in the electron column, these electrons interact with atoms within the sample at different depths to create signals (secondary and backscattered electrons), which are used to produce an image (Sharma & Bhardwaj, 2019).

The technique has been used extensively to study both single and binary gel structures (Fu & Nakamura, 2017; Kumar, Brennan, Brennan, & Zheng, 2022; Ren, Yu, Dong, Hou, & Cui, 2017; Wang *et al.*, 2020). Samples for SEM require careful preparation to prevent any artefacts, distortion of the structure, and potential interactions between components in the sample and chemicals used in sample preparation (*e.g.*, removal of lipid-soluble components in solvents used for dehydration step) (Sharma & Bhardwaj, 2019). During sample preparation, water is removed from the gel matrix while maintaining its original structure. This process results in samples having a porous structure. Examples of scanning electron micrographs of gels containing gelatinised tapioca and corn starch with or without WPI are shown in Figure 3-19.

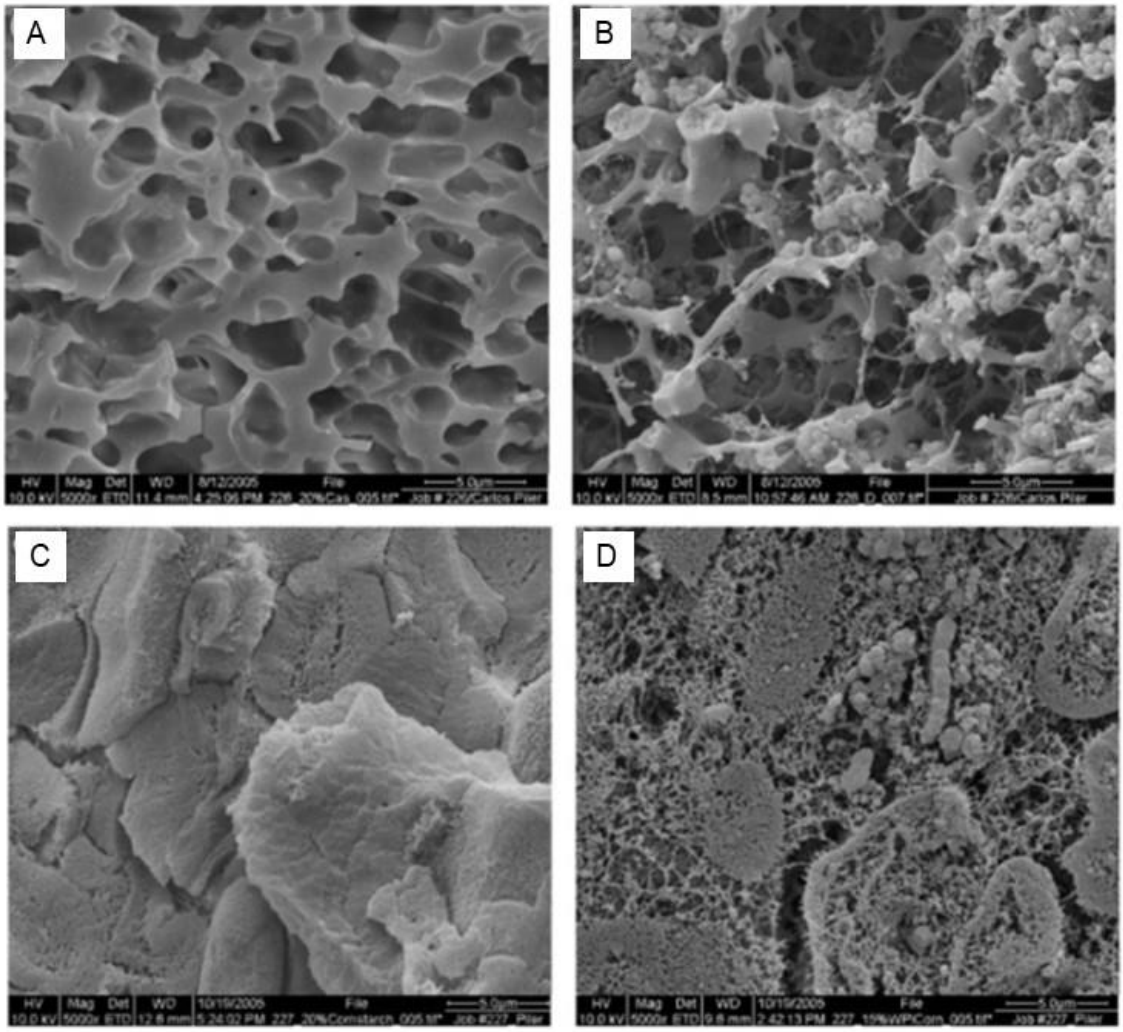

Figure 3-19 Scanning electron micrograph of (A) 20% w/w tapioca starch, (B) WPI and tapioca starch (1:1 ratio) at 15% w/w total solids, (C) 20% w/w corn starch and (D) WPI and corn starch (1:1 ratio) at 15% w/w total solid. Reprinted with permission from Carvalho, Onwulata, & Tomasula (2007). Copyright 2007 SAGE Publications.

The microstructure of native whey protein gels (~pH 7 and at low ionic strength) has been reported to have a fine-stranded network with the size of individual protein molecules ranging from ~3 to ~5 nm (Langton & Hermansson, 1992). With the addition of salt or adjustment of pH close to its isoelectric point, whey proteins form larger aggregates ranging from 0.1 to 1 µm (Urbonaite *et al.*, 2016). The scanning electron microscope used in this study can only produce a good resolution image up to 8000× magnification. Thus, SEM was used in the WPI + starch interaction study to study the effect of salts (*i.e.*, NaCl and $CaCl_2$), as the differences in microstructures of systems without salts (with finer microstructures) could not be detected at magnification ≤ 8000× (Appendix A).

3.5.2. Transmission electron microscopy (TEM)

The microstructure of WPI + starch gels with no salt added was studied using transmission electron microscopy (TEM) due to its excellent resolution at high magnification (Table 3-2). The working principles of TEM are similar to SEM. However, in TEM, the image is generated by focusing the electron beam through a thin section of the sample, rather than striking on the surface (Auty, 2019). Sample preparation for TEM of gel samples often requires embedding. The sample has to be chemically fixed and dehydrated before embedding into a polymer-based resin. In an earlier study by Langton & Hermansson (1992), the sample was cut into a thin section of ~60 nm and double-stained with lead citrate and uranyl acetate to increase contrast. As mentioned earlier in Section 3.5.1, native whey protein has a very fine-stranded structure. Micrographs of a 60% w/w whey protein isolate paste before and after extrusion at 100 °C are presented in Figure 3-20. Before extrusion, whey proteins existed in the form of irregular strands and granules—due to molecular aggregation—with sizes ranging from 10 to 200 nm. Upon extrusion, whey protein exhibited a uniform dense protein matrix with particle sizes of ~2–6 nm in diameter (Onwulata, Konstance, Cooke, & Farrell, 2003).

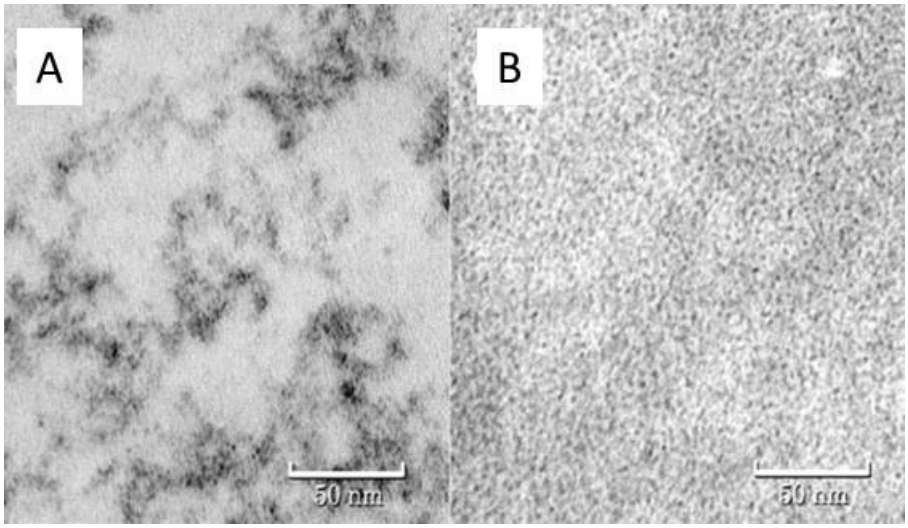

Figure 3-20 Transmission electron micrographs of whey protein isolate paste (60% w/w) (A) before and (B) extrusion at 100 °C. Reprinted from Onwulata *et al.* (2003), with permission from Elsevier.

3.5.3. Confocal scanning laser microscopy (CSLM)

Confocal scanning laser microscopy (CSLM) is a technique that enables the visualisation of internal food microstructure at different optical sections, which allows a 3-D image to be generated through a z-stack program. The principle of CSLM is illustrated in Figure 3-21, where the light from the laser (excitation source) is reflected by a dichroic mirror and focused on an area of the sample. This causes the fluorescence dye to be excited and emits light that passes through the objective lens. The reflected light rays from the focal plane will then be collected through the pinhole by the detector (illustrated

by blue lines). In contrast, the remaining light rays that are reflected from the out-of-focus planes are blocked out by the pinhole (illustrated by green lines). This collection of light rays from only fluorescence emission enables an excellent resolution image to be created within the focal plane. A 2-D image is created by scanning the sample in the x-y direction of the focal plane, while a 3-D image can be obtained with further scanning in the z-direction (Stanciu, 2012).

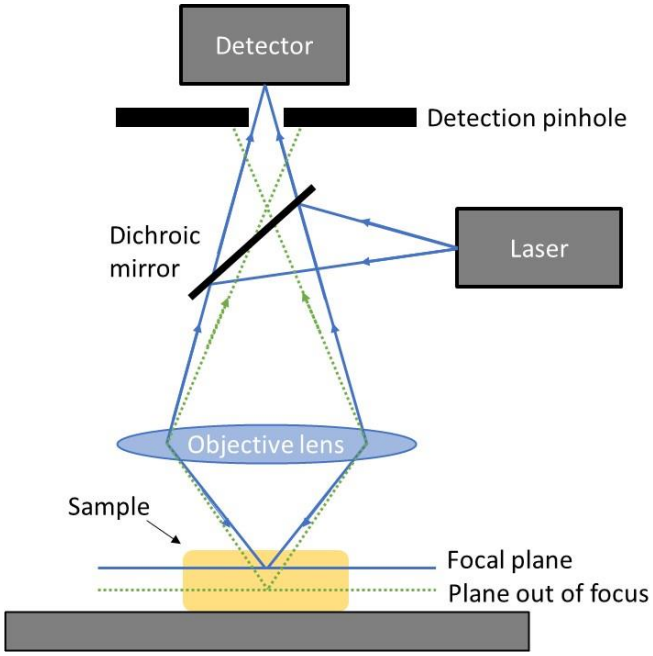

Figure 3-21 Schematic diagram of the principle of CSLM.

The CSLM technique gives the advantage to locate a material (*e.g.*, protein or starch) in a multiple-component system, where different fluorescence dyes can be used to stain specific materials (*e.g.*, protein, starch and fat). A set of lasers is then used to excite these fluorescent stains in the sample at different wavelengths and allows images to be taken separately. These images are overlayed to locate different components in the samples (van de Velde, Weinbreck, Edelman, van der Linden, & Tromp, 2003). An example of using CSLM to study a binary gel system is demonstrated by Çakır & Foegeding (2011). The authors used CSLM to study the microstructure of 13% w/w WPI and 0–0.6% w/w *k*-carrageenan gels. At 50 mM NaCl, the authors observed a transition of a continuous protein gel network at low *k*-carrageenan concentrations (0–0.2% w/w) to a bi-continuous microstructure (at 0.3 and 0.4% w/w *k*-carrageenan) and a continuous *k*-carrageenan phase was observed at ≤ 0.5% w/w *k*-carrageenan (Figure 3-22).

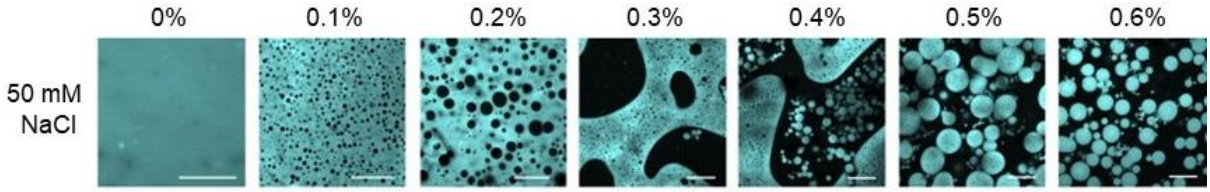

Figure 3-22 Confocal scanning laser micrographs of 13% w/w WPI gels with increasing concentration of k-carrageenan from 0–0.6% w/w at 50 mM NaCl. The scale bar is 50 µm. Reprinted from Çakır & Foegeding (2011), with permission from Elsevier.

In the preliminary study, different dyes were used to stain protein (rhodamine B and fast green) and starch (rhodamine B and 8-aminopyrene-1,3,6-trisulfonic acid, APTS) components in the gel samples. The details of these different fluorescence dyes are summarised in Table 3-3. Even though, rhodamine B stains both protein and starch, Rodriguez, Torrez Irigoyen, Navarro, & Yamul (2017) reported that rhodamine B preferentially stained protein over starch in dried gels prepared with whey proteins, honey and hydrocolloids mixture. Thus, rhodamine B and APTS were originally used to stain protein and starch for WPI + starch system, respectively. However, when starch granules were stained with either APTS or rhodamine B, good fluorescence was obtained with both dyes (Figure 3-23A and B). Thus, fast green was selected to replace rhodamine B for staining protein, as no signal was detected for starch granules stained with fast green (Figure 3-23C).

Table 3-3 Details of fluorescence dyes (rhodamine B, fast green and APTS) used in the study.

Fluorescent dye	**Excitation wavelength (nm)**	**Emission range (nm)**	**Stained material(s)**	**Reference**
Rhodamine B	546	580-670	Protein and starch	Rodriguez *et al.* (2017)
Fast green	633	650–700	Protein	Kasprzak, Macnaughtan, Harding, Wilde, & Wolf (2018)
APTS	488	500–520	Starch	Matignon *et al.* (2014)

The starch dye, APTS, was found to emit signals from a stained pure WPI gel (Figure 3-23D). This signal superimposed the protein network that was stained by fast green (Figure 3-23D–F). Moreover, an unstained whey protein gel was also found to emit weak fluorescence under the APTS channel (500–520 nm, result not shown), suggesting that the APTS signal in Figure 3-23D could either be due to (i) the inherent fluorescence from whey protein isolate or (ii) APTS interacting with the whey protein to

emit signals at the collection wavelengths. With these observations, APTS was concluded to be an unsuitable starch dye for this study. Thus, only the protein matrix was stained with fast green for CSLM experiments in Chapter 7 and 8. Further work on finding a suitable starch fluorescence dye for WPI + DWPS gel is recommended to fully utilise the CSLM technique.

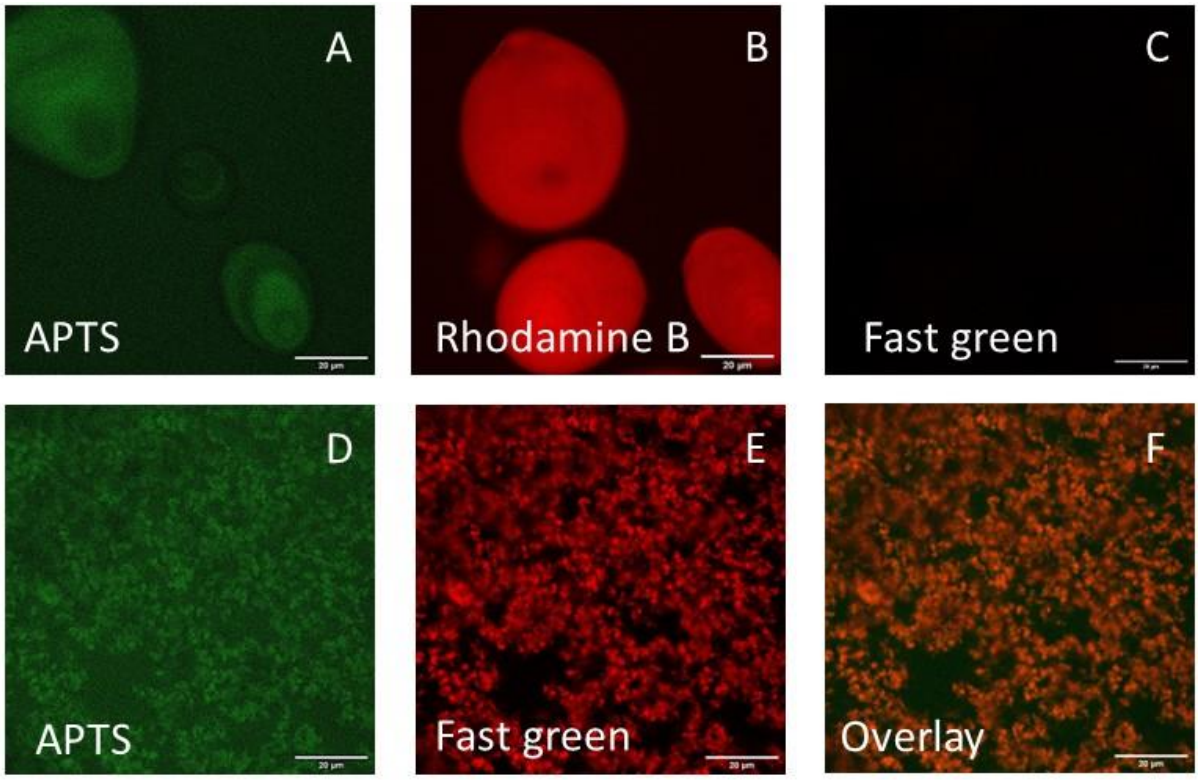

Figure 3-23 Confocal scanning laser micrographs of native waxy potato starch granules stained with (A) APTS, (B) Rhodamine B, (C) fast green, and 13% w/w whey protein gel with 500 mM NaCl stained with APTS and fast green with emissions under (D) APTS and (E) fast green channels and (F) their overlay. The scale bar is 20 µm.

3.6. Conclusions

The characterisation techniques listed in this chapter were employed to address the research objectives listed in Chapter 1. Molecular characterisation techniques (^{1}H-NMR, SEC and SEC-MALLS) coupled with particle sizing and rheological measurements were the approach taken to address the hypotheses on the starch de-structuring process and shear-induced structuring observed in DWPS samples (Chapters 4, 5 and 6). The combination of mechanical characterisation methods with microscopy techniques allowed the study of the influence of DWPS on the WPI gels under different pH and ionic strength conditions (Chapters 7 and 8).

Chapter 4 Characterisation of de-structured starch and its de-structuring mechanism[1,2]

4.1. Introduction

With the increased pursuit of natural food products, there is an increased pressure on food manufacturers to develop food products that are considered "clean-label". As such, there is an increasing trend to shift from using chemical additives to natural functional ingredients during food formulation.

Starch is a common ingredient used in formulating food products because of its gelling, stabilising, film-forming, and thickening properties. However, many of these commercial starches are chemically-modified to enhance their physicochemical properties and functionalities. Due to the use of synthetic chemical(s) during the modification process, such starches are unfit to be claimed as clean-label. Over the last decade, numerous research studies have been conducted to develop next-generation physical-based strategies to modify starches. In reference to the literature review (Chapter 2), some examples of these strategies include HMT, annealing, and high-pressure processing (HPP). Both HMT and annealing are hydrothermal-based processes where the treatments tend to result in increased gelatinisation temperature while retaining the integrity of the starch granular structure. As for HPP, partial or full gelatinisation of starches with intact granules is commonly observed with the application of high pressure between ~100 and 600 MPa (Bauer & Knorr, 2005; Knorr, Heinz, & Buckow, 2006). Different from these aforementioned modification strategies that allow the starch to retain its granular structure, a combination of physical treatments including thermal, pressure, shear, and duration was employed—starch de-structuring process at 120–150 °C for 30 min, under continuous shear at 300 rpm—in this study. Such modification is hypothesised to cause native waxy potato starch

Parts of this chapter are published as:
[1]Ang, C. L., Matia-Merino, L., Lim, K., & Goh, K. K. T. (2021b). Molecular and physico-chemical characterisation of de-structured waxy potato starch. *Food Hydrocolloids, 117*, 106667.
[2]Ang, C. L., Matia-Merino, L., Sims, I. M., Sargison, L., Edwards, P. J. B., Lim, K., & Goh, K. K. T. (2022b). Characterisation of de-structured starch and its shear-thickening mechanism. *Food Hydrocolloids, 132,* 107864.

granules to undergo disassembly into their macromolecular chains, forming DWPS as de-structured starch. These DWPS materials could exhibit physico-chemical properties that are different from conventionally physical-modified starches. To the best of this author's knowledge, DWPS obtained by such a physical treatment regime is not well-characterised and understood. Therefore, in this chapter, the effects of various physical conditions on the extent of starch de-structuring through molecular and physico-chemical characterisation of the respective DWPS samples were evaluated. These results help in elucidating the mechanism behind the starch de-structuring process as well as its potential applications as a clean-label food ingredient.

4.2. Materials and Methods

4.2.1. Sample preparation

The sample preparation of DWPS is described in Section 3.1. Rheological, DLS and zeta-potential measurements were carried out on fresh DWPS solutions (5% w/w), whereas the LD was carried out on DWPS samples (5% w/w) that were reconstituted from freeze-dried powder and Milli-Q water. The DWPS dispersions were heated in a boiling water-bath for 1 h. The mixing of samples was carried out using a vortex to ensure sample homogeneity. For comparison purposes (zeta-potential measurements and LD), 1% w/w and 5% w/w gelatinised starch were prepared respectively at 95 °C for 30 min under constant shear at 300 rpm. The samples were allowed to cool to room temperature (~15 min) before analysis.

4.2.2. Laser diffraction

The particle-size distribution of the DWPS samples was obtained using a LD particle analyser (MasterSizer Hydro 2000MU, Malvern Panalytical Ltd., Malvern, Worcestershire, England). The refractive indices of water and starch were 1.31 and 1.53, respectively. All experiments were repeated three times, each with three measurements.

4.2.3. Dynamic light scattering

The z-average hydrodynamic diameter of DWPS samples was determined *via* DLS (Nano partica SZ-100, Horiba Scientific, Kyoto, Japan) at sample concentrations ranging from 0.125–5.0% w/v. Each sample (3 mL) was filled in a cuvette and the z-average readings were taken at 90° scattering light using a refractive index of starch particles of 1.530 (Pinto *et al.*, 2015). The temperature of the samples was controlled at 20.0 ± 0.1 °C during the measurement. All experiments were repeated twice times, each with three measurements.

4.2.4. Zeta potential measurements

The zeta-potential value of the gelatinised starch and DWPS samples (at their native pHs) was determined by a ZetaSizer Nano ZS (Malvern Panalytical Ltd., Malvern, Worcestershire, England) *via* electrophoresis and laser Doppler velocimetry techniques at sample concentrations of 0.125–1.0 % w/v. The samples were measured in universal folded capillary cells (DTS1060C; Malvern Instruments Ltd, Worcestershire, England) at 20.00 ± 0.02 °C. All experiments were repeated twice times, each with three measurements.

4.2.5. Size-exclusion chromatography coupled with multi-angle laser light scattering (SEC-MALLS)

The weight-average M_w and z-average mean square radius (R_z) were determined *via* SEC-MALLS on a Shimadzu LC-20AD HPLC system (Kyoto, Japan). Samples were eluted from a size-exclusion column (OHpak SB-806 M HQ, 300 × 8.0 mm, Shodex, Tokyo, Japan) with a guard column (OHpak SB-G, 50 × 6.0 mm, Shodex, Tokyo, Japan) connected in series with 0.1 M sodium nitrate solution containing 0.02% w/w sodium azide (0.5 mL/min, 60 °C). The eluted materials were monitored using a multi-angle laser light scattering photometer (Dawn Heleos 8+, Wyatt Technology Corp., Goleta, CA, USA) and a refractive index detector (RID-20A, Shimadzu, Kyoto, Japan).

Pure amylopectin (BDH, Poole, England) and starch samples (native waxy potato starch and DWPS) were heated overnight at 80 °C in a shaking water-bath at 0.5 % w/w in 90 % DMSO. The samples were then precipitated with absolute ethanol at a 1:4 sample to ethanol volume ratio. The mixtures were then centrifuged at 4000 *g* for 10 min. The pellets were re-solubilised with the mobile phase (0.1 M sodium nitrate containing 0.02 % w/w sodium azide) and heated in a boiling water-bath for 1 h. A separate sample (120 °C DWPS was re-solubilised with the mobile phase) was also heated in a boiling water-bath for 1 h. The light scattering and differential refractive index signals were analysed using Astra software (version 6.1.1.17, Wyatt Technology Corp., Goleta, CA, USA) with a second-order Berry method and *dn/dc* value of 0.146 mL/g for starch (Yoo & Jane, 2002). All experiments were repeated twice times, each with three measurements.

4.2.6. High-performance size-exclusion chromatography

The side-chain length distribution of debranched native starch and DWPS samples was analysed by HP-SEC on an Agilent Technologies 1260 HPLC system (Santa Clara, CA, USA). Samples were eluted from three columns (TSK-Gel $G5000_{PWXL}$, $G4000_{PWXL}$, and $G3000_{PWXL}$, 300 × 7.8 mm, Tosoh Corp., Tokyo, Japan) connected in series with 0.25 M sodium nitrate containing 0.02% sodium azide (0.5 mL/min, 70 °C). The eluted materials were monitored using a dRI detector. The system was calibrated using a series of pullulan molar mass standards (0.180, 0.504, 0.991, 6.1, 9.8, 22.0, 47.1, 107, 194, 337, 708 and 1220 kDa, PSS Polymer Standards Service GmbH, Mainz, Germany).

Debranched native and DWPS samples were prepared using the method outlined in Han *et al.* (2017) with slight modifications. Briefly, starch samples (8 mg) were dispersed in 1.6 mL 90% v/v DMSO overnight in an 80 °C shaking water-bath. The samples were then precipitated with absolute ethanol at a 1:4 sample to ethanol volume ratio and centrifuged at 4000 *g* for 10 min. The pellet was re-solubilised in 1.6 mL of 10 mM sodium acetate buffer (pH 5.5) and heated in a boiling water-bath for 10 min. The starch solutions were then cooled to 37 °C before the addition of 8 µL of isoamylase (E-

ISAMY, EC 3.2.1.68, 180 U/mg, Megazyme International, Wicklow, Ireland) and pullulanase (E-PULKP, EC 3.2.1.41, 30 U/mg, Megazyme International, Wicklow, Ireland) each. The samples were incubated in a 37 °C shaking water-bath for 24 h. The samples were then heated in a boiling water-bath for 10 min to deactivate the enzymes, followed by neutralisation of the solutions with NaOH (0.15 M, 0.2 mL). Barium acetate (2 M, 30 µL) was added to precipitate sulphate ions from the samples as barium sulphate. All the samples were filtered through a 0.45 µm PTFE membrane filter before injecting into the columns. The samples were maintained at ≥ 40 °C to prevent any precipitation of debranched starch samples. All experiments were repeated three times.

4.2.7. ^{1}H-NMR Spectroscopy

The degree of branching (DB) of native starch and DWPS samples was determined using ^{1}H-NMR spectroscopy. Starch samples (3.3 mg) were dissolved in 500 µL of d_6-DMSO containing 0.5% lithium bromide. Immediately before the NMR analysis, d_1-TFA (33 µL) was added to the samples and transferred to 3 mm NMR tubes, filled to a depth of 40 mm. The ^{1}H NMR spectra were recorded at 321 K on a 700 MHz Bruker Avance Neo Spectrometer (Bruker Biospin, Rheinstetten, Germany) equipped with a cryoprobe. Spectra were sampled using a 90^{o} ^{1}H pulse, a spectral width of 13.9 kHz and an acquisition time of 2.36 s, followed by a relaxation delay of 12.64 s. Spectra were processed using Topspin 4.1.3 (Bruker Biospin, Billerica, MA, USA), with zero-filling to 64k points and apodisation with exponential line broadening (1 Hz), prior to Fourier transformation. Spectra were phased followed by 2nd order polynomial baseline correction between 7 ppm and 1 ppm. The DB is calculated using Equation 3-1. All experiments were repeated three times, each with two readings.

4.2.8. Rheological measurements

Rheological measurements were performed using the Anton Paar MCR 302 rheometer in a controlled shear rate (CSR) mode at 20.0 ± 0.1 °C (Anton-Paar, Graz, Austria). Approximately 5.0 mL of 5 % w/w DWPS sample was loaded into the double gap geometry (DG 26-7 and C-PTD 200) for measurement. The sample was subjected to shear from 0.1 to 1000 s^{-1}. Data points were collected using a log-ramp for both time (40 to 10 s, initial to final) and shear rate settings. All experiments were repeated twice times, each with three measurements.

4.2.9. Statistical analysis

The data are presented as means ± standard error. One-way analysis of variance with Tukey's test was used to test significant differences among mean values at a 95% confidence level using Minitab software (Minitab 18, Minitab Inc, Sydney, Australia).

4.3. Results and discussion

4.3.1. Particle size, viscosity and zeta-potential of DWPS samples

Generally, during the initial phase of the heat treatment in excess water, starch granules undergo gelatinisation, where the disruption of molecular organisation of starch granules occurs together with irreversible swelling and melting of starch crystalline regions occurs (Ai & Jane, 2018b; Allan *et al.*, 2020). The remnants of starch granules form 'ghost' structures that can often be observed under a light microscope and the suspension appears translucent or opaque due to the scattering of light by particles from the starch remnants. However, the high pressure with shearing at the elevated temperatures (120–150 °C for 30 min) applied in this study further disrupted the granule remnants releasing their macromolecules and resulting in a clear solution. These solutions were termed as 'de-structured' waxy potato starch (DWPS) solutions.

Measurements of the DWPS (120–150 °C) by DLS and rheological measurement showed a reduction in both the z-average hydrodynamic diameter and the viscosity of the starch solutions (Figure 4-1). The hydrodynamic diameter and viscosity results are further supported by the LD particle-size distribution data. Gelatinised starch at 95 °C was found to contain particles ranging from 1 to ~600 µm. Upon de-structuring process at 120 °C, the particle-size distribution of DWPS samples shifted left, indicating a decrease in particle size, where a portion of the larger particle size range shifted to a smaller molecular fraction (Figure 4-2). Such a shift increased at increasing temperature from 120 to 150 °C. These results suggest that starch degradation had occurred at temperatures higher than 120 °C, and the size of both starch fragments and polymer molecules was further reduced with increasing temperature.

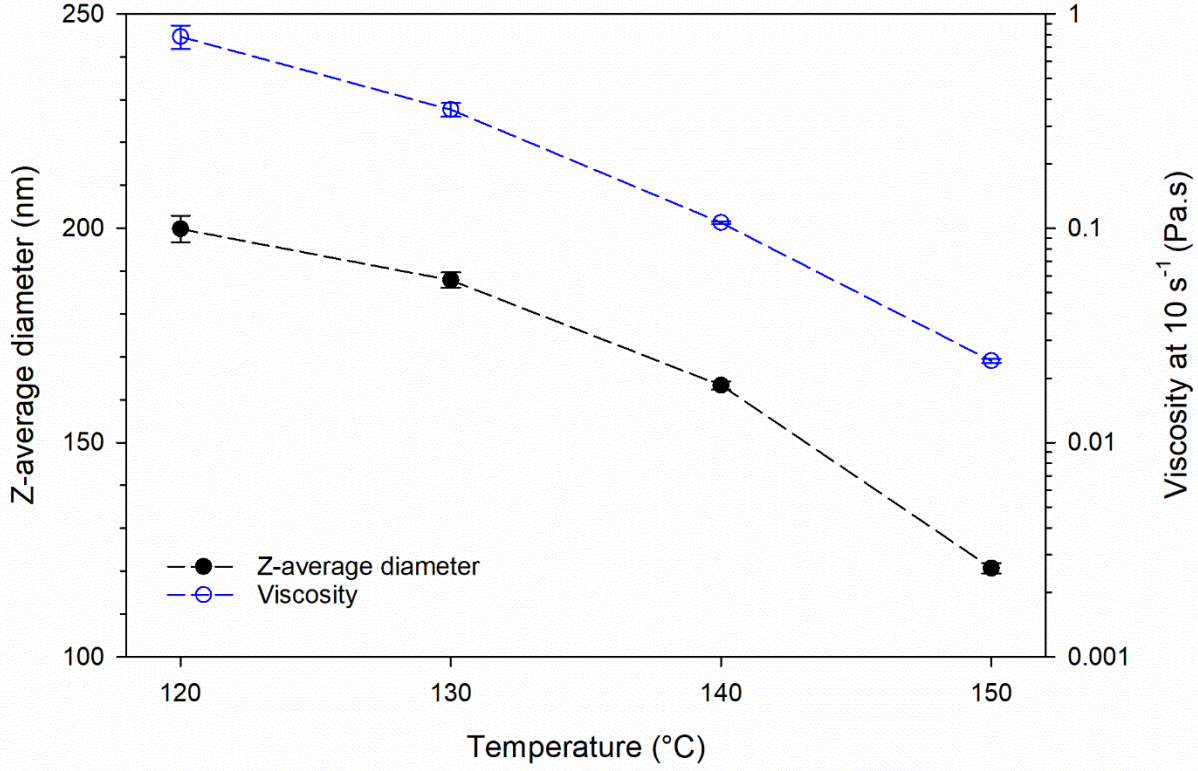

Figure 4-1 Effect of temperature on the z-average hydrodynamic diameter and viscosity at 10 s^{-1} of DWPS samples treated at 120, 130, 140, and 150 °C. Values are plotted with means ± standard error, with measurements taken at 20 °C.

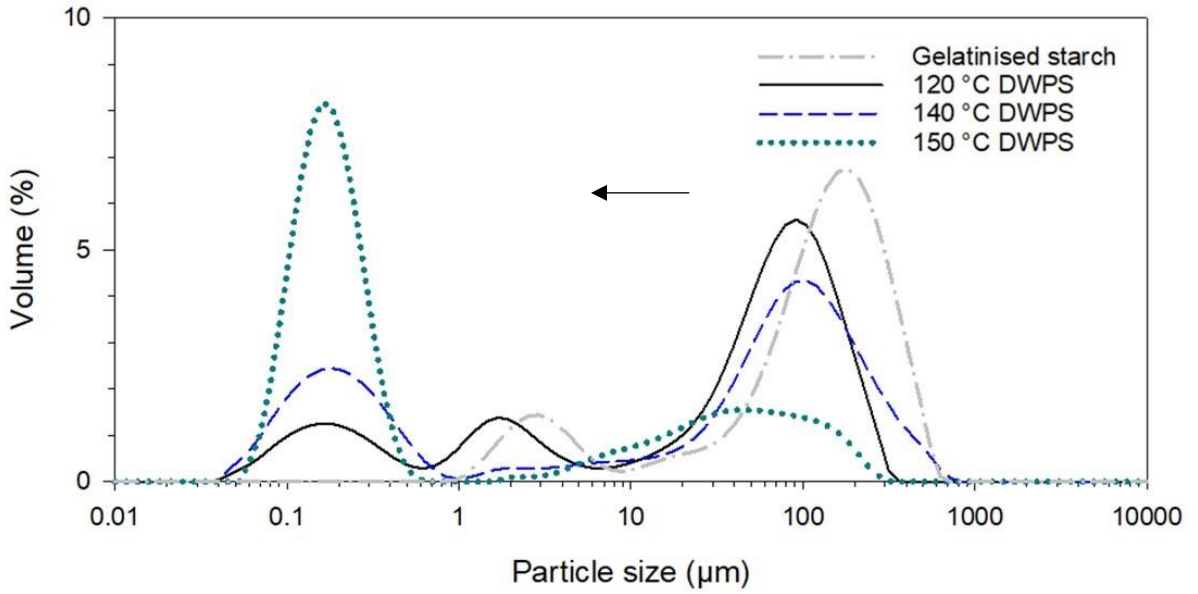

Figure 4-2 Particle-size distribution of gelatinised waxy potato starch (95 °C) and DWPS samples treated at 120, 140 and 150 °C determined by laser diffraction.

The zeta-potential of DWPS samples was observed to be less negative with increasing treatment temperature, where the zeta potential of the gelatinised starch was –31.0 ± 1.0 mV, and the DWPS samples treated at 120, 140 and 150 °C were –18.0 ± 1.1, –2.8 ± 0.6, and –2.1 ± 0.1 mV, respectively. Potato starch contains 0.5% phosphate group that contributes to its negative charges (Xu *et al.*, 2017).

Tabata & Hizukuri (1971) reported that the phosphate group is mono-esterified to glucose resides on the amylopectin chain at the positions of C-6 (61%), C-3 (38%), and C-2 (1%). The reduction in negative charges indicated that the de-structuring process had caused molecular changes to the starch polymers, as the zeta-potential measures the surface charge of the polymers (Lu & Gao, 2010). The reduction in the zeta-potential of DWPS samples would also mean that there was a decrease in the electrostatic repulsion between charged starch polymers. The reduced electrostatic repulsion can potentially alter how these DWPS samples behave in a pure system or mixed systems with other biopolymers.

4.3.2. Molar mass, size, and conformation of DWPS samples

Further analyses on weight-average M_w, z-average R_z, and polymer conformation of the DWPS samples were evaluated *via* SEC-MALLS. The determined M_w, R_z, and slope of the plot of M_w against the root-mean-square radius of starch samples are presented in Table 4-1. The M_w and R_z of native waxy potato starch were ~3.7×10^8 Da and 284 nm respectively, which corresponds well with the reported values in various studies, *i.e.* ~3.3×10^8 Da and 252 nm (Fang *et al.*, 2019; Szwengiel & Kubiak, 2020) and ~2.0×10^8 Da (Yoo & Jane, 2002).

Based on the data, the M_w of 120 °C DWPS was observed to be similar to that of the native starch, suggesting that the treatment at 120 °C did not affect the chain size (Table 4-1). To validate the claim, another 120 °C DWPS sample was prepared with mobile phase (without the use of DMSO) to check if there were any presence of starch clusters that were solubilised by DMSO in the sample preparation, as DMSO is commonly used to dissolve native starch granules into its individual macromolecular chains (Everett & Foster, 1959; Han & Lim, 2004). Very similar M_w values of $(3.6 \pm 0.2) \times 10^8$ and $(3.6 \pm 0.2) \times 10^8$ Da were observed for 120 °C samples treated with DMSO and without DMSO, respectively. The M_w results confirmed that 120 °C treatment disassembled starch into its native amylopectin chains without further chain fragmentation. The further increase in temperature from 120 to 140 and 150 °C decreased M_w from ~3.6×10^8 to 1.6×10^8 and 4.1×10^7 Da, respectively (Table 4-1). The chromatogram in Figure 4-3 shows two similar light scattering (LS) and differential refractive index (dRI) peaks for the native waxy potato starch and 120 °C DWPS. An increase in elution time with the peaks shifting from a bi-modal to mono-modal distribution when the treatment temperature was increased from 120 to 150 °C. Thus, the results indicated that amylopectin chain fragmentation had occurred at elevated temperatures above 120 °C. It is also noted that the M_w of the pure commercial potato amylopectin (~5.7×10^7 Da) was close to that of 150 °C DWPS. The low M_w of the pure amylopectin sample could either be due to the degradation of the amylopectin during the purification process or a different variety of potato starch. It is also worthy to note that the bi-modal distributions

observed for both native waxy potato starch and 120 °C DWPS could potentially be due to the fragmentation of large polymer chains caused by shear when samples were pumped through the size-exclusion column in SEC-MALLS, since the amylopectin being a highly branched chain is susceptible to shear degradation (Cave, Seabrook, Gidley, & Gilbert, 2009).

The conformation of a polymer chain can be deduced from the slope of a M_w against the root-mean-square radius plot. A slope value of 0.33 suggests a hard-sphere conformation and a slope value of 0.50 suggests a fully swollen randomly branched polymer in a good solvent (Stojanović, Jeremić, & Jovanović, 2013). The slope value of all samples ranged between 0.33 and 0.35, suggesting spherical conformation (Table 4-1). There is no significant difference in terms of slope value among all the tested samples. The results indicated that even at a high-temperature treatment of 150 °C, there was no significant change in the polymer conformation as all samples appeared to be spherical. Such spherical conformation is also commonly reported for corn amylopectin (0.36), normal corn starch (0.37), waxy rice starch (0.40), and potato starch (0.42) (Hanselmann, Burchard, Ehrat, & Widmer, 1996; Roger, Bello-Perez, & Colonna, 1999; Rolland-Sabaté, Guilois, Jaillais, & Colonna, 2011).

Table 4-1 Weight-average molar mass (M_w), root-mean-square radius (R_z), and slope from the plot of M_w against the root-mean-square radius of DMSO-solubilised native waxy potato starch, amylopectin (from potato), and DWPS samples treated at 120, 140, and 150 °C.

	Weight-average molar mass, $M_w \times 10^6$ (Da)	**Root-mean-square radius, R_z (nm)**	**Slope of the plot of M_w against root-mean-square radius**
Native starch	372.1 ± 27.9^a	284 ± 14^a	0.35 ± 0.00^a
Amylopectin (potato)	56.8 ± 4.7^c	163 ± 4^c	0.34 ± 0.02^a
120 °C DWPS	359.9 ± 7.6^a	330 ± 4^a	0.34 ± 0.00^a
140 °C DWPS	157.1 ± 4.0^b	238 ± 6^b	0.34 ± 0.01^a
150 °C DWPS	41.1 ± 3.0^c	117 ± 5^d	0.33 ± 0.01^a

Values are expressed as means ± standard error. Values in the same column denoted with the same superscripts are not significantly different ($p \leq 0.05$).

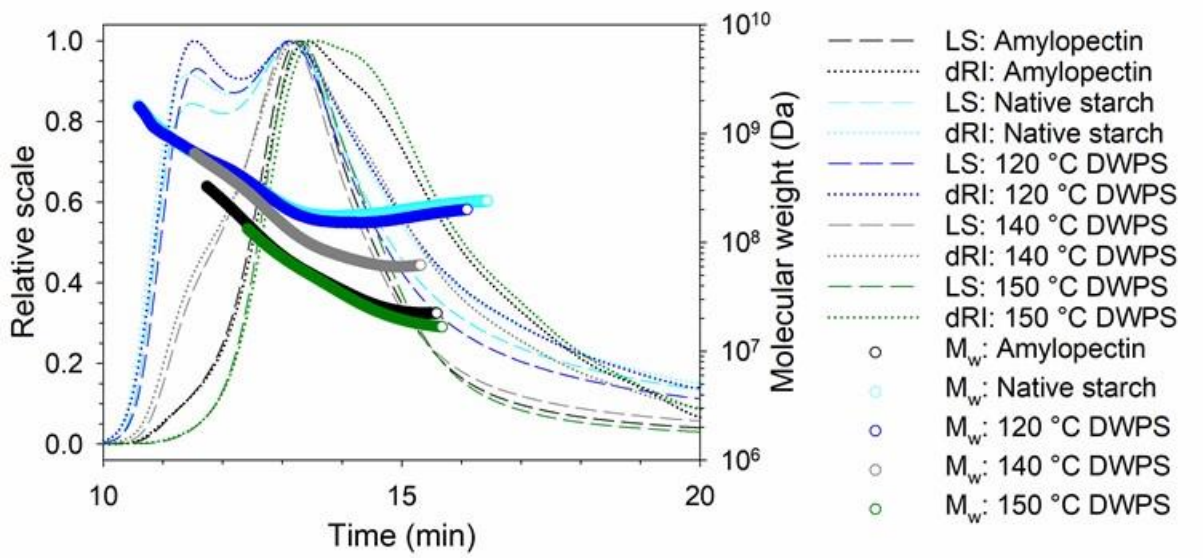

Figure 4-3 Light scattering (LS) signal, differential refractive index (dRI) signal and M_w distribution of native waxy potato starch, amylopectin (potato), and DWPS samples treated at 120, 140, and 150 °C eluted with 0.1 M sodium nitrate containing 0.02% sodium azide.

4.3.3. Side-chain length distributions and degree of branching of DWPS samples

Waxy potato starch consists of mainly amylopectin, which is a branched molecule. The branching points of the amylopectin are connected *via* α-1,6 linkages while the rest of the anhydroglucose monomers are joined by α-1,4 linkages. In this study, debranching enzymes (isoamylase and pullulanase) were used to cleave all the side-chain branches on the amylopectin molecules to yield linear starch chains. These chains are typically grouped into four categories according to their degree of polymerisation (DP), namely DP 6–12, DP 13–24, DP 25–36 and DP > 36 (Jane, 2009). The data on chain lengths according to the DP could reveal how original native amylopectin chains were degraded during the de-structuring treatment.

The side-chain length distributions of native waxy potato starch and DWPS samples treated at 120, 140 and 150 °C are presented in Figure 4-4. The results indicated that treatment at temperature between 120 °C and 150 °C did not exhibit significant differences in the side-chain length distributions during the de-structuring of waxy potato starch. Based on the data, it is likely that the cleavage of amylopectin during the de-structuring process occurred at the α-1,4 linkages along the main amylopectin backbone. Such cleavage will not affect the chain distributions due to the highly branched nature of amylopectin polymers and the low degree of polymerisation of the individual side-chain branches. A similar trend with minimal change in its side-chain length distribution was observed by Liu, Halley, & Gilbert (2010) in starch extruded at 140 °C. Even though amylopectin is a highly branched molecule that is expected to be susceptible to shear degradation (Cave *et al.*, 2009), a harsh mechanical treatment (as in this case, extrusion) where starch was subjected to high shear at high

starch concentration—with closely packed starch granules—did not result in further increased disruptions of side-chains. In contrast, Vermeylen *et al.* (2006) reported an increase in the proportion of side-chains with DP of 6–12 for potato starch that underwent HMT at 130 °C for 24 h (at 23% moisture content). The increased concentration of short side-chains (DP of 6-12) indicated that starch chain degradation occurred in side-chains longer than DP 12. Although the processing conditions of producing DWPS (fully gelatinised) were more severe than HMT (where its granular structure is retained), the results in this study, interestingly, did not show more severe degradation in amylopectin side-chains to result in higher fractions of starch chains with DP 6–12, as shown in the study from Vermeylen *et al.* (2006).

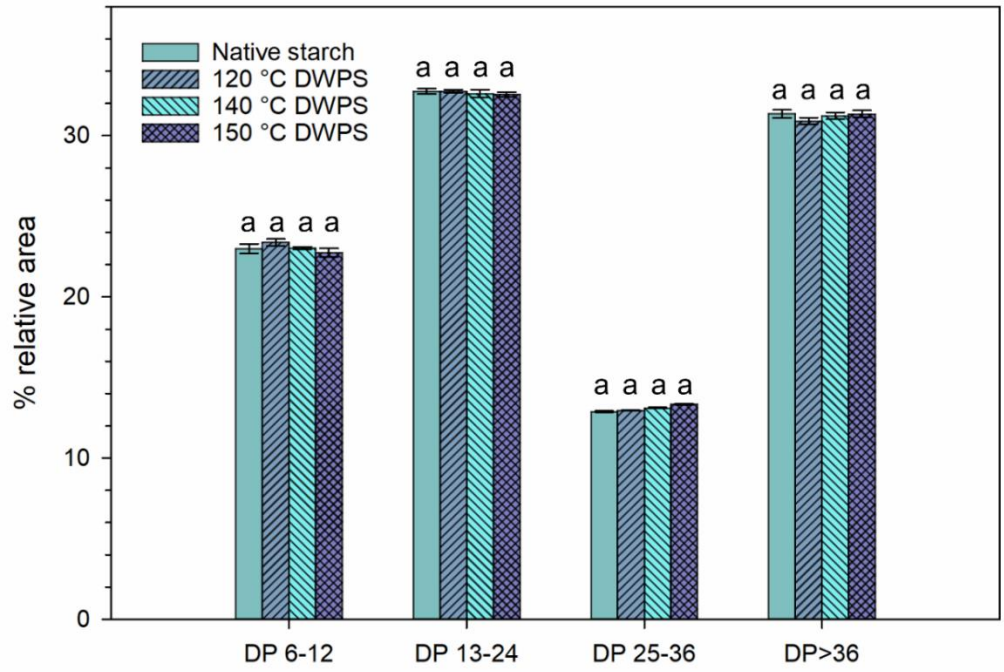

Figure 4-4 Starch side-chain length distribution of debranched native waxy potato starch and DWPS samples treated at 120, 140 and 150 °C, with the degree of polymerisation denoted as DP. Values are plotted as means ± standard error. Values in the same DP group denoted with the same superscripts are not significantly different ($p \leq 0.05$).

It is also worthy to note that the similar side-chain length distributions for native waxy potato starch and DWPS samples treated at 120, 140 and 150 °C may initially be interpreted as cleavage occurring preferentially at α-1,6 linkages (branching points) during the de-structuring process. In this case, the resultant side-chain of DWPS samples will be identical to that of its native form. To validate this claim, the DB of native starch and DWPS samples was determined using ^{1}H-NMR. If the cleavage of starch is specific to α-1,6 linkages, a lower DB for DWPS samples in comparison to its native form would be expected, as the resultant starch molecules would attain a more linear conformation (less branched structure).

The DB of native waxy potato starch and DWPS samples are presented in Table 4-2. There was no significant difference in the DB between 120 °C DWPS and its native form. A significant increase in DB was observed in DWPS samples treated at higher temperatures, *i.e.*, 140 and 150 °C, as compared to that of the native starch (Table 4-2). With reference to Equation 3-2, the DB of starch is defined as the ratio of the number of α-1,6 linkages to the total number of its α-1,4 and α-1,6 linkages (Tizzotti *et al.*, 2011). An increase in the DB of the 140 and 150 °C DWPS samples indicates a decrease in their α-1,4 linkages as compared to their native form, yielding a more branched structure. Hence, this data prove that the de-structuring process did not cleave the amylopectin chains specifically at α-1,6 linkages.

Table 4-2 Degree of branching of native waxy potato starch and DWPS samples treated at 120, 140 and 150 °C.

	Degree of branching (%)
Native starch	3.54 ± 0.07^{b}
120 °C DWPS	3.70 ± 0.04^{ab}
140 °C DWPS	3.76 ± 0.04^{a}
150 °C DWPS	3.74 ± 0.03^{a}

Values are expressed as means ± standard error. Values denoted with the same superscripts are not significantly different ($p \leq 0.05$).

4.3.4. Proposed mechanism of starch de-structuring

The reduction in the M_w, hydrodynamic diameter, and viscosity of the DWPS samples when waxy potato starch (5% w/w) was subjected to temperatures ranging from 120 to 150 °C for 30 min under continuous stirring at 300 rpm supports the proposed hypothesis that waxy potato starch granule had disassembled into its macromolecular chains. During the initial part of the de-structuring process, the native starch granules underwent gelatinisation below 100 °C. Upon gelatinisation, the starch granules began to swell irreversibly, and subsequent melting of the starch crystalline region occurred due to the disruption of hydrogen bonds (Wang, Li, Copeland, Niu, & Wang, 2015). The fragile granules continued to break into fragments and eventually degraded into their polymer chains under the presence of both shear and high temperatures. This was observed for the DWPS treated at 120 °C, with a gauge pressure of 1.2 bar under continuous shear. Furthermore, 120 °C DWPS had a similar M_w as the native waxy potato amylopectin chain suggesting that the amylopectin chains retain their native state. However, at temperatures above 120 °C, starch degradation (reduction in amylopectin chain size) occurred as indicated by the reduction in M_w and R_z of 140 and 150 °C DWPS samples. In addition, the presence of large fragments (> 1 µm) in 150 °C DWPS (laser diffraction particle-size distribution) suggests that the de-structuring process is incomplete. Thus, the degradation of starch materials during the de-structuring process at elevated temperatures between 120 and 150 °C is likely to occur

in both the amylopectin chains and starch granule fragments concurrently (Figure 4-5A). A significant increase in the DB was observed in 140 and 150 °C DWPS as compared to that of its native form, while there were no differences in the starch side-chain length distributions among the native starch and all the DWPS samples. It is important to note that since amylopectin chains are highly branched, only a few cleavages are needed to cause a significant drop in their molecular size. However, a large number of cleavages will be needed to impact their side-chain distributions, as the individual side-chains are of relatively low DP (DP 6–12, DP 13–24, DP 25–36 and DP > 36). Thus, it is likely that only a small number of cleavages were involved during the de-structuring process, resulting in a negligible change in side-chain distributions of DWPS. In addition, the mono-modal M_w distributions of DWPS shifted gradually to the right side (smaller M_w) with increased treatment temperature. This could infer that the amylopectin chains were mainly being cleaved close to their middle at α-1,4 linkages, along the main amylopectin backbone rather than from the outer branches. Cleavage of the amylopectin chains in the middle would yield products of similar molecular sizes (Figure 4-5B) as observed in the almost mono-modal dRI chromatograms in Figure 4.3. In contrast, if the cleavages were to occur at the outer chains, the dRI chromatograms would show a bi-modal distribution, containing two fractions: larger parent chains and markedly smaller outer chains, which was not observed from the dRI chromatographs.

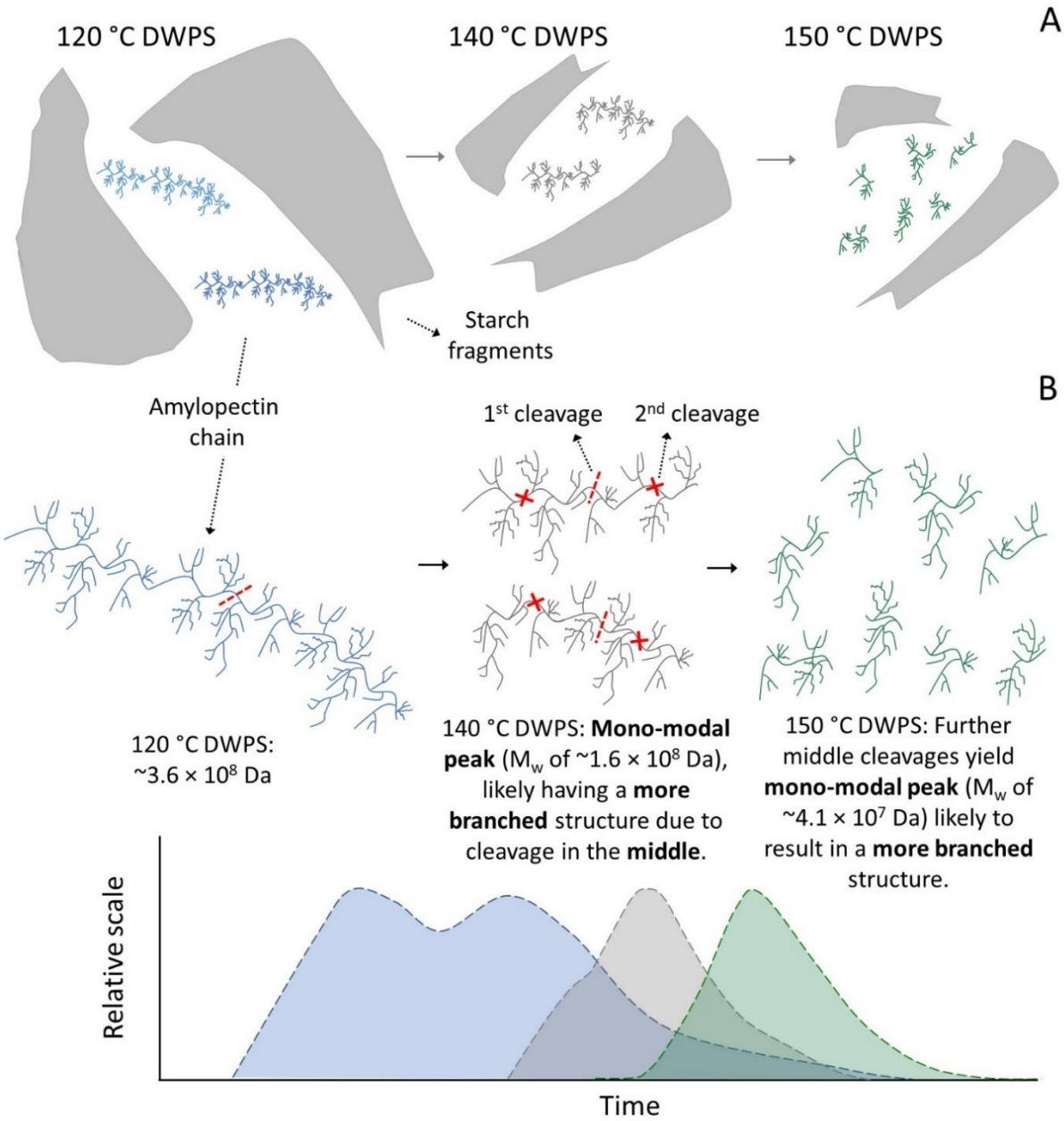

Figure 4-5 Schematic illustrations of (A) starch degradation during the de-structuring process from 120 to 150 °C and (B) dRI chromatograms of 120, 140 and 150 °C DWPS becoming more mono-modal due to amylopectin chains being cleaved near the middle.

4.4. Conclusions

An increased degree of starch disassembly was observed as the treatment temperature increased from 120 to 150 °C. The process reduced the M_w and hydrodynamic diameter of the starch samples through elevated temperature, pressure, and shear; to convert starch granules to their macromolecular chains. The de-structuring process caused a significant increase in the DB of 140 and 150 °C DWPS as compared to its native form. However, no changes in their side-chain profile were noted. The observations were attributed to the cleavage of the amylopectin chain occurring mainly close to the centre rather than its outer chains during de-structuring. The de-structuring process was found to be incomplete even at 150 °C due to the presence of a small amount of starch fragments (> 1 µm). These DWPS samples have the potential to aid in the assembly of new food structures for improved sensory and nutritional qualities that are different from conventionally gelatinised starch. In order to facilitate the use of DWPS ingredients in food formulation, further rheological characterisation of these materials was conducted, and the results are presented in Chapter 5.

Chapter 5 Rheological characterisation of de-structured starch [1,2,3]

5.1. Introduction

The rheological properties of gelatinised starch are highly dependent on its gelatinisation parameters such as temperature, heating rate and mechanical stress (Ai & Jane, 2015; Lagarrigue & Alvarez, 2001). During gelatinisation, starch granules (in the presence of heat and water) lose their crystallinity resulting in the loss of birefringence (Ai & Jane, 2015). The resulting gelatinised starch paste is a heterogeneous mixture of solubilised polymers (amylose and low molecular weight amylopectin chains), residual ghost granules and their fragments (made up mainly of amylopectin). The presence of shear during gelatinisation can impact the physico-chemical properties and rheological properties of the starch paste (Zhang, Dhital, Flanagan, & Gidley, 2014).

In Chapter 4, the de-structuring treatment from 120 to 150 °C reduced the native starch granules into their fragments and polymeric moieties at decreasing molar mass from ~3.6× 10^8 to ~4.1 × 10^7 Da. These structural changes during the starch de-structuring process are expected to impact on the rheological properties of the respective DWPS materials. To the best of this author's knowledge, the rheological properties of these DWPS materials are not well-characterised and understood. In this chapter, a combination of rotational and oscillatory shear rheological tests was used to study the time-, shear- and shear-history-dependencies of these DWPS materials. The acquired rheological data will enable a better understanding of the complex flow behaviour of DWPS, where such knowledge is important in the food formulation and the production of DWPS.

Parts of this chapter are published as:
[1]Ang, C. L., Goh, K. K. T., Lim, K., & Matia-Merino, L. (2021a). Rheological characterisation of a physically-modified waxy potato starch: Investigation of its shear-thickening mechanism. Food Hydrocolloids, 120, 106908.
[2]Ang, C. L., Matia-Merino, L., Lim, K., & Goh, K. K. T. (2021b). Molecular and physico-chemical characterisation of de-structured waxy potato starch. Food Hydrocolloids, 117, 106667.
[3]Ang, C. L., Matia-Merino, L., Sims, I. M., Sargison, L., Edwards, P. J. B., Lim, K., & Goh, K. K. T. (2022b). Characterisation of de-structured starch and its shear-thickening mechanism. Food Hydrocolloids, 132, 107864.

5.2. Materials and Methods

5.2.1. Sample preparation

Freeze-dried 120 °C DWPS from Section 3.1 was dispersed in Milli-Q water at varied starch concentrations of 0.5, 1.0, 2.5, 5.0, 7.5, and 10.0% w/w. Samples of 140 and 150 °C DWPS (5% w/w) were also prepared. The dispersions were heated in a boiling water-bath for ~1 h. Mixing of the sample was done with a vortex to ensure sample homogeneity. The reconstituted modified starch was then allowed to cool to ambient temperature (~15 min) before rheological measurements.

A control sample, ~19.0 mL of 5% w/w gelatinised waxy potato starch (Eliane 100, Avebe, Veendam, Netherlands), was prepared using a rheometer (Physica MCR 302, Anton-Paar, Graz, Austria) with a starch cell geometry (ST24-2D/2V/2V-30 and C-ETD 160/ST). Pre-shear was carried out at 960 rpm for 10 s to disperse the starch. The initial phase of heating was done in rotational mode at 300 rpm from 20 to 70 °C at a rate of 3.75 °C/min. Subsequent heating from 70 to 95 °C was done in an oscillatory mode at 1% strain and 1 Hz frequency to prevent disruption of the starch gel. Once the sample reached 95 °C, it was held for 30 min under the same oscillatory settings. Thereafter, the sample was cooled to 20 °C at 2.1 °C/min and held for another 15 min for thermal equilibrium before switching back to rotational mode for viscosity and shear stress measurements (Section 5.2.2.1).

5.2.2. Rheological measurements

Rheological measurements were performed using the Anton Paar MCR 302 rheometer (Anton-Paar, Graz, Austria) in a controlled shear rate (CSR) mode at 20.0 ± 0.1 °C, either with a cone-and-plate geometry (CP-40-4 and P-PTD200/56, gap = 0.049 mm) or double gap geometry (DG 26-7 and C-PTD 200). Prior to data collection, the samples were left unperturbed for 5 min upon loading to achieve temperature equilibrium. The data were collected using the Rheoplus software (v.3.62, Anton-Paar, Graz, Austria). All experiments were repeated at least two times, each with three measurements. A fresh sample was used for each measurement.

5.2.2.1. Rotational test

The flow behaviour of gelatinised starch and DWPS samples was analysed with either (i) viscosity curve or (ii) hysteresis area determined using the upward and downward flow curves at *log-ramp time setting* at initial to final interval of 40–10 s (for upward curve from 0.1 to 1000 s^{-1}) and 10–40 s (for downward curve from 1000 to 0.1 s^{-1}), respectively. The flow curves data were also fitted to a power-law model (Equation 5-1) to further characterise the flow properties:

$$\tau = K\dot{\gamma}^{n} \qquad \text{(Equation 5-1)}$$

where τ is the shear stress (Pa), $\dot{\gamma}$ is the shear rate (s^{-1}), *K* is the consistency index ($Pa.s^n$), and *n* is the flow behaviour index (dimensionless).

The effect of shear rate on the viscosity 120 °C DWPS was also investigated at varied constant shear rates of 1, 5, 10, 15, 30, 45, 60, 120, 300 and 1000 s^{-1} for 12 min. Viscosity readings were collected at 30 s (for ≤ 5 s^{-1}) and 10 s (for > 5 s^{-1}) intervals. The shear-history dependency of 120 °C DWPS was studied using three upward and downward shear cycles: (i) 0.1 to 5, (ii) 0.1 and 60, and (iii) 0.1 to 1000 s^{-1}. Both the viscosity and shear stress readings at varied shear rates were collected. The extent of the hysteresis was then quantified using Equation 5-1.

5.2.2.2. Oscillatory test

Oscillatory measurements were carried out at a fixed strain and frequency of 1% and 1 Hz respectively (within the LVR), to monitor any structural changes during measurements. The *G'* and *G"* readings were collected at 30 s intervals. A solvent trap was used to minimise evaporation during measurements.

5.3. Results and discussion

5.3.1. Shear-dependent viscosity of DWPS samples

The shear-dependent viscosity curves of gelatinised starch and DWPS (120–150 °C) samples are presented in Figure 5-1. Gelatinised waxy potato starch prepared at 95 °C for 30 min was used as the control sample to study the changes in rheological properties of the DWPS. The control sample exhibited shear-thinning behaviour throughout the shear rate region of 0.1 to 1000 s^{-1}. In contrast, DWPS samples modified at 120 and 130 °C exhibited shear-thickening behaviour at a shear rate of ~14 and 27 s^{-1}, respectively. When the temperature of de-structuring was increased to 140 and 150 °C, the samples approached Newtonian behaviour.

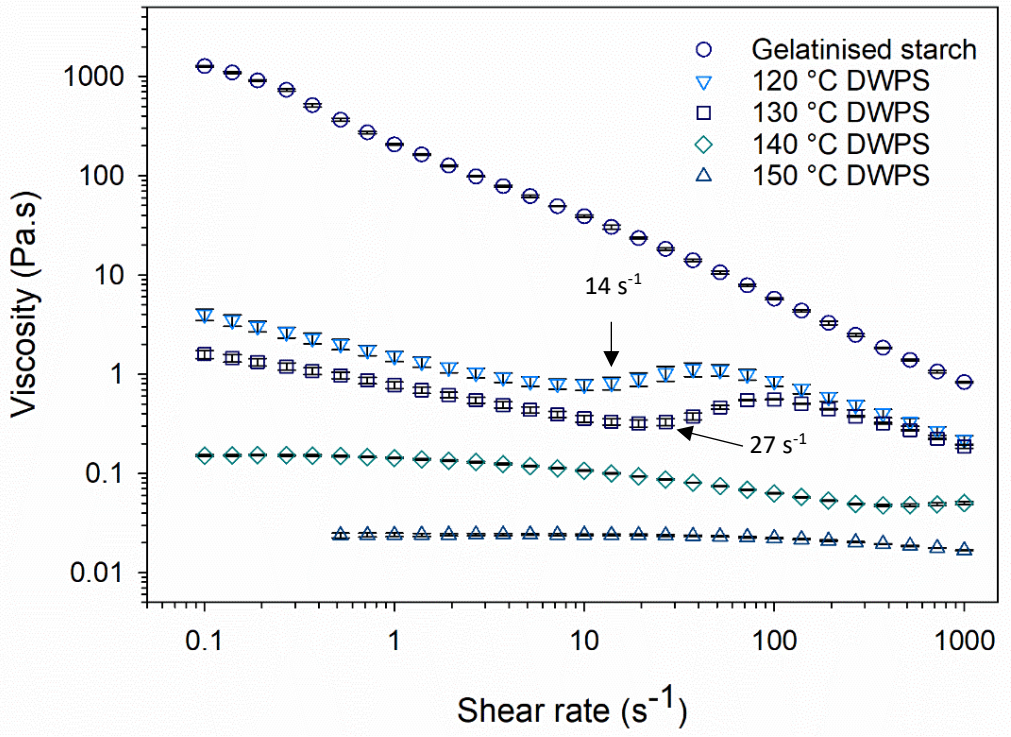

Figure 5-1 Shear-dependent viscosity of 5% w/w gelatinised waxy potato starch (95 °C) and DWPS samples treated at 120, 130, 140, and 150 °C. Values are plotted as means ± standard error with measurements taken at 20 °C.

Shear-thickening behaviour in starch has been reported in a couple of published reports, where the behaviour tends to occur under specific conditions such as low shear sample preparation of starch dispersion, for example, stirring using a spatula at room temperature with 0.2 KOH/NaOH (Bagley & Dintzis, 1999; Kim *et al.*, 2002); autoclaved at 140 °C (Bagley & Dintzis, 1999); or heating at 95 °C for 15 minutes at a low stirring rate such as 200 rpm (Fang *et al.*, 2019). Despite using the same waxy potato starch as Fang *et al.* (2019), shear-thickening was absent in the control sample (gelatinised starch) but observed in DWPS samples prepared in the reactor at much higher temperatures of 120 and 130 °C. It was probably due to the higher shearing speed (300 rpm) and longer heating duration

(30 min) used during sample preparation in the rheometer geometry cup. In addition, the presence of ghost remnants in starch pastes due to different sample preparation techniques, including different applied shear, could potentially cause a difference in the rheological properties (Feng *et al.*, 2014). In their follow-up study, Fang *et al.* (2020b) concluded that the shear-thickening behaviour in their study is attributed to the intermolecular double-helical aggregation of the waxy potato amylopectin chains that is governed by hydrogen bonding. The shear-thickening mechanism of the 120 °C DWPS will be investigated in the later section of this chapter (Section 5.3.4) and Chapter 6.

5.3.2. Time-dependent shear behaviour of DWPS samples

The time-dependent shear behaviour of gelatinised starch and DWPS was also characterised using the hysteresis area and a power-law model of the flow curves where shear stress is plotted as a function of shear rate. A hysteresis loop is commonly used to assess the extent of thixotropy of a material, where a hysteresis loop is an area generated between the upward and downward flow curves. Thixotropic behaviour is observed when the upward flow curve is higher than its downward flow curve, yielding a positive hysteresis loop area indicating a structural decomposition (Sikora *et al.*, 2015). In contrast to thixotropy, a structural build-up is observed when the downward curve is higher than its upward curve, giving a negative hysteresis loop area. A material exhibiting such behaviour is said to be anti-thixotropic (Mezger, 2011b). Furthermore, the total area of the hysteresis loop can be used to evaluate rheological stability under the influence of shear and time (Sikora *et al.*, 2015).

The calculated hysteresis loop areas and shear cycle plots of all the samples are presented in Table 5-1 and Figure 5-2, respectively. The control sample exhibited a pure thixotropy behaviour, which indicates a structural degradation during the shear cycle (Figure 5-2A). However, a mixed behaviour of thixotropy and anti-thixotropy was observed in the shear cycle of DWPS samples treated at 120 and 130 °C, as shown in Figure 5-2B and C, respectively. Anti-thixotropic behaviour was observed at the lower shear rate region: 0.1 to 37 s^{-1} in 120 °C DWPS and 0.1 to 87 s^{-1} in 130 °C DWPS. On the other hand, thixotropic behaviour was observed at the higher shear rate region: 37 to 1000 s^{-1} and 87 to 1000 s^{-1} for DWPS samples treated at 120 and 130 °C, respectively. At 140 °C, the sample exhibited anti-thixotropy behaviour across the broad shear rate range of 0.1–1000 s^{-1} (Figure 5-2D), whereas a negligible hysteresis loop was observed in 150 °C DWPS (Figure 5-2E), which indicates the disappearance of the time-dependency properties at 150 °C. Thus, increased stability was observed with the increment of treatment temperature, as a decrease in the total area through the structural formation and/or degradation was observed (Table 5-1).

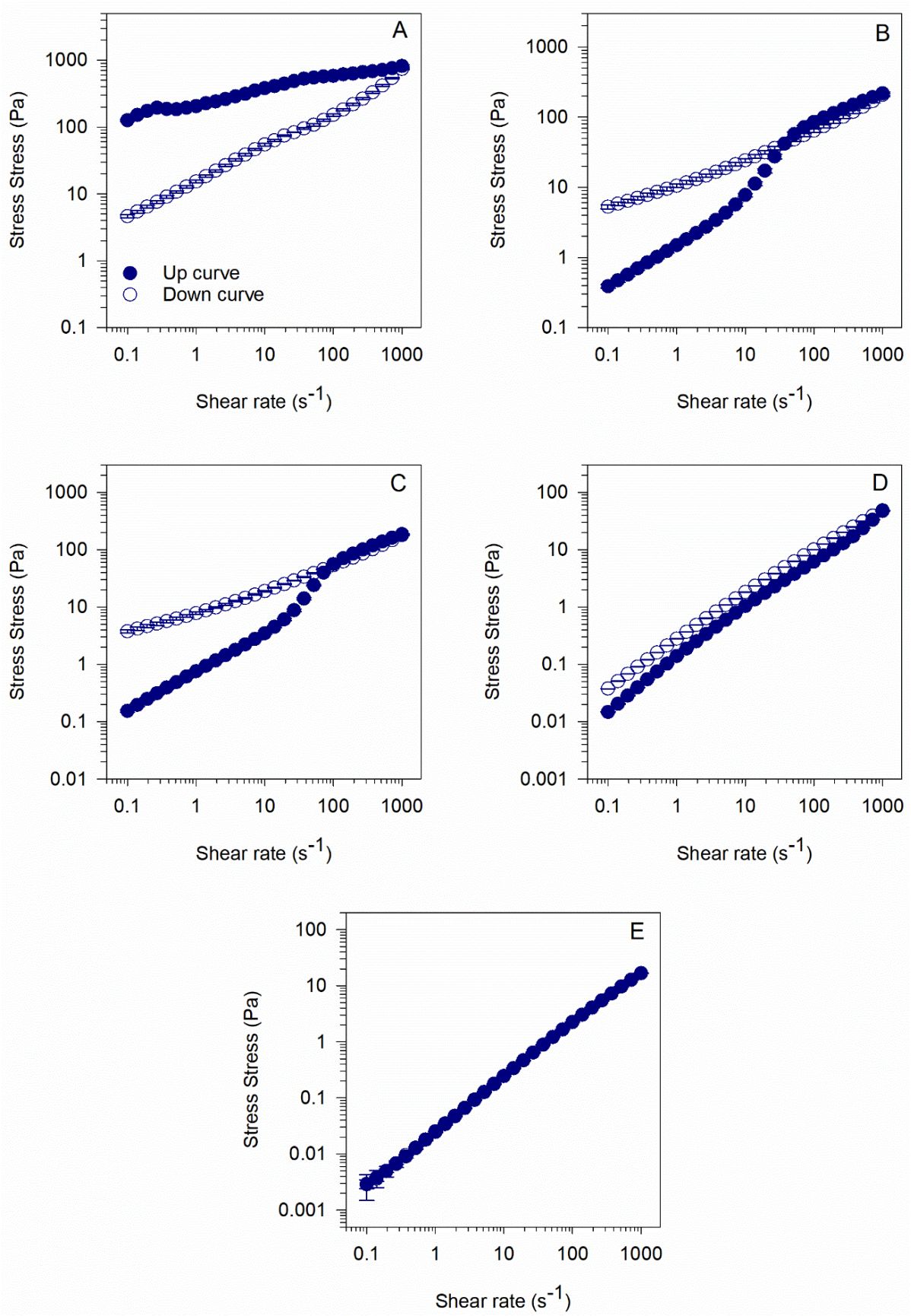

Figure 5-2 Hysteresis area between upward and downward flow curves of 5% w/w (A) gelatinised starch (95 °C) and DWPS samples treated at (B) 120, (C) 130, (D) 140, and (E) 150 °C DWPS. Values are plotted as means ± standard error with measurements taken at 20 °C.

Table 5-1 Hysteresis areas of the 5% w/w gelatinised starch (95 °C) and DWPS samples treated at 120, 130, 140, and 150 °C.

	Hysteresis areas (Pa.s^{-1})		
	Anti-thixotropy	**Thixotropy**	**Total area**
Gelatinised starch	-	294,528.6 ± 5,141.0^{a}	294,528.6 ± 5,141.0^{a}
120 °C DWPS	411.0 ± 27.8^{a}	22,834.5 ± 2,012.2^{b}	23,245.5 ± 2,035.3^{b}
130 °C DWPS	1,145.9 ± 53.5^{b}	12,452.3 ± 426.0^{c}	13,598.2 ± 384.1^{c}
140 °C DWPS	5,461.4 ± 19.4^{c}	-	5,461.4 ± 19.4^{cd}
150 °C DWPS	-	0.2 ± 0.2^{d}	0.2 ± 0.2^{d}

Values are expressed as means ± standard error. Values in the same column denoted with the same superscripts are not significantly different ($p \leq 0.05$).

The power-law model was used to fit the upward and downward flow curves to calculate the consistency coefficient (*K*) and flow behaviour index (*n*). For the control sample, a ~93% reduction in *K* value was noted when the downward flow curve was compared to its upward flow curve, which showed an overall thixotropy behaviour (Table 5-2). In contrast, anti-thixotropy behaviour was observed in 120, 130 and, 140 °C DWPS samples, with an increased *K* value of ~503, 926, 108% in comparison to their respective downward curves. No change in *K* values was noted in 150 °C DWPS. In addition, changes in the *n* values were also observed in the control and 120–140 °C DWPS samples (Table 5-2). A material exhibits shear-thinning properties when its $n < 1$ but for Newtonian fluid, $n = 1$. A reduction in *n* value was observed in 120–140 °C DWPS samples during the shear cycle. The shear cycle with a lower *n* value in a downward curve than in its upward curve suggested that the sample was more shear-sensitive in the downward curve than that of the upward curve. In other words, the structural breakdown was occurring faster than its structure recovery when the system was under shear. In contrast, no change in *n* value (~0.95) was observed for the upward and downward curves of 150 °C DWPS, which indicated that shear had a negligible effect on 150 °C DWPS (Table 5-2).

Table 5-2 Power-law model parameters for 5% w/w gelatinised starch (95 °C) and DWPS samples treated at 120, 130, 140, and 150 °C.

	Up curve			**Down curve**		
	K (Pa.s^n)*	***n***	***R*^{2}**	***K* (Pa.s^n)**	***n***	***R*^{2}**
Gelatinised starch	227.93 ± 4.50^{a**}	0.198 ± 0.13^a	0.980	15.35 ± 0.57^a	0.52 ± 0.01^c	0.997
120 °C DWPS	1.80 ± 0.07^b	0.77 ± 0.01^b	0.984	10.86 ± 0.68^b	0.39 ± 0.00^e	0.992
130 °C DWPS	0.79 ± 0.03^b	0.83 ± 0.01^c	0.987	8.11 ± 0.38^c	0.42 ± 0.01^d	0.992
140 °C DWPS	0.13 ± 0.00^b	0.85 ± 0.00^d	0.998	0.27 ± 0.00^d	0.78 ± 0.00^b	0.998
150 °C DWPS	0.03 ± 0.00^b	0.95 ± 0.00^e	0.999	0.03 ± 0.00^d	0.95 ± 0.01^a	0.999

Values are expressed as means ± standard error.
*K – Consistency coefficient, n – flow behaviour index, R2 – determination parameter.
**Values in the same column denoted with the same superscripts are not significantly different ($p \leq 0.05$).

5.3.3. Viscoelasticity of sheared and unsheared DWPS samples

The effect of shear (1000 s^{-1}, 5 min) on the viscoelastic properties of DWPS was investigated (Figure 5-3). The viscoelastic moduli results are in good agreement with the flow curve results (Figure 5-2). Before the application of shear (1000 s^{-1}, 5 min), all samples exhibited viscous behaviour with *G″* above their respective *G′*. Upon the application of shear, structural changes were observed in both 120 and 140 °C DWPS samples, where a marked increase in both viscoelastic moduli (*G′* and *G″*) was noted. In particular, sheared-120 °C DWPS exhibited *G′* > *G″*, indicating a gel-like behaviour. Similar to its flow curve profile (Figure 5-2), no noticeable differences in the loss moduli (*G″*) in 150 °C DWPS were observed.

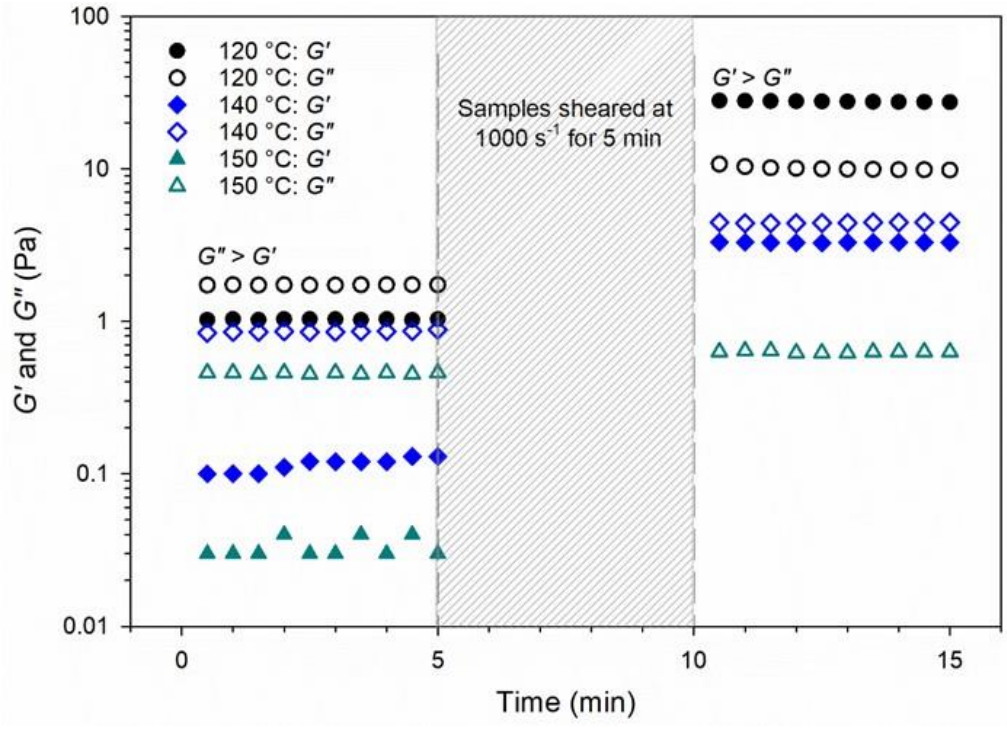

Figure 5-3 Effect of shear (1000 s^{-1} for 5 min) on the storage and loss moduli (*G′* and *G″*) of 5% w/w DWPS samples treated at 120, 140 and 150 °C. Measurements were taken at 20 °C. Note that the *G″* of 150 °C DWPS upon shear was outside of the detectable range of the rheometer.

5.3.4. Factors affecting shear-thickening behaviours of 120 °C DWPS

From the above rheological data, 120 °C DWPS showed interesting shear-thickening, anti-thixotropy and shear-induced gelation. Thus, further work was conducted on 120 °C DWPS to study the influences of shear rate, shear-history and concentration on its shear-thickening behaviour.

5.3.4.1. Effect of shear rate

The viscosity of 120 °C DWPS was determined at different shear rates (1, 5, 10, 15, 30, 45, 60, 120, 300 and 1000 s^{-1}) for 12 min to understand its time- and shear-dependencies. The development of viscosity over 12 min from 1 to 1000 s^{-1}—with an inset graph focusing on the first 4 min at shear rates between 10 and 60 s^{-1}—is presented in Figure 5-4. No time-dependency was observed at shear rates at 5 s^{-1} and below. A steady viscosity increase was observed throughout the 12 min experimental timeframe when the sample was sheared at 10 s^{-1}, with a final viscosity of 0.56 Pa.s. A similar observation was made at 15 s^{-1}, with a final viscosity of 0.67 Pa.s. When the shear rate was increased to 30 s^{-1}, the increase in viscosity plateaued at 11 min, with a final viscosity of 0.77 Pa.s. Samples sheared at 45 and 60 s^{-1} plateaued within 3.5 min, with their final viscosities reaching 0.68 and 0.72 Pa.s, respectively. The final viscosity of sample sheared at 120 s^{-1} (0.62 Pa.s) was developed within 30 s of the measurement. At 300 and 1000 s^{-1}, an initial reduction in viscosity was observed followed by viscosity plateauing off at 0.39 and 0.20 Pa.s, respectively. The data from these time sweep

measurements (Figure 5-4) are in good agreement with the steady-state viscosity data (Appendix B, obtained with "*no time setting*"), where an increase in viscosity at shear rates ≥ 10 s^{-1} occurred (in both time sweeps and steady-state viscosity curve in Appendix B). Moreover, maximum viscosity was achieved at ~60 s^{-1} (Figure 5-4), which was near the onset of maximum viscosity at ~63 s^{-1} in steady-state viscosity curve (Appendix B). The steady-state viscosity and time sweep curves indicate that the observed shear-thickening behaviour was not due to any artefact during the measurements.

The steady increase in viscosity at certain intermediate shear rates with time can be attributed to shear-induced intermolecular associations between 120 °C DWPS polymer chains. The viscosity results indicated that the sample not only showed strong time-dependency but also shear rate-dependency. A low shear rate at 5 s^{-1} was likely to be too weak to stretch the starch polymer for intermolecular association, but at 10 s^{-1}, the polymers appeared to be sufficiently stretched out with shear flow to allow some intermolecular associations between neighbouring polymer chains to occur. This means that the rate of association dominated over the rate of dissociation upon the applied shear, resulting in a net increase in viscosity with time. With an increase in shear rate to 60 s^{-1}, a shorter duration was required for intermolecular interactions to occur as polymer chains probably stretch further, increasing intermolecular interactions among neighbouring chains. However, when the shear rate was further increased to ≥ 120 s^{-1} (in the shear-thinning region), a drop in viscosity was observed before the viscosity plateaued off. This drop in viscosity could be attributed to the disruption of intermolecular interactions as the applied shear force exceeded the intermolecular forces among the polymer chains. Such behaviour could be due to the rate of intermolecular disruptions exceeding the rate of association, which resulted in shear-thinning behaviour. Such time-dependency has been observed in Mamaku gum (Wee, Matia-Merino, & Goh, 2015b), poly(ethylene oxide) solutions in Aroclor (Laufer, Jalink, & Staverman, 1973) and semi-dilute solutions of poly(2-hydroxyethyl methacrylamide) in glycerine (Kosvintsev, Riande, Velarde, & Guzmán, 2001). In the case of Mamaku gum, the polymer chains stretched and unfolded under shear, which allowed intermolecular association to occur *via* cooperative zipping (hydrogen bonding) between aligned Mamaku polymer chains.

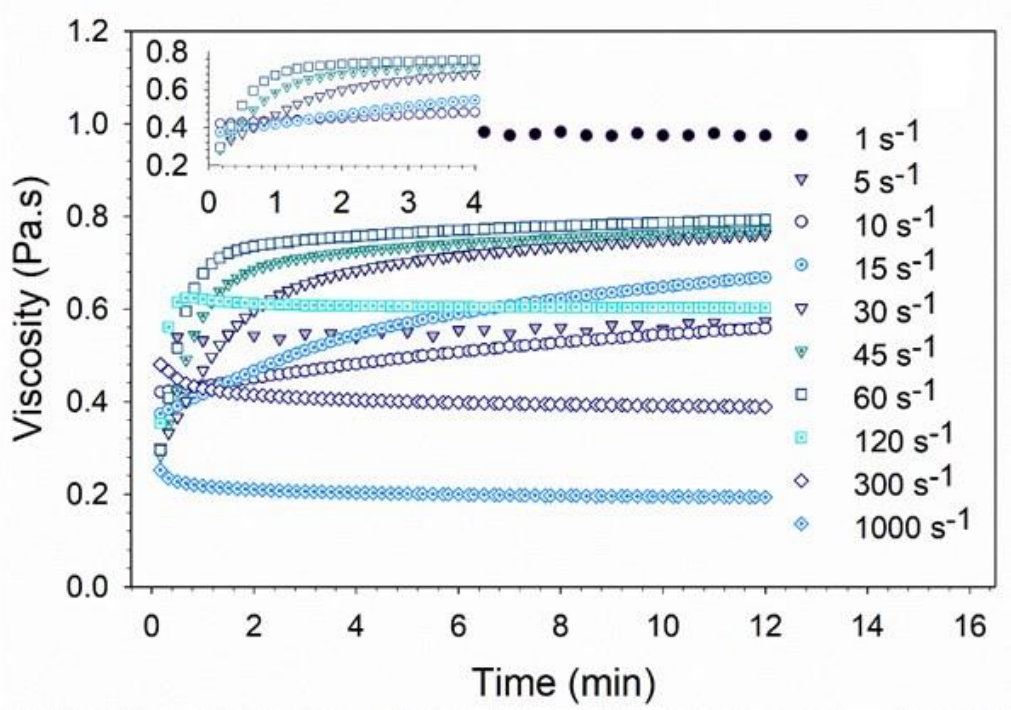

Figure 5-4 Effect of shear rate on the viscosity of 5% w/w 120 °C DWPS, at 1, 5, 10, 15, 30, 45, 60, 120, 300 and 1000 s^{-1} for 12 min, with an inset graph at 10, 15, 30, 45, and 60 s^{-1} during the first 4 min of the measurement. Measurements were taken at 20 °C.

5.3.4.2. Effect of shear-history

The shear-history dependence of 120 °C DWPS viscosity was investigated with three shear-up and down cycles to determine the extent of hysteresis (Figure 4-3). As shown in Figure 4-3A, the shear-up curve overlapped with its shear-down curve when the sample was sheared up to 5 s^{-1} and back, with no hysteresis observed. A distinct hysteresis was observed when the sample was sheared up to 60 s^{-1} (Figure 4-3B), which coincided with the shear rate at which maximum viscosity was observed in the time sweep measurements (Figure 5-4). When the sample was sheared up to 1000 s^{-1}, a further increase in hysteresis was observed, where the total area of hysteresis increased from 490 (Figure 4-3B) to 13,249 Pa.s^{-1} (Figure 4-3C). The higher viscosity obtained in the shear-down curve (upon shear to 1000 s^{-1} as opposed to only 60 s^{-1}) could be explained by an increased intermolecular association when the starch polymer chains were presumably fully extended at a high shear rate, allowing increased interactions during shearing down. In addition, a complex rheological anti-thixotropic and thixotropic behaviour was observed when the sample was sheared for a complete up and down cycle up to 1000 s^{-1} (Figure 4-3C). This could be explained by interactions and disruptions of bonds among molecular chains at different stages of applied shear. In other words, the onset of increased viscosity was the result of intermolecular association and that occurred at shear rate of ≥ 10 s^{-1} during the shear up cycle. The intermolecular associations were broken at a faster rate than their formation at shear rate of ≥ 120 s^{-1} (Figure 5-5). For the shear down cycle from 1000 to 120 s^{-1}, the structural bond

disruption dominated over the structural bond formation, which resulted in thixotropy behaviour. When the shear rate fell below 120 s^{-1}, intermolecular interactions were allowed to recur, resulting in the observed anti-thixotropy behaviour.

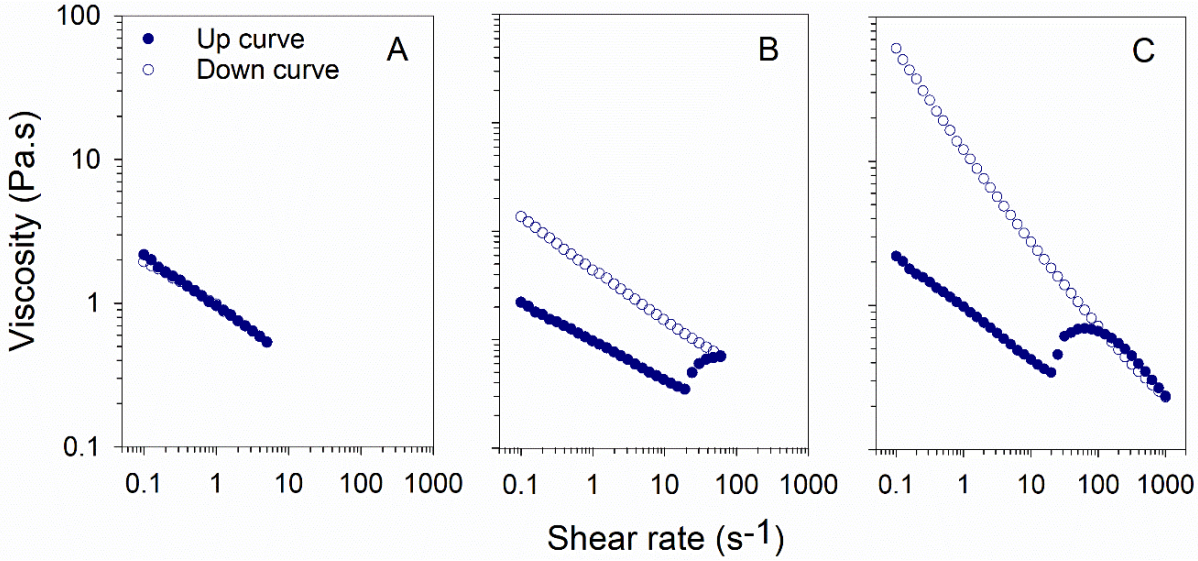

Figure 5-5 Hysteresis behaviour of 5% w/w 120 °C DWPS upon increasing or decreasing shear rate at 20 °C: (A) 0.1 to 5 s^{-1}, (B) 0.1 to 60 s^{-1}, and (C) 0.1 to 1000 s^{-1}. Measurements were taken at 20 °C.

The effect of shear-history on the viscoelasticity of 120 °C DWPS is shown in Figure 5-6A, where the viscoelastic moduli were monitored after the sample was subjected to pre-shear at 0.1, 1, 10, 100, or 1000 s^{-1} for 5 min. Both the *G'* and *G"* of 120 °C DWPS were unaffected by pre-shears between 0.1 and 10 s^{-1}, where no noticeable changes in viscoelastic moduli were observed. However, the sample showed a strong shear-history dependency at pre-shear of ≥ 100 s^{-1}. When the sample was sheared at 100 s^{-1}, a steady increase in viscosity was observed with time (Figure 5-6A). The increase in viscosity was an indication of the presence of shear-induced associations at 100 s^{-1}. In addition, the *G'* of the sample was also found to be higher than its *G"* after the sample was sheared at 100 s^{-1} for 5 min, which suggested that shear-induced gelation had occurred (Mezger, 2011b). When the shear rate was increased to 1000 s^{-1}, a further increase in both *G'* and *G"* was observed. This increased viscoelasticity was attributed to an enhanced association promoted by the high shear rate. Similar shear-induced gelation had been observed by Kim *et al.* (2002) in 2% waxy maize starch dispersion prepared by spatula stirring at room temperature with 0.2 N NaOH. The pattern of shear-induced aggregation was reported to have disappeared upon storage after a few days. Thus, leading the researchers to believe that the aggregation was reversible upon storage. In this study, the structural stability of the shear-induced gels was evaluated *via* a small amplitude oscillatory test, to monitor the viscoelastic moduli after the formation of the shear-induced gels (Figure 5-6B). A marked increase in viscoelastic moduli and shear-induced gelation was observed when the sample was subjected to one shear cycle (from

0.1 to 1000 s^{-1}) and then held at 1000 s^{-1} for 5 min. A slight decrease in both *G'* and *G"* was observed during the first hour of the recovery period. The drop in *G'* and *G"* could be attributed to the initial reorganisation of associated starch chains upon the removal of shear (Deshmukh, Kovářík, Muzaffar, Basheer Ahamed, & Khadheer Pasha, 2020; Zaccarelli, 2007). However, no further noticeable changes in *G'* and *G"* were observed for the remaining experimental timeframe of 72 h. Thus, the data suggest that the shear-induced structure is permanent as it remained stable even after 72 h. In addition, the viscosity data before and after shear-induced gelation are in good agreement with the viscoelastic moduli data. No marked differences were observed in the initial shear down curve as compared to those of the viscosity curves obtained from the shear cycle after a 72 h recovery period (inset graph of Figure 5-6B). The observed shear discrepancy between this study and Kim *et al.* (2002) in the structural stability of starch, could be due to the differences in starch polymer structures caused by different starch sources (waxy potato versus waxy maize) and sample preparation techniques.

It is also important to note that amylopectin gelation requires a long duration and high concentration of at least 10% w/w to occur (Biliaderis, 2009). In this study, a weak gel (~40 Pa) was observed at 5% w/w concentration after applying shear at 1000 s^{-1} for 5 min (Figure 5-6A). A similar observation of weak amylopectin gels (~4 Pa, at 5% w/w) was reported in an earlier study by Cameron, Durrani, & Donald (1994). The authors attributed the weak gel formation to limited helix formation between the external A-chains of the amylopectin molecules, rather than the aggregation of the pair of chains or further chain reorientation to become a more ordered structure. In their experiment, pure waxy maize amylopectin was prepared in a boiling water-bath under constant shear (stirring speed is not specified) for 5 min. Without the information on shear applied—such as stirring speed used for their sample preparation—it is inconclusive of whether the amylopectin gel observed by the authors is similar to that of what was observed in 120 °C DWPS as shear-induced gelation.

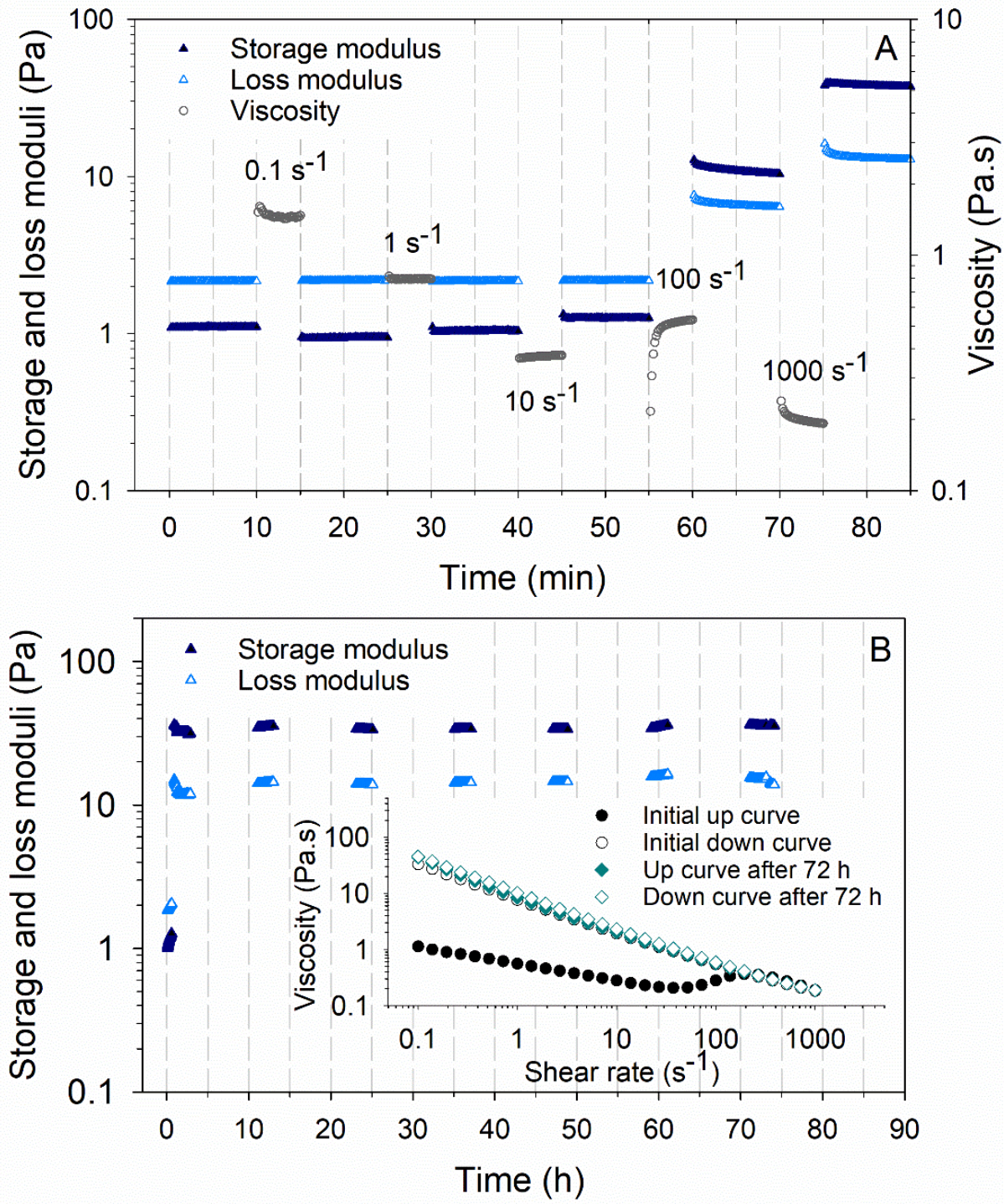

Figure 5-6 Effect of shear history on the *G'* and *G"* of 5% w/w 120 °C DWPS: (A) in-shear structural recovery with a step increase of pre-shear from 1, 10, 100 to 1000 s^{-1} for 5 min; and (B) long-term structural recovery over 72 h at 12 h intervals (measurement were only taken during the first 2 h) after shear-induced gelation at one shear cycle (0.1 to 1000 s^{-1}) and 1000 s^{-1} for 5 min, with an inset graph of viscosity of the same sample before and after shear-induced gelation. Measurements were taken at 20 °C.

5.3.4.3. Effect of concentration

The viscosity of 120 °C DWPS at varied concentrations from 0.5 to 10.0% w/w is presented in Figure 5-7A. Shear-thickening was observed at a minimum concentration of 1.0% w/w, which is in good agreement with the reported critical overlap concentration (*c**) of a waxy maize amylopectin at 0.9% w/w (Ring *et al.*, 1987). Three regions of flow behaviour were noted above 1.0% w/w; the initial shear-thinning behaviour in the first region could be attributed to the alignment of starch polymers in the direction of flow. Thus, leading to the reduction in viscosity with increasing shear rate. At shear rate above critical shear rate ($\dot{\gamma}_{crit}$), the shear exposed interactive sites on the polymer chain causing the neighbouring chains to associate through aggregation, raising the viscosity. The gradual increment in shear rate allowed better alignment of polymers, which caused a higher tendency for association interaction, and eventually resulting in a maximum viscosity. The subsequent shear-thinning behaviour after this viscosity peak at higher shear rates could be explained by the rate of polymer disentanglement or chain-chain disruption exceeding the rate of intermolecular association among polymer chains (Egmond, 1998).

In addition, the $\dot{\gamma}_{crit}$ was observed to occur at a lower shear rate with increased concentration. At a higher starch concentration, there is an increased frequency for the polymer chains to interact. This resulted in a lower $\dot{\gamma}_{crit}$ observed in a more concentrated system. Photographs showing the flowability of samples (2.5, 5.0, 7.5, and 10% w/w) before and after shear are presented in Figure 5-7B. A drastic reduction in the flowability of the sample was observed at concentrations of 7.5 and 10% w/w after the samples were sheared. Sheared-120 °C DWPS with reduced flowability also appeared to be more turbid as compared to that of the unsheared sample at a similar concentration. These observations are consistent with the shear-induced association of the starch polymer molecules, which will be further discussed in Chapter 6.

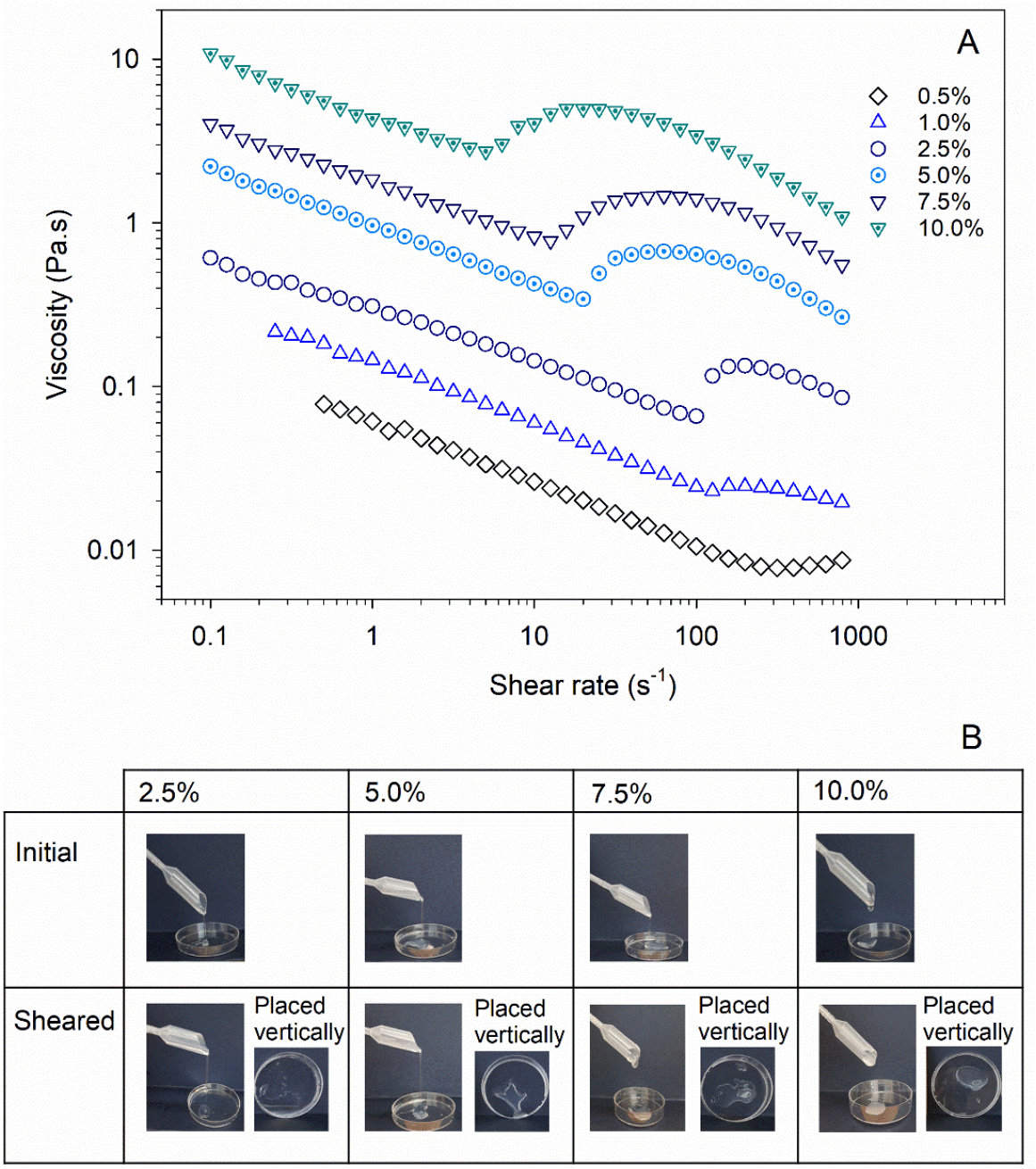

Figure 5-7 Effect of concentration on the: (A) viscosity of 0.5, 1.0, 2.5, 5.0, 7.5, and 10.0% w/w 120 °C treated waxy potato starch, and (B) visual appearance of 2.5, 5.0, 7.5, and 10.0% w/w 120 °C treated waxy potato starch before and after rheological measurements. Measurements were taken at 20 °C.

5.3.5. General remarks

The shear-induced gelation of 120 °C DWPS appeared to be stable once it is formed, such novel functionality has potential application in food products, especially where an enhanced structure is desired upon shear (*e.g.*, in whipping cream, where the enhanced structure will aid in the foam stability of whipped cream). In addition, no heat is required to induce the structure formation. Thus, the 120 °C DWPS can also be used as an effective stabiliser in the presence of heat-sensitive ingredients in food applications.

5.4. Conclusions

DWPS samples treated at 120–150 °C exhibited different rheological properties, which could be shear-dependent (shear-thickening and shear-thinning) and/or time-dependent (anti-thixotropy and thixotropy) or Newtonian. In particular, 120 °C DWPS exhibited shear-thickening, anti-thixotropy and shear-induced gelation. Once the shear-induced structure of 120 °C DWPS was formed, the weak gel structure (~20–40 Pa) was relatively stable during storage. Such enhanced structure may be used to enhance food structure like whipped cream. To facilitate the application of DWPS, further work on elucidating the mechanism of its shear-thickening, anti-thixotropy and shear-induced gelation was conducted in Chapter 6.

Chapter 6 Mechanism of shear-thickening, anti-thixotropy and shear-induced gelation of de-structured starch[1,2]

6.1. Introduction

In Chapter 5, DWPS samples were found to exhibit a wide range of rheological properties—Newtonian, shear-thinning, shear-thickening and anti-thixotropy behaviours—depending on their treatment temperature (120–150 °C). In particular, 120 °C DWPS exhibited interesting shear-induced behaviours such as shear-thickening, anti-thixotropy and shear-induced gelation. These rheological properties were different from the shear-thinning and thixotropy behaviours observed in most conventional gelatinised waxy potato starches treated at 95 °C.

As mentioned in the Literature Review (Section 2.1.3.4), shear-thickening behaviour in starches has been reported by several groups of researchers (Dintzis *et al.*, 1995; Fang *et al.*, 2020b; Kim *et al.*, 2002). Even though a number of hypotheses on shear-thickening in starches have been proposed, the exact mechanism responsible for shear-thickening behaviour is still debatable. The possible interactions that cause shear-thickening in the 120 °C DWPS could be related to mechanisms observed in other polymer systems including: (i) hydrogen bonding, as reported for a tree fern gum where the stretching of polymer chains upon shear exposes interactive sites for cooperative zipping to occur between aligned chains (Wee *et al.*, 2015b); (ii) electrostatic interactions due to the presence of negatively charged phosphate groups on waxy potato starch. For instance, Lewandowska (2007) reported shear-thickening behaviour in "hydrolysed polyacrylamide" (HPAM) solution. The observed shear-thickening effect was attributed to the increased repulsive forces originating from negatively

Parts of this chapter are published as:
[1]Ang, C. L., Goh, K. K. T., Lim, K., & Matia-Merino, L. (2021a). Rheological characterisation of a physically-modified waxy potato starch: Investigation of its shear-thickening mechanism. Food Hydrocolloids, 120, 106908.
[2] Ang, C. L., Matia-Merino, L., Sims, I. M., Sargison, L., Edwards, P. J. B., Lim, K., & Goh, K. K. T. (2022b). Characterisation of de-structured starch and its shear-thickening mechanism. Food Hydrocolloids, 132, 107864.

charged HPAM chains being forced together under shear; (iii) hydrophobic interactions, where shear-thickening was observed in hydrophobic ethoxylated urethane (HEUR) under shear. The formation of flower micelles occurs due to bridging interactions between HEUR polymer chains (Tam, Jenkins, Winnik, & Bassett, 1998). Hence, aggregates formed *via* hydrogen bonds, electrostatic attractions and hydrophobic interactions by polymers with associating groups, and together with the starch fragments present, could potentially result in characteristic rheological properties such as shear-thickening at the low shear rate (Tanaka, 2002).

To the best of this author's knowledge, the exact mechanism of shear-thickening, anti-thixotropy and shear-induced gelation in starch are not well-characterised and understood. Thus, the objectives of this chapter are to elucidate the effect of: (i) molecular/particle sizes and (ii) various environmental conditions (*i.e.*, urea, ionic strength, and temperature) on the rheological properties of DWPS materials. The acquired data will aid in the elucidation of the shear-thickening, anti-thixotropy and shear-induced gelation mechanism and provide insights into how DWPS can be used as a next-generation "clean-label" ingredient to create foods with unique structures.

6.2. Materials and Methods

6.2.1. Sample preparation

Samples of 120 °C DWPS at 5.0, 6.25, 7.5 and 8.0% w/w, and 140 and 150 °C DWPS at 5 % w/w were prepared as per Section 5.2.1.

6.2.1.1. Addition of urea to 120 °C DWPS

Stock urea solution (10 M, prepared with milli-Q water, LabServ) and 120 °C DWPS (7.5% w/w) were mixed to obtain samples with a final starch concentration of 5% w/w at varied urea concentrations of 0, 0.5, 1.5, 2.5, and 3.0 M.

6.2.1.2. Addition of NaCl to 120 °C DWPS

Sodium chloride (NaCl) stock solutions with concentrations ranging from 5 mM to 5.0 M were prepared with milli-Q water. The NaCl stock solutions and 120 °C DWPS (6.25% w/w) were mixed to give samples with a final starch concentration of 5% w/w at varied salt concentrations of 0.001, 0.005, 0.01, 0.05, 0.1, 0.25, and 0.5 M.

6.2.1.3. Addition of urea and NaCl to 120 °C DWPS

Stock urea and NaCl solutions (10 M and 2 M respectively) were mixed with 120 °C DWPS (8.0 % w/w) to give a final starch concentration of 5% w/w with 3 M urea and 0.1 M NaCl.

6.2.2. Rheological measurements

Rheological measurements were performed as per Section 5.2.2 with slight modifications at 20.0 ± 0.1 °C (unless specified). All experiments were repeated at least two times, each with three measurements.

6.2.2.1. Rotational test

The viscosity of 120 °C DWPS was characterised at varied: (i) urea concentrations (0–3 M), (ii) NaCl concentrations (0.01–0.5 M) and (iii) temperatures (20, 35, 65, 80 and 95 ± 0.1 °C). The measurements were taken with *log-ramp time setting* of initial to final interval of 40–10 s. The sheared samples (5.0% w/w) studied in Section 6.2.3–6.2.7 were pre-sheared at 1000 s^{-1} for 5 min.

6.2.2.2. Oscillatory test

For the thermal stability test, the sample was (i) heated from 20 to 90 ± 0.1 °C, at a rate of 3.75 °C/min, (ii) held at 90 ± 0.1 °C for 20 min and (iii) cooled from 90 to 20 ± 0.1 °C at a rate of 2.1 °C/min. A solvent trap and a thin layer of mineral oil around the exposed sample were used to minimise evaporation during measurements. The measurements were carried out at a 1% fixed strain and 1 Hz frequency (within the LVR), with *G'* and *G"* collected at 30 s intervals.

6.2.3. Size-exclusion chromatography coupled with multi-angle laser light scattering (SEC-MALLS)

The M_w and R_z of the original (without pre-shear) and sheared DWPS samples were determined as per Section 4.2.5. The original (Section 5.2.1) and sheared (Section 5.2.2.1) samples were diluted to a final concentration of 0.5% w/w with the mobile phase (0.1 M sodium nitrate containing 0.02% sodium azide). All experiments were repeated three times, each with two measurements.

6.2.4. Laser diffraction

The particle-size distribution of the original (Section 5.2.1) and sheared (Section 5.2.2.1) DWPS samples was determined as per section 4.2.2. All experiments were repeated three times, each with three measurements.

6.2.5. Dynamic light scattering

The z-average hydrodynamic diameter of the original (Section 5.2.1) and sheared (Section 5.2.2.1) DWPS samples was determined *via* DLS (ZetaSizer Pro, Malvern Panalytical Ltd., Malvern, Worcestershire, England) as per Section 4.2.3. All experiments were repeated three times, each with three measurements.

6.2.6. Starch content determination

The original (Section 5.2.1) and sheared (Section 5.2.2.1) DWPS samples were filtered through a 5.0 µm syringe filter (Minisart® Syringe Filters, Sartorius AG, Göttingen, Germany). Starch content was determined using the phenol-sulphuric acid method (Dubois, Gilles, Hamilton, Rebers, & Smith, 1956) with some modifications. Briefly, 0.15 mL of DWPS (diluted right ~625 times), standard or blank was added to a test tube, followed by the addition of 0.15 mL phenol (5% w/w) and 0.75 mL of concentrated sulphuric acid. The mixture was vortexed and heated in a boiling water-bath for 10 min. The samples were then cooled to room temperature and the aliquots were loaded into a 96-well plate after 30 min. Absorbance readings were taken at 490 nm *via* a multi-plate reader (SPECTROstar Nano, BMG LABTECH, Ortenberg, Germany) at 20 °C. Standard curves were plotted with DWPS at concentrations of 20, 40, 60, 80, 100 and 160 mg/kg. All experiments were repeated three times, each with three measurements.

The remained unsheared and sheared DWPS after passing through a 5.0 µm filter was calculated using Equation 6-1:

$$Remaining\ DWPS\ with\ respect\ to\ original\ unsheared\ DWPS\ (\%\ w/w) = \frac{Quantity\ of\ starch\ in\ the\ filtered\ and/or\ sheared\ sample}{Quantity\ of\ starch\ in\ the\ original\ sample} \times 100\% \qquad \text{(Equation 6-1)}$$

6.2.7. Turbidity measurements

The absorbance of the original and sheared DWPS samples (Section 5.2.2.1) was obtained using a 96-well plate and multi-plate reader (SPECTROstar Nano, BMG LABTECH, Ortenberg, Germany) at 640 nm (at 20 °C). All experiments were repeated three times, each with three measurements. The absorbance was determined against blank. The turbidity of the samples was calculated using Equation 6-2 (Pearce & Kinsella, 1978):

$$Turbidty = \frac{2.303 \times Absorbance\ at\ 640\ nm}{path\ length\ (cm)} \qquad \text{(Equation 6-2)}$$

Where 2.303 = $\ln 10$ (a constant) is the conversion factor between common to natural logarithms.

6.2.8. Statistical analysis

A one-way analysis of variance (ANOVA) with Tukey's test was used to test significant differences among mean values using Minitab (Minitab 18, Minitab Inc, Sydney, Australia).

6.3. Results and discussion

6.3.1. Turbidity of unsheared and sheared DWPS samples

In Section 5.3.4.3, the turbidity of 120 °C DWPS was observed to increase upon shear. The turbidity reading of DWPS samples (120–150 °C) before and upon shear at 1000 s^{-1} for 5 min was quantified (Figure 6-1). As expected, the turbidity of 120 and 140 °C DWPS samples increased significantly upon shear. In contrast, no change in turbidity upon shear was detected for 150 °C DWPS (Figure 6-1). The increase in turbidity is usually attributed to an increase in particle size, as a result of polymer-polymer interactions (Liu, Oey, Bremer, Carne, & Silcock, 2017b; Lu & Baik, 2015). However, the increased turbidity could also be caused by other physical mechanisms. The shear action could cause mechanical fragmentation of starch polymers and generate an increased number of smaller starch particles (Cave *et al.*, 2009; Hall *et al.*, 2016). The change in the number of particles and conformation of starch polymer fragments could influence the refractive index of the sheared starch sample and alter its turbidity (Linke & Drusch, 2016; Niskanen *et al.*, 2019). Thus, to understand how shear affects the polymer chains and fragments of DWPS samples, characterisation of the molecular and particle sizes of original and sheared DWPS samples was conducted in Section 6.3.2 and Section 6.3.3, respectively.

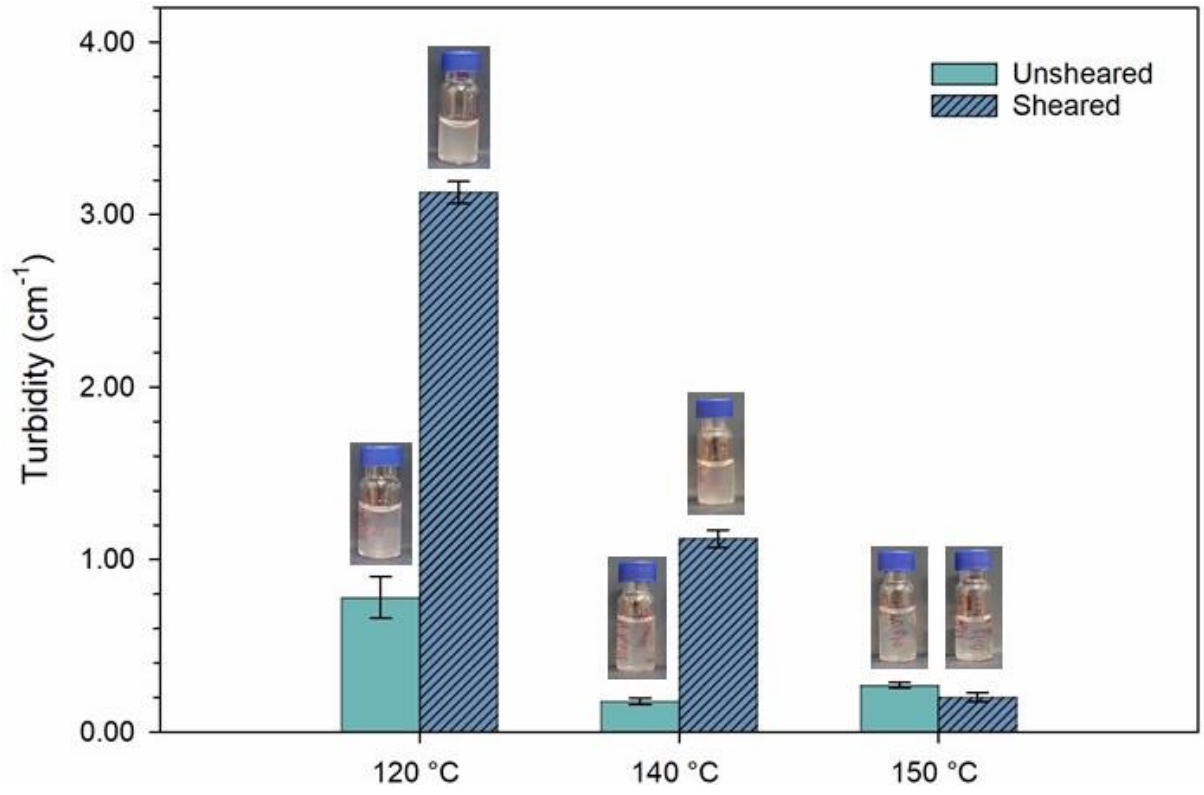

Figure 6-1 Turbidity of 5% w/w unsheared and sheared DWPS samples treated at 120, 140 and 150 °C. Values are plotted as means ± standard error, with measurements taken at 20 °C.

6.3.2. Molecular parameters of unsheared and sheared DWPS samples

The LS and dRI chromatograms of unsheared and sheared DWPS samples obtained by SEC-MALLS are presented in Figure 6-2. Note that the chromatographs of unsheared DWPS samples shifted right compared to the chromatographs of DWPS shown in Figure 4-3. The shift (disappearance of the larger molecular fraction) could be due to the ageing of DWPS (~2.5 years), where the DWPS polymers had degraded during storage. It is to be noted that the degradation did not affect the shear-induced rheological properties of DWPS (Appendix C).

An increase in elution time through the size-exclusion column was observed in 120 and 140 °C DWPS samples upon shear (Figure 6-2A and B). The longer elution time suggests a decrease in the size of the molecular fractions upon shear. From the molar mass data, the M_w of sheared 120 and 140 °C DWPS samples decreased by ~4-fold and 3-fold respectively, as compared to their unsheared samples (Table 6-1). A similar decreasing trend was also noted in their R_z (Table 6-1). However, the chromatograph, M_w and R_z of 150 °C DWPS were unaffected by shear action (Figure 6-2C and Table 6-1). The trend is consistent with their rheological properties where an increase in consistency coefficient (Table 5-2) and viscoelasticity moduli (Figure 5-3) was observed for DWPS samples treated at 120 and 140 °C, while no change was noted for 150 °C DWPS.

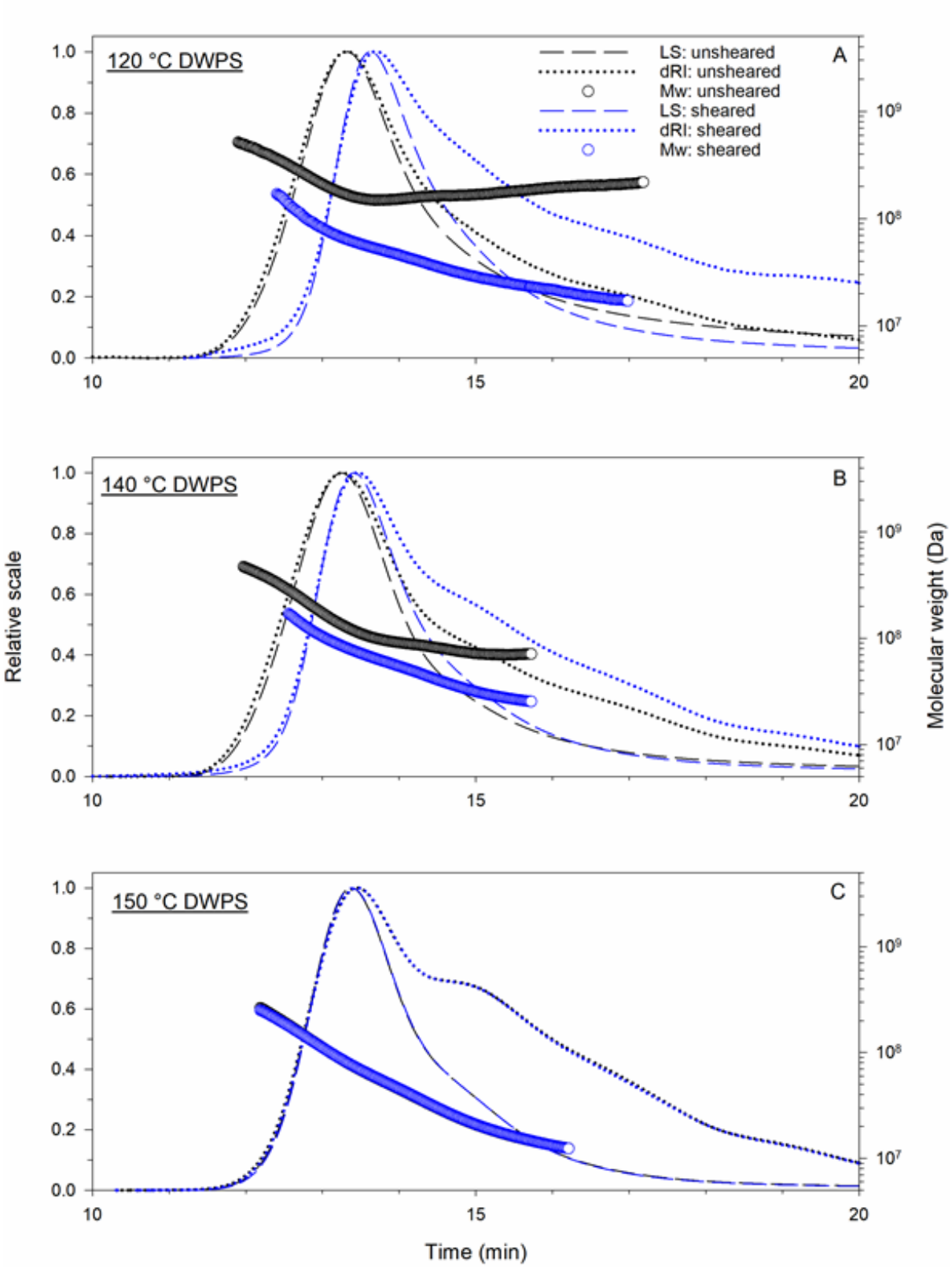

Figure 6-2 Light scattering (LS) signal, differential refractive index (dRI) signal and weight-average molar mass (M_w) of unsheared and sheared DWPS samples treated at (A) 120, (B) 140 and (C) 150 °C eluted with 0.1 M sodium nitrate containing 0.02% sodium azide.

Table 6-1 Weight-average molar mass (M_w) and root-mean-square radius (R_z) of unsheared and sheared DWPS samples treated at 120, 140 and 150 °C.

		Weight-average molar mass, $M_w \times 10^6$ (Da)	**Root mean square radius, R_z (nm)**
120 °C	Unsheared	178.6 ± 7.8^{a}	217 ± 4^{a}
	Sheared	47.4 ± 2.6^{d}	124 ± 3^{d}
140 °C	Unsheared	141.6 ± 3.4^{b}	204 ± 3^{b}
	Sheared	65.4 ± 2.1^{c}	136 ± 2^{c}
150 °C	Unsheared	56.3 ± 0.7^{cd}	145 ± 1^{c}
	Sheared	56.1 ± 0.3^{cd}	144 ± 0^{c}

Values are expressed as means ± standard error. Values denoted with the same superscripts in the same column are not significantly different ($p \leq 0.05$).

6.3.3. Particle size of unsheared and sheared DWPS samples

From Chapter 4, DWPS samples were found to contain starch fragment > 1 µm. As such, the size and concentration of these fragments could also be responsible for the shear-induced rheological properties seen at 120 and 140 °C DWPS samples. Thus, the particle-size distributions of unsheared and sheared DWPS samples were characterised using DLS and LD. Based on the manufacturer's specifications, the reliable ranges of particle size measurement for the ZetaSizer Pro (DLS) and MasterSizer 2000 (LD) are 0.3 nm to 10 µm and 0.02–2000 µm, respectively (Malvern Panalytical, 2021a, 2021b). Thus, the use of both techniques is required to measure the complete size range of DWPS as the samples contained both nano-size polymers and micro-size fragments. Both techniques showed multiple size fractions in unsheared-120 °C DWPS. DLS results revealed that unsheared-120 °C DWPS consisted of polymers and fragments ranging from 10 nm to 10 µm, whereas LD showed a particle-size distribution between 30 nm and 400 µm (Figure 6-3A). Upon shear, DLS results showed that the particle-size distribution shifted right, indicating an increase in particle size, as the smaller molecular fraction shifted to a larger particle size range. However, in the case of LD measurements, upon shear, 120 °C DWPS was reduced to a smaller particle size range, with the major peak shifting from ~90 to 9 µm particles. The results suggest that the larger fractions in 120 °C DWPS were fragmented into smaller sizes. The shift to a larger size range detected in DLS for the smaller particles/molecules could be attributed to amylopectin chain associations (discussed in Chapter 5). In addition, small fragments that were disrupted by shear from the large starch fragments could also be contributing to the larger size range in DLS. The results imply that the shear-induced rheological properties (*i.e.*, shear-thickening, anti-thixotropy and shear-induced gelation) for 120 °C DWPS are

possibly due to the changes in fragment size and its distributions. To further validate the claim of a reduction in particle size of large molecular fractions in 120 °C DWPS upon shear, attempts were made to pass the unsheared and sheared samples through a 5 µm filter. The unsheared-120 °C DWPS was unable to pass through a 5 µm filter but the sheared-120 °C DWPS could pass through it, which was evidence, that the sheared-120 °C sample was indeed smaller in particle size than that of the unsheared-120 °C DWPS (Figure 6-4). Similar observations were made by Kim *et al.* (2002), where the authors explained the observed shear-thickening behaviour in their experiment as a cluster-breaking process. The authors believe that the original starch samples contained a high concentration of starch clusters, which are broken down by the shear action from the rheometer, dispersing these clusters. The dispersed clusters probably led to an increase in the effective starch volume fraction and hence, its viscosity.

Similar observations in particle-size distributions were also made with 140 °C DWPS, with an increase in DLS particle size (major peak shifted from 15 nm to peaks at 126 nm and 5400 nm) and a decrease in LD particle-size distribution (major peak shifted from ~100 to ~8 µm) upon shear. The change in particle-size distribution (Figure 6-3B) was accompanied by a slight increase in rheological properties (anti-thixotropy behaviour in Figure 5-2D and increased viscoelastic moduli in Figure 5-3) upon shear. The lower extent of shear-induced structure in 140 °C DWPS (compared to 120 °C DWPS), could be explained by a high concentration of smaller particles (80–300 nm) in the sheared-140 °C DWPS observed in DLS data. In the case of 150 °C DWPS, no change in particle-size distribution (Figure 6-3C) and rheological properties (Figure 5-2E and Figure 5-3) were observed upon shear. These results further supported the hypothesis that the change in size distribution of DWPS led to the alteration in its rheology, where a generation of smaller particle sizes ranging from 2 to 20 µm (seen in both DLS and LD analyses) is critical for shear-induced behaviours (absented in 150 °C DWPS). It is also noteworthy that although 140 °C DWPS contained large fragments (peak ~100 µm) that were similar to those in 120 °C DWPS (Figure 6-3A and Figure 6-3B), 140 °C DWPS was able to pass through a 5 µm filter, but not 120 °C DWPS. The result could suggest that the large fragments in 140 °C DWPS dissociated easily under shear force when the samples were pushed through the filter (Figure 6-4).

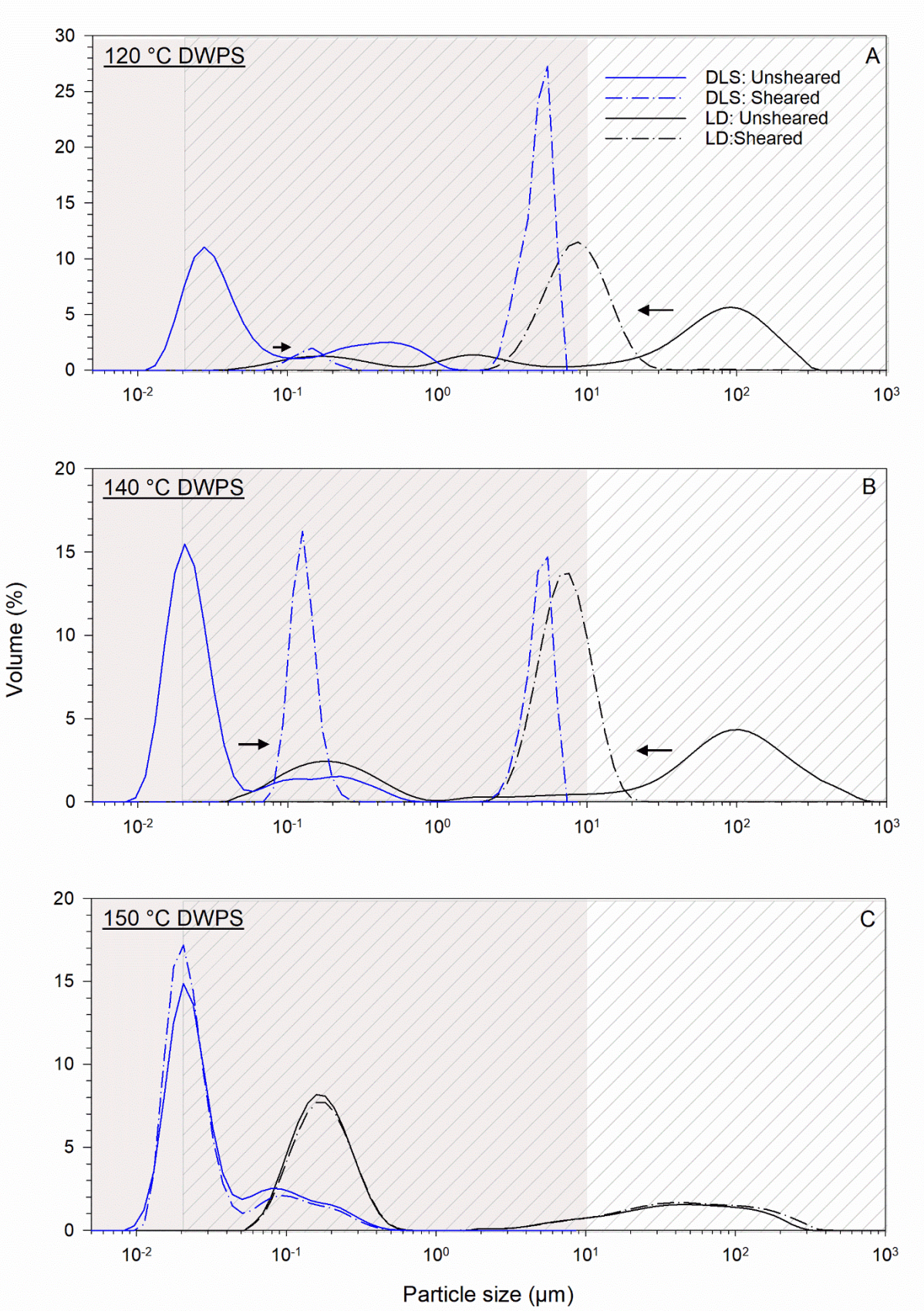

Figure 6-3 Particle-size distribution of unsheared and sheared DWPS samples treated at: (A) 120, (B) 140 and (C) 150 °C determined using dynamic light scattering (DLS; with measurable region coloured in grey) and laser diffraction (LD; with measurable region shaded in grey).

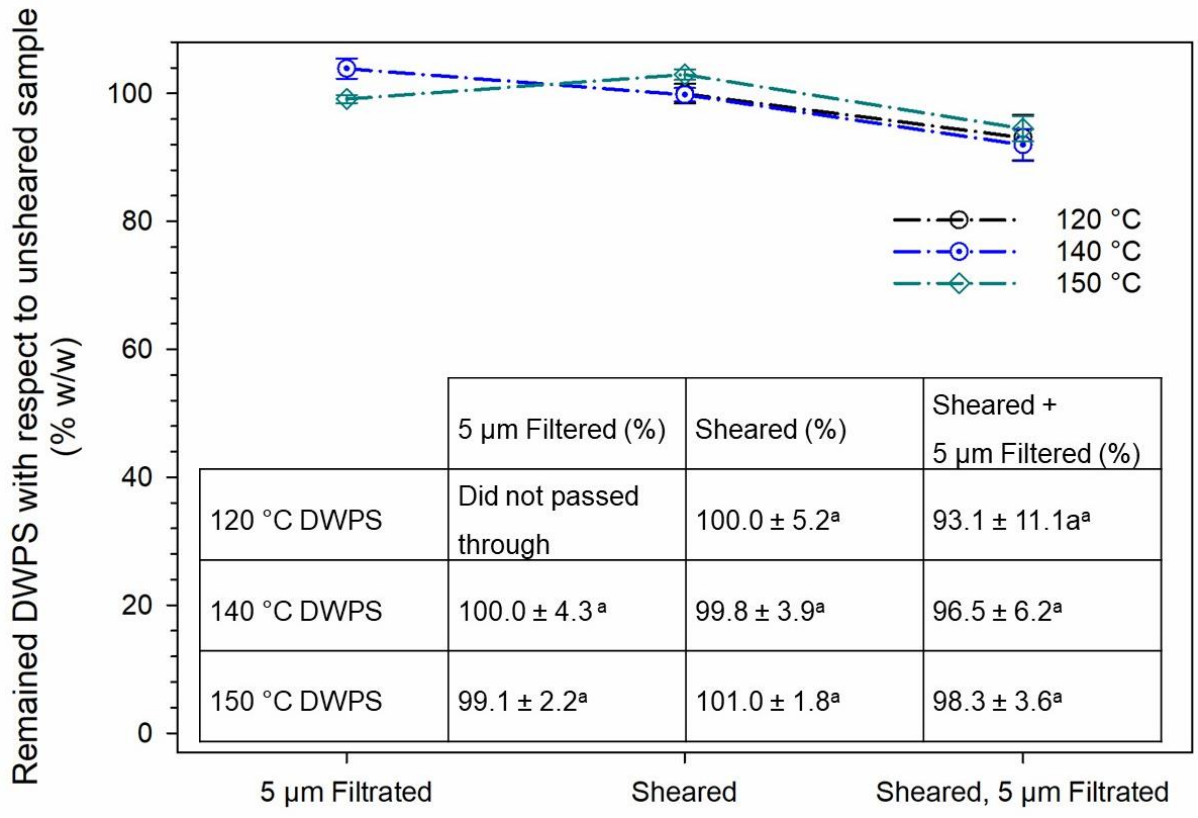

	5 µm Filtered (%)	Sheared (%)	Sheared + 5 µm Filtered (%)
120 °C DWPS	Did not passed through	100.0 ± 5.2[a]	93.1 ± 11.1a[a]
140 °C DWPS	100.0 ± 4.3 [a]	99.8 ± 3.9[a]	96.5 ± 6.2[a]
150 °C DWPS	99.1 ± 2.2[a]	101.0 ± 1.8[a]	98.3 ± 3.6[a]

Figure 6-4 DWPS samples treated at 120, 140 and 150 °C that remained (% w/w, with respect to the original unsheared sample) after passing through a 5 µm filter or sheared at 1000 s^{-1} for 5 min or sheared at 1000 s^{-1} for 5 min and then passed through a 5 µm filter. Note that unsheared-120 °C DWPS cannot be filtered through a 5 µm filter. Values are plotted as means ± standard error, with measurements taken at 20 °C.

6.3.4. Effect of environmental conditions on the shear-thickening behaviour of 120 °C DWPS

The shear-thickening mechanism of 120 °C DWPS was studied in the presence of different environmental conditions, *i.e.*, at varied urea and ionic strength concentrations, and temperatures to probe for hydrogen bonding, electrostatic and hydrophobic interactions respectively, as these interaction forces could be responsible for the mechanism.

6.3.4.1. Effect of urea

The influence of urea (0–3.0 M) on the viscosity curve of 5% w/w 120 °C DWPS is shown in Figure 6-5. Interestingly, no noticeable changes in the extent of shear-thickening behaviour (*i.e.*, the ratio between maximum viscosity and viscosity at critical shear rate; η_{max}/η_{crit}) were observed when urea concentration was increased from 0 to 3.0 M. Urea behaves as a chaotropic agent that competes for binding sites to disrupt hydrogen bonds (Bennion & Daggett, 2003; Kuo & Wang, 2006). Thus, the shear-thickening behaviour for 120 °C DWPS was unlikely to be contributed by hydrogen bonding. The result was interesting, as amylopectin chains contain a high amount of hydroxyl groups, with the

potential for hydrogen bonds to occur (De Azeredo, Rosa, De Sá, Souza Filho, & Waldron, 2014; Tako & Hizukuri, 2002). Moreover, hydrogen bonding is often responsible for shear-thickening and/or anti-thixotropy behaviour in polymers such as pectin solutions (Kjøniksen, Hiorth, Roots, & Nyström, 2003) and Mamaku gum (Jaishankar *et al.*, 2015). A slight increase in the viscosity of 120 °C DWPS was also observed at increased urea concentration (Figure 6-5). Such an increase in polymer viscosity has been reported in chitosan (Tsaih & Chen, 1997), fenugreek gum and xyloglucan (Winkworth-Smith, MacNaughtan, & Foster, 2016) in the presence of added urea. Urea is believed to cause the breakage of intra-molecular hydrogen bonding of these polymer chains, resulting in a more extended polymer chain conformation, which led to the observed increment in viscosity. Moreover, Chen *et al.* (2019) reported that 12% w/w urea (~2.0 M) increased the solubility of native maize starch granules from ~3% w/w to ~28% w/w. The samples containing higher urea concentration could have caused further solubilisation of starch fragments in 120 °C DWPS, leading to increased viscosity.

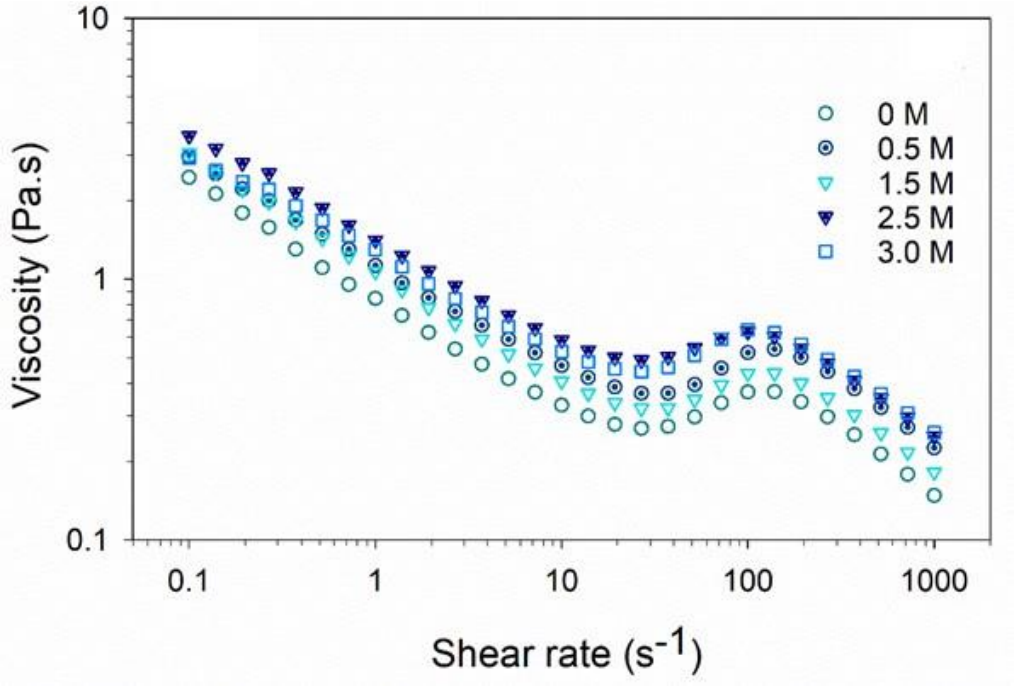

Figure 6-5 Effect of urea on the viscosity of 5% w/w 120 °C DWPS at 0, 0.5, 1.5, 2.5, and 3.0 M urea. Measurements were taken at 20 °C.

6.3.4.2. Effect of ionic strength

Waxy potato starch contains phosphate groups that carry negative charges, which present the potential for electrostatic interactions to occur among the starch polymers and/or with the dissolved salt in the sample (Fang *et al.*, 2020a; Wee, Matia-Merino, & Goh, 2015a). Thus, 120 °C DWPS samples (5.0 % w/w) containing varied NaCl concentrations (0–0.5 M) were used to investigate if the shear-thickening phenomenon was contributed by electrostatic interactions. The addition of NaCl up to 0.5 M did not affect the extent of shear-thickening behaviour in this sample (Figure 6-6). In a separate

experiment, no changes in shear-thickening behaviour were noted in 120 °C DWPS (~2% w/w) after 48 h of dialysis (Appendix D). Hence, these results suggest that shear-thickening mechanism is unlikely to be contributed by electrostatic interactions (Wee *et al.*, 2015a). A slight reduction in viscosity was observed at NaCl concentration as low as 0.001 M. A further decrease in viscosity profile was observed at 0.005 M NaCl. No further reduction in viscosity was observed at NaCl concentrations greater than 0.005 M. The reduction in sample viscosity could be due to the shielding effect provided by sodium ions on the phosphate group of the 120 °C DWPS, which decreased electrostatic repulsion between the negatively charged starch polymers. The reduced repulsion could lead to a decrease in the hydrodynamic volume of polymer chains, causing a subsequent viscosity reduction (Tan, Tam, & Jenkins, 2001; Zhang, Zhou, Zhai, Liu, & Gao, 2008).

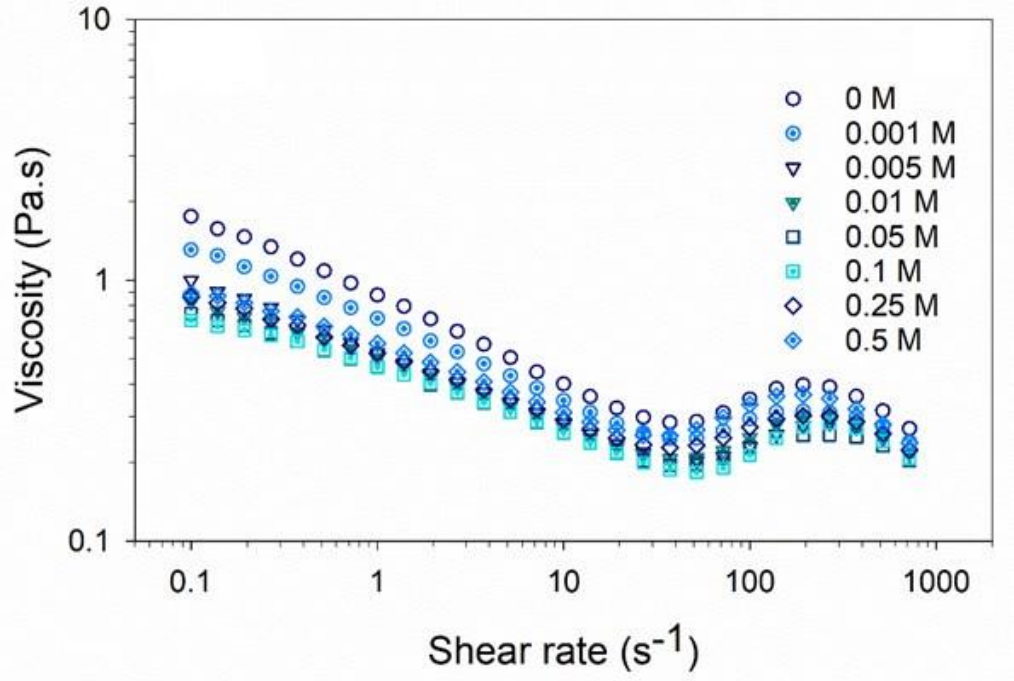

Figure 6-6 Effect of NaCl on the viscosity of 5% w/w 120 °C DWPS, at 0, 0.001, 0.005, 0.01, 0.05, 0.1, 0.25, and 0.5 M NaCl. Measurements were taken at 20 °C.

6.3.4.3. Effect of temperature

The effect of temperature (20–95 °C) on the viscosity of 5% w/w 120 °C DWPS is presented in Figure 6-7A, where an overall shift along the x-axis and y-axis of the viscosity profile was observed with increasing temperature. The reduction in viscosity is to be expected as an increase in temperature results in provision of additional thermal energy to the system, directly increasing the polymer chain mobility. In addition, the free volume of the system would also increase with temperature, providing further intermolecular distance between polymer chains. Thus, a reduced flow resistance experienced by the polymer chains led to an overall reduction in viscosity. The results are in agreement with the effect of temperature on other polymer solutions (Briscoe, Luckham, & Zhu, 1998; Kulicke & Clasen,

2004; Waxham, 2007). Both $\dot{\gamma}_{crit}$ and viscosity at critical shear rate (η_{crit}) at different temperatures (20–95 °C) were found to obey the Arrhenius model (Figure 6-7B). In other words, the interactions governing the mechanism of shear-thickening were weakened with increasing temperature. Moreover, the maximum viscosity (η_{max}) and the inverse of its corresponding shear rate at η_{max} ($1/\dot{\gamma}_{max}$) exhibited similar exponential dependencies (~$e^{-0.02T}$) on temperature (Figure 6-7C), where $1/\dot{\gamma}_{max}$ can be interpreted as the mean relaxation time of the associations. The observed shear-thickening region at shear rate below $\dot{\gamma}_{max}$ is probably a result of a longer mean relaxation time (due to sample association) compared to the experimental timescale (Kosvintsev *et al.*, 2001). These similar exponential dependencies (~$e^{-0.02T}$) indicate that the stress required for the onset of shear-thinning after shear-thickening remained relatively constant at shear stress values between ~28 and 45 Pa within the temperature range studied. Tan *et al.* (2001) attributed the stress required for the onset of shear-thinning to the number and strength of intermolecular associations that contributed to the total structural strength needed to induce shear-thinning upon reaching η_{max}. Thus, the results suggest that the increment in temperature had shortened the relaxation time but had a minimal effect on the number of associations. Therefore, based on these results, the effect of shear-thickening was unlikely to be contributed by hydrophobic interactions; these interactions get stronger with temperature. Taking the example of whey protein denaturation, when the hydrophobic regions are exposed upon heating, the hydrophobic bonds get stronger, resulting in subsequent aggregation that leads to an increment in structure/viscosity (Benoit, Afizah, Ruttarattanamongkol, & Rizvi, 2013; Oldfield, Singh, Taylor, & Pearce, 1998). Burckbuchler *et al.* (2006) also reported an enhancement of shear-thickening at increased temperatures of 35 and 45 °C from 15 °C in hydrophobically-modified alginate solution with added cyclodextrin compounds. Since no increment in the viscosity/shear-thickening behaviour of 120 °C DWPS was observed with increased temperature, the data suggest that shear-thickening was not likely to be influenced by hydrophobic interactions.

The thermal stability of the shear-induced gel was also studied by heating the sheared-120 °C DWPS at 90 °C for 20 min as presented in Figure 6-7D. The sample remained as a gel throughout the heating and cooling cycles, with an expected reduction in both *G'* and *G"* when the temperature was increased from 20 to 90 °C. There was no phase change from gel to sol when the sample was heated to 90 °C and held at 90 °C for 20 min. Such observations indicated that the gel sample was thermally irreversible. The thermal irreversible property is not typical of an amylopectin gel (Biliaderis, 2009; Durrani & Donald, 1995). Briscoe *et al.* (1998) observed a weaker gel structure when the shear-induced gel was heated up to 90 °C, the weakened structure was attributed to a greater intermolecular distance between polymer chains when compared to the original intermolecular distance before heat treatment. In a recent study by Fang (2017), 10% w/w waxy potato starch was sheared at 20 s^{-1} for 10

min to attain a shear-induced structure, where the *G'* of the sheared sample was significantly higher than that of the unsheared sample. The researchers attributed this observed shear-induced structure to double-helical aggregation between amylopectin chains *via* hydrogen bonding upon shear. When this shear-induced structure was subjected to a temperature sweep from 25 to 95 °C, the shear-induced structure was found to be thermal reversible at 65 °C (similar *G'* values were observed in both the sheared and unsheared samples at temperatures ≥ 65 °C), which differed from the experimental data of 120 °C DWPS. Thus, the thermal irreversibility of 120 °C DWPS at 90 °C further validated that hydrogen bonding was not responsible for the shear-induced structure.

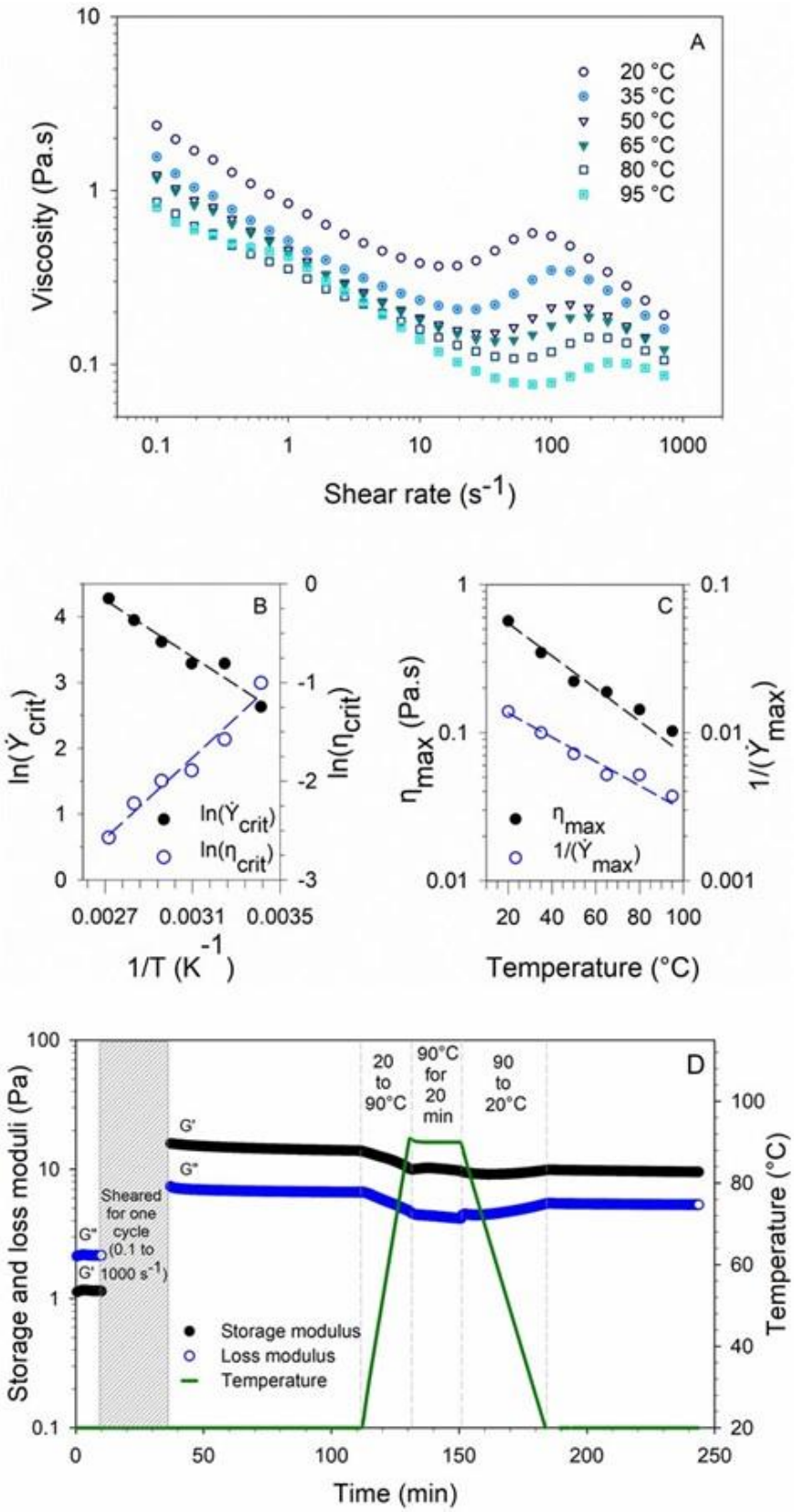

Figure 6-7 The effect of temperature on 5% w/w 120 °C DWPS: (A) viscosity at varied temperatures of 20, 35, 50, 65, 80, and 90 °C, (B) Arrhenius plots of critical shear rate ($\dot{\gamma}_{crit}$) and critical viscosity (η_{crit}), and (C) maximum viscosity (η_{max}) and characteristic time scale ($1/\dot{\gamma}_{max}$), and D) viscoelastic moduli of shear-induced structure heated at 90 °C for 20 min. The viscoelasticity was measured at 1% strain and 1 Hz frequency.

6.3.4.4. Combined effects of urea, ionic strength and temperature

As clearly evident from the presented results, hydrogen bonding, electrostatic or hydrophobic interactions was not the sole contributor to the observed shear-thickening phenomenon. A combined effect of: (i) 3 M urea and 0.1 M NaCl and (ii) 3 M urea, 0.1 M NaCl and temperature (95 °C) was tested on 5% w/w 120 °C DWPS, to validate if the shear-thickening behaviour could also be a result of the combination of the mentioned interactions acting synergistically. The viscosity results are presented in Figure 6-8. The addition of urea and NaCl did not result in the elimination of the shear-thickening behaviour in 120 °C DWPS measured at 20 and 95 °C (Figure 6-8). Hence, these observations suggest that the shear-thickening is not caused by a combined effect of hydrogen bonding, electrostatic and hydrophobic interactions.

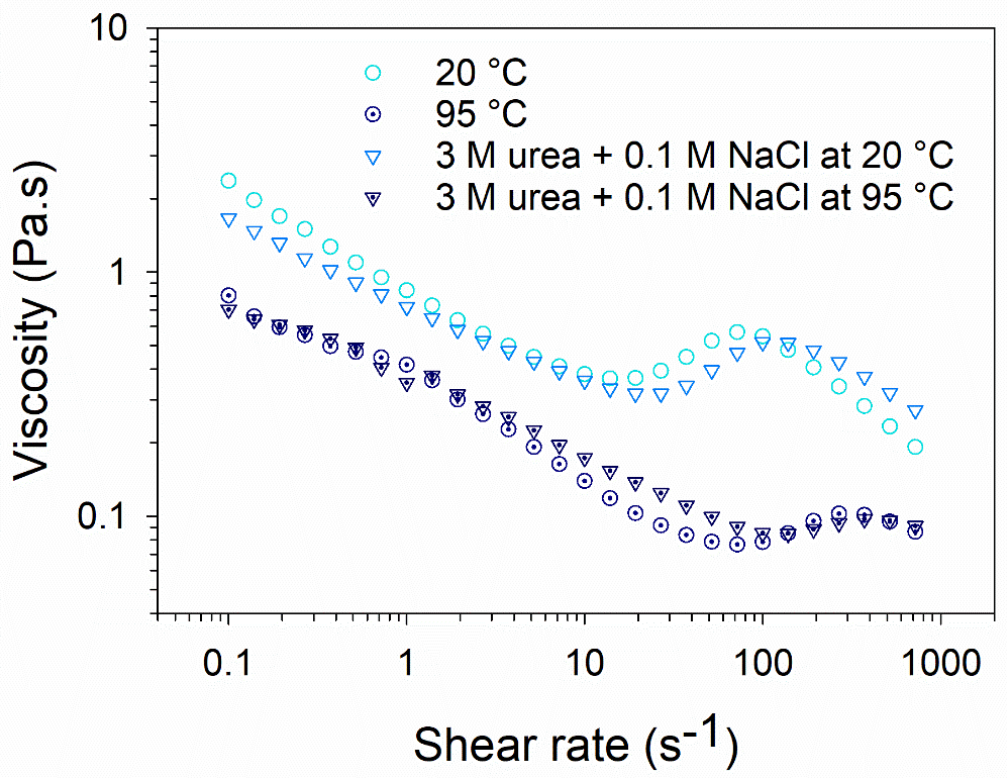

Figure 6-8 Combined effects of urea (3 M) and NaCl (0.1 M) with and without temperature (20 or 95 °C) on the viscosity of 5% w/w 120 °C DWPS.

6.3.5. Proposed mechanism for shear-thickening, anti-thixotropy and shear-induced gelation of DWPS

The DWPS was modified from waxy potato starch that contains mainly amylopectin chains. Amylopectin has a highly branched structure, which prevents intra- and intermolecular chain association due to the presence of high steric hindrance (Liu *et al.*, 2019). It is hypothesised that upon shear above their critical shear rate, the polymer chains of 120 and 140 °C DWPS samples are forced to realign in the direction of shear allowing reorientation of amylopectin chains to occur. The narrow

range of applied shear rates facilitates close proximity between polymer chains to occur, which causes reassociation between polymers to take place. This hypothesis is supported by the DLS results of 120 and 140 °C DWPS as the particle-size distribution shifted right, indicating that the small molecular fraction shifted to a larger particle size range. In addition to amylopectin chain reassociation, the maximum value of the major LD peak of 120 and 140 °C DWPS samples shifted from ~100 to 10 µm upon shear (Figure 6-3A and Figure 6-3B). The shift suggests that the shear-induced behaviours seen in 120 and 140 °C DWPS can also be attributed to the presence of a higher number of small starch fragments (2-20 µm), which increase the overall effective volume fraction of starch fragments in the solvent. The forces involved in the mechanism were not caused by hydrogen bonding, electrostatic, hydrophobic interactions, or the combination of these interactions. Thus, with the current findings, it is hypothesised that the mechanism for shear-induced behaviours (*i.e.*, anti-thixotropy together with or without shear-thickening and gelation) is likely to be a two-step process where: (i) the starch fragments were reduced in size and (ii) the subsequent shear action allows the amylopectin chains and smaller fragments to be in very close proximity, which could lead to generation of network from amylopectin chain associations and physical interlocking of fragments when these soft particles slide past each other during shear (Figure 6-9). Further work on identifying the exact mechanism that governs the shear-induced interactions is recommended.

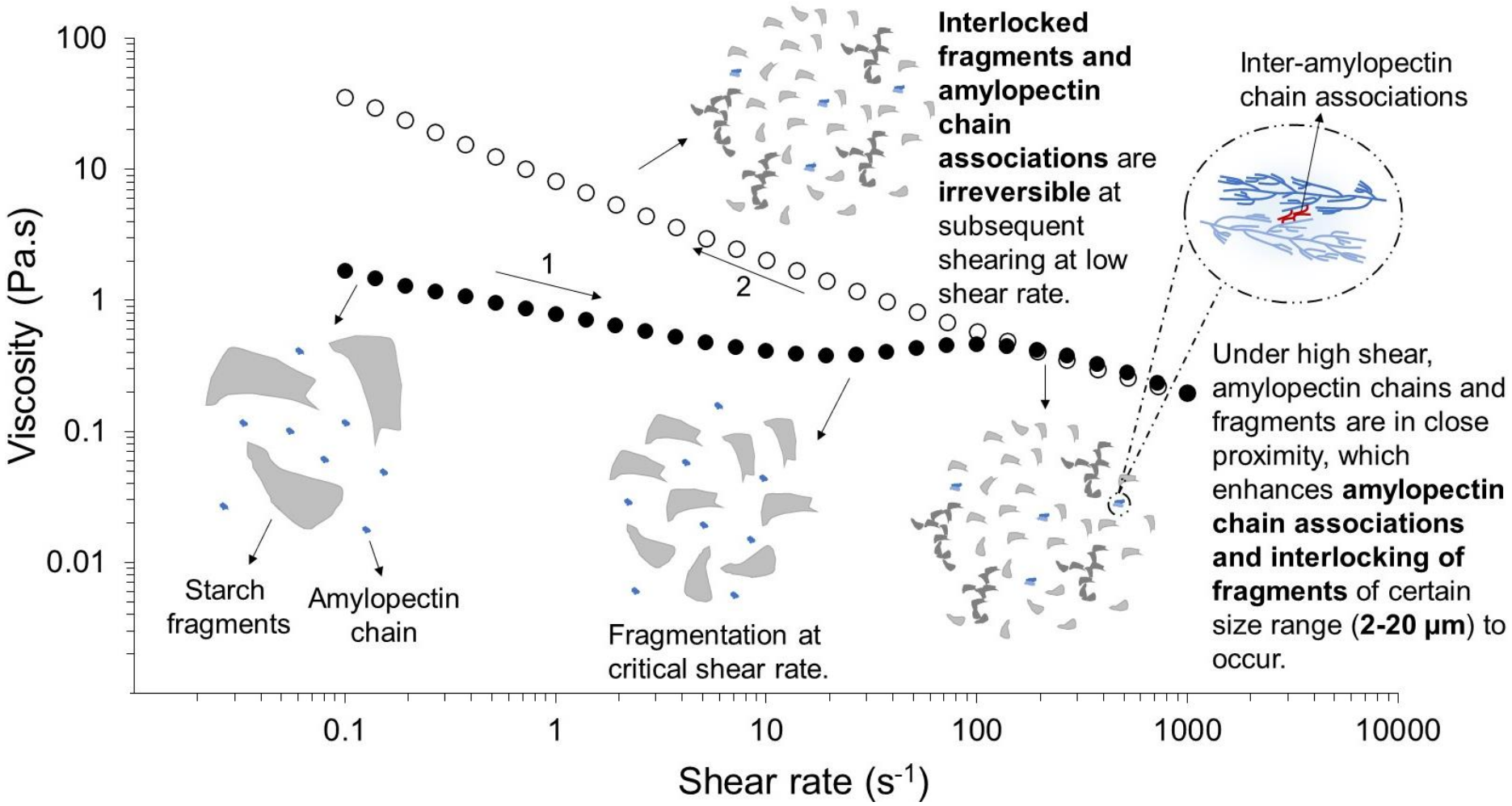

Figure 6-9 Schematic illustration of shear-thickening and anti-thixotropy mechanism of 120 °C DWPS.

6.4. Conclusions

The shear-induced behaviours (*i.e.*, anti-thixotropy together with or without shear-thickening and gelation) observed in the DWPS were attributed to the presence of starch fragments in the samples. Upon shear, the starch fragments were broken down into smaller fragments, which caused an increase in the effective starch volume fraction. The subsequent shear resulted in the amylopectin chains and smaller fragments being in very close proximity, probably leading to amylopectin physical chain associations and interlocking of fragments of a certain size range (2–20 μm). These mechanisms would then generate a network, resulting in an irreversible weak gel structure of DWPS. The results from this chapter have provided further insights into the structural behaviour of DWPS dependent on its temperature treatment and shear post-processing. In the next chapter, the feasibility of DWPS as an ingredient in a food gel matrix system was evaluated by studying the influence of DWPS in a WPI gel (Chapter 7).

Chapter 7 The influence of de-structured starch on the mechanical properties, microstructure, and water immersion stability of polymeric and particulate whey protein isolate gels[1]

7.1. Introduction

Whey protein has excellent gelling properties. The mechanical and microstructural properties of whey protein gels are strongly affected by the environmental conditions (*i.e.*, ionic strength and pH) at which the gels are formed (Twomey, Keogh, Mehra, & O'Kenndey, 1997). A clear fine-stranded gel is formed at low ionic strength and at pH away (< pH 4 or > pH 6) from the isoelectric point of whey (p*I* ~5.1). On the other hand, an opaque particulate gel with a coarse-stranded structure is formed when pH is close to the p*I* of whey (4 < pH < 6) or at high ionic strength (Langton & Hermansson, 1992; Urbonaite *et al.*, 2016). Studies have shown that particulate gels are stiffer, less elastic and have poorer water-holding capacity than fine-stranded polymeric gels (Lefèvre & Subirade, 2000; Lucey, 2008).

The mechanical and microstructural properties of whey protein gels can be altered by adding another polymer, such as starch polymers (Aguilera, 2000; Fu & Nakamura, 2017; Lavoisier & Aguilera, 2019). The resulting gel properties are hence dependent on the thermodynamic compatibility between these two polymers. In the case of thermodynamic incompatibility (segregative interactions), phase separation occurs (Çakır & Foegeding, 2011). When these binary polymer systems are being heated, phase separation—enhanced with raising temperature (Bryant & McClements, 2000)—and gelation can occur concurrently. The phase separation largely ceases once the gel network is formed. A wide range of gel textures can be obtained by manipulating the thermodynamic incompatibility to create

[1]Parts of this chapter were submitted as Ang, C. L., Matia-Merino, L., Lim, K., & Goh, K. K. T. (2023). Influence of de-structured starch on fine-stranded polymeric and coarse-stranded particulate whey protein gels. *Food Hydrocolloids, 135*, 108201.

different degrees of phase separation and rate of gelation of these mixed polymer systems. The thermodynamic incompatibility of a mixed system can also be altered by changing the M_w of polymers, pH and ionic strength (Tolstoguzov, 2000). It is hypothesised that the addition of DWPS materials with varied molecular sizes can alter the gel properties of whey protein. Such gel manipulation can be useful in structuring new "clean-label" high-protein foods that are different from WPI-based gel containing conventional gelatinised starch. To the best of this author's knowledge, there is no literature reporting on the interaction between WPI and DWPS. Thus, in this study, the influence of DWPS on WPI gels was elucidated, by characterising the phase stability of the liquid mixed polymers, and the mechanical properties, microstructure, and water-immersion stability of WPI + DWPS composite gels at pH 5 and 7. Gels formed at pH 5 and 7 represent coarse-stranded particulate and fine-stranded polymeric protein gel systems, respectively. The results from this interaction study are beneficial for using DWPS to structure foods with different textural and functional properties.

7.2. Materials and Methods

7.2.1. Sample preparation of whey protein + starch mixtures at pH 7 and pH 5

Stock samples of 25% WPI (SureProtein^{TM} WPI 895, Fonterra Co-operative Group Limited, Auckland, New Zealand) and 11% w/w of DWPS (120–150 °C) were dispersed in Milli-Q water. Stock WPI solution was hydrated overnight at 4 °C under constant stirring. The DWPS stock dispersions were immersed in a boiling water-bath for 1 h while being mixed with a vortex to ensure sample homogeneity. For comparison purposes, two additional samples (11 % w/w) were used as control samples against DWPS samples: (i) waxy potato starch gelatinised at 95 °C for 30 min under continuous shear at 300 rpm and (ii) maltodextrin heated in boiling water-bath for 1 h. All the stock solutions were degassed for 2 h (under vacuum) and equilibrated to room temperature before use. The pH of samples was adjusted to either pH 5 or 7 with 0.5 M HCl or 0.5 M NaOH solution, respectively. The stock samples were then combined to achieve WPI solutions containing 13, 14, 15, 16 and 17% w/w WPI and mixtures containing 13% w/w WPI + 4% w/w maltodextrin or gelatinised starch or DWPS. The samples were stirred for 30 min to ensure proper mixing.

7.2.2. Phase stability

The phase stability of pure WPI solutions and mixtures at pH 5 and 7 was determined visually (*i.e.*, signs of phase separation) over 24 h at 20 °C. Sodium azide (0.02% w/w) was added as preservative.

7.2.3. Rheological measurements

Rheological measurements were performed using a Paar Physica MCR 302 rheometer in controlled shear rate (CSR) mode (Anton-Paar, Graz, Austria). Approximately 0.8 mL of a pure WPI solution or a mixture (WPI + gelatinised starch or maltodextrin or DWPS samples) was loaded onto a 25 mm serrated plate geometry (PP25/2 and P-PTD 200/56/I) at 1 mm sample gap. The sample was pre-sheared at 10 s^{-1} for 60 s and rested for 5 min at 20.0 ± 0.1 °C. To minimise evaporation, a thin layer of mineral oil around the sample and a solvent trap were used during measurement. The heat-induced gelation was carried out at 5 °C/min from 20 to 95 °C, followed by cooling to 20 °C at 5 °C/min. Readings of G', G'' and tan δ were collected at 1% strain and 1 Hz frequency (within the LVR) during the heating and cooling phases. The sample was then allowed to rest for 5 min at 20 °C before a frequency sweep from 0.1 to 20 Hz at 1% strain was conducted. Note that all the samples in this chapter can be defined rheologically as gels, as the G' were above their G'' with tan $\delta < 0.2$. Thus, only G' values were presented. Each set of experiments was repeated three times with at least two measurements.

7.2.4. Zeta-potential measurements

The zeta-potential of maltodextrin at its native pH was determined as per Section 0. All experiments were repeated three times, each with five measurements.

7.2.5. Textural measurements

7.2.5.1. Gel preparation

The WPI solutions and mixtures (~5 g) as described in 7.2.1 were loaded into a round silicone mould (20 mm diameter, 15 mm height). To ensure homogeneity, all samples were gently stirred prior to loading. Heat-induced gelation of samples was carried out in a 90 °C water-bath for 30 min. The gels were stored overnight at 20 °C before removal from the mould for further analysis.

7.2.5.2. Gel hardness

The textural hardness of the prepared gel samples was determined using a TA.XT plus texture analyser (Stable Micro System, Godalming, England) *via* a compression test. A 35 mm cylindrical metal probe and a 50 kg load cell were used. Measurements were conducted at pre-test, test and post-test speeds of 0.5 mm/s, 1 mm/s and 5 mm/s, respectively, with a trigger force of 0.049 N and 75% deformation. The textural hardness is determined from the resulting plots of force versus time as the maximum force during the compression. Each set of experiments was repeated three times with at least five measurements.

7.2.6. Syneresis measurements

The syneresis of the gel samples was determined using the method by Charoenrein, Tatirat, & Muadklay (2008) with modifications. Gels were placed into cylindrical tubes, where the end of each cylindrical tube was covered with a filter paper. The cylindrical tube was then attached to the cap of a centrifuge tube. The samples were then centrifuged at 1000 *g* for 5 min. The released serum from the gel was absorbed by the filter paper and accumulated at the bottom of the centrifuge tube as supernatant. Syneresis of the gels is calculated using Equation 7-1:

$$Syneresis\ (\%\ w/w) = \frac{Weight\ of\ supernatant}{Weight\ of\ original\ gel} \times 100\% \qquad \text{(Equation 7-1)}$$

Each set of experiments was repeated three times with at least two measurements. Note that due to the high water-holding capacity of gels at pH 7, no syneresis was detected for all gel samples, thus only results for gels at pH 5 are presented.

7.2.6.1. Protein leaching

The quantity of leached protein from the gel during centrifugation was determined *via* Bradford protein assay. The Bradford assay dye reagent concentrate (5000006, Bio-rad, Hercules, CA, USA) was diluted five-fold with Milli-Q water and filtered through a Grade 1 filter paper (Whatman plc, Maidstone, England). Briefly, 10 µL of supernatant (at diluted concentration with absorbance ranging from 0.2–0.8), standard or blank, were pipetted into a 96-well plate. The diluted reagent (200 µL) was then added to each well and the samples were kept at room temperature for 15 min. The absorbance of samples was measured at 595 nm with a multi-plate reader (SPECTROstar Nano, BMG LABTECH, Ortenberg, Germany). BSA was used as a standard for calibration curve at protein concentrations of 0.05, 0.1, 0.2, 0.4 and 0.5 mg/mL. The degree of protein leaching is calculated using Equation 7-2:

$$Leached\ protein\ (\%\ w/w) = \frac{Weight\ of\ protein\ in\ supernatant}{Weight\ of\ total\ protein\ in\ original\ gel} \times 100\% \qquad \text{(Equation 7-2)}$$

Each set of experiments was repeated three times with at least two measurements.

7.2.6.2. Carbohydrate leaching

The quantity of leached carbohydrate from the gel after centrifugation was determined *via* phenol-sulphuric acid method as per Section 6.2.6. Maltodextrin, waxy potato starch and DWPS were used as the standards for their respective calibration curves at carbohydrate concentrations between 20 and 140 mg/kg. The degree of carbohydrate leaching is calculated using Equation 7-3:

$$Leached\ carbohydrate\ (\%\ w/w) =$$

$$\frac{Weight\ of\ carbohydrate\ in\ supernatant}{Weight\ of\ total\ carbohydrate\ in\ original\ gel} \times 100\% \qquad \text{(Equation 7-3)}$$

Each set of experiments was repeated three times with at least two measurements.

7.2.7. Gel water-immersion test

The gel water-immersion stability was evaluated by immersing the gel samples in Milli-Q water containing 0.02 % w/w sodium azide at a 1:9 gel to water ratio at room temperature for 40 h. The gels were separated from the liquid at time intervals of 0, 2, 4, 6, 8, 16, 20, 26, 32 and 40 h using a filter and funnel setup with Whatman® grade 1 filter paper (pore size of 11 µm, Whatman plc, Maidstone, England). The gels were left to drain for 10 min, and both the retentates (gels) and filtrates were collected and weighed. The degree of water absorption by the gels is calculated using Equation 7-4:

$$Water\ absorption\ (\%\ w/w) = \frac{Weight\ of\ drained\ gel\ after\ x\ h - weight\ of\ original\ gel}{Weight\ of\ original\ gel} \times 100\% \quad \text{(Equation 7-4)}$$

The quantity of leached protein and carbohydrate from the gel into the filtrate was determined as per Section 7.2.6.1 and Section 7.2.6.2, respectively. The degrees of protein leaching and carbohydrate leaching are calculated using Equation 7-5 and Equation 7-6, respectively:

$$Leached\ protein\ (\%\ w/w) = \frac{Soluble\ protein\ in\ filtrate}{Total\ protein\ in\ original\ gel} \times 100\% \quad \text{(Equation 7-5)}$$

$$Leached\ carbohydrate\ (\%\ w/w) = \frac{Soluble\ carbohydrate\ in\ filtrate}{Total\ carbohydrate\ in\ original\ gel} \times 100\% \quad \text{(Equation 7-6)}$$

Each set of experiments was repeated three times with at least two measurements.

7.2.8. Microscopy analysis

The influence of DWPS on the gel microstructure of samples was studied using TEM and CSLM for systems at pH 7 and pH 5, respectively.

7.2.8.1. Transmission electron microscopy (TEM)

Tubes of gel samples (2–3 mm) at pH 7 were submerged in a fixation solution containing 0.25 M glutaraldehyde and 0.1 M sodium cacodylate buffer (pH 7.2) for 16 h. The samples were rinsed thrice in a 0.1 M sodium cacodylate buffer (pH 7.2), before a secondary fixation with 1% osmium tetroxide in 0.1 M sodium cacodylate buffer for 1 h at room temperature. The samples were then rinsed thrice in a 0.1 M sodium cacodylate buffer. The samples were dehydrated with a series of acetone at increasing concentrations of 25, 50, 76, 95 and 100% for 45 min each. The dried samples were infiltrated in 50:50 resin:acetone and incubated overnight. The mixture was then replaced twice with 100% epoxy resin (Procure 812, ProSciTech, Thuringowa Central, Australia) and incubated for 8 h. The samples were embedded in moulds with fresh resin and cured at 60 °C for 48 h. A thin section of the

sample (~70 nm thickness) was cut from each resin block and mounted on copper grids. The grids were then stained with saturated uranyl acetate contained in 50% ethanol for 4 min, washed with 50% ethanol and Milli-Q water, and then stained in lead citrate for 4 min. The samples were finally washed with Milli-Q water and left to dry. Micrographs (60 000× magnification) were taken using a Tecnai G2 Spirit BioTWIN transmission electron microscope (FEI Corp., Brno-Černovice, Czech Republic).

7.2.8.2. Confocal scanning laser microscopy (CSLM)

The microstructure of gels at pH 5 was studied using a confocal scanning laser microscope (Zeiss LSM900 with Airyscan 2 super-resolution microscope, Carl Zeiss AG, Jena, Germany), with a 63× N.A. 1.4 oil immersion objective. The liquid samples at pH 5 from Section 7.2.1 were loaded into laboratory-made welled slides and gelation was carried out in a 90 °C water-bath for 30 min. The gels were stored at room temperature for 6 h before Fast green dye (~5 µL, 0.2% w/w) was added. To ensure good dye penetration, the samples were then stored overnight at 20 °C. The dye was excited at 633 nm using a helium/neon laser to detect protein. Emission was collected between 650 and 700 nm. Images were scanned twice (5–10 µm below the coverslip). The signals were averaged to minimise noise. Each set of experiments was repeated twice.

7.2.9. Statistical analysis

A one-way analysis of variance (ANOVA) with Tukey's test was used to test significant differences among mean values using Minitab (Minitab 18, Minitab Inc, Sydney, Australia).

7.3. Results and discussion

7.3.1. Phase stability of WPI + 140 °C DWPS mixtures at pH 7 and 5

The phase stability of 13% w/w WPI solution and the mixtures with the carbohydrate fraction (13% w/w WPI + 4% w/w maltodextrin or gelatinised waxy potato starch or DWPS) after 24 h at pH 7 and pH 5 is presented in Figure 7-1. Both WPI samples containing maltodextrin or gelatinised starch served as control samples. The former represents a system with similar total solids as in the mixed samples, while the latter represents a conventionally gelatinised starch in order to compare with the influence of DWPS in these mixtures. No visual phase separation was noted for samples at pH 7 (Figure 7-1A), whereas mixtures containing gelatinised starch or DWPS samples (120–150 °C) exhibited phase separation after 24 h at pH 5 (Figure 7-1B). At pH 7, the protein molecules exist in their native state and have better phase stability when mixed with other polymers (Quiroga & Bergenståhl, 2008). From Figure 7-1A, all samples showed excellent compatibility with WPI in the mixed samples at pH 7. When the pH of the system was adjusted to pH 5, near the isoelectric point of whey protein (pI ~5.1), the neutralisation of surface charges on proteins resulted in protein self-association, which reduced the overall stability of the mixtures (Li, Ould Eleya, & Gunasekaran, 2006). At pH 5, a higher HCl amount was added to liquid mixtures as compared to the NaOH volume (of the same molarity) required to adjust pH to 7, as the pH of the native WPI solution was ~6.7. With the unfavourable conformational changes in proteins (from protein self-association) and a higher ionic strength in pH 5 systems, phase separation was prominent in these mixtures (except for the mixtures containing maltodextrin). In contrast to the phase separation observed in the mixed systems containing gelatinised starch or DWPS (polymers of larger molecular sizes), the phase stability of WPI + maltodextrin could be due to the small molecular size of maltodextrin, which tend to be thermodynamically more stable in partially aggregated WPI samples (at pH 5). It is generally known that smaller molecules in a mixed polymer system tend to contribute to higher entropy of mixing than the large molecular species, which is favourable for the mixed system (Higgins, Lipson, & White, 2010; Tolstoguzov, 2000).

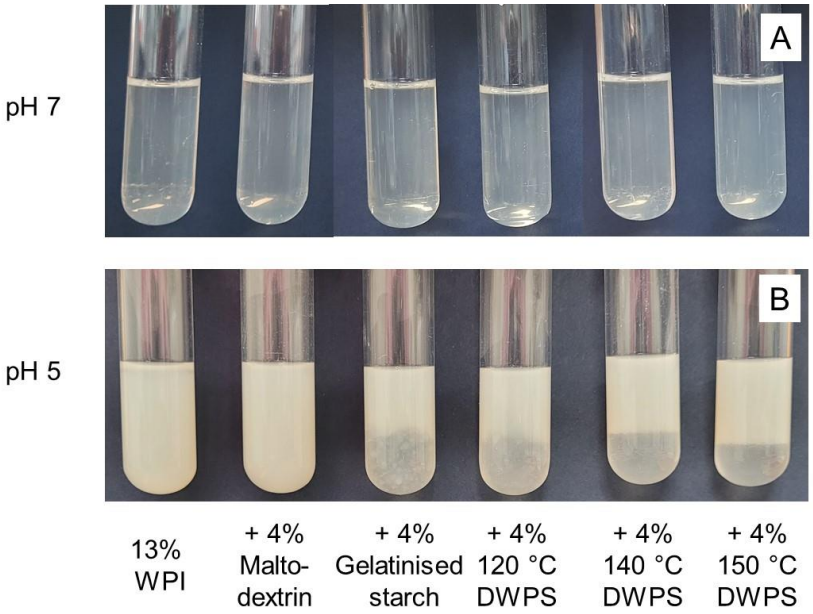

Figure 7-1 Phase stability of 13% w/w WPI solutions and mixtures of 13% w/w WPI + 4% maltodextrin or gelatinised starch or DWPS (120–150 °C) at (A) pH 7 and (B) pH 5, after 24 h storage at 20 °C.

7.3.2. Influence of 140 °C DWPS on fine-stranded WPI polymeric gels (pH 7)

7.3.2.1. Rheological, textural and microstructural properties

The *G'*, textural hardness and microstructure (obtained by TEM) of 13% w/w WPI gels and composite gels containing 13% w/w WPI + 4 % w/w maltodextrin or gelatinised starch or DWPS at pH 7 are presented in Figure 7-2. The addition of solids to WPI caused a significant increase in both *G'* and gel hardness. All the gels at pH 7 had fine-stranded structure (Figure 7-2B). Faint aggregates were observed in the gel that contained maltodextrin. With the addition of gelatinised starch or DWPS to WPI, the composite gels appeared to form a grainy structure. In particular, WPI + 140 °C DWPS gel appeared to have the densest and finest microstructure among the composite gels. It is worth noting that 60 000× was the highest magnification that could be used on these samples without compromising the resolution of the micrographs. The observation of the densest microstructure structure corresponds with the synergistic increase in the *G'* and hardness values observed in WPI + 140 °C DWPS gel, where the hardness was almost two times greater than that of other composite gels (Figure 7-2A). The results suggest that the mechanical properties of the composite gels were dependent on the degree of interactions (junction zones) among whey protein chains and how the presence of DWPS had either interfered with or aided in the network formation. Since 140 °C DWPS carried almost no charges (–3 mV), the DWPS could potentially be in close proximity to interact with WPI (probably involving hydrogen bonds) due to minimum electrostatic repulsion between negatively-charged WPI and 140 °C DWPS at pH 7. In contrast, the more negatively-charged gelatinised starch (–

31.0 mV) or 120 °C DWPS (–18.0 mV) are less likely to be in close proximity with WPI due to electrostatic repulsion between WPI and these starch polymers. On the other hand, even though 150 °C DWPS and maltodextrin also carry minimal charges (–2.1 mV and –8.5 mV respectively), 140 °C DWPS being a larger molecule (~157 × 10^6 Da as compared to 150 °C DWPS at ~41 × 10^6 Da and maltodextrin at ~6 × 10^3 Da (Castro, Durrieu, Raynaud, & Rouilly, 2016)), could mean that there are more available sites for interaction with protein molecules. Thus, these mechanisms could probably explain the synergistic increase in gel strength observed in WPI + 140 °C DWPS. A similar synergistic increase in gel strength was also reported by Liu *et al.* (2017a) in a mixed WPI + lotus root amylopectin system. The authors observed a drastic increase in *G'* from ~300 Pa (10% w/v WPI) and ~100 Pa (1% w/v amylopectin) to ~8000 Pa in the resulting mixed gel system. They attributed the increased *G'* to the increased levels of the reactive sulfhydryl group, C—N and/or N—H bonds in the composite gel. Their results suggest that the addition of lotus root amylopectin to WPI may have caused an increased number of junction zones and resulted in a stronger gel matrix. A similar mechanism could also be occurring in WPI + 140 °C DWPS, where the densest microstructure (resulted from increased junction zones) was observed among all the samples.

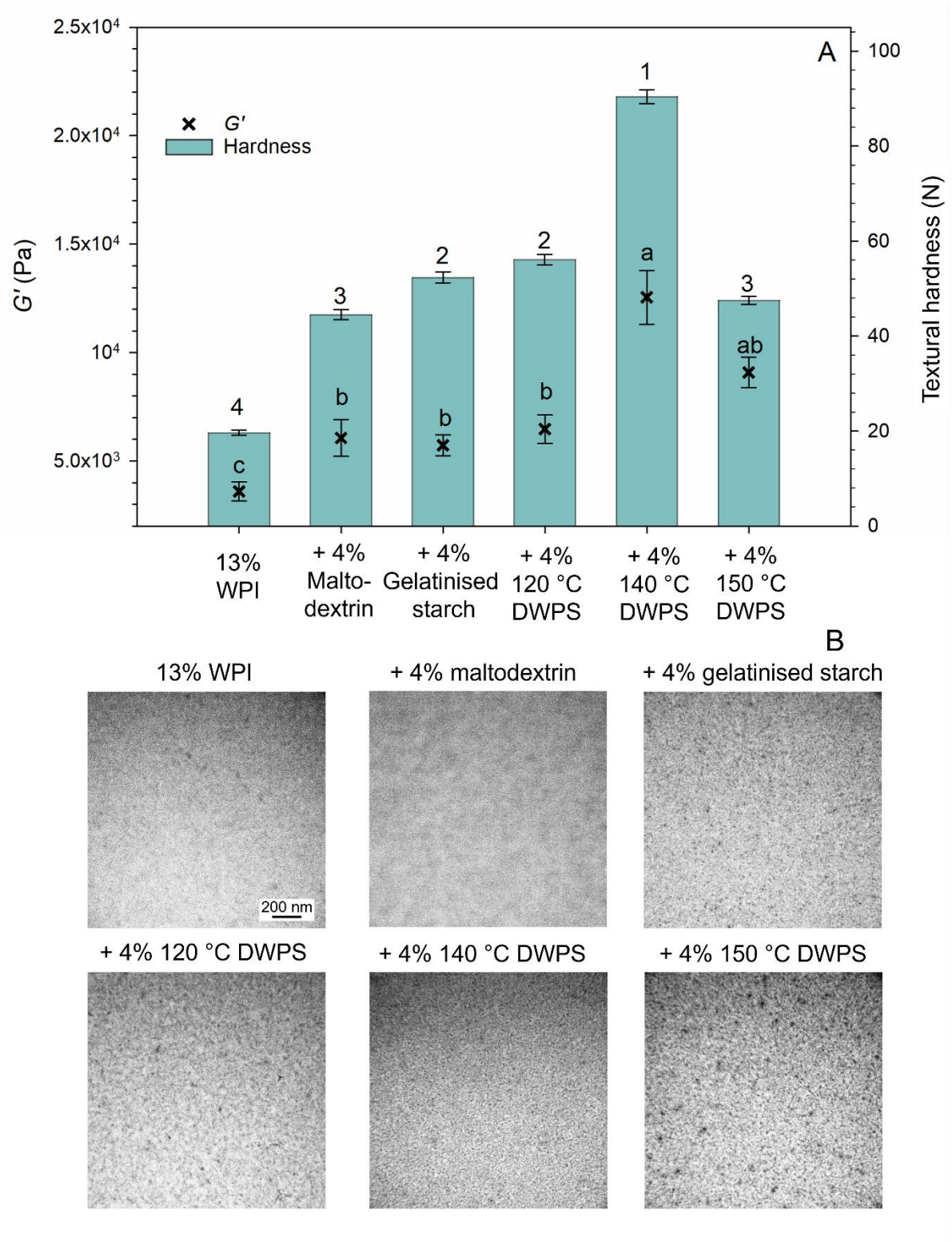

Figure 7-2 Influence of DWPS on fine-stranded polymeric protein gels (13 % w/w WPI, 13% w/w + 4% w/w maltodextrin or gelatinised starch or DWPS (120–150 °C) at pH 7): (A) *G′* from frequency sweep at 1% strain and 1 Hz frequency at 20 °C and gel hardness at room temperature, and (B) TEM micrographs (60 000×) with a scale bar of 200 nm. Values are presented as means ± standard error. Values denoted with the same superscript/number are not significantly different ($p \leq 0.05$).

It is also noteworthy that the hardness and *G'* values of WPI + 140 °C DWPS were similar to that of a pure WPI gel at ~15% w/w protein (Figure 7-3). Such observation could be used to develop cost-effective formulations by replacing whey protein with a cost-friendly DWPS to lower the cost of the product.

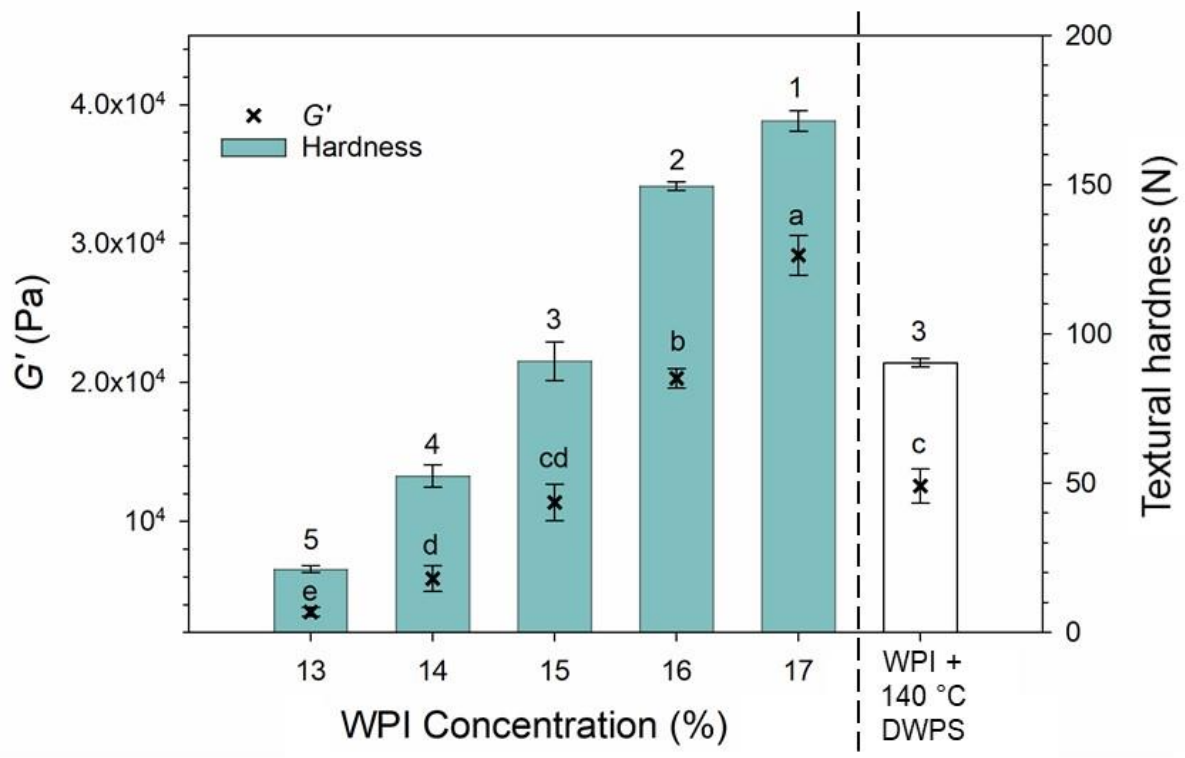

Figure 7-3 *G'* from frequency sweep at 1% strain and 1 Hz frequency at 20 °C and textural hardness at room temperature of 13–17% w/w WPI and 13% w/w WPI + 4% w/w 140 °C DWPS at pH 7. Values are presented as means ± standard error. Values denoted with the same superscript/number are not significantly different ($p \leq 0.05$).

7.3.2.2. Gel immersion in water

The gel stability of pure WPI and composite gels made at pH 7, was evaluated by immersing them in water for 40 h. The degrees of water absorption and leached components (protein and maltodextrin or gelatinised starch or DWPS samples) are presented in Figure 7-4. As shown in Figure 7-4A, pure WPI gels exhibited the highest degree of water absorption among the samples throughout a 40 h duration. In addition, a disintegrated WPI gel (broken into smaller pieces) was noted after immersing in water for 6 h, with water absorption at 259% w/w (Figure 7-4B). At 12 h, the WPI gel pieces became very swollen with further water absorption (334% w/w). At 20 h, the disintegrated gel pieces continued to absorb more water (437% w/w). At this stage, the WPI gels became a very weak fluid-like gel. A disintegrated gel was also observed for WPI + maltodextrin at 40 h, with water absorption reaching 384% w/w. In contrast, the other samples (WPI + gelatinised starch or DWPS samples) appeared as intact swollen gels at 40 h with water absorption ranging between 305 and 338% w/w. The water

absorption data suggest that the gelatinised starch and DWPS aided in strengthening the gel integrity since at ~259% w/w water absorption, the pure WPI gels broke apart, whereas gels containing gelatinised starch or DWPS samples remained intact.

The trend for protein leaching was similar to that of the degree of water absorption. Pure WPI gel exhibited the highest amount of protein leaching (15.2% w/w) among the gel samples. This observation was consistent throughout the experimental period of 40 h. The remaining composite gel samples containing maltodextrin or gelatinised starch or DWPS samples exhibited a similar degree of protein leaching (0.9–1.6% w/w) up to ~20 h. At 26 h, WPI + maltodextrin had a slightly higher amount of protein leaching (2.4% w/w) as compared to WPI + gelatinised starch or DWPS (1.6–1.9% w/w) (Figure 7-4C). Thus, the data suggest that both the degrees of water absorption and protein leaching are unlikely to be affected solely by the total solids content of the gel. Furthermore, the gel hardness appears to have no direct correlation with gel stability and protein leaching, as the water absorption and the amount of protein leaching for WPI + 140 °C DWPS (the sample that exhibited the highest hardness values in Figure 7-2A) were not significantly different from the other WPI + starch gels (and Figure 7-4A and C). In fact, the results indicate that the added starch samples (gelatinised starch and DWPS samples) reinforced the gel network and hindered continuous water absorption into the matrix, which will eventually lead to the loss of gel integrity.

As for carbohydrate leaching, WPI + maltodextrin had a markedly higher degree of leaching (~5.3–35.0% w/w) as compared to other composite gels (≤ 3.6% w/w) throughout the whole period when the gels were immersed in water. Among the WPI + starch samples, the WPI + 150 °C DWPS exhibited significantly higher carbohydrate leaching (3.6% w/w) than WPI + 140 °C DWPS (1.0% w/w) and even lower leaching was observed in WPI + gelatinised starch (0.7% w/w) and WPI + 120 °C DWPS (0.5% w/w) (Figure 7-4D). The M_w of the starch samples (Table 4-1) and maltodextrin (~6×10^3 Da, reported by Castro *et al.* (2016)) can possibly explain the observed trend. Based on Figure 7-5, the degree of carbohydrate leaching was observed to exhibit logarithmic decline with an increasing M_w of the added carbohydrates. Such observation is likely due to larger carbohydrate polymers such as the gelatinised starch or the 120 °C DWPS, which were less likely to diffuse out of the gel matrix as compared to the smaller polymer species, particularly maltodextrin which has the lowest M_w (Castro *et al.*, 2016; Demirel, 2007).

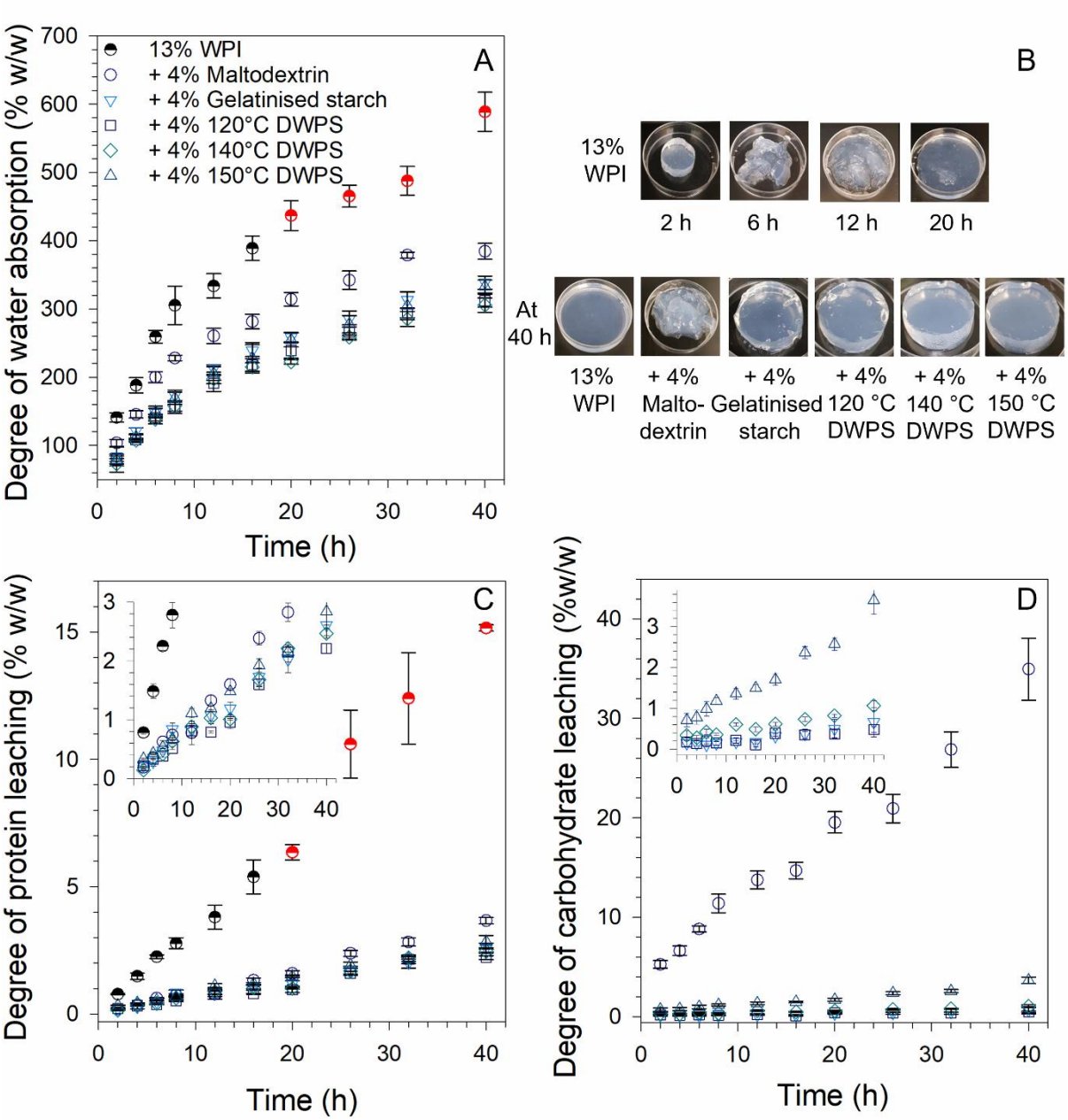

Figure 7-4 Influence of DWPS on the water-immersion stability of fine-stranded polymeric protein gels (13% w/w WPI and 13% w/w WPI + 4% w/w maltodextrin or gelatinised starch or DWPS (120–150 °C) at pH 7) over 40 h: (A) degree of water absorption, (B) appearance of drained gels (13 % w/w WPI gels after 2, 6, 12 and 20 h, and all gel samples at 40 h), (C) degree of protein leaching, with an inset graph showing 0–3% w/w of protein leaching, and (D) degree of carbohydrate leaching with an inset graph showing 0–3.9% w/w of carbohydrate leaching. Values are plotted as means ± standard error with measurements taken at room temperature. The red marker indicates fluid gel.

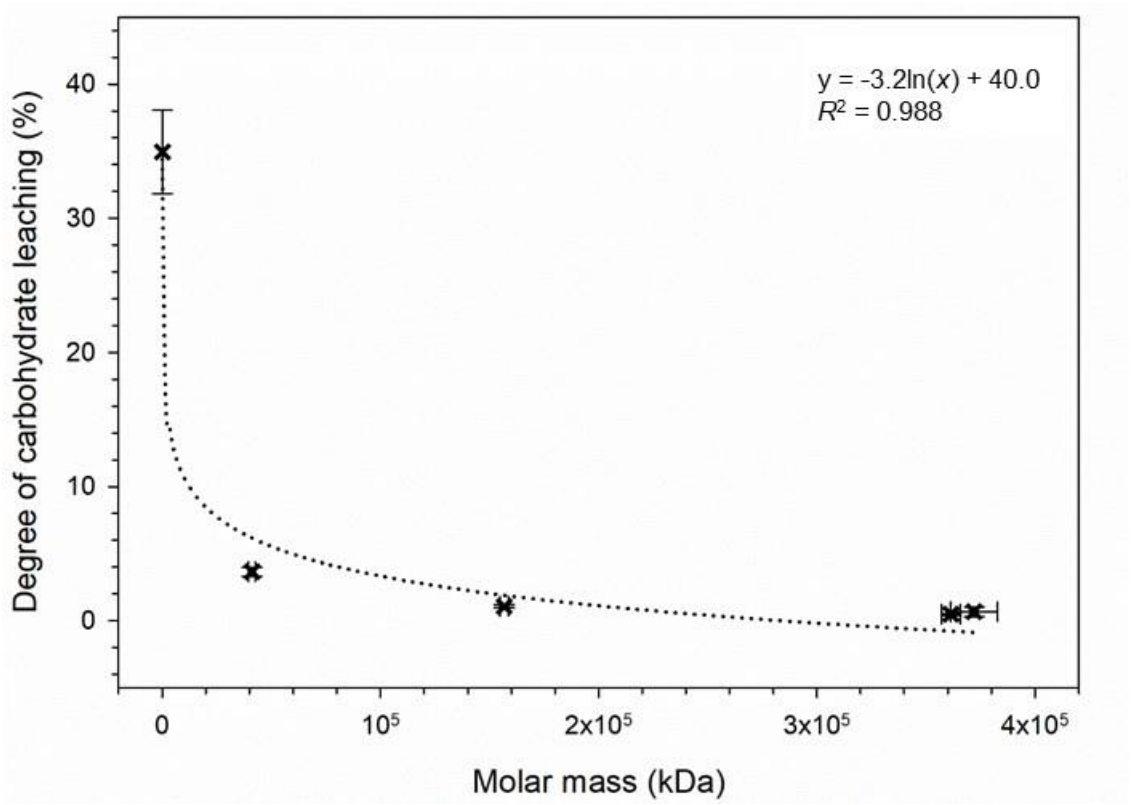

Figure 7-5 Effect of the molar mass of added carbohydrates on the degree of carbohydrate leaching from fine-stranded polymeric protein gels (at pH 7) containing maltodextrin or gelatinised starch or DWPS (120–150 °C) at 40 h water-immersion. Values are plotted as means ± standard error.

7.3.3. Influence of 140 °C DWPS on coarse-stranded WPI particulate gels (pH 5)

7.3.3.1. Rheological, textural and microstructural properties

Pure WPI gels made at pH 5—near the *pI* values of whey protein—exhibited significantly higher hardness and *G'* values (~142 N and ~94.3 kPa respectively) as compared to gels made at pH 7 (19 N and 4.8 kPa respectively) as showed in Figure 7-2A and Figure 7-6. This has been previously reported based on increased protein-protein interactions during gel formation (Ryan, Zhong, & Foegeding, 2013). The reduced electrostatic repulsion at pH near the p*I* of whey, leads to the domination of attractive forces (Van der Waals and hydrophobic interactions) and resulted in an increased aggregation after the protein chains unfold during heating.

The addition of starch (*i.e.*, gelatinised or DWPS samples) to WPI gels at pH 5 caused a significant reduction in the hardness of the resulting composite gels (Figure 7-6). The reduction of gel hardness was observed to be following a logarithmic trend with increasing M_w of the added carbohydrates, *i.e.*, maltodextrin, gelatinised starch and DWPS samples (Figure 7-7). Since the addition of maltodextrin did not cause any significant change in gel hardness (Figure 7-6), the results could imply that the composite gel strength is dependent on the M_w of the carbohydrate molecules. As M_w is related to

the amount of space occupancy, above a certain hydrodynamic volume, there is the possibility that the added starch molecules will disrupt and weaken the WPI gel network. The micrographs (obtained by CSLM) of the composite gels in Figure 7-7 supported this hypothesis, where a well-connected protein network was observed in composite gels with smaller polymers (*i.e.*, maltodextrin and 150 °C DWPS). In contrast, micrographs of gels containing larger polymers (*i.e.*, gelatinised starch or 120 °C DWPS) had a protein network with poorer connectivity (Figure 7-7). The observations from this study are different from an earlier study by Olsson *et al.* (2003). The authors observed an increase in *G'* value in composite gels of 6% w/w β-lactoglobulin and 3.6% w/w of amylopectin at pH 5.4 at increased amylopectin M_w from 3.2×10^5 to 2.7×10^7 Da. The authors attributed the increased *G'* to a coarser protein network caused by larger amylopectin molecules, which resulted in a more porous gel matrix. The differences in their results could be due to multiple factors including the source of amylopectin, M_w, degree of branching and conformation, etc. Amylopectin molecules of a smaller M_w range (3.2×10^5 to 2.7×10^7 Da) were used in their studies and differed markedly from the larger amylopectin molecules (4.1×10^7 to 3.7×10^8 Da) used in this study. The larger M_w of the starch samples in this study could be one of the reasons that caused partial disruption of the protein network.

In addition to the above hypothesis (*i.e.*, incorporation of larger starch polymers resulting in poorer protein connectivity), incompatible polymer systems have been reported to form gels with large pore sizes, *i.e.*, WPI and starch components (Kuhn, Cavallieri, & da Cunha, 2011; Ziegler & Foegeding, 1990). Thus, the reduced hardness values are likely caused by the combined effects of: (i) thermodynamic incompatibility between WPI and gelatinised starch or DWPS samples (Figure 7-1B) and (ii) the disruption of protein network by added starch components creating a more open structure (Figure 7-7). Such a claim is also supported by the study conducted by Andoyo, Guyomarc'h, & Famelart (2016), where the authors manipulated the pore size distributions of acidified whey protein gels and found that the gel with the largest pore sizes showed the lowest *G'* values due to its weakest structure.

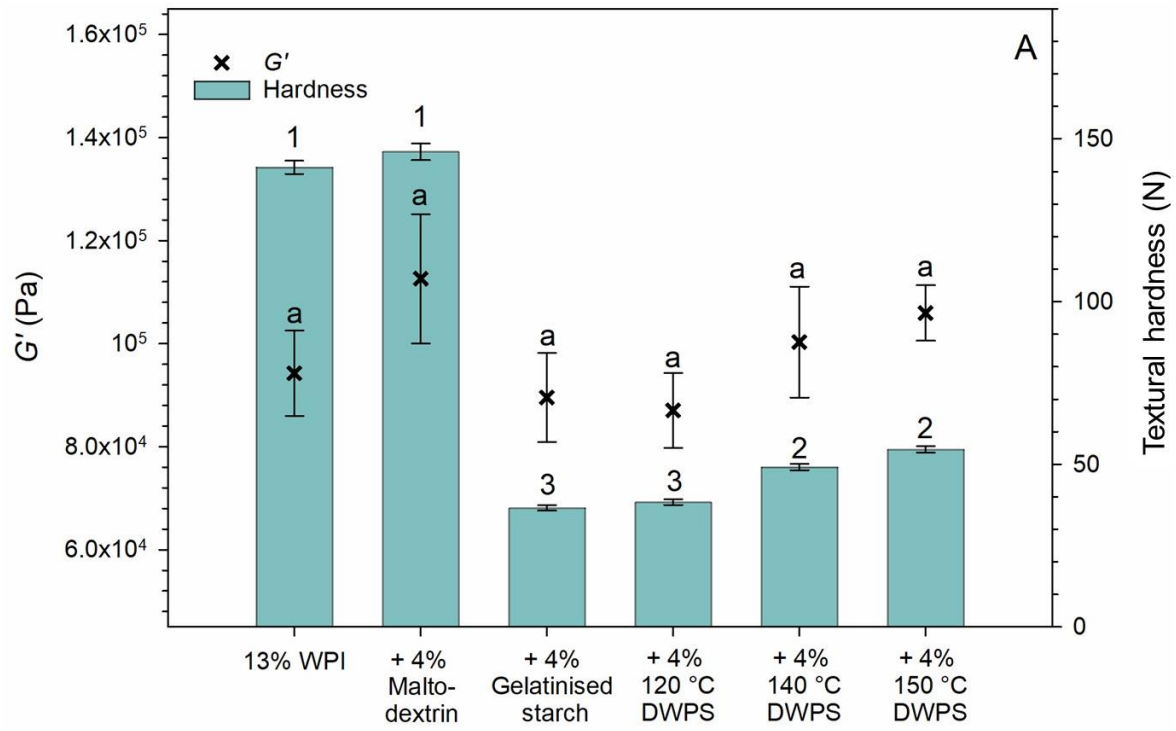

Figure 7-6 Influence of DWPS on the *G'* (from frequency sweep at 1% strain and 1 Hz frequency) at 20 °C and gel hardness at room temperature of coarse-stranded particulate protein gels (13% w/w WPI and 13% w/w + 4% w/w maltodextrin or gelatinised starch or DWPS (120–150 °C) at pH 5. Values denoted with the same superscript/number are not significantly different ($p \leq 0.05$).

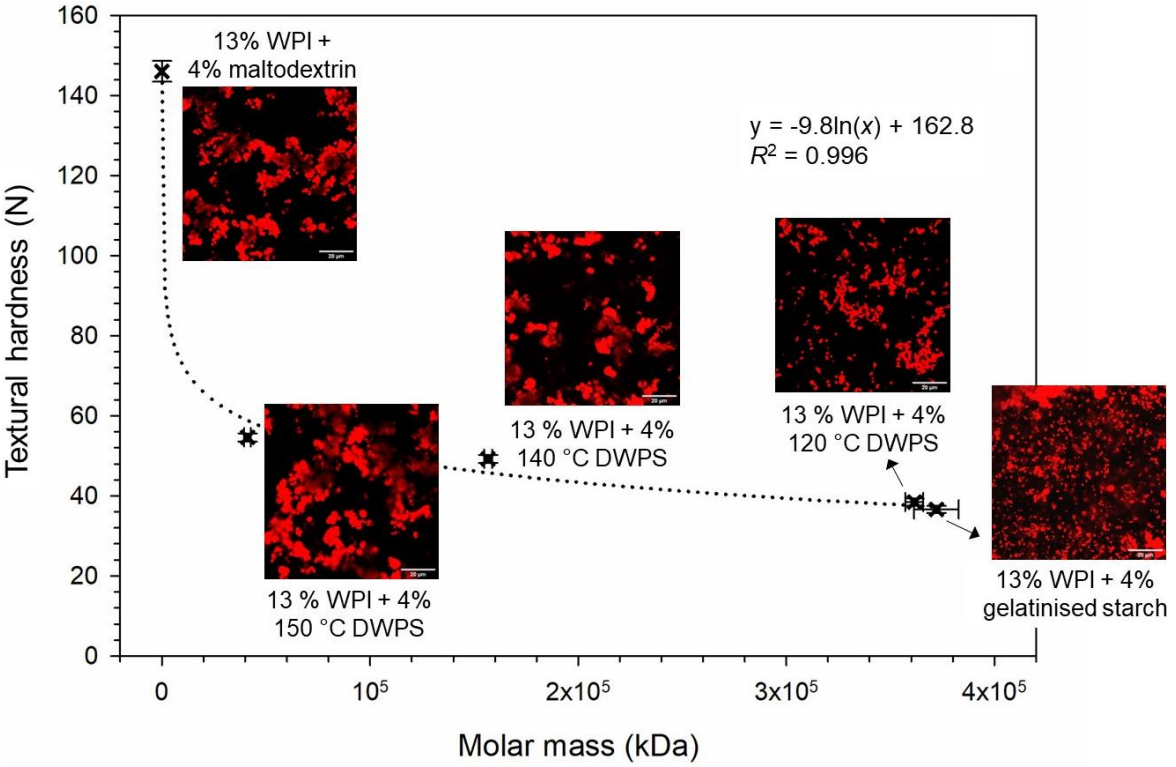

Figure 7-7 Effect of molar mass of carbohydrates on the gel hardness and microstructure of coarse-stranded particulate protein gels (13% w/w WPI + 4% w/w maltodextrin or gelatinised starch or DWPS (120–150 °C)) at pH 5. Values are plotted with means ± standard error. Confocal scanning laser micrographs were taken at 630× magnification, with a scale bar of 20 µm.

7.3.3.2. Water-holding capacity

Whey protein gels at pH 5 were generally found to have poor water-holding capacity (Picone *et al.*, 2011; Stading, Langton, & Hermansson, 1993). A clear serum was squeezed out when pure WPI and WPI + maltodextrin gels were compressed (Figure 7-8A), whereas a white/turbid serum was observed during the compression of WPI + gelatinised starch or DWPS gels (Figure 7-8B). Gels with large pore sizes were also observed in the deformed gels (after compression test) containing gelatinised starch or 120 °C DWPS or 140 °C DWPS (Figure 7-8C). The observation is in good agreement with the *G'* and textural hardness and microstructure results presented earlier (Figure 7-6 and Figure 7-7), where the hypothesis that two concurrent mechanisms (*i.e.*, phase separation and the disruption of the protein network by starch polymers) led to open microstructures. Moreover, these observations suggest that the starch polymers are acting as inactive fillers in the protein network. Previously, Dille, Draget, & Hattrem (2015) have also defined inactive fillers as components that are weakly bound to the polymer network, which reduced the mechanical properties of the composite gel. A large fraction of these trapped inactive fillers in the pores of the gel matrix was found to be released upon shear. These polymer leaching events described by Dille *et al.* (2015) were similar to those in this study.

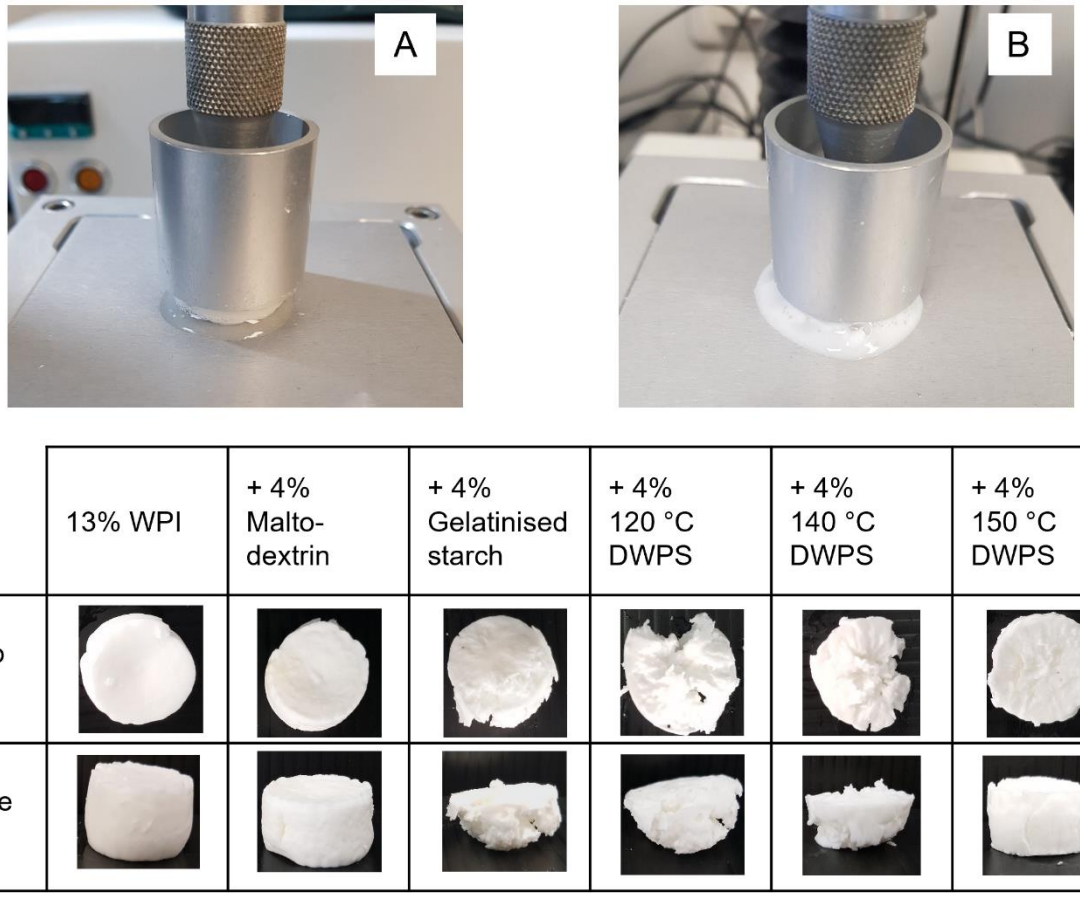

Figure 7-8 Appearance of serum released from coarse-stranded particulate protein gels at pH 5 during compression test: (A) 13% w/w WPI or 13% w/w WPI + 4% w/w maltodextrin (B) 13% w/w WPI + 4% w/w gelatinised starch or DWPS (120–150 °C), and (C) visual appearance of deformed particulate protein gels of 13% w/w WPI and 13% w/w WPI + 4% w/w maltodextrin or gelatinised starch or DWPS (120–150 °C) after compression test.

In order to further investigate the amount and content of the released serum, the gels were centrifuged to determine the degree of syneresis (amount of serum or supernatant released), and the amount of protein and carbohydrate contents from the serum. The results are presented in Table 7-1. Both pure WPI and WPI + maltodextrin gels exhibited high percentages of syneresis (60.1% w/w and 55.6% w/w respectively), followed by WPI + 150 °C DWPS (25.4% w/w), whereas WPI + gelatinised starch or 120 °C DWPS or 140 °C DWPS showed significantly lower levels of syneresis (5.0–7.4% w/w). The high syneresis results of WPI + maltodextrin or 150 °C DWPS were attributed to the lower water-holding capacity of maltodextrin (and the small 150 °C DWPS) as compared to that of the larger starch polymers. The composite gels containing small polymers had a lower water-holding capacity, which is aligned with the data reported by Adetoro, Opara, & Fawole (2020) and Liu, Hong, Gu, Li, & Cheng (2015). Adetoro *et al.* (2020) found waxy starch exhibited ~64% w/w higher water-holding capacity than that of maltodextrin and Liu *et al.* (2015) reported that smaller enzymatically-hydrolysed starch

polymer had lower water-holding capacity (3.2 g/g) compared to its larger counterparts (4.3 g/g), due to a lower tendency to form a well-established network to hold water.

In terms of the amount of protein in the leached serum, very low protein levels (< 0.30% w/w) were detected in all the samples (Table 7-1). In contrast to leached protein, the amount of leached carbohydrate detected in the serum varied widely and occurred at higher values (~4–82% w/w). A logarithmic decline in carbohydrate leaching was observed with increasing M_w of the added starch polymers (Figure 7-9). This trend is similar to the logarithmic trend in Figure 7-5 (carbohydrate leaching in polymeric protein composite gels at pH 7) described earlier. WPI + maltodextrin had ~82% w/w of its maltodextrin leached out from the gel matrix, followed by WPI + 150 °C DWPS (~40% w/w of its starch leached out). Larger starch fractions like gelatinised starch, 120 and 140 °C DWPS showed low markedly lower values (≤ 8.5% w/w). These observations could be attributed to the low amount of starch polymers diffusing out of the protein matrix as the starch polymers remained entrapped within the protein network (Demirel, 2007).

Table 7-1 Degree of syneresis, protein leaching, and carbohydrate leaching from coarse-stranded particulate protein gels (13 % w/w WPI and 13% w/w + 4% w/w maltodextrin or gelatinised starch or DWPS (120–150 °C) at pH 5).

	% Syneresis	**Leached protein (% w/w)**	**Leached carbohydrate (% w/w)**
13% w/w WPI	60.1 ± 0.2^{a}	0.28 ± 0.01^{a}	Not applicable
+ 4% w/w Maltodextrin	55.6 ± 0.4^{a}	0.24 ± 0.01^{b}	81.9 ± 1.8^{a}
+ 4% w/w Gelatinised starch	6.3 ± 0.7^{c}	Not detected	3.7 ± 0.2^{d}
+ 4% w/w 120 °C DWPS	5.0 ± 1.0^{c}	0.03 ± 0.02^{d}	4.2 ± 0.2^{d}
+ 4% w/w 140 °C DWPS	7.4 ± 0.7^{c}	0.13 ± 0.08^{c}	8.5 ± 0.2^{c}
+ 4% w/w 150 °C DWPS	25.4 ± 2.8^{b}	0.10 ± 0.00^{c}	40.3 ± 0.9^{b}

Values are expressed as means ± standard error. Values in the same column denoted with the same superscripts are not significantly different ($p \leq 0.05$).

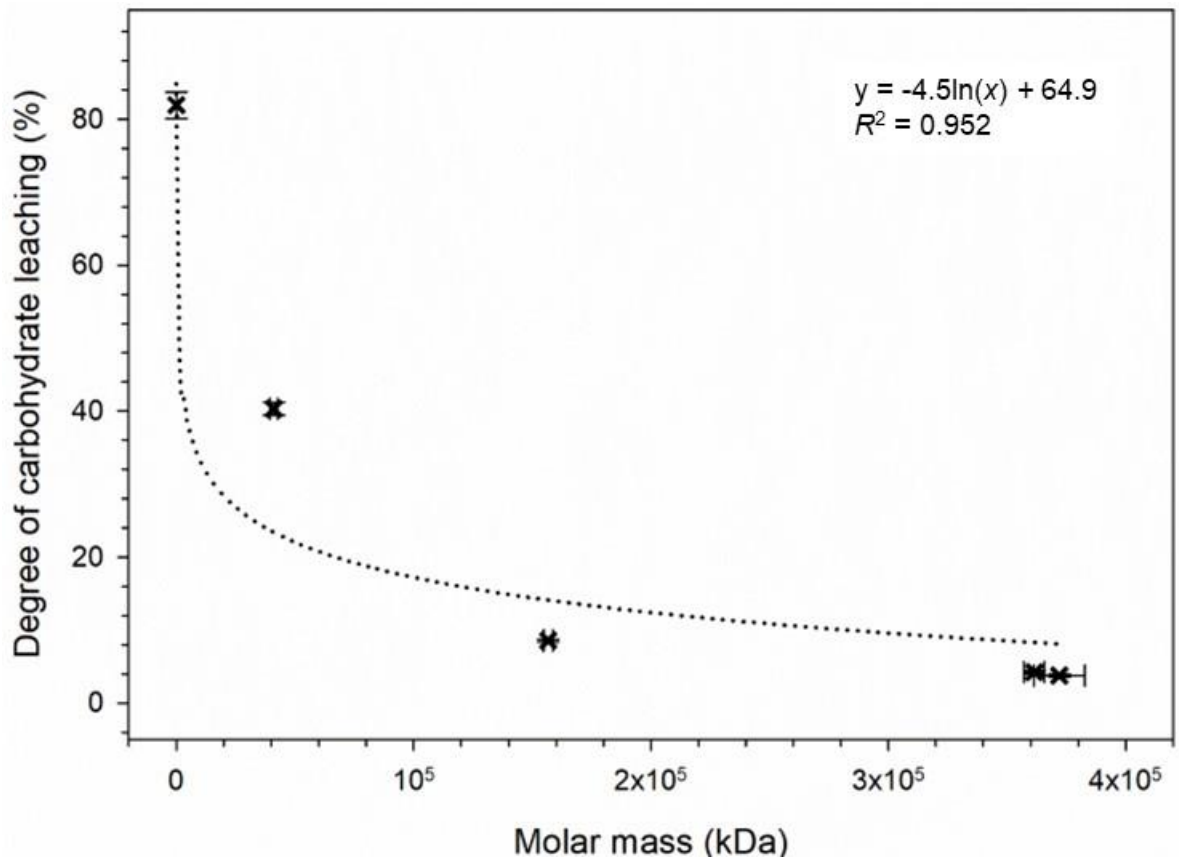

Figure 7-9 Effect of molar mass of carbohydrates on the degree of carbohydrate leaching of centrifuged coarse-stranded particulate protein gels containing maltodextrin or gelatinised starch or DWPS (120–150 °C) at pH 5. Values are plotted as means ± standard error.

7.3.3.3. Gel immersion in water

The water-immersion stability of particulate protein gels at pH 5 was also evaluated (Figure 7-10). All drained gels were intact at the end of the experiment after 40 h immersion (Figure 7-10B). All the gels exhibited low levels of water absorption (≤ 12% w/w), where the degree of water absorption at 40 h were 5, 4, 12, 11, 9 and 1% w/w for pure WPI, WPI + maltodextrin, WPI+ gelatinised starch, WPI + 120 °C DWPS, WPI + 140 °C DWPS and WPI + 150 °C DWPS, respectively (Figure 7-10A). The low water absorption was attributed to the extensively aggregated protein network, which led to the formation of particulate gels with large pores that in turn resulted in poor water-holding capacities (Picone *et al.*, 2011). The slightly higher degree of water absorption observed in gels containing gelatinised starch or 120 °C DWPS or 140 °C DWPS could be attributed to the water-holding capacity of the starch polymers within the composite gels as discussed earlier. Very low protein leaching (≤ 0.4% w/w) was observed in all gel samples at 40 h as expected (Figure 7-10C). The observation was due to the formation of an insoluble protein matrix near its p*I* value (Cavallieri, Netto, Menossi, & Cunha, 2007). In contrast to protein leaching, high amounts of carbohydrate leaching (29–71% w/w) were noted in all composite gels, where the M_w of carbohydrates seemed to affect the carbohydrate leaching of particulate gels

(Figure 7-10D). The highest leaching values were noted in gels containing the smaller carbohydrate polymers such as maltodextrin (71% w/w) and 150 °C DWPS (60% w/w), which had a higher chance of diffusing out of the protein matrix (Demirel, 2007). The high leaching values (29–71% w/w) also suggest that the carbohydrate polymers are unlikely to be bound to the protein matrix, which reinforced that the carbohydrate polymers are likely to be entrapped as inactive fillers in the protein network.

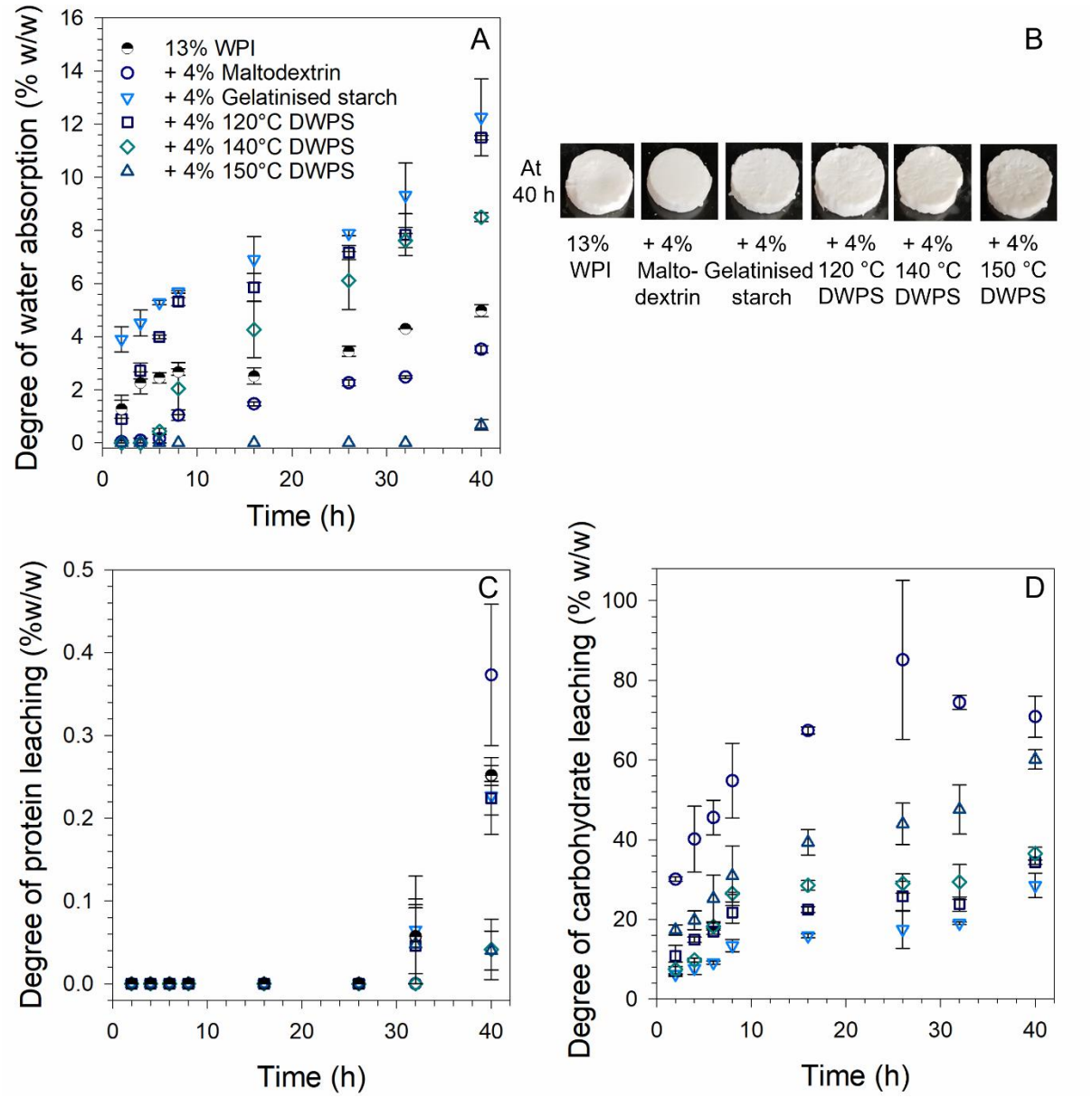

Figure 7-10 Influence of DWPS on the water-immersion stability of coarse-stranded particulate protein gels (13 % w/w WPI and 13% w/w + 4% w/w maltodextrin or gelatinised starch or DWPS (120–150 °C) at pH 5) over 40 h: (A) degree of water absorption, (B) appearance of drained gels at 40 h, (C) degree of protein leaching, and (D) degree of carbohydrate leaching. Values are plotted as means ± standard error with measurements taken at room temperature.

7.3.4. General remarks

At pH 5 and 7, WPI forms coarse-stranded particulate and fine-stranded polymeric gels, respectively. The above findings have shown that DWPS can be used to manipulate the microstructure and mechanical properties of these two types of heat-induced WPI gels. At neutral pH, the added DWPS samples did not result in any segregation of mixed systems prior to heat-induced gelation. In particular, the addition of 140 °C DWPS, caused a synergistic increase in its gel strength. Such an increase is likely to be due to a combined effect of optimum negative charges and polymer size of 140 °C DWPS, allowing more available sites for interaction with the protein molecules. However, the exact mechanism of the interactions requires further investigation. On the other hand, phase separation was observed at pH 5 with the addition of starch (gelatinised starch or DWPS), resulting in the formation of particulate gels with decreasing hardness and increasing pore size at increasing molar mass of starch polymers. The knowledge is useful to food product developers when structuring protein-enriched foods, in particular: (i) the synergistic increase of hardness in WPI + 140 °C DWPS can be advantageous in designing cost-effective protein-based food products, as the cost of proteins is generally higher than modified starches, (ii) the enhanced gel integrity of a fine-stranded composite gel containing gelatinised starch or DWPS at neutral pH could potentially be used in aqua feed formula, where good shape retention in water is desired. As good gel stability ensures that the feed remains available for the marine animals as long as possible in the water, and (iii) the ability to produce particulate gels with varied pore size and hardness by incorporating DWPS samples of different molar masses, as these gel matrices could be used to provide different degrees of liquid (*e.g.*, carrying flavour) being released during mastication to provide a unique texture and sensory experience.

7.4. Conclusions

The mechanical properties and microstructure of WPI gels can be altered by the addition of a novel physically-modified DWPS. In a pH neutral environment, the fine-stranded WPI gels can be markedly strengthened with the addition of DWPS samples such as synergistic increase in gel hardness in WPI + 140 °C DWPS and good shape retention of WPI + DWPS when immersed in water over a prolonged period of 40 h. On the other hand, in an acidic environment (pH 5), DWPS has also been shown to alter the gel hardness and porosity of particulate WPI gels creating other gel matrices that could be used in applications where the controlled release of liquid carriers is desired. The potential of using DWPS as a clean-label ingredient to structure foods is a cost-effective and innovative avenue for the development of protein-dense foods with its unique functionality and sensory properties. In the next chapter, the effects of NaCl and $CaCl_2$ (*i.e.*, ionic strength and type of salts) on WPI + 140 °C DWPS gels were further evaluated, as ionic strength and salt type are likely to impact on the mechanical and microstructural properties of composite gels (Chapter 8).

Chapter 8 Manipulation of mechanical properties and microstructure of whey protein gels using DWPS and salts [1]

8.1. Introduction

In Chapter 7, WPI + DWPS was studied in two types of protein gel systems: fine-stranded polymeric (at pH 7, near-native protein pH ~6.7) and coarse-stranded particulate (at pH 5, near p*I* ~5.1) protein gels. Other than pH adjustment, particulate WPI gel can also be formed at neutral pH conditions at high ionic strength (Urbonaite *et al.*, 2016). The addition of DWPS was found to affect the mechanical and microstructural properties of WPI gels. In particular, a synergistic increase in gel strength was observed in neutral WPI + 140 °C DWPS gels. From the preliminary trials, the control of ionic strength in combination with 140 °C DWPS can be used to alter the gel structure of WPI, yielding gels with desirable textural attributes. These gel matrices could be useful in structuring "clean-label" foods. Of special interest is to produce textures that tackle the problem of dysphagia, a medical condition that hinders normal swallowing. Due to the risk of choking or aspiration, foods with a soft texture and thickened fluids are used for dysphagia management to slow down the swallowing process, minimise chewing and protect the airway (Giura, Urtasun, Belarra, Ansorena, & Astiasarán, 2021).

Currently, there is no literature reporting on the interaction between WPI and DWPS and limited publications on the effect of salt on WPI + starch gels. Thus, in this chapter, the influence of salts on the interaction between WPI and 140 °C DWPS was studied by characterising the mechanical and microstructural properties of heat-induced WPI + 140 °C DWPS gels at various ionic strengths (0–500 mM NaCl and $CaCl_2$). Maltodextrin and gelatinised starch will also be used as controls. The results from this interaction study are essential for predicting the outcome when formulating high-protein foods for dysphagia as well as for food gel design in 3-D printing.

[1]Parts of this chapter are published as Ang, C. L., Goh, K. K. T., Lim, K., & Matia-Merino, L. (2022a). High-protein foods for dysphagia: Manipulation of mechanical and microstructural properties of whey protein gels using de-structured starch and salts. *Gels, 8*(7), 399.

8.2. Materials and Methods

8.2.1. Sample preparation of whey protein + starch mixtures at varied NaCl and $CaCl_2$ concentrations

Stock solution of 25% w/w WPI and stock suspension of 11% w/w of gelatinised starch or maltodextrin or 140 °C DWPS were prepared as per Section 7.2.1. Stock NaCl solution (5 M) was added to stock samples to produce 13% w/w WPI solution and mixtures (13% w/w WPI + 4% w/w maltodextrin or gelatinised starch or 140 °C DWPS at varied NaCl concentrations of 0–500 mM). Same procedure was repeated with stock $CaCl_2$ solutions (0.1 or 5 M) to obtain 13% w/w WPI and mixtures (13% w/w WPI + 4% w/w carbohydrate) at varied $CaCl_2$ concentrations (0–500 mM). The pH values of pure WPI and mixed systems were ~6.5–6.7 and ~6.3–6.7 at varied NaCl and $CaCl_2$ concentrations, respectively.

8.2.2. Phase stability

The phase stability of pure WPI solutions and mixtures at various salts concentrations was determined as per Section 7.2.2.

8.2.3. Rheological measurements

Rheological measurements of pure WPI and mixture at varied salt concentrations were performed as per Section 7.2.3. Each set of experiments was repeated three times with at least two measurements. Note that all the samples in this chapter can be defined rheologically as gels, as the *G'* were above their *G"* (tan δ < 0.2). Thus, only *G'* values were presented.

8.2.4. Textural hardness measurements

The pure WPI solutions and mixtures (~5 g) from Section 8.2.1 were made into gels as per Section 7.2.5.1. and the textural hardness of the gel samples was determined as per Section 7.2.5.2. Each set of experiments was repeated three times with at least five measurements.

8.2.5. Microscopy analysis

The effects of salts on the gel microstructure were analysed *via* both scanning electron microscopy (SEM) and CSLM. SEM was only conducted on self-supporting gels (not paste-like samples).

8.2.5.1. Scanning electron microscopy (SEM)

The prepared gel samples were cut into small pieces (~3 mm) and soaked in a 0.1 M phosphate buffer containing 3% w/v glutaraldehyde and 2% w/v formaldehyde (pH 7.2) for 24 h at room temperature. The samples were washed three times in a 0.1 M phosphate buffer (pH 7.2) for 10 min, followed by dehydration using a series of ethanol solutions at increasing concentrations, *i.e.,* 25, 50, 75, and 95% for 10 min each and at 100% for 1 h. Critical-point drying was carried out using liquid carbon dioxide

and 100% ethanol with samples placed in a Polaron E3000 series II apparatus (Quorum, East Sussex, England). Samples were then fractured and mounted on the aluminium stubs using double-sided tape samples and sputter-coated with ~100 nm of gold (Bal-Tec SVD050, Los Angeles, CA, U.S.A.). The microstructure (2500× magnification) was taken using Quanta 200 Environmental scanning electron microscope (FEI Co., Hillsboro, OR, USA) at an accelerating voltage of ~10–15 kV.

8.2.5.2. Confocal scanning microscopy (CSLM)

Samples from Section 8.2.1 were prepared and analysed as per Section 7.2.8.2. Each set of experiments was repeated twice.

8.2.6. Statistical analysis

A one-way analysis of variance (ANOVA) with Tukey's test was used to test significant differences among mean values using Minitab (Minitab 18, Minitab Inc, Sydney, Australia).

8.3. Results and discussion

8.3.1. Effect of ionic strength on phase stability of WPI + DWPS mixtures

According to New Zealand Nutrition Foundation (2022b), foods can be categorised into low-, medium- and high-salt foods, which contain < 120, 120–600 and > 600 mg sodium per 100 g of food that translates into NaCl concentrations of approximately < 50, 50 – 260 and > 260 mM. On the other hand, calcium is one of the most important minerals for the human body, and the recommended dietary allowance (RDA) for calcium is ~1000 mg for an adult. Dairy products such as yoghurt are a source of calcium, which contains 195 mg of calcium per serving (150 g, ~33 mM) (New Zealand Nutrition Foundation, 2022a). However, one serving of yoghurt only supplies ~20% of the daily RDA for calcium, making calcium-fortified foods the effective alternative to increase calcium intake. The effect of NaCl and $CaCl_2$ was evaluated at the relevant concentrations between 0 and 500 mM.

The phase stability of 13% w/w WPI and 13% w/w WPI + 4% w/w maltodextrin or gelatinised starch or 140 °C DWPS with the addition of NaCl or $CaCl_2$ (0–500 mM) after 24 h at 20 °C is presented in Figure 8-1. Similar to Chapter 7, mixtures containing maltodextrin or gelatinised starch served as control samples, as the former represents a system with similar total solids as in the mixed systems and, the latter is the control using unmodified starch needed to investigate the influence of DWPS on these mixtures. Samples with added NaCl did not show any visual phase separation (Figure 8-1). Similarly, no phase separation was noted in pure WPI solutions at $CaCl_2$ concentrations between 0 and 500 mM. However, increasing visual turbidity was observed at increasing $CaCl_2$ concentrations between 10 and 100 mM. The results are in agreement with previous studies, where a higher ionic strength caused the formation of larger protein aggregates that scatter the light (Schmitt, Bovay, Rouvet, Shojaei-Rami, & Kolodziejczyk, 2007). The subsequent increase in $CaCl_2$ above 100 mM resulted in a decrease in sample turbidity. The decrease in turbidity is likely due to the dissociation effect contributed by the excess of chloride ions in the system. Some of the aggregated proteins cross-linked via calcium ions could dissociate in the presence of an increasing amount of counter-ions, which affect the electrostatic interactions, hence, lowering the turbidity of the samples. Such observations have been made in 7S and 11S soy protein solutions with $CaCl_2$ and $MgCl_2$, where a decrease in turbidity was observed after maximum divalent salt concentration at ~30–40 mM (Tay, Tan, & Perera, 2006).

In contrast to NaCl systems, visual phase separation was noted in mixed systems between 50 and 500 mM $CaCl_2$ for WPI + maltodextrin, and between 10 and 75 mM $CaCl_2$ for WPI + gelatinised starch or DWPS systems. The observed phase separation in the presence of calcium could be explained by the unfavourable protein conformational changes induced by the divalent calcium ions due to bridging

effect (Tolstoguzov, 2000). Moreover, the phase separation occurring at lower $CaCl_2$ concentrations in protein + starch mixtures could be attributed to the gelatinised starch and DWPS being larger molecules than maltodextrin, which better facilitated the thermodynamic incompatibility (higher Gibbs free energy value) leading to separation (Higgins *et al.*, 2010; Tolstoguzov, 2000). This also led to a difference in the location of the polysaccharide-rich phase in the phase-separated samples—at the bottom (in the presence of the starches) or the top (in the presence of maltodextrin).

At concentrations ≥ 100 mM $CaCl_2$, only single-phase systems were observed in the mixtures that contained gelatinised starch or DWPS. Given that both the gelatinised starch and whey proteins are all initially negatively charged, the single-phase system may be the result of an optimum balance between attractive and repulsion forces among proteins and starch polymers at high $CaCl_2$ concentrations, which results in thermodynamic compatibility. It could also be related to the dissociative effect on proteins as described above, contributed by high concentrations of chloride ions, which reverse the shielding and bridging effects of calcium ions resulting in some of the protein molecules regaining their negative charges and getting dissociated, decreasing the incompatibility with the polysaccharide fraction (Higgins *et al.*, 2010; Tolstoguzov, 2000).

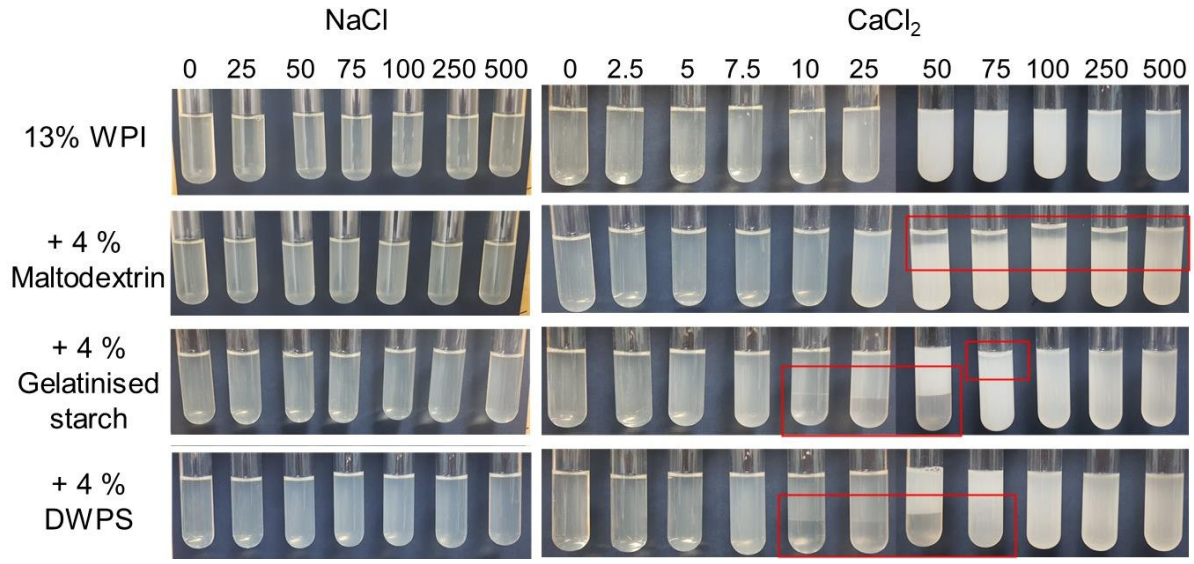

Figure 8-1 Effect of NaCl (0, 25, 50, 75, 100, 250 and 500 mM) and $CaCl_2$ (0, 2.5, 5, 7.5, 10, 25, 50, 75, 100, 250 and 500 mM) on the phase stability of 13% w/w WPI solutions and mixtures of 13% w/w WPI + 4% w/w maltodextrin or gelatinised starch or 140 °C DWPS after 24 h storage at 20 °C.

8.3.2. Effect of ionic strength on gelation temperature of WPI + DWPS mixtures

The individual effects of NaCl (0–500 mM) and $CaCl_2$ (0–500 mM) on the gelation temperature of pure WPI and mixed systems are presented in Figure 8-2A and B respectively, as well as the plot against the calculated ionic strength (0–1500 mM) in Figure 8-2C. The gelation temperature of WPI was not significantly affected by the addition of maltodextrin or 140 °C DWPS, whereas gelatinised starch significantly decreased the gelation temperature from 95 to 91 °C (Figure 8-2A). Such observation could be due to gelatinised starch being a larger and more negatively charged molecule (~3.6×10^8 Da and -31.0 mV) as compared to maltodextrin (~6×10^3 Da and –8.5 mV) and 140 °C DWPS (~157×10^6 Da and –2.8 mV). Thus, gelatinised starch was better at promoting segregative interactions between starch and protein molecules, causing enhanced protein denaturation and aggregation (Bryant & McClements, 2000; Fitzsimons, Mulvihill, & Morris, 2008b). The addition of small quantities of both NaCl and $CaCl_2$ rapidly reduced the gelation temperature of the system by ~10–15 °C (Figure 8-2A and B). The reduction plateaued off at 75 mM NaCl and 25 mM $CaCl_2$, which corresponds to a similar ionic strength of ~75 mM (Figure 8-2C). However, $CaCl_2$ was clearly more effective than NaCl at reducing gelation temperature (Figure 8-2C). A similar observation was made by Puyol, Pérez, & Horne (2001), where the increase in salt concentrations resulted in a reduction in the gelation temperature of WPI. Such reduction can be attributed to the enhanced aggregation contributed by the shielding of charged protein molecules by cations and intra- and inter-molecular bridges formed by calcium ions between negatively charged protein molecules (Hongsprabhas *et al.*, 1999; Joyce, Kelly, & O'Mahony, 2018). In conclusion, at ≥ 75 mM added ionic strength for any of the systems (NaCl or $CaCl_2$), the gelation temperature of both pure WPI and mixed systems was no longer significantly affected by further salt addition. Hence, the results indicate that both salts, especially $CaCl_2$, could be used to lower gelation temperatures to minimise energy consumption during gel formation.

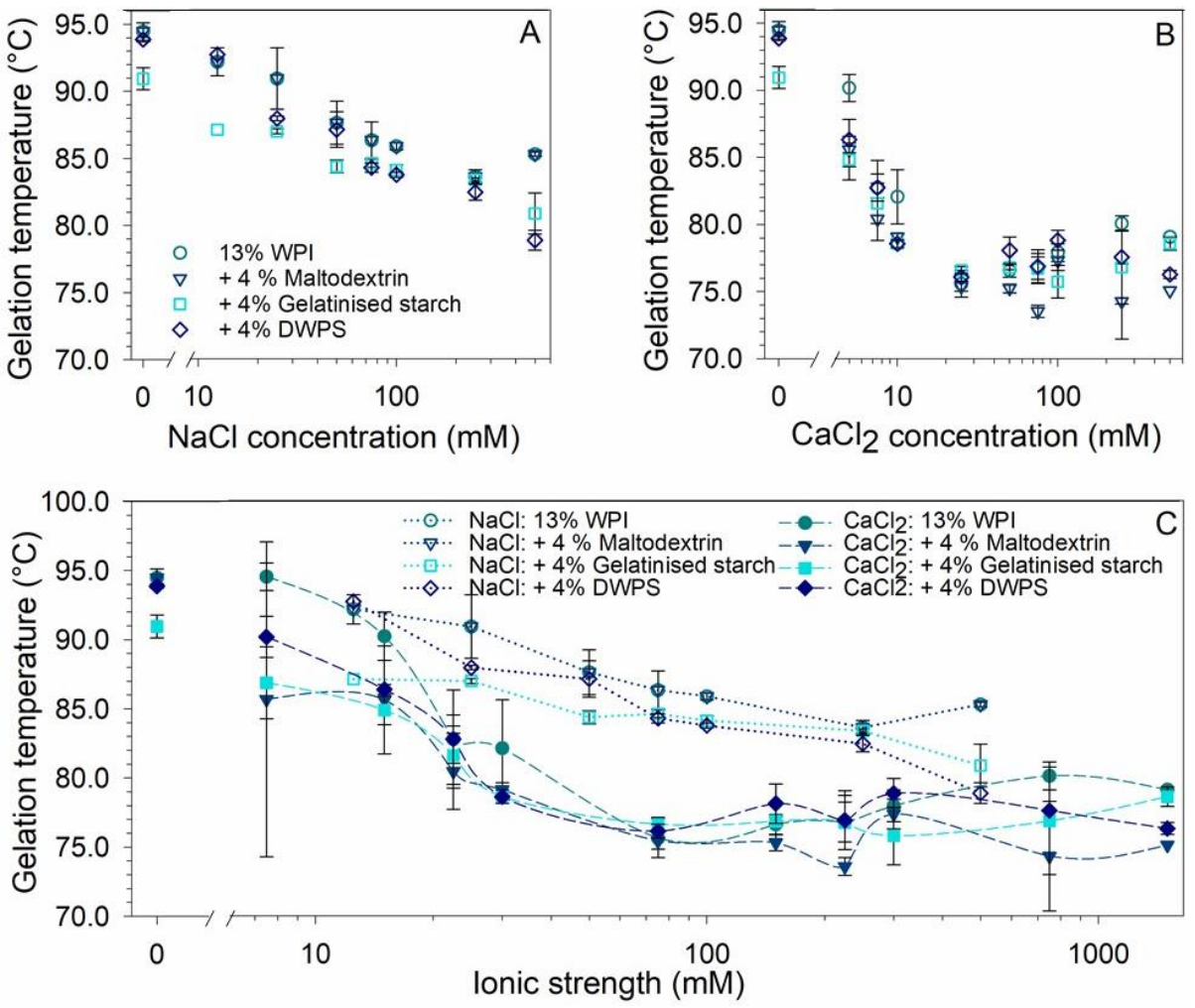

Figure 8-2 Effect of salts on the gelation temperature of 13 % w/w WPI and 13 % w/w WPI + 4% w/w maltodextrin or gelatinised starch or 140 °C DWPS at varied: (A) NaCl concentrations of 0, 12.5, 25, 50, 75, 100, 250 and 500 mM, and (B) $CaCl_2$ concentrations of 0, 2.5, 5, 7.5, 10, 25, 50, 75, 100, 250 and 500 mM, and (C) effect of NaCl and $CaCl_2$ on gelation temperature at equivalent ionic strengths (lines serve as visual aids). The gelation temperatures were obtained from temperature sweep when *G'* crossed over *G"* (tan δ = 1, at 1% strain and 1 Hz frequency) during the heat-induced gelation. Values are plotted as means ± standard error.

8.3.3. Effect of ionic strength on the rheological, textural and microstructural properties of WPI + DWPS gels

8.3.3.1. Effect of NaCl

The effect of NaCl on the *G'* of pure WPI and composite gels is presented in Figure 8-3A. Pure WPI and WPI + maltodextrin showed similar increasing trends in *G'* values with increasing NaCl concentrations up to 100 and 75 mM, respectively. Further increase in NaCl concentrations caused a slight reduction in *G'* and the values plateaued off to ~36.8 and 15.7 kPa respectively at 250 mM NaCl. Such behaviour of NaCl in WPI gels was also noted by Urbonaite *et al.* (2016) when NaCl increased from 0 to 300 mM. The authors observed an increase in WPI gel stiffness where the network strands grew thicker up to an optimum NaCl concentration of 150 mM. Further increase in NaCl after this optimum concentration (from 150 to 300 mM) led to even thicker strands, where microstructure with a coarser network (from 1.6 to 2.0 µm) and a lower protein connectivity was noted, leading to a decrease in the gel stiffness values from ~430 to ~80 kPa.

As mentioned in Chapter 7, without NaCl, WPI + 140 °C DWPS exhibited a unique synergistic increase in *G'* and hardness values (~11.4 kPa and ~90 N) that was almost twice the values of that WPI + gelatinised starch (~5.7 kPa and ~52 N). However, the unique synergistic effect of DWPS in WPI gel diminished with the addition of NaCl. Similar *G'* and hardness values were noted among the mixed systems (*i.e.*, WPI + maltodextrin or gelatinised starch or DWPS) at 12.5 mM NaCl (Figure 8-3A and C). Further increase in *G'* values were noted in WPI + gelatinised starch and WPI + DWPS up to NaCl concentrations of 50 mM and 25 mM, respectively. The subsequent increase in NaCl concentrations for WPI + gelatinised starch (75 mM) and WPI + DWPS (50 mM) led to lower *G'* values. With WPI + gelatinised starch gels, *G'* plateaued off at ≥ 250 mM. In contrast, a recovery in *G'* value was noted in WPI + DWPS at 75 mM, followed by a gradual decrease in *G'* at 100 mM before plateauing at ≥ 250 mM.

In order to understand further the texture and microstructure of these samples, gels of pure WPI and WPI + gelatinised starch or DWPS containing 0–500 mM NaCl were formed, where their textural attributes (consistency and homogeneity) were evaluated visually at macroscopic and microscopic scales (Figure 8-3B & Figure 8-4), and measured using a texture analyser to obtain the hardness values (Figure 8-3C). Self-supporting gels were obtained throughout the tested NaCl concentrations of 0–500 mM for pure WPI gels. As for WPI + gelatinised starch, gels with different textural properties were observed at increasing NaCl concentrations, including: (i) self-supporting gels, (ii) self-supporting gels with a liquid centre and (iii) paste-like weak gels at ≤ 75, 100, ≥ 250 mM NaCl, respectively. WPI + DWPS samples exhibited an even more varied range of textural properties, including those observed

in WPI + gelatinised starch as above (i, ii and iii at ≤ 25, 50–75 and 100 mM NaCl concentrations respectively) and additional recovery of texture at ≥ 250 mM NaCl, where soft self-supporting gels were formed.

In general, *G'*, the visual properties of the samples (consistency and homogeneity), and the hardness values correlated well with each other. The decreased *G'* values observed for WPI + gelatinised starch or DWPS (Figure 8-3A) could be explained by the inhomogeneity of the gels (Figure 8-3B), where self-supporting gels with a liquid centre were observed at 100 mM and 50 mM NaCl, respectively. A further increase of NaCl concentrations to ≥ 250 mM in WPI + gelatinised starch and 100 mM in WPI + DWPS, resulted in weak gels with a paste-like consistency, hence, the observation of lower *G'* values compared to those at the lower NaCl concentrations.

These differences in the gel texture can be further explained by observing the microstructure of the composite gels (Figure 8-4). At a low NaCl concentration of 25 mM, the addition of gelatinised starch or DWPS to WPI seems to cause increased protein aggregation, which is evidenced by the increased roughness observed in the micrographs of composite gels as compared to that of a pure WPI sample. At 75 mM, the liquid portion of WPI + DWPS was analysed using CSLM, whereas the gel portion was imaged with SEM. For the liquid portion, WPI existed as dispersed spherical droplets in the continuous phase (CSLM micrograph in Figure 8-4 with DWPS). Such microstructure is typical of micro-phase separation of incompatible biopolymers, where the adoption of such spherical conformation minimises the overall surface tension of the system (Ponchel & Cauchois, 2016). Similar micro-phase separation has also been observed in a binary system containing 13% w/w WPI + 0.5% w/w carrageenan at 50–100 mM NaCl (Çakır & Foegeding, 2011). The gel portion of WPI + DWPS at 75 mM was different from that observed at 25 mM NaCl, where the former appeared to be a more open network (SEM micrographs in Figure 8-4 with DWPS). With these observations, the occurrence of thermodynamic incompatibility resulting in an inhomogeneous gel could be a plausible reason for the reduced *G'* value of WPI + DWPS (Figure 8-3A). The increase of NaCl from 75 to 100 mM caused a change in texture from a self-supporting gel with a liquid centre to a weak gel with paste-like consistency (Figure 8-3B). The paste-like texture is likely due to the thermodynamic incompatibility between WPI and DWPS at 100 mM NaCl, resulting in a microstructure resembling that of the liquid portion of WPI + DWPS at 75 mM, *i.e.*, WPI unable to form a continuous network (de Jong & van de Velde, 2007).

At high NaCl concentrations (500 mM), the good protein connectivity seen in the micrographs of WPI + DWPS (Figure 8-4 with DWPS) suggests that the recovery of a self-supporting gel structure in WPI + DWPS was due to the dominating protein-protein interactions. Hence, such enhanced interactions

were facilitated by high levels of NaCl. In contrast, poor protein connectivity was noted in WPI + gelatinised starch at 500 mM NaCl (Figure 8-4 with gelatinised starch). The poor protein connectivity could explain the lower *G'* values and the paste-like consistency observed in WPI + gelatinised starch as compared to WPI + DWPS. Gelatinised starch is more negatively charged (-31.0 mV) than 140 °C DWPS (-2.8 mV), which suggests that the former, is likely to compete with proteins for sodium ions. The competition between protein and gelatinised starch for positive ions led to a lower amount of available sodium ions to neutralise the negative charges on protein molecules. Hence, the remaining negative charges on the proteins were able to cause protein-protein repulsions and prevented good connectivity. Another possible reason for the observed weaker structure in WPI + gelatinised starch, could be that the gelatinised starch, being a larger molecule (~3.6×10^8 Da as compared to M_w of 140 °C DWPS at 1.6×10^7 Da), was more effective in disrupting the connectivity of the protein network.

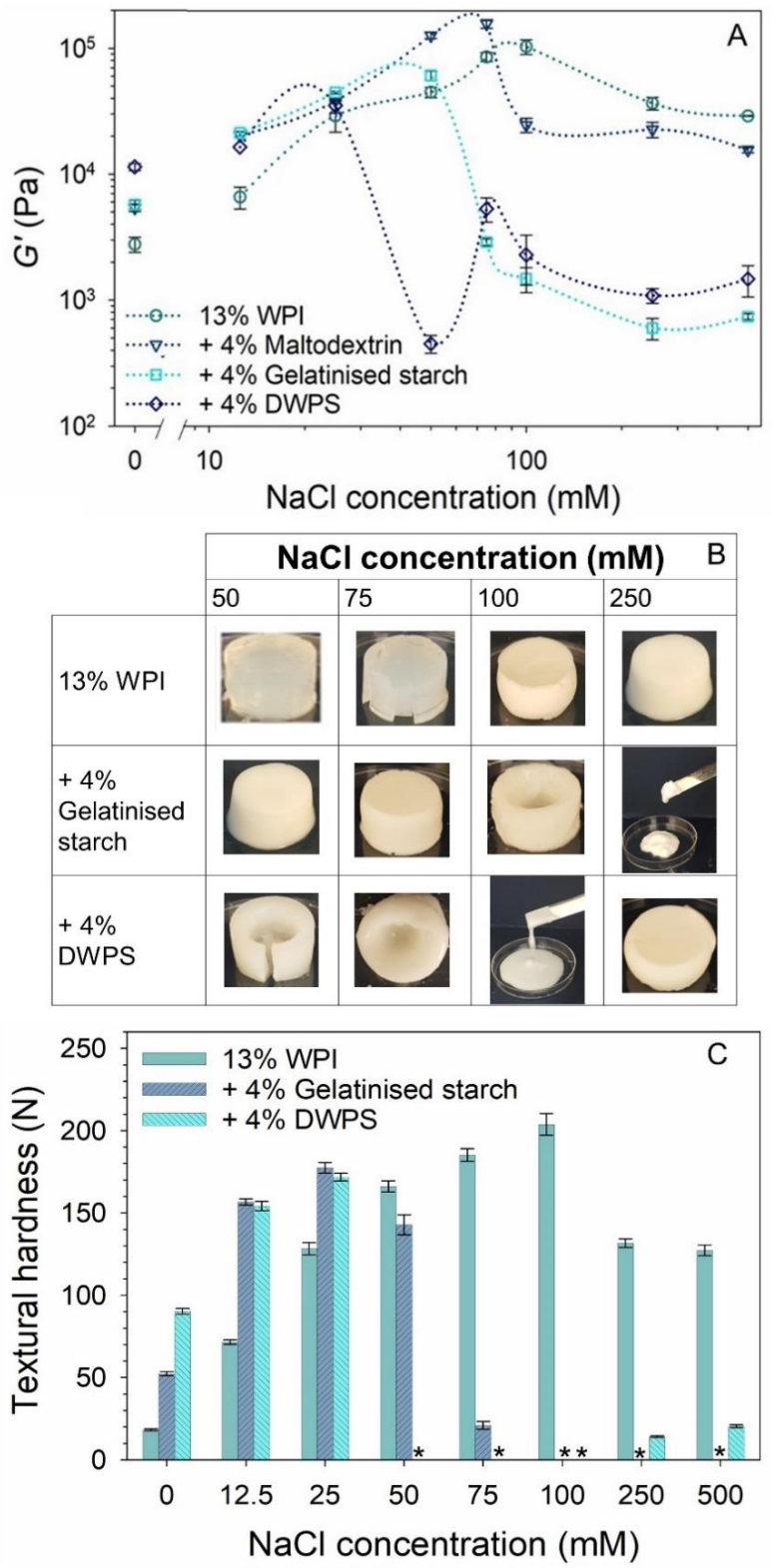

Figure 8-3 Effect of NaCl on the: (A) *G′* from frequency sweep at 1% strain and 1 Hz frequency of 13% w/w WPI and 13% w/w WPI + 4% w/w maltodextrin or gelatinised starch or 140 °C DWPS with 0–500 mM NaCl at 20 °C. Lines in the graphs serve as visual aids, (B) visual appearance of 13% w/w WPI and 13% w/w WPI + 4% w/w gelatinised starch or 140 °C DWPS at 50, 75, 100 and 250 mM NaCl, (C) textural hardness of 13% w/w WPI and 13% w/w WPI + 4% w/w gelatinised starch or DWPS with 0–500 mM NaCl at room temperature. Values are plotted as means ± standard error. Note that compression test was not performed on inhomogeneous/paste-like gels (denoted with *).

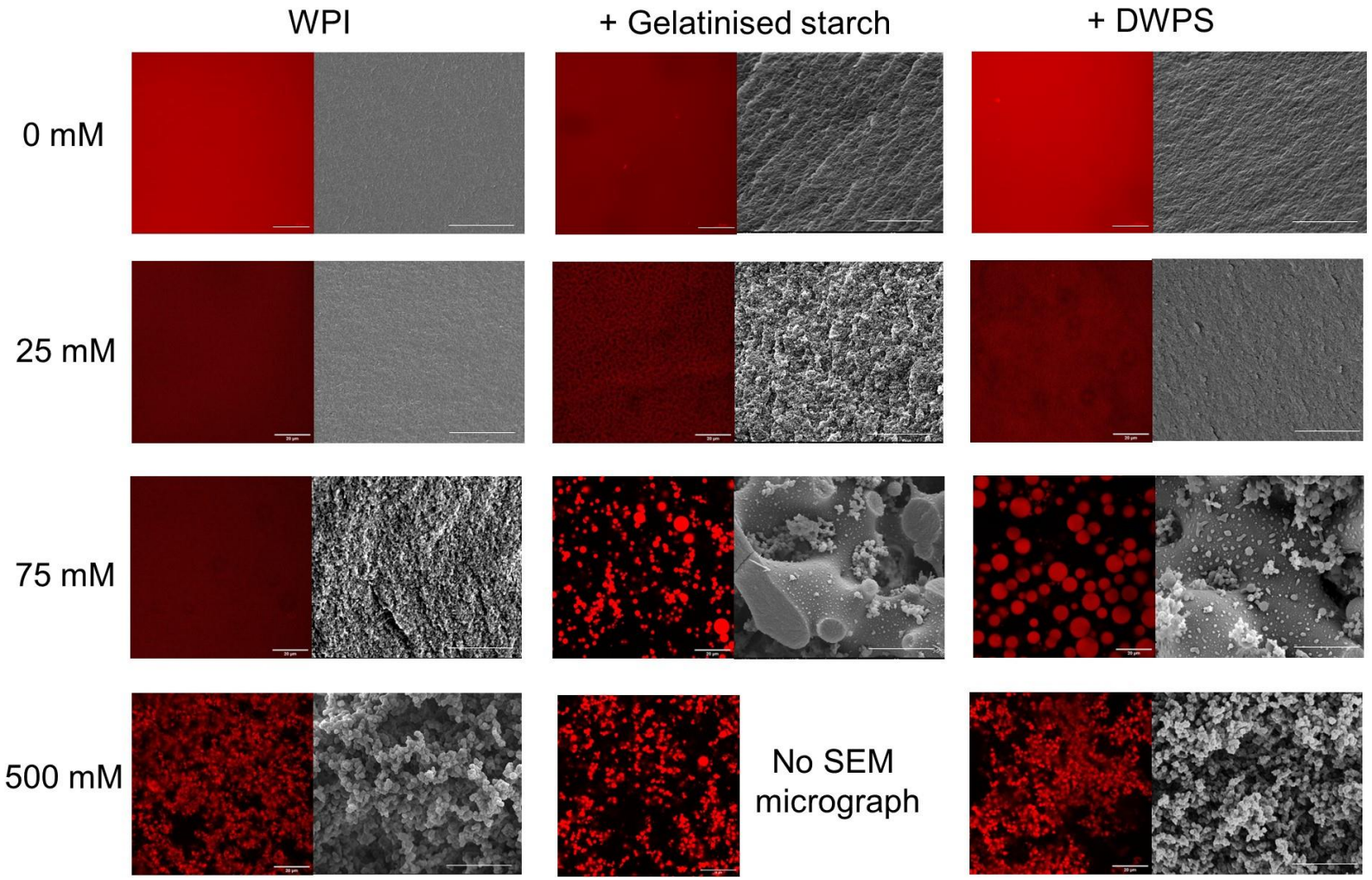

Figure 8-4 Effect of NaCl on the microstructure of 13% w/w WPI and 13% w/w WPI + 4% w/w gelatinised starch or 140 °C DWPS gels at 0, 25, 75 and 500 mM NaCl: CSLM micrographs (630×) and SEM micrographs (2500×). Note that SEM was not done on paste-like samples. The scale bars are 20 µm.

8.3.3.2. Effect of $CaCl_2$

The effect of $CaCl_2$ on the *G'*, visual appearance and gel hardness of pure WPI and composite gels is presented in Figure 8-5. Like NaCl, increasing trends were observed in both *G'* and hardness values at the initial increase of $CaCl_2$ concentrations (Figure 8-5A and C). However, the occurrence of maximum *G'* and hardness values was observed at considerably lower concentrations in the presence of calcium (~5 mM $CaCl_2$ versus ~25 mM NaCl for WPI + gelatinised starch or DWPS). These observations could again be attributed to the ability of calcium ions to form bridges between protein molecules, which facilitated protein aggregation (Hongsprabhas *et al.*, 1999; Joyce *et al.*, 2018). At ≤ 10 mM $CaCl_2$, all the gels were self-supporting with good protein connectivity as observed in both the CSLM and SEM micrographs (Figure 8-6). However, at 25 mM, inhomogeneous gels were noted for WPI + gelatinised starch or DWPS (Figure 8-5B), which were attributed to the phase separation between WPI and starch polymers (Figure 8-1) occurring during gel formation. These two opposing forces present during gelation—segregative and associative—are likely to result in heterogeneous gels (Matia-Merino, Lau, & Dickinson, 2004). At 75 mM $CaCl_2$, gelatinised starch or DWPS in the composite gels disrupted the connectivity of protein network (Figure 8-6), resulting in the formation of a weak gel with paste-like consistency (Figure 8-5B). Even though, increased protein connectivity was observed in CSLM micrographs of WPI + gelatinised starch or DWPS at 500 mM $CaCl_2$ (Figure 8-6), the gels still retained their paste-like consistency (Figure 8-5B). The observations in this study were different from Yang *et al.* (2014), where the authors noted self-supporting composite gels containing 15% w/w WPI + 3–5% w/w wheat starch at $CaCl_2$ concentration from 5 to 192 mM. In their system, starch existed as a filler that was trapped in the protein continuous network. The differences in gel properties could be due to the differences in sample preparation. In this study, starch gelatinisation was carried out under shear before mixing with WPI stock solution, followed by the heating of this mixture, whereas in Yang *et al.* (2014), the starch was gelatinised during the heat-induced gelation of the composite gel. It is likely that the starch in Yang *et al.* (2014) was less gelatinised and had some of its granular structure, which led to the entrapment of starch in the protein network. Consequently, their gelatinised starch might not be as effective in disrupting the connectivity of the protein network at high $CaCl_2$ concentrations as compared to the inclusion of gelatinised starch or DWPS in WPI gels of this study. In addition, a higher protein concentration (15% w/w protein) was also used in their system as compared to 13% w/w protein in this study, which could result in a gel having prominent protein gel characteristics with a stronger network.

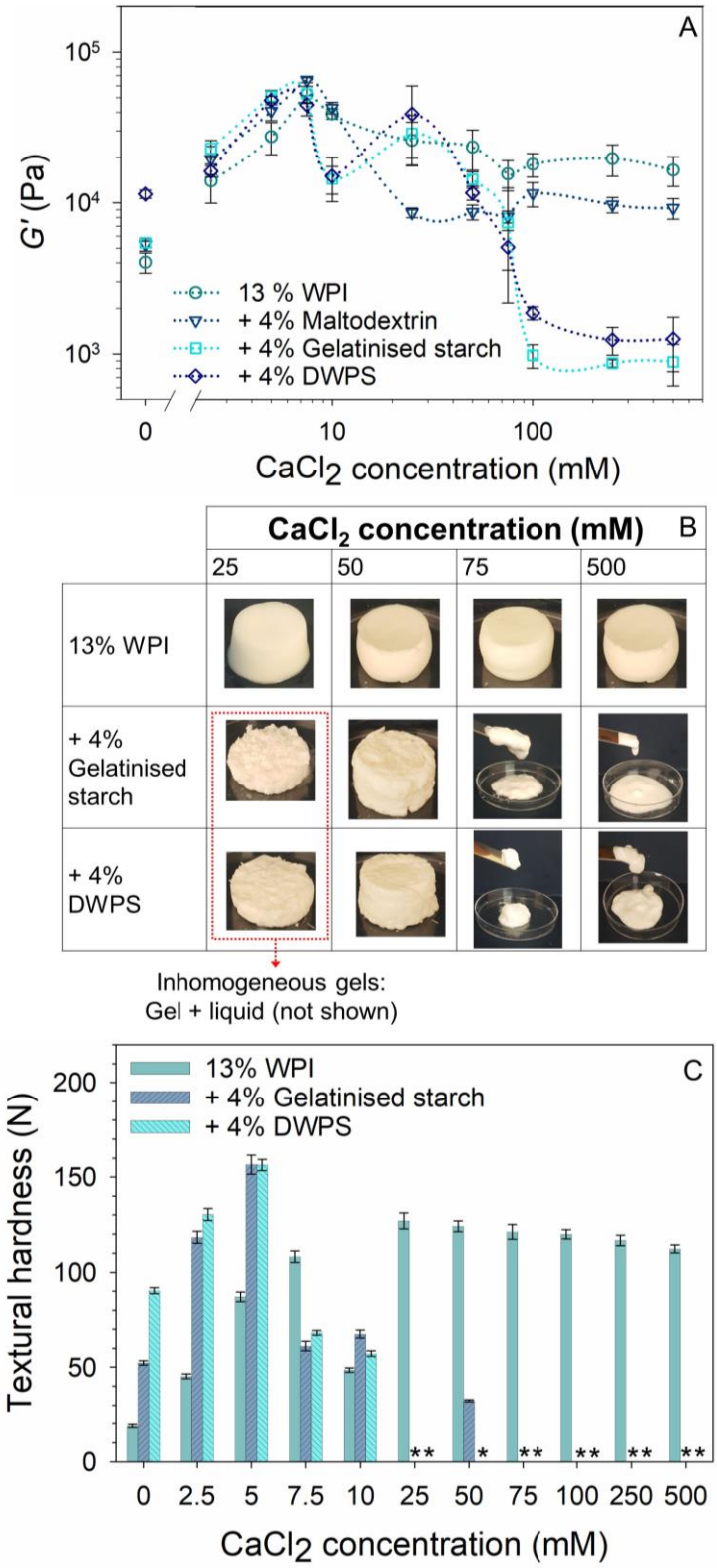

Figure 8-5 Effect of $CaCl_2$ on the: (A) *G'* from frequency sweep at 1% strain and 1 Hz frequency of 13% w/w WPI and 13% w/w WPI + 4% w/w maltodextrin or gelatinised starch or 140 °C DWPS with 0–500 mM $CaCl_2$ at 20 °C. Lines in the graphs serve as visual aids, (B) visual appearance of 13% w/w WPI and 13% w/w WPI + 4% w/w gelatinised starch or 140 °C DWPS at 25, 50, 75 and 500 mM $CaCl_2$, (C) textural hardness of 13 % w/w WPI and 13% w/w + 4% w/w gelatinised starch or 140 °C DWPS with 0–500 mM $CaCl_2$ at room temperature. Values are plotted as means ± standard error. Note that compression test was not performed on inhomogeneous/paste-like gels (denoted with *).

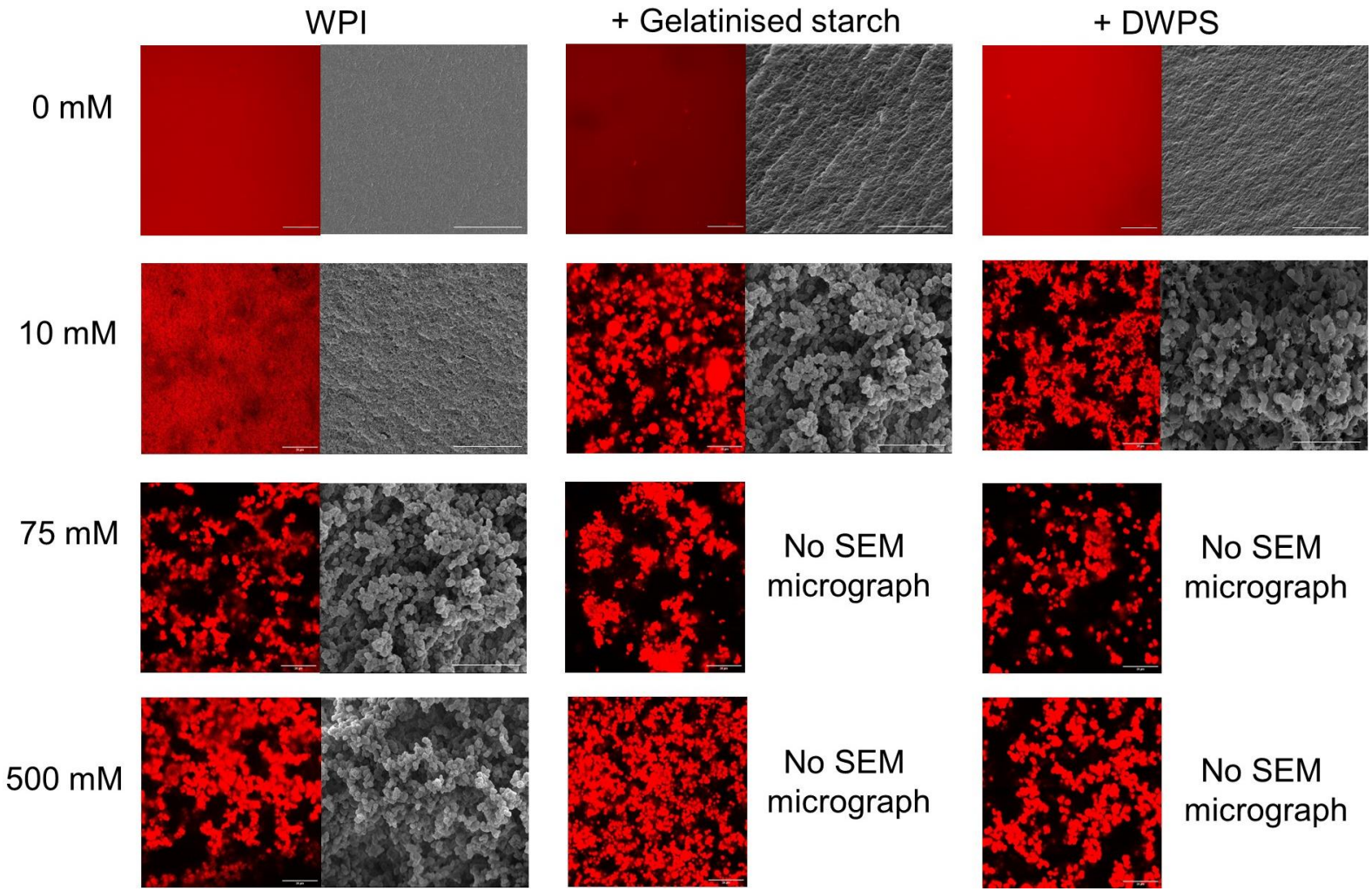

Figure 8-6 Effect of $CaCl_2$ on the microstructure of 13% w/w WPI and 13% w/w WPI + 4% w/w gelatinised starch or 140 °C DWPS gels at 0, 10, 75 and 500 mM $CaCl_2$: CSLM micrographs (630×) and SEM micrographs (2500×). Note that SEM was not done for paste-like samples. The scale bars are 20 µm.

8.4. General remarks

The above findings have demonstrated that both NaCl and $CaCl_2$ can be used to manipulate the microstructure and mechanical properties of composite systems based on heat-induced whey protein gels with added starch—such knowledge is valuable in food formulations. In particular, the WPI + 140 °C DWPS system was able to yield a plethora of gel textures with desirable attributes at varying NaCl concentrations that can be used in different food applications. The range of possible textures with WPI + DWPS gels include paste-like texture (100 mM NaCl or 75–500 mM $CaCl_2$) and soft self-supporting gels (250–500 mM NaCl). These gels can be used in 3-D printed foods as well as when formulating pH neutral high-protein-dense foods with or without calcium fortification for the growing senior population and dysphagia sufferers. It is worthy to note that the effect of NaCl as a monovalent salt has been verified using KCl at similar concentrations (Appendix E). Future work is recommended to evaluate the feasibility of textural manipulation using 140 °C DWPS in combination with ionic strength variations, for specific high-protein food matrices.

8.5. Conclusions

Visual macro-phase separation was only observed in mixtures containing $CaCl_2$ (not NaCl) and the separations were observed at 50–500 mM in WPI + maltodextrin and 10–75 mM in WPI + gelatinised starch or 140 °C DWPS systems. By controlling the NaCl concentration in WPI + 140 °C DWPS systems—affecting micro-phase separation and/or protein connectivity—a plethora of gel textures suitable for different food applications can be obtained. Such gel textures include homogeneous strong self-supporting gels, inhomogeneous self-supporting gels with a liquid centre, and weak gels with a paste-like consistency. Recovery of self-supporting gel structures was also noted at ≥ 250 mM NaCl, where gels exhibited a soft texture. Weak gels with paste-like consistency were also noted in WPI + 140 °C DWPS systems containing 75–500 mM $CaCl_2$. These systems can serve as a form of mineral carrier for calcium-fortified foods. The ability to generate a range of textures in WPI gelation-based foods by using DWPS under different ionic conditions is a feasible strategy for formulating high-protein foods (with or without calcium fortification) for 3-D printing as well as for dysphagia sufferers, where the range of food textures include thickened fluids and soft solids.

Chapter 9 Overall conclusions and recommendations

9.1. Overall conclusions

The general overview of the DWPS characteristics and its interactions under investigation in this thesis is summarised in Figure 9-1.

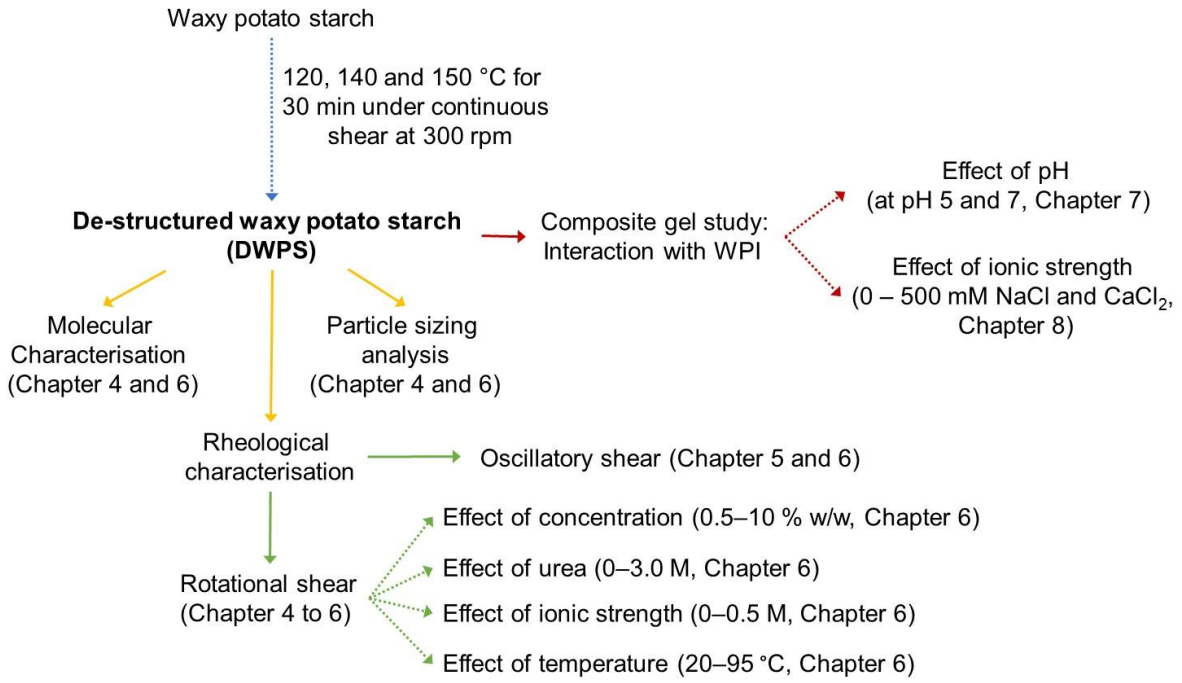

Figure 9-1 General overview of the DWPS characteristics and its interactions under investigation in this thesis.

In this study, native waxy potato starch was modified at 120–150 °C for 30 min, under continuous shear at 300 rpm to produce DWPS materials (containing starch fragments and macromolecules). Due to the physical method employed in the modification, these DWPS materials can be considered to possess "clean-label" status. This thesis includes work by the author that has been published (Page xxiii) as referenced in the text with key focus areas including molecular, rheological and physico-chemical properties of the modified starch. The influence of the different DWPS ingredients was also explored in a WPI-based gel system at different pHs (*i.e.*, pH 5 and 7) and ionic strengths, where their mechanical and microstructural properties were extensively investigated. With the established

knowledge, the research questions were answered (in Section 9.1.1 to 9.1.4) and suggested applications for DWPS are presented in Section 9.1.5:

9.1.1. How does the de-structuring process disassemble the waxy potato starch granules? (Chapter 4)

- At 120 °C, 5% w/w waxy potato starch granules were disassembled into their macromolecular chains, without degradation of amylopectin chains (similar bi-modal molar mass (M_w) distributions and M_w values as native amylopectin).
- At elevated temperatures from 120 to 150 °C, the cleavage of individual amylopectin chains occurred.
- The amylopectin chains were likely to be cleaved at α-1,4 linkages approximately near the middle of the main amylopectin backbone.
- The de-structuring process was deemed to be incomplete even at 150 °C (remnants of large fragments ≥ 1 µm were present in 150 °C DWPS).

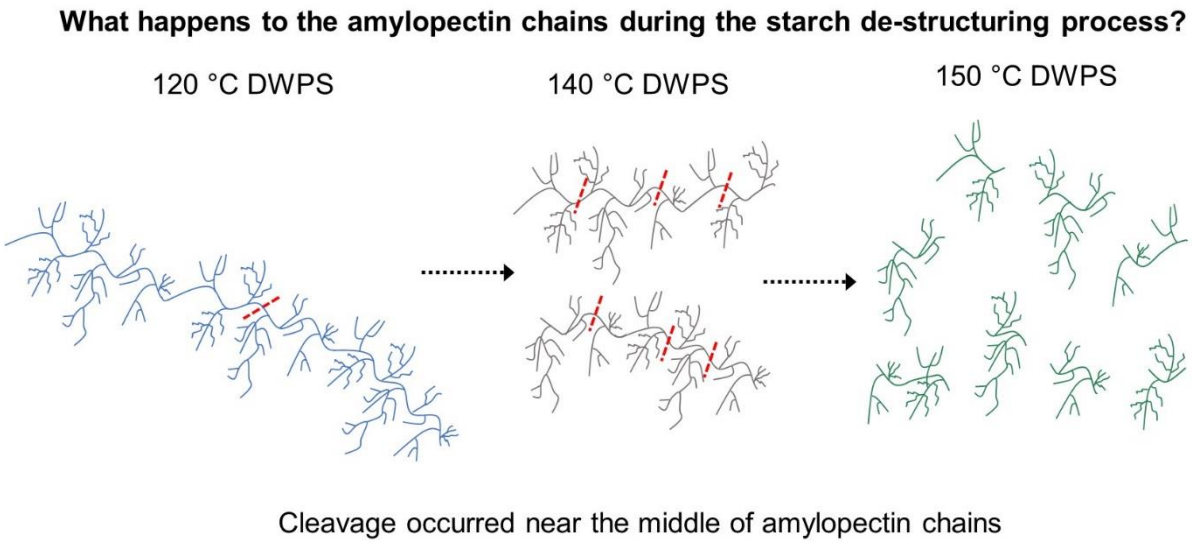

Figure 9-2 Schematic illustration of amylopectin degradation during the de-structuring process from 120 to 150 °C.

9.1.2. How do the structural changes of DWPS during the de-structuring process alter its rheological properties? (Chapter 5 and 6)

- DWPS samples showed different degrees of shear- and time-dependencies, which are different from conventionally gelatinised (Figure 9-3) and enzymatically-modified starches (Appendix F).
- At 120 °C, DWPS exhibited shear-thickening at ~10–20 s^{-1} during its shear-up viscosity curve, and complex thixotropy and anti-thixotropy characteristics were noted upon a complete shear cycle. Such behaviours were absent in the control sample (gelatinised starch) that exhibited solely shear-thinning and thixotropy behaviours.
- At 140 °C, DWPS lost its shear-thickening behaviour, demonstrating a slight shear-thinning behaviour and anti-thixotropy properties.
- At 150 °C, DWPS showed Newtonian properties.

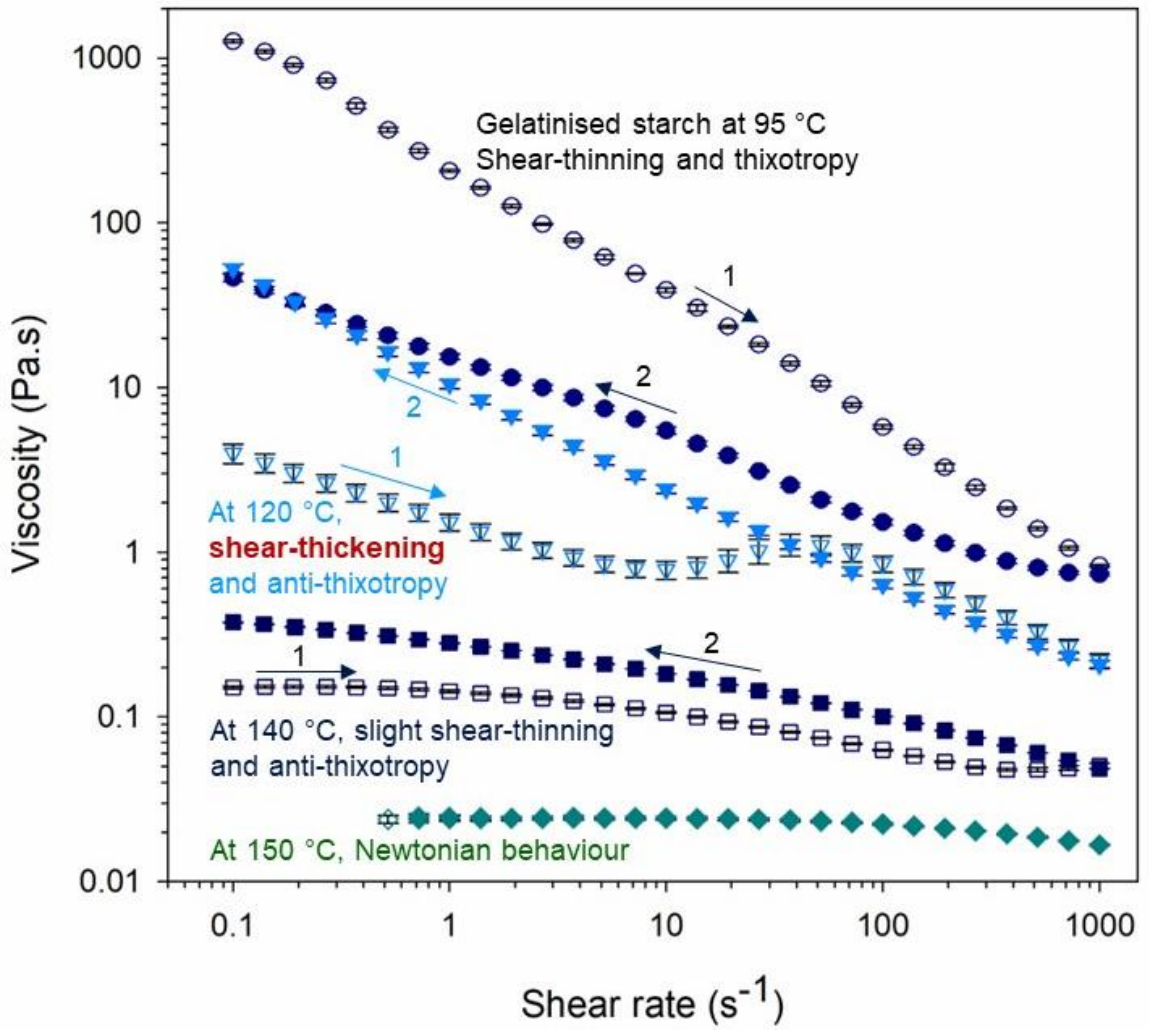

Figure 9-3 Rheological profiles of gelatinised starch (95 °C) and DWPS treated at 120, 140 and 150 °C upon increasing (unfilled markers, 1) or decreasing shear rate (filled markers, 2). Measurements were taken at 20 °C.

- The mechanism for the interesting shear-thickening and/or anti-thixotropy (shear-induced) behaviours of 120 and 140 °C DWPS is proposed to be a two-step process:
    i. Upon shear at the critical shear rate, the shear stress caused a size reduction in the starch fragments.
    ii. The increased number of small fragments together with the amylopectin chains in very close proximity could lead to the formation of a complex network probably consisting of amylopectin chains and fragments (2–20 µm). Shear thickening properties were attributed largely to these soft fragment particles colliding and sliding past each other during shear.
- The mechanism for shear-thickening and anti-thixotropy was determined to be not caused by hydrogen bonding, electrostatic, hydrophobic interactions, or the combination of these interactions.

9.1.3. How does DWPS affect the mechanical properties, microstructure and water-immersion stability of polymeric and particulate whey protein isolate gels (Chapter 7)?

At neutral pH, upon the addition of 4% w/w DWPS to 13% w/w polymeric WPI gel, the following was concluded:

- A unique synergistic increase of gel strength in WPI + 140 °C DWPS (~twice as high as those in the control samples) was observed. The synergistic increase coincided with the densest gel microstructure among the composite gels. These properties could be due to molecular interactions between WPI and DWPS.
- Enhanced water-immersion gel stability (*i.e.*, gel integrity and leaching properties) was noted in WPI + DWPS (or gelatinised starch remained as intact gels) as compared to pure WPI gel (fluid gel) and WPI + maltodextrin (disintegrated gel) upon 40 h water-immersion.

At pH 5 (near p*I* of whey protein), upon the addition of 4% w/w DWPS to 13% w/w particulate WPI, the following was concluded:

- The hardness of composite gels declined logarithmically with increasing molar mass of the DWPS polymers (120 °C DWPS).
- The decreased gel hardness was attributed to the combined effects of: (i) thermodynamic incompatibility between WPI and DWPS, and (ii) the disruption of the protein network by starch materials (both of which were affected by the molar mass of starch polymers).
- DWPS acted as inactive fillers trapped in the protein gel matrix.

- The porous structure and insoluble protein gel matrix led to good water-immersion stability with poor water absorption (< 12 % w/w), low protein leaching (≤ 0.4% w/w) and high carbohydrate leaching (~29–71% w/w) when gels were immersed in water for 40 h.

9.1.4. What are the effects of NaCl and $CaCl_2$ on the interaction between WPI and DWPS (Chapter 8)?

For NaCl systems of WPI + 140 °C DWPS:

- The addition of NaCl concentration (0–500 mM) to the WPI + DWPS system—affecting the micro-phase separation and/or protein connectivity—yielded a plethora of gels with different textures (Figure 9-4) suitable for various food applications.
- The recovery of a gel network at high NaCl concentration of ≥ 250 mM (forming a soft self-supporting gel from paste-like consistency at 100 mM) was unique, as it was not seen in WPI + gelatinised starch.

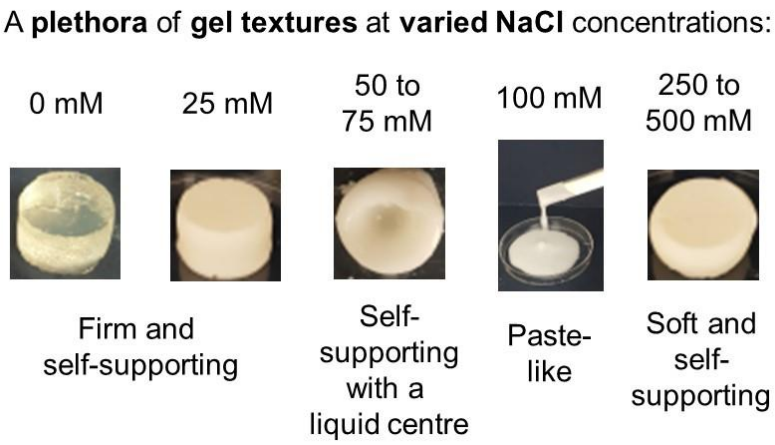

Figure 9-4 Varied gel textures of 13% w/w WPI + 4% w/w 140 °C DWPS at different NaCl concentrations (0 – 500 mM).

For $CaCl_2$ systems of WPI + 140 °C DWPS:

- Three different types of gels were formed:
  i. Firm and self-supporting
  ii. Phase-separated
  iii. Paste-like consistency
- The strong thermodynamic incompatibility between WPI and DWPS at 25 mM $CaCl_2$ caused phase separation between polymers, which preceded the network formation during the gelation process, resulting in an inhomogeneous gel with separated layers.
- At ≥ 75 mM $CaCl_2$, paste-like weak gels with low *G'* values (~1.3–5.5 kPa) was formed. These weak gels were attributed to the disrupted protein connectivity by DWPS. The weak gel

structures with paste-like consistency were distinctly different from the firm self-supporting gel structures (high *G'* values) of pure WPI (~16–20 kPa) and WPI + maltodextrin (~9–12 kPa), but similar to those of WPI + gelatinised starch (~0.9–8.0 kPa) at the similar $CaCl_2$ concentrations.

9.1.5. Potential applications of de-structured starch

The findings from this study indicate several potential applications for DWPS samples:

1. As a stabiliser to enhance structure upon shear

The shear-induced structure (*i.e.*, gelation and thickening properties) exhibited by 120 °C DWPS was found to be stable up to at least 72 h, which can potentially be used in food applications such as whipping cream where the DWPS could be used to enhance the foam stability of aerated emulsions.

2. As a stabiliser in heat-sensitive formulations

The development of the rheological properties of DWPS is shear-induced as opposed to most of the polysaccharides such as agar and carrageenan, where their gelling ability is heat-mediated. Thus, DWPS could be a suitable stabiliser for food systems containing heat-sensitive ingredients (*e.g.*, vitamins and flavours).

3. As a co-texturiser in cost-effective protein-based foods

The synergistic increase of gel hardness in 13% w/w WPI + 4% w/w 140 °C DWPS can be advantageous in enhancing the firmness of protein-enriched food products (neutral pH) without the need to further increase protein levels and cost, as proteins are generally more costly than modified starches.

4. As a co-texturiser to control the release of flavour in food matrices

DWPS can be added to acidified high-protein foods to control different degrees of liquid (*e.g.*, carry flavour) being released during mastication, to provide unique textural and sensory experiences. The pore size and hardness of particulate gels at pH 5 can be manipulated by incorporating DWPS samples of different molar masses.

5. As a co-texturiser in high-protein 3-D printed foods and dysphagia foods

The ability to generate a range of textures in WPI composite gels by using 140 °C DWPS and salts (*i.e.*, NaCl and $CaCl_2$ at different ionic strengths) is a feasible strategy for formulating high-protein foods (with or without calcium fortification) for applications such as 3-D printed foods as well as soft-textured foods for dysphagia sufferers, where the range of food textures fabricated include from thickened fluids to soft solids.

6. As an enhancer of water-immersion stability of aqua feed

The enhanced gel integrity of fine-stranded polymeric WPI + DWPS gel at neutral pH could be used in aqua feed formula, to ensure that the feed remains available for the marine animals as long as possible in the water.

7. As a raw material for papermaking and biodegradable packaging

Starch is one of the main components of papermaking. Traditionally, cationic starch, amphoteric starch or native starch are usually used added to the pulp during the wet-end operation for internal sizing. The molar mass of starch is an important parameter, where non-degraded starch with a higher molar mass is suitable for wet-end application due to higher binding power, whereas degraded starch is suited for surface application due to its lower viscosity (Maurer, 2009). Since DWPS samples exhibited a wide range of molar masses and viscosities, making them potential materials in both the wet-end and surface applications of papermaking. In addition, DWPS could potentially be used in sustainable and bio-based packaging to reinforce the properties of packaging materials.

9.2. Recommendations

1. Quantification of starch fragments and macromolecules

The disassembly of starch fragments and macromolecules needs quantification in terms of the proportions of fragments and amylopectin polymer chains since the proportions could impact the mechanical properties of food systems in which DWPS is used.

2. De-structuring starch of other starch types and varieties

In this study, only waxy potato starch (a B-type starch) is evaluated. Thus, there are still questions on how other starch types (*i.e.*, A- and C-types) and varieties (*i.e.*, starch that contains amylose such as normal and high-amylose varieties) would behave in comparison to DWPS.

3. Shear-thickening mechanism

The mechanism of shear-thickening remains inconclusive based on our current findings. We found that the shear-thickening was associated with the generation of smaller fragments (2–20 μm) upon shear. The size reduction led to the hypothesis that the shear-thickening mechanism is due to the physical interlocking of starch fragments within the amylopectin chains. However, the hypothesis remains to be proven.

In a separate study, a loss in shear-thickening properties was found for 5% w/w 120 °C DWPS prepared in 50 or 100% w/w DMSO. The results can be found in Appendix G. DMSO is a common solvent used to solubilise starch macromolecules. At lower DMSO concentrations (0–25% w/w DMSO) exhibited both anti-thixotropy and shear-thickening behaviours in their shear-up curves, whereas samples containing 50 and 100% w/w DMSO exhibited a higher viscosity profile with only thixotropy behaviour, and no shear-thickening was noted. Similar to the observations (a shift in particle size and shear-thickening in 0% DMSO system—the studied system in Chapter 5), samples containing 0–25% w/w DMSO showed a shift in particle size to a 2–20 μm region upon shear. In contrast, minimal changes were noted in the particle-size distribution of samples containing 50 and 100% w/w DMSO. These results are consistent with what was observed in Chapter 5. Further studies are recommended to elucidate the role of DMSO in preventing shear-thickening behaviour at higher concentrations (*i.e.*, ≥ 50% w/w DMSO). The knowledge of how DMSO prevents shear-thickening could aid in the elucidation of the shear-thickening mechanism of DWPS in a pure water system (0% w/w DMSO).

4. Fluorescence dye for CSLM starch staining

A covalent-specific starch dye is recommended for further analysis of the WPI + DWPS system (prior work on identifying a starch-specific stain was unsuccessful, as the starch dye interfered with the protein matrix, see Section 3.5.3). A covalent-specific starch dye that stains starch components only in the composite gels will aid in differentiating starch and proteins under CSLM and provides stronger evidence in elucidating the interactions between WPI and DWPS.

5. Interactions between WPI and DWPS

The synergistic increase in *G'* and gel hardness of WPI + 140 °C DWPS was attributed to the highly dense microstructure generated among the composite gel samples. However, the exact mechanism for such an increase in the gel strength is still unclear. Further studies on the interaction between WPI and DWPS using FTIR and solid-state NMR are recommended. These analyses may be beneficial in detecting new chemical bonds and/or identifying molecular interactions between the polymer chains.

6. **Further studies on the effect of DWPS concentration on the interaction between WPI and DWPS**

The composite gel studied in this thesis contained 13% w/w WPI and 4% w/w DWPS, which was a protein-based system. Investigation on composite gel systems with DWPS concentration greater than 4% w/w should be conducted. Composite gels with a higher DWPS concentration could result in a different gel matrix, such as starch being the continuous network or producing an interpenetrating binary gel network.

7. Further interactions study of DWPS with other biopolymers

For the interaction study of a mixed system, WPI was the only biopolymer (neutral WPI in Chapter 7 and Chapter 8, and acidic WPI in Appendix H) that was evaluated. A further interaction study of DWPS with other proteins or polysaccharides is recommended, to explore the applications of DWPS in other biopolymer-based systems.

8. Formulation of whipping cream with DWPS

Based on the shear-thickening and shear-induced gelation of DWPS, DWPS appears promising with the potential to be used in applications such as in whipping cream to enhance foam stability. However, further work to validate the functionality of DWPS in such applications is needed.

9. Formulation of high-protein dense foods with DWPS

At appropriate salts (NaCl or $CaCl_2$) concentrations, DWPS can be used to manipulate the firm texture of WPI gels. Future work is recommended to evaluate the feasibility of using DWPS in combination with variations of ionic strength to manipulate the firm texture of an actual high-protein food, to produce soft solids or thickened fluids (with or without calcium fortification) for 3D printing and dysphagia sufferers.

10. Exploring DWPS as a material to replace soft plastic applications

In recent years, due to the environmental issues associated with plastic pollution, there has been increasing research on biodegradable materials. Starch-based material is one of the most frequently studied natural biodegradable ingredients due to its advantage of being naturally abundant, renewable, low-cost, non-toxic and film-forming ability (Cheng *et al.*, 2021). Thus, it will be beneficial to explore the applications of DWPS as a biodegradable material for packaging and other soft plastic applications.

References

Aberle, T., Burchard, W., Vorwerg, W., & Radosta, S. (1994). Conformational Contributions of Amylose and Amylopectin to the Structural Properties of Starches from Various Sources. *Starch - Stärke, 46*(9), 329-335. doi:10.1002/star.19940460903.

Abioye, V. F., Adeyemi, I. A., Akinwande, B. A., Kulakow, P., & Maziya-Dixon, B. (2017). Effect of steam cooking and storage time on the formation of resistant starch and functional properties of cassava starch. *Cogent Food & Agriculture, 3*(1), 1296401. doi:10.1080/23311932.2017.1296401.

Adebowale, K. O., Henle, T., Schwarzenbolz, U., & Doert, T. (2009). Modification and properties of African yam bean (Sphenostylis stenocarpa Hochst. Ex A. Rich.) Harms starch I: Heat moisture treatments and annealing. *Food Hydrocolloids, 23*(7), 1947-1957. doi:https://doi.org/10.1016/j.foodhyd.2009.01.002.

Adetoro, A. O., Opara, U. L., & Fawole, O. A. (2020). Effect of Carrier Agents on the Physicochemical and Technofunctional Properties and Antioxidant Capacity of Freeze-Dried Pomegranate Juice (Punica granatum) Powder. *Foods (Basel, Switzerland), 9*(10), 1388. doi:10.3390/foods9101388.

Aguilera, J. M. (2000). Microstructure and food product engineering. *Food Technology, 54,* 56–65.

Aguilera, J. M., & Baffico, P. (1997). Structure-Mechanical Properties of Heat-Induced Whey Protein/Cassava Starch Gels. *Journal of Food Science, 62*(5), 1048-1066. doi:https://doi.org/10.1111/j.1365-2621.1997.tb15035.x.

Ai, Y., & Jane, J.-l. (2015). Gelatinization and rheological properties of starch. *Starch - Stärke, 67*(3-4), 213-224. doi:https://doi.org/10.1002/star.201400201.

Ai, Y., & Jane, J.-l. (2018a). Chapter 3 - Understanding Starch Structure and Functionality. In M. Sjöö & L. Nilsson (Eds.), *Starch in Food (Second Edition)* (pp. 151-178): Woodhead Publishing.

Ai, Y., & Jane, J.-l. (2018b). Understanding Starch Structure and Functionality. In M. Sjöö & L. Nilsson (Eds.), *Starch in Food (Second Edition)* (pp. 151-178): Woodhead Publishing.

Allan, M. C., Chamberlain, M., & Mauer, L. J. (2020). Effects of Sugars and Sugar Alcohols on the Gelatinization Temperatures of Wheat, Potato, and Corn Starches. *Foods, 9*(6), 757. doi:10.3390/foods9060757.

Ambigaipalan, P., Hoover, R., Donner, E., & Liu, Q. (2014). Starch chain interactions within the amorphous and crystalline domains of pulse starches during heat-moisture treatment at different temperatures and their impact on physicochemical properties. *Food Chemistry, 143*, 175-184. doi:https://doi.org/10.1016/j.foodchem.2013.07.112.

Andoyo, R., Guyomarc'h, F., & Famelart, M.-H. (2016). Acid gelation of whey protein microbeads of different sizes. *Dairy Science & Technology, 96*(2), 213-225. doi:10.1007/s13594-015-0260-3.

Ang, C. L., Goh, K. K. T., Lim, K., & Matia-Merino, L. (2021a). Rheological characterization of a physically-modified waxy potato starch: Investigation of its shear-thickening mechanism. *Food Hydrocolloids, 120*, 106908. doi:https://doi.org/10.1016/j.foodhyd.2021.106908.

Ang, C. L., Goh, K. K. T., Lim, K., & Matia-Merino, L. (2022a). High-Protein Foods for Dysphagia: Manipulation of Mechanical and Microstructural Properties of Whey Protein Gels Using De-Structured Starch and Salts. *Gels, 8*(7), 399.

Ang, C. L., Matia-Merino, L., Lim, K., & Goh, K. K. T. (2021b). Molecular and physico-chemical characterization of de-structured waxy potato starch. *Food Hydrocolloids, 117*, 106667. doi:https://doi.org/10.1016/j.foodhyd.2021.106667.

Ang, C. L., Matia-Merino, L., Lim, K., & Goh, K. K. T. (2023). Influence of de-structured starch on fine-stranded polymeric and coarse-stranded particulate whey protein gels. *Food Hydrocolloids, 135*, 108201. doi:https://doi.org/10.1016/j.foodhyd.2022.108201.

Ang, C. L., Matia-Merino, L., Sims, I. M., Sargison, L., Edwards, P. J. B., Lim, K., & Goh, K. K. T. (2022b). Characterisation of de-structured starch and its shear-thickening mechanism. *Food Hydrocolloids, 132*, 107864. doi:https://doi.org/10.1016/j.foodhyd.2022.107864.

Anton Paar. (2022). Particle size analysis methods: Dynamic light scattering vs. laser diffraction. Retrieved from https://wiki.anton-paar.com/nz-en/particle-size-analysis-methods-dynamic-light-scattering-vs-laser-diffraction/

Arp, C. G., Correa, M. J., & Ferrero, C. (2020). Production and Characterization of Type III Resistant Starch from Native Wheat Starch Using Thermal and Enzymatic Modifications. *Food and Bioprocess Technology, 13*(7), 1181-1192. doi:10.1007/s11947-020-02470-5.

Atkin, N. J., Cheng, S. L., Abeysekera, R. M., & Robards, A. W. (1999). Localisation of amylose and amylopectin in starch granules using enzyme-gold labelling. In (Vol. 51, pp. 163-172).

Atta-ur-Rahman. (1986). *Nuclear Magnetic Resonance : Basic Principles*: Springer US.

Auty, M. (2019). Microscopy tools for product innovation. *Food Science and Technology, 33*(4), 51-55. doi:https://doi.org/10.1002/fsat.3304_14.x.

Bagley, E. B., & Dintzis, F. R. (1999). Shear thickening and flow induced structures in foods and biopolymer systems. In D. A. Siginer, D. De Kee, & R. P. Chhabra (Eds.), *Rheology Series* (Vol. 8, pp. 63-86): Elsevier.

Bauer, B. A., & Knorr, D. (2005). The impact of pressure, temperature and treatment time on starches: pressure-induced starch gelatinisation as pressure time temperature indicator for high hydrostatic pressure processing. *Journal of Food Engineering, 68*(3), 329-334. doi:https://doi.org/10.1016/j.jfoodeng.2004.06.007.

Beck, M., Jekle, M., & Becker, T. (2011). Starch re-crystallization kinetics as a function of various cations. *Starch - Stärke, 63*(12), 792-800. doi:doi:10.1002/star.201100071.

Becker, A., Hill, S. E., & Mitchell, J. R. (2001). Relevance of Amylose-Lipid Complexes to the Behaviour of Thermally Processed Starches. *Starch/Stärke, 53*, 121-130. doi:10.1002/1521-379X(200104)53:3/4<121::AID-STAR121>3.0.CO;2-Q.

Bello-Pérez, L. A., Roger, P., Baud, B., & Colonna, P. (1998). Macromolecular Features of Starches Determined by Aqueous High-performance Size Exclusion Chromatography. *Journal of Cereal Science, 27*(3), 267-278. doi:https://doi.org/10.1006/jcrs.1998.0186.

BeMiller, J. N. (2019a). 6 - Starches: Molecular and Granular Structures and Properties. In J. N. BeMiller (Ed.), *Carbohydrate Chemistry for Food Scientists (Third Edition)* (pp. 159-189): AACC International Press.

BeMiller, J. N. (2019b). 7 - Starches: Conversions, Modifications, and Uses. In J. N. BeMiller (Ed.), *Carbohydrate Chemistry for Food Scientists (Third Edition)* (pp. 191-221): AACC International Press.

Bennion, B. J., & Daggett, V. (2003). The molecular basis for the chemical denaturation of proteins by urea. *Proceedings of the National Academy of Sciences of the United States of America, 100*(9), 5142-5147. doi:10.1073/pnas.0930122100.

Benoit, S. M., Afizah, M. N., Ruttarattanamongkol, K., & Rizvi, S. S. H. (2013). Effect of pH and Temperature on the Viscosity of Texturized and Commercial Whey Protein Dispersions. *International Journal of Food Properties, 16*(2), 322-330. doi:10.1080/10942912.2011.552015.

Bertoft, E. (2017). Understanding Starch Structure: Recent Progress. *Agronomy, 7*(3). doi:10.3390/agronomy7030056.

Bertoft, E. (2018). Chapter 2 - Analyzing Starch Molecular Structure. In M. Sjöö & L. Nilsson (Eds.), *Starch in Food (Second Edition)* (pp. 97-149): Woodhead Publishing.

Bhattacharjee, S. (2016). DLS and zeta potential – What they are and what they are not? *Journal of Controlled Release, 235*, 337-351. doi:https://doi.org/10.1016/j.jconrel.2016.06.017.

Biliaderis, C. G. (2009). Structural Transitions and Related Physical Properties of Starch. In J. BeMiller & R. Whistler (Eds.), *Starch (Third Edition)* (pp. 293-372). San Diego: Academic Press.

Boye, J. I., & Alli, I. (2000). Thermal denaturation of mixtures of α-lactalbumin and β-lactoglobulin: a differential scanning calorimetric study. *Food Research International, 33*(8), 673-682. doi:https://doi.org/10.1016/S0963-9969(00)00112-5.

Briscoe, B., Luckham, P., & Zhu, S. (1998). Rheological properties of poly(ethylene oxide) aqueous solutions. *Journal of Applied Polymer Science, 70*(3), 419-429. doi:https://doi.org/10.1002/(SICI)1097-4628(19981017)70:3<419::AID-APP1>3.0.CO;2-Q.

Brumovsky, J. O., & Thompson, D. B. (2001). Production of Boiling-Stable Granular Resistant Starch by Partial Acid Hydrolysis and Hydrothermal Treatments of High-Amylose Maize Starch. *Cereal Chemistry, 78*(6), 680-689. doi:10.1094/cchem.2001.78.6.680.

Bryant, C. M., & McClements, D. J. (2000). Influence of xanthan gum on physical characteristics of heat-denatured whey protein solutions and gels. *Food Hydrocolloids, 14*(4), 383-390. doi:https://doi.org/10.1016/S0268-005X(00)00018-7.

Burckbuchler, V., Kjøniksen, A.-L., Galant, C., Lund, R., Amiel, C., Knudsen, K. D., & Nyström, B. (2006). Rheological and Structural Characterization of the Interactions between Cyclodextrin Compounds and Hydrophobically Modified Alginate. *Biomacromolecules, 7*(6), 1871-1878. doi:10.1021/bm060149o.

Çakır, E., & Foegeding, E. A. (2011). Combining protein micro-phase separation and protein–polysaccharide segregative phase separation to produce gel structures. *Food Hydrocolloids, 25*(6), 1538-1546. doi:https://doi.org/10.1016/j.foodhyd.2011.02.002.

Cameron, R. E., Durrani, C. M., & Donald, A. M. (1994). Gelation of Amylopectin without Long Range Order. *Starch - Stärke, 46*(8), 285-287. doi:https://doi.org/10.1002/star.19940460802.

Carreau, P. J., De, D. C. R., & Chhabra, R. P. (2021). *Rheology of Polymeric Systems: Principles and Applications*: Carl Hanser GmbH.

Carvalho, C. W. P., Onwulata, C. I., & Tomasula, P. M. (2007). Rheological Properties of Starch and Whey Protein Isolate Gels. *Food Science and Technology International, 13*(3), 207-216. doi:10.1177/1082013207079897.

Castro, N., Durrieu, V., Raynaud, C., & Rouilly, A. (2016). Influence of DE-value on the physicochemical properties of maltodextrin for melt extrusion processes. *Carbohydrate Polymers, 144*, 464-473. doi:https://doi.org/10.1016/j.carbpol.2016.03.004.

Cavallieri, A., Netto, A., Menossi, M., & Cunha, R. (2007). Whey protein interactions in acid cold-set gels at different pH values. *http://dx.doi.org/10.1051/lait:2007032, 87*. doi:10.1051/lait:2007032.

Cave, R. A., Seabrook, S. A., Gidley, M. J., & Gilbert, R. G. (2009). Characterization of Starch by Size-Exclusion Chromatography: The Limitations Imposed by Shear Scission. *Biomacromolecules, 10*(8), 2245-2253. doi:10.1021/bm900426n.

Chandla, N. K., Saxena, D. C., & Singh, S. (2017). Processing and evaluation of heat moisture treated (HMT) amaranth starch noodles; An inclusive comparison with corn starch noodles. *Journal of Cereal Science, 75*, 306-313. doi:https://doi.org/10.1016/j.jcs.2017.05.003.

Charoenrein, S., Tatirat, O., & Muadklay, J. (2008). Use of centrifugation–filtration for determination of syneresis in freeze–thaw starch gels. *Carbohydrate Polymers, 73*(1), 143-147. doi:https://doi.org/10.1016/j.carbpol.2007.11.012.

Chassenieux, C., Nicolai, T., & Benyahia, L. (2011). Rheology of associative polymer solutions. *Current Opinion in Colloid & Interface Science, 16*(1), 18-26. doi:https://doi.org/10.1016/j.cocis.2010.07.007.

Chen, H., Chen, L., Dang, X., Shan, Z., Dai, R., & Wang, Y. (2019). The structure and properties of granular cold-water-soluble starch by a NaOH/urea aqueous solution. *International Journal of Biological Macromolecules, 141*, 732-737. doi:https://doi.org/10.1016/j.ijbiomac.2019.08.226.

Chen, X., He, X., Fu, X., & Huang, Q. (2015). In vitro digestion and physicochemical properties of wheat starch/flour modified by heat-moisture treatment. *Journal of Cereal Science, 63*, 109-115. doi:https://doi.org/10.1016/j.jcs.2015.03.003.

Cheng, H., Chen, L., McClements, D. J., Yang, T., Zhang, Z., Ren, F., . . . Jin, Z. (2021). Starch-based biodegradable packaging materials: A review of their preparation, characterization and diverse applications in the food industry. *Trends in Food Science & Technology, 114*, 70-82. doi:https://doi.org/10.1016/j.tifs.2021.05.017.

Chung, H.-J., Hoover, R., & Liu, Q. (2009a). The impact of single and dual hydrothermal modifications on the molecular structure and physicochemical properties of normal corn starch. *International Journal of Biological Macromolecules, 44*(2), 203-210. doi:https://doi.org/10.1016/j.ijbiomac.2008.12.007.

Chung, H.-J., Liu, Q., & Hoover, R. (2009b). Impact of annealing and heat-moisture treatment on rapidly digestible, slowly digestible and resistant starch levels in native and gelatinized corn, pea and lentil starches. *Carbohydrate Polymers, 75*(3), 436-447. doi:https://doi.org/10.1016/j.carbpol.2008.08.006.

Collado, L. S., Mabesa, L. B., Oates, C. G., & Corke, H. (2001). Bihon-Type Noodles from Heat-Moisture-Treated Sweet Potato Starch. *Journal of Food Science, 66*(4), 604-609. doi:https://doi.org/10.1111/j.1365-2621.2001.tb04608.x.

Conde-Petit, B. (2003). 4 - The structure and texture of starch-based foods. In B. M. McKenna (Ed.), *Texture in Food* (pp. 86-108): Woodhead Publishing.

Cornejo-Ramírez, Y. I., Martínez-Cruz, O., Del Toro-Sánchez, C. L., Wong-Corral, F. J., Borboa-Flores, J., & Cinco-Moroyoqui, F. J. (2018). The structural characteristics of starches and their functional properties. *CyTA - Journal of Food, 16*(1), 1003-1017. doi:10.1080/19476337.2018.1518343.

De Azeredo, H. M. C., Rosa, M. F., De Sá, M., Souza Filho, M., & Waldron, K. W. (2014). The use of biomass for packaging films and coatings. In K. Waldron (Ed.), *Advances in Biorefineries* (pp. 819-874): Woodhead Publishing.

de Jong, S., & van de Velde, F. (2007). Charge density of polysaccharide controls microstructure and large deformation properties of mixed gels. *Food Hydrocolloids, 21*(7), 1172-1187. doi:https://doi.org/10.1016/j.foodhyd.2006.09.004.

Debet, M. R., & Gidley, M. J. (2006). Three classes of starch granule swelling: Influence of surface proteins and lipids. *Carbohydrate Polymers, 64*(3), 452-465. doi:https://doi.org/10.1016/j.carbpol.2005.12.011.

Deeth, H., & Bansal, N. (2019). Whey Proteins: An Overview. In H. C. Deeth & N. Bansal (Eds.), *Whey Proteins* (pp. 1-50): Academic Press.

Demirel, Y. (2007). Diffusion. In Y. Demirel (Ed.), *Nonequilibrium Thermodynamics (Second Edition)* (pp. 319-362). Amsterdam: Elsevier Science B.V.

Deshmukh, K., Kovářík, T., Muzaffar, A., Basheer Ahamed, M., & Khadheer Pasha, S. K. (2020). Mechanical analysis of polymers. In M. A. A. AlMaadeed, D. Ponnamma, & M. A. Carignano (Eds.), *Polymer Science and Innovative Applications* (pp. 117-152): Elsevier.

Dias, A. R. G., da Rosa Zavareze, E., Spier, F., de Castro, L. A. S., & Gutkoski, L. C. (2010). Effects of annealing on the physicochemical properties and enzymatic susceptibility of rice starches with different amylose contents. *Food Chemistry, 123*(3), 711-719. doi:https://doi.org/10.1016/j.foodchem.2010.05.040.

Dille, M. J., Draget, K. I., & Hattrem, M. N. (2015). The effect of filler particles on the texture of food gels. In J. Chen & A. Rosenthal (Eds.), *Modifying Food Texture* (pp. 183-200): Woodhead Publishing.

Dintzis, F. R., & Bagley, E. B. (1995). Shear-thickening and transient flow effects in starch solutions. *Journal of Applied Polymer Science, 56*(5), 637-640. doi:10.1002/app.1995.070560513.

Dintzis, F. R., Bagley, E. B., & Felker, F. C. (1995). Shear-thickening and flow-induced structure in a system of DMSO containing waxy maize starcha). *Journal of Rheology, 39*(6), 1399-1409. doi:10.1122/1.550643.

Dintzis, F. R., Berhow, M. A., Bagley, E. B., Wu, Y. V., & Felker, F. C. (1996). Shear-thickening behavior and shear-induced structure in gently solubilized starches

Cereal Chemistry, v. 73(no. 5), pp. 638-643-1996 v.1973 no.1995.

Dubois, M., Gilles, K. A., Hamilton, J. K., Rebers, P. A., & Smith, F. (1956). Colorimetric Method for Determination of Sugars and Related Substances. *Analytical Chemistry, 28*(3), 350-356. doi:10.1021/ac60111a017.

Dundar, A. N., & Gocmen, D. (2013). Effects of autoclaving temperature and storing time on resistant starch formation and its functional and physicochemical properties. *Carbohydrate Polymers, 97*(2), 764-771. doi:https://doi.org/10.1016/j.carbpol.2013.04.083.

Durrani, C. M., & Donald, A. M. (1995). Physical characterisation of amylopectin gels. *Polymer Gels and Networks, 3*(1), 1-27. doi:https://doi.org/10.1016/0966-7822(94)00005-R.

Egmond, J. W. V. (1998). Shear-thickening in suspensions, associating polymers, worm-like micelles, and poor polymer solutions. *Current Opinion in Colloid & Interface Science, 3*(4), 385-390. doi:https://doi.org/10.1016/S1359-0294(98)80054-X.

Englyst, H. N. N., Kingman, S. M. M., & Cummings, J. (1992). Classification and Measurement of Nutritionally Important Starch Fractions. *European Journal of Clinical Nutrition, 46 Suppl 2*, S33-50.

Escarpa, A., González, M. C., Mañas, E., García-Diz, L., & Saura-Calixto, F. (1996). Resistant Starch Formation: Standardization of a High-Pressure Autoclave Process. *Journal of Agricultural and Food Chemistry, 44*(3), 924-928. doi:10.1021/jf950328p.

Everett, W. W., & Foster, J. F. (1959). The Subfractionation of Amylose and Characterization of the Subfractions by Light Scattering1,2. *Journal of the American Chemical Society, 81*(13), 3459-3464. doi:10.1021/ja01522a076.

Falco, C., Baccile, N., & Titirici, M.-M. (2011). Morphological and structural differences between glucose, cellulose and lignocellulosic biomass derived hydrothermal carbons. *Green Chemistry, 13*(11), 3273-3281. doi:10.1039/C1GC15742F.

Fang, F. (2017). *Shear-induced aggregation and ordering of amylopectin dispersion affected by hydrocolloids.* Purdue University, MI, United State.

Fang, F., Luo, X., BeMiller, J. N., Schaffter, S., Hayes, A. M. R., Woodbury, T. J., . . . Campanella, O. H. (2020a). Neutral hydrocolloids promote shear-induced elasticity and gel strength of gelatinized waxy potato starch. *Food Hydrocolloids, 107*, 105923. doi:https://doi.org/10.1016/j.foodhyd.2020.105923.

Fang, F., Martinez, M. M., Campanella, O. H., & Hamaker, B. R. (2020b). Long-term low shear-induced highly viscous waxy potato starch gel formed through intermolecular double helices. *Carbohydrate Polymers, 232*, 115815. doi:https://doi.org/10.1016/j.carbpol.2019.115815.

Fang, F., Tuncil, Y. E., Luo, X., Tong, X., Hamaker, B. R., & Campanella, O. H. (2019). Shear-thickening behavior of gelatinized waxy starch dispersions promoted by the starch molecular characteristics. *International Journal of Biological Macromolecules, 121*, 120-126. doi:https://doi.org/10.1016/j.ijbiomac.2018.09.137.

Fang, Y., Li, L., Inoue, C., Lundin, L., & Appelqvist, I. (2006). Associative and Segregative Phase Separations of Gelatin/κ-Carrageenan Aqueous Mixtures. *Langmuir, 22*(23), 9532-9537. doi:10.1021/la061865e.

Fathi, B., Aalami, M., Kashaninejad, M., & Sadeghi Mahoonak, A. (2016). Utilization of Heat-Moisture Treated Proso Millet Flour in Production of Gluten-Free Pound Cake. *Journal of Food Quality, 39*(6), 611-619. doi:https://doi.org/10.1111/jfq.12249.

Feng, T., Su, Q., Zhuang, H., Ye, R., Gu, Z., & Jin, Z. (2014). Ghost Structures, Pasting, Rheological and Textural Properties between Mesona Blumes Gum and Various Starches. *Journal of Food Quality, 37*(2), 73-82. doi:https://doi.org/10.1111/jfq.12076.

Fitzsimons, S. M., Mulvihill, D. M., & Morris, E. R. (2008a). Co-gels of whey protein isolate with crosslinked waxy maize starch: Analysis of solvent partition and phase structure by polymer

blending laws. *Food Hydrocolloids, 22*(3), 468-484. doi:https://doi.org/10.1016/j.foodhyd.2007.01.011.

Fitzsimons, S. M., Mulvihill, D. M., & Morris, E. R. (2008b). Large enhancements in thermogelation of whey protein isolate by incorporation of very low concentrations of guar gum. *Food Hydrocolloids, 22*(4), 576-586. doi:https://doi.org/10.1016/j.foodhyd.2007.01.013.

Fredriksson, H., Silverio, J., Andersson, R., Eliasson, A. C., & Åman, P. (1998). The influence of amylose and amylopectin characteristics on gelatinization and retrogradation properties of different starches. *Carbohydrate Polymers, 35*(3), 119-134. doi:https://doi.org/10.1016/S0144-8617(97)00247-6.

Freitas, C. M. P., Coimbra, J. S. R., Souza, V. G. L., & Sousa, R. C. S. (2021). Structure and Applications of Pectin in Food, Biomedical, and Pharmaceutical Industry: A Review. *Coatings, 11*(8), 922.

French, D. (1972). Fine Structure of Starch and its Relationship to the Organization of Starch Granules. *Journal of the Japanese Society of Starch Science, 19*(1), 8-25. doi:10.5458/jag1972.19.8.

Fu, W., & Nakamura, T. (2017). Explaining the texture properties of whey protein isolate/starch co-gels from fracture structures. *Bioscience, Biotechnology, and Biochemistry, 81*(4), 839-847. doi:https://doi.org/10.1080/09168451.2017.1282812.

Gallant, D. J., Bouchet, B., & Baldwin, P. M. (1997). Microscopy of starch: evidence of a new level of granule organization. *Carbohydrate Polymers, 32*(3), 177-191. doi:https://doi.org/10.1016/S0144-8617(97)00008-8.

Gawkowska, D., Cybulska, J., & Zdunek, A. (2018). Structure-Related Gelling of Pectins and Linking with Other Natural Compounds: A Review. *Polymers, 10*(7), 762. doi:10.3390/polym10070762.

Giura, L., Urtasun, L., Belarra, A., Ansorena, D., & Astiasarán, I. (2021). Exploring Tools for Designing Dysphagia-Friendly Foods: A Review. *Foods, 10*(6), 1334. doi:https://doi.org/10.1080/09168451.2017.1282812.

Gunaratne, A., & Hoover, R. (2002). Effect of heat–moisture treatment on the structure and physicochemical properties of tuber and root starches. *Carbohydrate Polymers, 49*(4), 425-437. doi:https://doi.org/10.1016/S0144-8617(01)00354-X.

Guo, M., & Wang, C. (2019a). Chemistry of Whey Proteins. In *Whey Protein Production, Chemistry, Functionality, and Applications* (pp. 39-65).

Guo, M., & Wang, G. (2019b). History of Whey Production and Whey Protein Manufacturing. In *Whey Protein Production, Chemistry, Functionality, and Applications* (pp. 1-12).

Hall, D., Zhao, R., Dehlsen, I., Bloomfield, N., Williams, S. R., Arisaka, F., . . . Carver, J. A. (2016). Protein aggregate turbidity: Simulation of turbidity profiles for mixed-aggregation reactions. *Analytical Biochemistry, 498*, 78-94. doi:https://doi.org/10.1016/j.ab.2015.11.021.

Han, J.-A., & Lim, S.-T. (2004). Structural changes of corn starches by heating and stirring in DMSO measured by SEC-MALLS-RI system. *Carbohydrate Polymers, 55*(3), 265-272. doi:https://doi.org/10.1016/j.carbpol.2003.09.007.

Han, W., Zhang, B., Li, J., Zhao, S., Niu, M., Jia, C., & Xiong, S. (2017). Understanding the fine structure of intermediate materials of maize starches. *Food Chemistry, 233*, 450-456. doi:https://doi.org/10.1016/j.foodchem.2017.04.155.

Han, X. Z., & Hamaker, B. R. (2002). Location of Starch Granule-associated Proteins Revealed by Confocal Laser Scanning Microscopy. *Journal of Cereal Science, 35*(1), 109-116. doi:https://doi.org/10.1006/jcrs.2001.0420.

Hanashiro, I., Itoh, K., Kuratomi, Y., Yamazaki, M., Igarashi, T., Matsugasako, J.-i., & Takeda, Y. (2008). Granule-Bound Starch Synthase I is Responsible for Biosynthesis of Extra-Long Unit Chains of Amylopectin in Rice. *Plant and Cell Physiology, 49*(6), 925-933. doi:10.1093/pcp/pcn066.

Hanselmann, R., Burchard, W., Ehrat, M., & Widmer, H. M. (1996). Structural Properties of Fractionated Starch Polymers and Their Dependence on the Dissolution Process. *Macromolecules, 29*(9), 3277-3282. doi:10.1021/ma951452c.

Hernández, J. M., Gaborieau, M., Castignolles, P., Gidley, M. J., Myers, A. M., & Gilbert, R. G. (2008). Mechanistic Investigation of a Starch-Branching Enzyme Using Hydrodynamic Volume SEC Analysis. *Biomacromolecules, 9*(3), 954-965. doi:10.1021/bm701213p.

Higgins, J. S., Lipson, J. E. G., & White, R. P. (2010). A simple approach to polymer mixture miscibility. *Philosophical Transactions of the Royal Society A: Mathematical, Physical and Engineering Sciences, 368*(1914), 1009-1025. doi:https://doi.org/10.1098/rsta.2009.0215.

Hizukuri, S. (1986). Polymodal distribution of the chain lengths of amylopectins, and its significance. *Carbohydrate Research, 147*(2), 342-347. doi:https://doi.org/10.1016/S0008-6215(00)90643-8.

Hongsprabhas, P. (2010). *Physicochemical Aspects of Food Engineering and Processing* (S. Devahastin Ed.). Boca Raton, FL, USA: CRC Press.

Hongsprabhas, P., Barbut, S., & Marangoni, A. G. (1999). The Structure of Cold-Set Whey Protein Isolate Gels Prepared With Ca++. *LWT, 32*(4), 196-202. doi:https://doi.org/10.1006/fstl.1998.0522.

Hoover, R. (2010). *The Impact of Heat-Moisture Treatment on Molecular Structures and Properties of Starches Isolated from Different Botanical Sources* (Vol. 50).

Hoover, R., & Manuel, H. (1996). The Effect of Heat–Moisture Treatment on the Structure and Physicochemical Properties of Normal Maize, Waxy Maize, Dull Waxy Maize and Amylomaize V Starches. *Journal of Cereal Science, 23*(2), 153-162. doi:https://doi.org/10.1006/jcrs.1996.0015.

Hoover, R., & Zhou, Y. (2003). In vitro and in vivo hydrolysis of legume starches by α-amylase and resistant starch formation in legumes—a review. *Carbohydrate Polymers, 54*(4), 401-417. doi:https://doi.org/10.1016/S0144-8617(03)00180-2.

Hopkins, R. H., & Jelinek, B. (1948). The fractionation of potato starch. *Biochem J, 43*(1), 28-32. doi:10.1042/bj0430028.

Hormdok, R., & Noomhorm, A. (2007). Hydrothermal treatments of rice starch for improvement of rice noodle quality. *LWT - Food Science and Technology, 40*(10), 1723-1731. doi:https://doi.org/10.1016/j.lwt.2006.12.017.

Huang, T.-T., Zhou, D.-N., Jin, Z.-Y., Xu, X.-M., & Chen, H.-Q. (2016). *Effect of repeated heat-moisture treatments on digestibility, physicochemical and structural properties of sweet potato starch* (Vol. 54).

Huang, V. T., & Perdon, A. A. (2020). Major changes in cereal biopolymers during ready-to-eat cereal processing. In A. A. Perdon, S. L. Schonauer, & K. S. Poutanen (Eds.), *Breakfast Cereals and How They Are Made (Third Edition)* (pp. 109-140). Oxford: AACC International Press.

Jackson, D. S. (2003). Starch - Structure, Properties, and Determination. In B. Caballero (Ed.), *Encyclopedia of Food Sciences and Nutrition (Second Edition)* (pp. 5561-5567). Oxford: Academic Press.

Jacobs, H., & Delcour, J. A. (1998). Hydrothermal Modifications of Granular Starch, with Retention of the Granular Structure: A Review. *Journal of Agricultural and Food Chemistry, 46*(8), 2895-2905. doi:10.1021/jf980169k.

Jaishankar, A., Wee, M., Matia-Merino, L., Goh, K. K. T., & McKinley, G. H. (2015). Probing hydrogen bond interactions in a shear thickening polysaccharide using nonlinear shear and extensional rheology. *Carbohydrate Polymers, 123*, 136-145. doi:https://doi.org/10.1016/j.carbpol.2015.01.006.

Jane, J.-l. (2009). Starch. In J. BeMiller & R. Whistler (Eds.), *Starch (Third Edition)* (pp. 193-236). San Diego: Academic Press.

Jane, J., Chen, Y. Y., Lee, L. F., McPherson, A. E., Wong, K. S., Radosavljevic, M., & Kasemsuwan, T. (1999). Effects of Amylopectin Branch Chain Length and Amylose Content on the Gelatinization and Pasting Properties of Starch. *Cereal Chemistry, 76*(5), 629-637. doi:10.1094/cchem.1999.76.5.629.

Joyce, A. M., Kelly, A. L., & O'Mahony, J. A. (2018). Controlling denaturation and aggregation of whey proteins during thermal processing by modifying temperature and calcium concentration. *International Journal of Dairy Technology, 71*(2), 446-453. doi:https://doi.org/10.1111/1471-0307.12507.

Kalichevsky, M. T., & Ring, S. G. (1987). *Incompatibility of amylose and amylopectin in aqueous solution* (Vol. 162).

Kasprzak, M. M., Macnaughtan, W., Harding, S., Wilde, P., & Wolf, B. (2018). Stabilisation of oil-in-water emulsions with non-chemical modified gelatinised starch. *Food Hydrocolloids, 81*, 409-418. doi:https://doi.org/10.1016/j.foodhyd.2018.03.002.

Kawabata, A., Takase, N., Miyoshi, E., Sawayama, S., Kimura, T., & Kudo, K. (1994). Microscopic Observation and X-Ray Diffractometry of Heat/Moisture-Treated Starch Granules. *Starch - Stärke, 46*(12), 463-469. doi:10.1002/star.19940461204.

Kim, H. S., Kim, B. Y., & Baik, M. Y. (2012). Application of ultra high pressure (UHP) in starch chemistry. *Crit Rev Food Sci Nutr, 52*(2), 123-141. doi:10.1080/10408398.2010.498065.

Kim, S., Willett, J. L., Carriere, C. J., & Felker, F. C. (2002). Shear-thickening and shear-induced pattern formation in starch solutions. *Carbohydrate Polymers, 47*(4), 347-356. doi:https://doi.org/10.1016/S0144-8617(01)00181-3.

Kjøniksen, A.-L., Hiorth, M., Roots, J., & Nyström, B. (2003). Shear-Induced Association and Gelation of Aqueous Solutions of Pectin. *The Journal of Physical Chemistry B, 107*(26), 6324-6328. doi:10.1021/jp0302358.

Knorr, D., Heinz, V., & Buckow, R. (2006). High pressure application for food biopolymers. *Biochimica et Biophysica Acta (BBA) - Proteins and Proteomics, 1764*(3), 619-631. doi:https://doi.org/10.1016/j.bbapap.2006.01.017.

Kong, L., & Ziegler, G. R. (2014). Molecular encapsulation of ascorbyl palmitate in preformed V-type starch and amylose. *Carbohydrate Polymers, 111*, 256-263. doi:https://doi.org/10.1016/j.carbpol.2014.04.033.

Kosvintsev, S. R., Riande, E., Velarde, M. G., & Guzmán, J. (2001). Rheological behaviour of solutions of poly(2-hydroxyethyl methacrylamide) in glycerine. *Polymer, 42*(17), 7395-7401. doi:https://doi.org/10.1016/S0032-3861(01)00195-1.

Kuhn, K. R., Cavallieri, Â. L. F., & da Cunha, R. L. (2011). Cold-set whey protein–flaxseed gum gels induced by mono or divalent salt addition. *Food Hydrocolloids, 25*(5), 1302-1310. doi:https://doi.org/10.1016/j.foodhyd.2010.12.005.

Kulicke, W.-M., & Clasen, C. (2004). *Viscosimetry of Polymers and Polyelectrolytes*. Berlin: Springer.

Kumar, L., Brennan, M., Brennan, C., & Zheng, H. (2022). Influence of whey protein isolate on pasting, thermal, and structural characteristics of oat starch. *Journal of Dairy Science, 105*(1), 56-71. doi:10.3168/jds.2021-20711.

Kumar, R., & Khatkar, B. S. (2017). Thermal, pasting and morphological properties of starch granules of wheat (Triticum aestivum L.) varieties. *Journal of food science and technology, 54*(8), 2403-2410. doi:10.1007/s13197-017-2681-x.

Kuo, M.-I., & Wang, Y.-J. (2006). Effects of Urea Concentration on Thermal and Rheological Properties of Rice Starches. *Cereal Chemistry, 83*(5), 478-481. doi:https://doi.org/10.1094/CC-83-0478.

Lagarrigue, S., & Alvarez, G. (2001). The rheology of starch dispersions at high temperatures and high shear rates: a review. *Journal of Food Engineering, 50*(4), 189-202. doi:https://doi.org/10.1016/S0260-8774(00)00239-9.

Lan, H., Hoover, R., Jayakody, L., Liu, Q., Donner, E., Baga, M., . . . Chibbar, R. N. (2008). Impact of annealing on the molecular structure and physicochemical properties of normal, waxy and high amylose bread wheat starches. *Food Chemistry, 111*(3), 663-675. doi:https://doi.org/10.1016/j.foodchem.2008.04.055.

Langton, M., & Hermansson, A.-M. (1992). Fine-stranded and particulate gels of β-lactoglobulin and whey protein at varying pH. *Food Hydrocollids, 5*(6), 523-539. doi:https://doi.org/10.1016/S0268-005X(09)80122-7.

Laufer, Z., Jalink, H. L., & Staverman, A. J. (1973). Time dependence of shear and normal stresses of polystyrene and poly(ethylene oxide) solutions. *Journal of Polymer Science: Polymer Chemistry Edition, 11*(11), 3005-3015. doi:https://doi.org/10.1002/pol.1973.170111119.

Lavoisier, A., & Aguilera, J. M. (2019). Starch gelatinization inside a whey protein gel formed by cold gelation. *Journal of Food Engineering, 256*, 18-27. doi:https://doi.org/10.1016/j.jfoodeng.2019.03.013.

Le Bail, P., Bizot, H., Ollivon, M., Keller, G., Bourgaux, C., & Buléon, A. (1999). Monitoring the crystallization of amylose–lipid complexes during maize starch melting by synchrotron x-ray diffraction. *Biopolymers, 50*(1), 99-110. doi:10.1002/(sici)1097-0282(199907)50:1<99::Aid-bip9>3.0.Co;2-a.

Lee, C. J., Kim, Y., Choi, S. J., & Moon, T. W. (2012). Slowly digestible starch from heat-moisture treated waxy potato starch: Preparation, structural characteristics, and glucose response in mice. *Food Chemistry, 133*(4), 1222-1229. doi:https://doi.org/10.1016/j.foodchem.2011.09.098.

Lefèvre, T., & Subirade, M. (2000). Molecular differences in the formation and structure of fine-stranded and particulate β-lactoglobulin gels. *Biopolymers, 54*(7), 578-586. doi:https://doi.org/10.1002/1097-0282(200012)54:7<578::AID-BIP100>3.0.CO;2-2.

Lewandowska, K. (2007). Comparative studies of rheological properties of polyacrylamide and partially hydrolyzed polyacrylamide solutions. *Journal of Applied Polymer Science, 103*(4), 2235-2241. doi:https://doi.org/10.1002/app.25247.

Li, J., Ould Eleya, M. M., & Gunasekaran, S. (2006). Gelation of whey protein and xanthan mixture: Effect of heating rate on rheological properties. *Food Hydrocolloids, 20*(5), 678-686. doi:https://doi.org/10.1016/j.foodhyd.2005.07.001.

Li, Z., & Wei, C. (2020). Morphology, structure, properties and applications of starch ghost: A review. *International Journal of Biological Macromolecules, 163*, 2084-2096. doi:https://doi.org/10.1016/j.ijbiomac.2020.09.077.

Lim, S. T., Kasemsuwan, T., & Jane, J. L. (1994). Characterization of phosphorus in starch by 31P-nuclear magnetic resonance spectroscopy. *Cereal chemistry., 71*(5), 488-493.

Lin, A. H.-M., Chang, Y.-H., Chou, W.-B., & Lu, T.-J. (2011). Interference Prevention in Size-Exclusion Chromatographic Analysis of Debranched Starch Glucans by Aqueous System. *Journal of Agricultural and Food Chemistry, 59*(11), 5890-5898. doi:10.1021/jf104393q.

Linke, C., & Drusch, S. (2016). Turbidity in oil-in-water-emulsions — Key factors and visual perception. *Food Research International, 89*, 202-210. doi:https://doi.org/10.1016/j.foodres.2016.07.019.

Liu, G., Hong, Y., Gu, Z., Li, Z., & Cheng, L. (2015). Pullulanase hydrolysis behaviors and hydrogel properties of debranched starches from different sources. *Food Hydrocolloids, 45*, 351-360. doi:https://doi.org/10.1016/j.foodhyd.2014.12.006.

Liu, K., Li, Q.-M., Pan, L.-H., Qian, X.-P., Zhang, H.-L., Zha, X.-Q., & Luo, J.-P. (2017a). The effects of lotus root amylopectin on the formation of whey protein isolate gels. *Carbohydrate Polymers, 175*, 721-727. doi:https://doi.org/10.1016/j.carbpol.2017.08.041.

Liu, K., Li, Q.-M., Zha, X.-Q., Pan, L.-H., Bao, L.-J., Zhang, H.-L., & Luo, J.-P. (2019). Effects of calcium or sodium ions on the properties of whey protein isolate-lotus root amylopectin composite gel. *Food Hydrocolloids, 87*, 629-636. doi:https://doi.org/10.1016/j.foodhyd.2018.08.050.

Liu, W.-C., Halley, P. J., & Gilbert, R. G. (2010). Mechanism of Degradation of Starch, a Highly Branched Polymer, during Extrusion. *Macromolecules, 43*(6), 2855-2864. doi:10.1021/ma100067x.

Liu, Y.-F., Oey, I., Bremer, P., Carne, A., & Silcock, P. (2017b). Effects of pH, temperature and pulsed electric fields on the turbidity and protein aggregation of ovomucin-depleted egg white. *Food Research International, 91*, 161-170. doi:https://doi.org/10.1016/j.foodres.2016.12.005.

Lopes, G. K., Alviano, D. S., Torres, D., Gonçalves, M. P., & Andrade, C. T. (2006). Gelation of whey protein concentrate in the presence of partially hydrolyzed waxy maize starch and urea at pH 7.5. *Colloid and Polymer Science, 285*(2), 203-210. doi:10.1007/s00396-006-1551-2.

Lu, G. W., & Gao, P. (2010). Emulsions and Microemulsions for Topical and Transdermal Drug Delivery. In V. S. Kulkarni (Ed.), *Handbook of Non-Invasive Drug Delivery Systems* (pp. 59-94). Boston: William Andrew Publishing.

Lu, L., & Baik, B.-K. (2015). Starch Characteristics Influencing Resistant Starch Content of Cooked Buckwheat Groats. *Cereal Chemistry, 92*(1), 65-72. doi:https://doi.org/10.1094/CCHEM-04-14-0062-R.

Lucey, J. A. (2008). Milk proteins. In A. Thompson, M. Boland, & H. Singh (Eds.), *Milk Proteins* (pp. 449-481). San Diego: Academic Press.

Maache-Rezzoug, Z., Zarguili, I., Loisel, C., Queveau, D., & Buléon, A. (2008). Structural modifications and thermal transitions of standard maize starch after DIC hydrothermal treatment. *Carbohydrate Polymers, 74*(4), 802-812. doi:https://doi.org/10.1016/j.carbpol.2008.04.047.

Malvern Panalytical. (2010). Mie theory the first 100 years. In.

Malvern Panalytical. (2021a). Mastersizer range. Retrieved from https://www.malvernpanalytical.com/en/support/product-support/mastersizer-range

Malvern Panalytical. (2021b). Zetasizer Pro. Retrieved from https://www.malvernpanalytical.com/en/products/product-range/zetasizer-range/zetasizer-advance-range/zetasizer-pro

MarketWatch. (2022). Clean Label Ingredients Market Size In 2022 : 7.4% CAGR with Top Countries Data, What trends are influencing the growth of the Clean Label Ingredients Industry? | In-depth 135 Pages Report. Retrieved from https://www.marketwatch.com/press-release/clean-label-ingredients-market-size-in-2022-74-cagr-with-top-countries-data-what-trends-are-influencing-the-growth-of-the-clean-label-ingredients-industry-in-depth-135-pages-report-2022-03-14

Matia-Merino, L., Lau, K., & Dickinson, E. (2004). Effects of low-methoxyl amidated pectin and ionic calcium on rheology and microstructure of acid-induced sodium caseinate gels. *Food Hydrocolloids, 18*(2), 271-281. doi:https://doi.org/10.1016/S0268-005X(03)00083-3.

Matignon, A., Moulin, G., Barey, P., Desprairies, M., Mauduit, S., Sieffermann, J. M., & Michon, C. (2014). Starch/carrageenan/milk proteins interactions studied using multiple staining and Confocal Laser Scanning Microscopy. *Carbohydrate Polymers, 99*, 345-355. doi:https://doi.org/10.1016/j.carbpol.2013.09.002.

Maurer, H. W. (2009). Starch in the Paper Industry. In J. BeMiller & R. Whistler (Eds.), *Starch (Third Edition)* (pp. 657-713). San Diego: Academic Press.

Meullenet, J.-F., Lyon, B. G., Carpenter, J. A., & Lyon, C. E. (1998). Relationship between sensory and instrumental texture profile attributes. *Journal of Sensory Studies, 13*(1), 77-93. doi:https://doi.org/10.1111/j.1745-459X.1998.tb00076.x.

Mezger, T. G. (2011a). *The rheology handbook* (3rd edition ed.). Germany: Vincentz Network.

Mezger, T. G. (2011b). *The rheology handbook : for users of rotational and oscillatory rheometers* (3rd ed ed.). Hanover, Germany: Vincentz Network.

Miri, T. (2011). Viscosity and Oscillatory Rheology. *Practical Food Rheology*, 7-28. doi:https://doi.org/10.1002/9781444391060.ch2.

Mori, S., & Barth, H. G. (1999). *Size Exclusion Chromatography*: Springer Berlin Heidelberg.

Morr, C. V., & Ha, E. Y. W. (1993). Whey protein concentrates and isolates: Processing and functional properties. *Critical Reviews in Food Science and Nutrition, 33*(6), 431-476. doi:10.1080/10408399309527643.

Morris, G. A., Adams, G. G., & Harding, S. E. (2014). On hydrodynamic methods for the analysis of the sizes and shapes of polysaccharides in dilute solution: A short review. *Food Hydrocolloids, 42*, 318-334. doi:https://doi.org/10.1016/j.foodhyd.2014.04.014.

Morrison, W. R. (1988). Lipids in cereal starches: A review. *Journal of Cereal Science, 8*(1), 1-15. doi:https://doi.org/10.1016/S0733-5210(88)80044-4.

Nanoscience Instruments. (2022). Mechanical Properties. Retrieved from https://www.nanoscience.com/techniques/nanoindentation/mechanical-properties/

New Zealand Nutrition Foundation. (2022a). Calcium. Retrieved from https://nutritionfoundation.org.nz/nutrition-facts/nutrients/minerals/calcium/

New Zealand Nutrition Foundation. (2022b). Sodium. Retrieved from https://nutritionfoundation.org.nz/nutrition-facts/nutrients/minerals/sodium/

Nilsson, G. S., Gorton, L., Bergquist, K.-E., & Nilsson, U. (1996). Determination of the Degree of Branching in Normal and Amylopectin Type Potato Starch with 1H-NMR Spectroscopy Improved resolution and two-dimensional spectroscopy. *Starch - Stärke, 48*(10), 352-357. doi:https://doi.org/10.1002/star.19960481003.

Niskanen, I., Forsberg, V., Zakrisson, D., Reza, S., Hummelgård, M., Andres, B., . . . Thungström, G. (2019). Determination of nanoparticle size using Rayleigh approximation and Mie theory. *Chemical Engineering Science, 201*, 222-229. doi:https://doi.org/10.1016/j.ces.2019.02.020.

Nobbmann, U. (2014). Size Exclusion chromatography – when to use MALS? Retrieved from https://www.materials-talks.com/size-exclusion-chromatography-when-to-use-mals/

Olayinka, O. O., Adebowale, K. O., & Olu-Owolabi, B. I. (2008). Effect of heat-moisture treatment on physicochemical properties of white sorghum starch. *Food Hydrocolloids, 22*(2), 225-230. doi:https://doi.org/10.1016/j.foodhyd.2006.11.004.

Oldfield, D. J., Singh, H., Taylor, M. W., & Pearce, K. N. (1998). Kinetics of Denaturation and Aggregation of Whey Proteins in Skim Milk Heated in an Ultra-high Temperature (UHT) Pilot Plant. *International Dairy Journal, 8*(4), 311-318. doi:https://doi.org/10.1016/S0958-6946(98)00089-2.

Olsson, C., Frigård, T., Andersson, R., & Hermansson, A.-M. (2003). Effects of Amylopectin Structure and Molecular Weight on Microstructural and Rheological Properties of Mixed β-Lactoglobulin Gels. *Biomacromolecules, 4*(5), 1400-1409. doi:10.1021/bm030038e.

Olsson, C., Langton, M., & Hermansson, A.-M. (2002). Microstructures of β-lactoglobulin/amylopectin gels on different length scales and their significance for rheological properties. *Food Hydrocolloids, 16*(2), 111-126. doi:https://doi.org/10.1016/S0268-005X(01)00069-8.

Onwulata, C. I., Konstance, R. P., Cooke, P. H., & Farrell, H. M. (2003). Functionality of Extrusion—Texturized Whey Proteins1. *Journal of Dairy Science, 86*(11), 3775-3782. doi:https://doi.org/10.3168/jds.S0022-0302(03)73984-8.

Pasch, H., & Trathnigg, B. (1999). *HPLC of Polymers*: Springer Berlin Heidelberg.

Pearce, K. N., & Kinsella, J. E. (1978). Emulsifying properties of proteins: evaluation of a turbidimetric technique. *Journal of Agricultural and Food Chemistry, 26*(3), 716-723. doi:10.1021/jf60217a041.

Pedrosa Silva Clerici, M. T., Sampaio, U. M., & Schmiele, M. (2019). Identification and Analysis of Starch. In M. T. P. Silva Clerici & M. Schmiele (Eds.), *Starches for Food Application* (pp. 23-69): Academic Press.

Pérez, S., & Bertoft, E. (2010). The molecular structures of starch components and their contribution to the architecture of starch granules: A comprehensive review. *Starch - Stärke, 62*(8), 389-420. doi:10.1002/star.201000013.

Picone, C. S. F., Takeuchi, K. P., & Cunha, R. L. (2011). Heat-Induced Whey Protein Gels: Effects of pH and the Addition of Sodium Caseinate. *Food Biophysics, 6*(1), 77-83. doi:10.1007/s11483-010-9177-9.

Pinto, V. Z., Moomand, K., Vanier, N. L., Colussi, R., Villanova, F. A., Zavareze, E. R., . . . Dias, A. R. G. (2015). Molecular structure and granule morphology of native and heat-moisture-treated pinhão starch. *International Journal of Food Science & Technology, 50*(2), 282-289. doi:10.1111/ijfs.12608.

Ponchel, G., & Cauchois, O. (2016). Shape-Controlled Nanoparticles for Drug Delivery and Targeting Applications. In C. Vauthier & G. Ponchel (Eds.), *Polymer Nanoparticles for Nanomedicines: A Guide for their Design, Preparation and Development* (pp. 159-184). Cham: Springer International Publishing.

Purwani, E. Y., Widaningrum, W., Thahir, R., & Muslich, M. (2006). Effect of Heat Moisture Treatment of Sago Starch on Its Noodle Quality. *Indonesian Journal of Agricultural Science, 7*(1), 8-14. doi:10.21082/ijas.v7n1.2006.p8-14.

Puyol, P., Pérez, M. D., & Horne, D. S. (2001). Heat-induced gelation of whey protein isolates (WPI): effect of NaCl and protein concentration. *Food Hydrocolloids, 15*(3), 233-237. doi:https://doi.org/10.1016/S0268-005X(01)00018-2.

Quiroga, C. C., & Bergenståhl, B. (2007). Characterization of the Microstructure of Phase Segregated Amylopectin and β-Lactoglobulin Dry Mixtures. *Food Biophysics, 2*(4), 172-182. doi:10.1007/s11483-007-9041-8.

Quiroga, C. C., & Bergenståhl, B. (2008). Phase segregation of amylopectin and β-lactoglobulin in aqueous system. *Carbohydrate Polymers, 72*(1), 151-159. doi:https://doi.org/10.1016/j.carbpol.2007.07.041.

Rahayu, N. S., Praseptiangga, D., Samanhudi, & Hariyanto, B. (2020). Yield and color changes of starch from Cilacap breadfruit for producing breadfruit's resistant starch type 3. *AIP Conference Proceedings, 2219*(1), 070008. doi:10.1063/5.0003481.

Rawle, A., & Sagar, C. (Producer). (2017, 05 January 2022). The basic principles of particle size analysis. Retrieved from https://www.malvernpanalytical.com/en/learn/events-and-training/webinars/W170216BasicsParticleSize

Ren, F., & Wang, S. (2019). Effect of modified tapioca starches on the gelling properties of whey protein isolate. *Food Hydrocolloids, 93*, 87-91. doi:https://doi.org/10.1016/j.foodhyd.2019.02.025.

Ren, F., Yu, B., Dong, D., Hou, Z.-h., & Cui, B. (2017). Rheological, thermal and microstructural properties of whey protein isolate-modified cassava starch mixed gels at different pH values. *International Journal of Food Science & Technology, 52*(11), 2445-2454. doi:https://doi.org/10.1111/ijfs.13529.

Ridout, M. J., Parker, M. L., Hedley, C. L., Bogracheva, T. Y., & Morris, V. J. (2003). Atomic force microscopy of pea starch granules: granule architecture of wild-type parent, r and rb single mutants, and the rrb double mutant. *Carbohydrate Research, 338*(20), 2135-2147. doi:https://doi.org/10.1016/S0008-6215(03)00309-4.

Rincón-Londoño, N., Vega-Rojas, L. J., Contreras-Padilla, M., Acosta-Osorio, A. A., & Rodríguez-García, M. E. (2016). Analysis of the pasting profile in corn starch: Structural, morphological, and thermal transformations, Part I. *International Journal of Biological Macromolecules, 91*, 106-114. doi:https://doi.org/10.1016/j.ijbiomac.2016.05.070.

Ring, S. G., Colonna, P., I'Anson, K. J., Kalichevsky, M. T., Miles, M. J., Morris, V. J., & Orford, P. D. (1987). The gelation and crystallisation of amylopectin. *Carbohydrate Research, 162*(2), 277-293. doi:https://doi.org/10.1016/0008-6215(87)80223-9.

Risi, A. D., Sante, R. D., & Colangelo, G. (2005). *Optical Characterization of a Diesel Spray at High Temperature and Pressure*.

Rocha, T. S., Felizardo, S. G., Jane, J.-l., & Franco, C. M. L. (2012). Effect of annealing on the semicrystalline structure of normal and waxy corn starches. *Food Hydrocolloids, 29*(1), 93-99. doi:https://doi.org/10.1016/j.foodhyd.2012.02.003.

Rodriguez, A. C., Torrez Irigoyen, M. R., Navarro, A. S., & Yamul, D. K. (2017). Obtention and characterization of dried gels prepared with whey proteins, honey and hydrocolloids mixture. *Journal of the Science of Food and Agriculture, 97*(14), 4969-4977. doi:https://doi.org/10.1002/jsfa.8375.

Roger, P., Bello-Perez, L. A., & Colonna, P. (1999). Contribution of amylose and amylopectin to the light scattering behavior of starches in aqueous solution. *Polymer, 40*(25), 6897-6909. doi:https://doi.org/10.1016/S0032-3861(99)00051-8.

Roger, P., Bello-Pérez, L. A., & Colonna, P. (1999). Contribution of amylose and amylopectin to the light scattering behaviour of starches in aqueous solution. *Polymer, 40*, 6897-6909.

Rolland-Sabaté, A., Guilois, S., Jaillais, B., & Colonna, P. (2011). Molecular size and mass distributions of native starches using complementary separation methods: Asymmetrical Flow Field Flow Fractionation (A4F) and Hydrodynamic and Size Exclusion Chromatography (HDC-SEC). *Analytical and Bioanalytical Chemistry, 399*(4), 1493-1505. doi:10.1007/s00216-010-4208-4.

Ross, S. A., & Lowe, G. (2000). Downfield displacement of the NMR signal of water in deuterated dimethylsulfoxide by the addition of deuterated trifluoroacetic acid. *Tetrahedron Letters, 41*(17), 3225-3227. doi:https://doi.org/10.1016/S0040-4039(00)00355-5.

Ryan, K. N., Zhong, Q., & Foegeding, E. A. (2013). Use of Whey Protein Soluble Aggregates for Thermal Stability—A Hypothesis Paper. *Journal of Food Science, 78*(8), R1105-R1115. doi:https://doi.org/10.1111/1750-3841.12207.

Sandhu, K. S., Siroha, A. K., Punia, S., & Nehra, M. (2020). Effect of heat moisture treatment on rheological and in vitro digestibility properties of pearl millet starches. *Carbohydrate Polymer Technologies and Applications, 1*, 100002. doi:https://doi.org/10.1016/j.carpta.2020.100002.

Schmiele, M., Sampaio, U. M., & Pedrosa Silva Clerici, M. T. (2019). Basic Principles: Composition and Properties of Starch. In M. T. P. Silva Clerici & M. Schmiele (Eds.), *Starches for Food Application* (pp. 1-22): Academic Press.

Schmitt, C., Bovay, C., Rouvet, M., Shojaei-Rami, S., & Kolodziejczyk, E. (2007). Whey Protein Soluble Aggregates from Heating with NaCl: Physicochemical, Interfacial, and Foaming Properties. *Langmuir, 23*(8), 4155-4166. doi:https://doi.org/10.1021/la0632575.

Schokker, E. P., Singh, H., & Creamer, L. K. (2000). Heat-induced aggregation of β-lactoglobulin A and B with α-lactalbumin. *International Dairy Journal, 10*(12), 843-853. doi:https://doi.org/10.1016/S0958-6946(01)00022-X.

Sharma, M., Yadav, D. N., Singh, A. K., & Tomar, S. K. (2015). Effect of Heat-Moisture Treatment on Resistant Starch Content as well as Heat and Shear Stability of Pearl Millet Starch. *Agricultural Research, 4*(4), 411-419. doi:10.1007/s40003-015-0177-3.

Sharma, V., & Bhardwaj, A. (2019). Scanning electron microscopy (SEM) in food quality evaluation. In J. Zhong & X. Wang (Eds.), *Evaluation Technologies for Food Quality* (pp. 743-761): Woodhead Publishing.

Sievert, D., & Pomeranz, Y. (1989). Enzyme-resistant starch. I. Characterization and evaluation by enzymatic, thermoanalytical, and microscopic methods. *Cereal chemistry., 66*(4), 342-347.

Sievert, D., & Wüsch, P. (1993). Amylose Chain Association Based On Differential Scanning Calorimetry. *Journal of Food Science, 58*(6), 1332-1335. doi:10.1111/j.1365-2621.1993.tb06177.x.

Sikora, M., Adamczyk, G., Krystyjan, M., Dobosz, A., Tomasik, P., Berski, W., . . . Izak, P. (2015). Thixotropic properties of normal potato starch depending on the degree of the granules pasting. *Carbohydrate Polymers, 121*, 254-264. doi:https://doi.org/10.1016/j.carbpol.2014.12.059.

Stading, M., Langton, M., & Hermansson, A.-M. (1993). Microstructure and rheological behaviour of particulate β-lactoglobulin gels. *Food Hydrocolloids, 7*(3), 195-212. doi:https://doi.org/10.1016/S0268-005X(09)80172-0.

Stanciu, S. G. (2012). *Digital Image Processing*. doi: https://doi.org/10.5772/1796

Stojanović, Ž., Jeremić, K., & Jovanović, S. (2013). Molecular structure of carboxymethyl starch in dilute aqueous sodium chloride solutions. *Starch - Stärke, 65*(11-12), 902-911. doi:10.1002/star.201200225.

Striegel, A. M., Yau, W. W., Kirkland, J. J., & Bly, D. D. (2009). *Modern size-exclusion liquid chromatography : practice of gel permeation and gel filtration chromatography*. Hoboken, N.J.: Wiley.

Sui, Z., & Kong, X. (2018). *Physical Modifications of Starch*: Springer.

Sun, Y., Shi, Q. H., Zhang, L., Zhao, G. F., & Liu, F. F. (2011). Adsorption and Chromatography. In M. Moo-Young (Ed.), *Comprehensive Biotechnology (Second Edition)* (pp. 665-679). Burlington: Academic Press.

Szcesniak, A. S., Brandt, M. A., & Friedman, H. H. (1963). Development of Standard Rating Scales for Mechanical Parameters of Texture and Correlation Between the Objective and the Sensory Methods of Texture Evaluation. *Journal of Food Science, 28*(4), 397-403. doi:https://doi.org/10.1111/j.1365-2621.1963.tb00217.x.

Szwengiel, A., & Kubiak, P. (2020). Molecular Dispersion of Starch as a Crucial Parameter during Size-Exclusion Chromatography. *Foods, 9*(9), 1024. doi:https://doi.org/10.3390/foods9091204.

Tabata, S., & Hizukuri, S. (1971). Studies on Starch Phosphate. Part 2. Isolation of Glucose 3-Phosphate and Maltose Phosphate by Acid Hydrolysis of Potato Starch. *Starch - Stärke, 23*(8), 267-272. doi:https://doi.org/10.1002/star.19710230803.

Takeda, Y., Hizukuri, S., Takeda, C., & Suzuki, A. (1987). Structures of branched molecules of amyloses of various origins, and molar fractions of branched and unbranched molecules. *Carbohydrate Research, 165*(1), 139-145. doi:https://doi.org/10.1016/0008-6215(87)80089-7.

Tako, M., & Hizukuri, S. (2002). Gelatinization mechanism of potato starch. *Carbohydrate Polymers, 48*(4), 397-401. doi:https://doi.org/10.1016/S0144-8617(01)00287-9.

Tako, M., Tamaki, Y., Teruya, T., & Takeda, Y. (2014). The Principles of Starch Gelatinization and Retrogradation. *Food and Nutrition Sciences, Vol.05No.03*, 12. doi:10.4236/fns.2014.53035.

Tam, K. C., Jenkins, R. D., Winnik, M. A., & Bassett, D. R. (1998). A Structural Model of Hydrophobically Modified Urethane−Ethoxylate (HEUR) Associative Polymers in Shear Flows. *Macromolecules, 31*(13), 4149-4159. doi:10.1021/ma980148r.

Tan, H., Tam, K. C., & Jenkins, R. D. (2001). Network structure of a model HASE polymer in semidilute salt solutions. *Journal of Applied Polymer Science, 79*(8), 1486-1496. doi:10.1002/1097-4628(20010222)79:8<1486::Aid-app160>3.0.Co;2-8.

Tanaka, F. (2002). Theoretical Study of Molecular Association and Thermoreversible Gelation in Polymers. *Polymer Journal, 34*(7), 479-509. doi:10.1295/polymj.34.479.

Tay, S. L., Tan, H. Y., & Perera, C. (2006). The Coagulating Effects of Cations and Anions on Soy Protein. *International Journal of Food Properties, 9*(2), 317-323. doi:https://doi.org/10.1080/10942910600596340.

Tekade, R. K. (2018). *Dosage form design considerations*: Academic Press, an imprint of Elsevier.

Tester, R. F., Karkalas, J., & Qi, X. (2004). Starch—composition, fine structure and architecture. *Journal of Cereal Science, 39*(2), 151-165. doi:https://doi.org/10.1016/j.jcs.2003.12.001.

Tester, R. F., & Morrison, W. R. (1990). Swelling and gelatinization of cereal starches. I. Effects of amylopectin, amylose, and lipids. *Cereal chemistry., 67*(6), 551-557.

Thakur, B. R., Singh, R. K., Handa, A. K., & Rao, M. A. (1997). Chemistry and uses of pectin — A review. *Critical Reviews in Food Science and Nutrition, 37*(1), 47-73. doi:10.1080/10408399709527767.

Tiefenbacher, K. F. (2019). Glossary of Terms in Wafers, Waffles and Adjuncts. In K. F. Tiefenbacher (Ed.), *The Technology of Wafers and Waffles II* (pp. 325-411): Academic Press.

Tizzotti, M. J., Sweedman, M. C., Tang, D., Schaefer, C., & Gilbert, R. G. (2011). New 1H NMR Procedure for the Characterization of Native and Modified Food-Grade Starches. *Journal of Agricultural and Food Chemistry, 59*(13), 6913-6919. doi:10.1021/jf201209z.

Tobitani, A., & Ross-Murphy, S. B. (1997). Heat-Induced Gelation of Globular Proteins. 2. Effect of Environmental Factors on Single-Component and Mixed-Protein Gels. *Macromolecules, 30*(17), 4855-4862. doi:10.1021/ma970113b.

Tolstoguzov, V. (2000). Phase behaviour of macromolecular components in biological and food systems. *Nahrung, 44*(5), 299-308. doi:https://doi.org/10.1002/1521-3803(20001001)44:5<299::AID-FOOD299>3.0.CO;2-9.

Tsaih, M. L., & Chen, R. H. (1997). Effect of molecular weight and urea on the conformation of chitosan molecules in dilute solutions. *International Journal of Biological Macromolecules, 20*(3), 233-240. doi:https://doi.org/10.1016/S0141-8130(97)01165-3.

Twomey, M., Keogh, K. M., Mehra, R., & O'Kenndey, B. T. (1997). Gel characteristics of β-lactoglobulin, whey protein concentrate and whey protein isolate. *Journal of Texture Studies, 28*(4), 387-403. doi:https://doi.org/10.1111/j.1745-4603.1997.tb00124.x.

Urbonaite, V., van der Kaaij, S., de Jongh, H. H. J., Scholten, E., Ako, K., van der Linden, E., & Pouvreau, L. (2016). Relation between gel stiffness and water holding for coarse and fine-stranded protein gels. *Food Hydrocolloids, 56*, 334-343. doi:https://doi.org/10.1016/j.foodhyd.2015.12.011.

van de Velde, F., Weinbreck, F., Edelman, M. W., van der Linden, E., & Tromp, R. H. (2003). Visualisation of biopolymer mixtures using confocal scanning laser microscopy (CSLM) and covalent labelling techniques. *Colloids and Surfaces B: Biointerfaces, 31*(1), 159-168. doi:https://doi.org/10.1016/S0927-7765(03)00135-8.

Varatharajan, V., Hoover, R., Li, J., Vasanthan, T., Nantanga, K. K. M., Seetharaman, K., . . . Chibbar, R. N. (2011). Impact of structural changes due to heat-moisture treatment at different temperatures on the susceptibility of normal and waxy potato starches towards hydrolysis by porcine pancreatic alpha amylase. *Food Research International, 44*(9), 2594-2606. doi:https://doi.org/10.1016/j.foodres.2011.04.050.

Vasanthan, T., & Hoover, R. (1992). A comparative study of the composition of lipids associated with starch granules from various botanical sources. *Food Chemistry, 43*(1), 19-27. doi:https://doi.org/10.1016/0308-8146(92)90236-U.

Vermeylen, R., Goderis, B., & Delcour, J. A. (2006). An X-ray study of hydrothermally treated potato starch. *Carbohydrate Polymers, 64*(2), 364-375. doi:https://doi.org/10.1016/j.carbpol.2005.12.024.

Waduge, R. N., Hoover, R., Vasanthan, T., Gao, J., & Li, J. (2006). Effect of annealing on the structure and physicochemical properties of barley starches of varying amylose content. *Food Research International, 39*(1), 59-77. doi:https://doi.org/10.1016/j.foodres.2005.05.008.

Wang, C., & Guo, M. (2019a). Whey Protein Structure and Denaturation and Interactions with Other Food Components. In *Whey Protein Production, Chemistry, Functionality, and Applications* (pp. 67-101).

Wang, G., & Guo, M. (2019b). Manufacturing Technologies of Whey Protein Products. In *Whey Protein Production, Chemistry, Functionality, and Applications* (pp. 13-37).

Wang, L., Zhang, C., Chen, Z., Wang, X., Wang, K., Li, Y., . . . Li, J. (2018). Effect of annealing on the physico-chemical properties of rice starch and the quality of rice noodles. *Journal of Cereal Science, 84*, 125-131. doi:https://doi.org/10.1016/j.jcs.2018.10.004.

Wang, S., & Copeland, L. (2013). Molecular disassembly of starch granules during gelatinization and its effect on starch digestibility: a review. *Food & Function, 4*(11), 1564-1580. doi:10.1039/c3fo60258c.

Wang, S., Li, C., Copeland, L., Niu, Q., & Wang, S. (2015). Starch Retrogradation: A Comprehensive Review. *Comprehensive Reviews in Food Science and Food Safety, 14*(5), 568-585. doi:https://doi.org/10.1111/1541-4337.12143.

Wang, Y., Zhao, J., Zhang, W., Liu, C., Jauregi, P., & Huang, M. (2020). Modification of heat-induced whey protein gels by basic amino acids. *Food Hydrocolloids, 100*, 105397. doi:https://doi.org/10.1016/j.foodhyd.2019.105397.

Waxham, M. N. (2007). Molecular Mobility in Cells Examined with Optical Methods. In A. J. Bean (Ed.), *Protein Trafficking in Neurons* (pp. 3-27). Burlington: Academic Press.

Wee, M. S. M., Goh, A. T., Stieger, M., & Forde, C. G. (2018). Correlation of instrumental texture properties from textural profile analysis (TPA) with eating behaviours and macronutrient composition for a wide range of solid foods. *Food & Function, 9*(10), 5301-5312. doi:10.1039/C8FO00791H.

Wee, M. S. M., Matia-Merino, L., & Goh, K. K. T. (2015a). The cation-controlled and hydrogen bond-mediated shear-thickening behavior of a tree-fern isolated polysaccharide. *Carbohydrate Polymers, 130*, 57-68. doi:https://doi.org/10.1016/j.carbpol.2015.03.086.

Wee, M. S. M., Matia-Merino, L., & Goh, K. K. T. (2015b). Time- and shear history-dependence of the rheological properties of a water-soluble extract from the fronds of the black tree fern, Cyathea medullaris. *Journal of Rheology, 59*(2), 365-376. doi:10.1122/1.4905006.

Werlang, S., Bonfante, C., Oro, T., Biduski, B., Bertolin, T. E., & Gutkoski, L. C. (2021). Native and annealed oat starches as a fat replacer in mayonnaise. *Journal of Food Processing and Preservation, 45*(3), e15211. doi:https://doi.org/10.1111/jfpp.15211.

Wijayanti, H. B., Brodkorb, A., Hogan, S. A., & Murphy, E. G. (2019). Thermal Denaturation, Aggregation, and Methods of Prevention. In H. C. Deeth & N. Bansal (Eds.), *Whey Proteins* (pp. 185-247): Academic Press.

Winkworth-Smith, C. G., MacNaughtan, W., & Foster, T. J. (2016). Polysaccharide structures and interactions in a lithium chloride/urea/water solvent. *Carbohydrate Polymers, 149*, 231-241. doi:https://doi.org/10.1016/j.carbpol.2016.04.102.

Wu, C., Ji, G., Gao, F., Qian, J.-Y., Zhang, L., Li, Q., & Zhang, C. (2021). Effect of heat-moisture treatment on the structural and physicochemical characteristics of sand rice (Agriophyllum squarrosum) starch. *Food Science & Nutrition, 9*(12), 6720-6727. doi:https://doi.org/10.1002/fsn3.2622.

Wyatt Technology. (2021). Absolute molar mass and size. Retrieved from https://www.wyatt.com/solutions/techniques/sec-mals-molar-mass-size-multi-angle-light-scattering.html

Xiong, Y. L., Dawson, K. A., & Wan, L. (1993). Thermal Aggregation of β-Lactoglobulin: Effect of pH, Ionic Environment, and Thiol Reagent1. *Journal of Dairy Science, 76*(1), 70-77. doi:https://doi.org/10.3168/jds.S0022-0302(93)77324-5.

Xu, X., Huang, X.-F., Visser, R. G. F., & Trindade, L. M. (2017). Engineering Potato Starch with a Higher Phosphate Content. *PLOS ONE, 12*(1), e0169610-e0169610. doi:10.1371/journal.pone.0169610.

Yamashita, Y., & Hirai, N. (1966). Single crystals of amylose V complexes. II. Crystals with 71 helical configuration. *Journal of Polymer Science Part A-2: Polymer Physics, 4*(2), 161-171. doi:https://doi.org/10.1002/pol.1966.160040201.

Yang, C., Zhong, F., Goff, D. H., & Li, Y. (2019a). Study on starch-protein interactions and their effects on physicochemical and digestible properties of the blends. *Food Chemistry, 280*, 51-58. doi:https://doi.org/10.1016/j.foodchem.2018.12.028.

Yang, N., Luan, J., Ashton, J., Gorczyca, E., & Kasapis, S. (2014). Effect of calcium chloride on the structure and in vitro hydrolysis of heat induced whey protein and wheat starch composite gels. *Food Hydrocolloids, 42*, 260-268. doi:https://doi.org/10.1016/j.foodhyd.2014.02.022.

Yang, Q., Zhang, W., Luo, Y., Li, J., Gao, J., Yang, P., . . . Feng, B. (2019b). Comparison of structural and physicochemical properties of starches from five coarse grains. *Food Chemistry, 288*, 283-290. doi:https://doi.org/10.1016/j.foodchem.2019.02.134.

Yang, X., Li, A., Li, D., Guo, Y., & Sun, L. (2021). Applications of mixed polysaccharide-protein systems in fabricating multi-structures of binary food gels—A review. *Trends in Food Science & Technology, 109*, 197-210. doi:https://doi.org/10.1016/j.tifs.2021.01.002.

Yao, H.-Y.-Y., Wang, J.-Q., Yin, J.-Y., Nie, S.-P., & Xie, M.-Y. (2021). A review of NMR analysis in polysaccharide structure and conformation: Progress, challenge and perspective. *Food Research International, 143*, 110290. doi:https://doi.org/10.1016/j.foodres.2021.110290.

Yasui, T., Ashida, K., & Sasaki, T. (2009). Chain-length Distribution Profiles of Amylopectin Isolated from Endosperm Starch of Waxy and Low-amylose Bread Wheat (Triticum aestivum L.) Lines with Common Genetic Background. *Starch - Stärke, 61*(12), 677-686. doi:https://doi.org/10.1002/star.200900177.

Yeh, Y., & Lai, L.-S. (2021). Effect of Single and Dual Hydrothermal Treatments on the Resistant Starch Content and Physicochemical Properties of Lotus Rhizome Starches. *Molecules, 26*(14), 4339.

Yokoyama, W., Renner-Nantz, J. J., & Shoemaker, C. F. (1998). Starch Molecular Mass and Size by Size-Exclusion Chromatography in DMSO-LiBr Coupled with Multiple Angle Laser Light Scattering. *Cereal Chemistry, 75*(4), 530-535. doi:https://doi.org/10.1094/CCHEM.1998.75.4.530.

Yoo, S.-H., & Jane, J.-l. (2002). Molecular weights and gyration radii of amylopectins determined by high-performance size-exclusion chromatography equipped with multi-angle laser-light

scattering and refractive index detectors. *Carbohydrate Polymers, 49*(3), 307-314. doi:https://doi.org/10.1016/S0144-8617(01)00339-3.

Yuryev, V. P., Krivandin, A. V., Kiseleva, V. I., Wasserman, L. A., Genkina, N. K., Fornal, J., . . . Schiraldi, A. (2004). Structural parameters of amylopectin clusters and semi-crystalline growth rings in wheat starches with different amylose content. *Carbohydrate Research, 339*(16), 2683-2691. doi:https://doi.org/10.1016/j.carres.2004.09.005.

Zaccarelli, E. (2007). Colloidal gels: equilibrium and non-equilibrium routes. *Journal of Physics: Condensed Matter, 19*(32), 323101. doi:10.1088/0953-8984/19/32/323101.

Zavareze, E. d. R., & Dias, A. R. G. (2011). Impact of heat-moisture treatment and annealing in starches: A review. *Carbohydrate Polymers, 83*(2), 317-328. doi:https://doi.org/10.1016/j.carbpol.2010.08.064.

Zhang, B., Dhital, S., Flanagan, B. M., & Gidley, M. J. (2014). Mechanism for Starch Granule Ghost Formation Deduced from Structural and Enzyme Digestion Properties. *Journal of Agricultural and Food Chemistry, 62*(3), 760-771. doi:10.1021/jf404697v.

Zhang, Q., Zhou, J.-s., Zhai, Y.-a., Liu, F.-q., & Gao, G. (2008). Effect of salt solutions on chain structure of partially hydrolyzed polyacrylamide. *Journal of Central South University of Technology, 15*(1), 80-83. doi:10.1007/s11771-008-0319-x.

Zheng, Y., Wei, Z., Zhang, R., Deng, Y., Tang, X., Zhang, Y., . . . Zhang, M. (2020). Optimization of the autoclave preparation process for improving resistant starch content in rice grains. *Food Science & Nutrition, 8*(5), 2383-2394. doi:https://doi.org/10.1002/fsn3.1528.

Zhou, Z., Robards, K., Helliwell, S., & Blanchard, C. (2002). Ageing of Stored Rice: Changes in Chemical and Physical Attributes. *Journal of Cereal Science, 35*(1), 65-78. doi:https://doi.org/10.1006/jcrs.2001.0418.

Ziegler, G. R., & Foegeding, E. A. (1990). The gelation of proteins. In J. E. Kinsella (Ed.), *Advances in Food and Nutrition Research* (Vol. 34, pp. 203-298): Academic Press.

Appendices

Appendix A: TEM microstructures of composite gels at pH 7

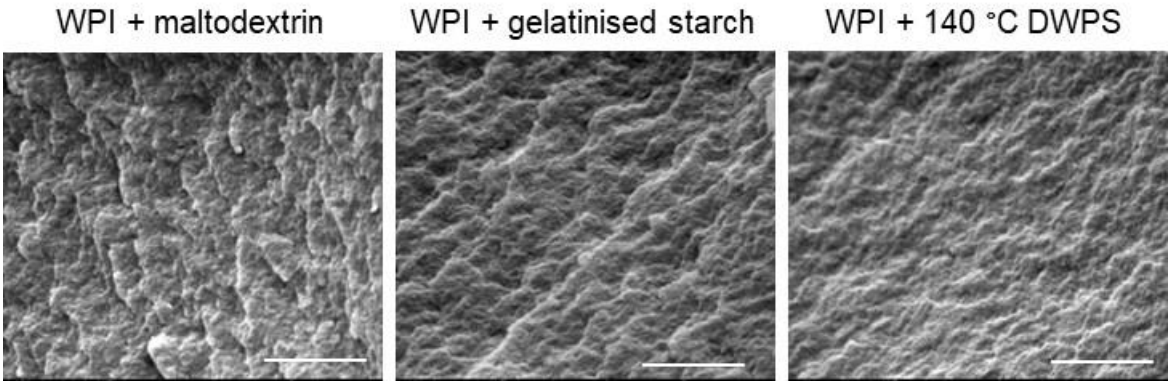

Figure 0-1: Scanning electron micrograph (8000× magnification) of (A) 13% w/w WPI + 4% w/w maltodextrin, (B) 13% w/w WPI + 4% w/w gelatinised starch, and (C) 13% w/w WPI + 4% w/w 140 °C DWPS. The scale bars are 5 µm.

Appendix B: Effect rheometer time setting on the viscosity of 120 °C DWPS

The time-dependency viscosity of 120 °C DWPS from 0.1 to 1000 s^{-1} was studied at different rheometer time settings, namely, *no time setting* (*i.e.*, steady-state measurement), *log-ramp time setting* of 40–10 s and *fixed interval* of 1, 10 and 60 s (Figure B-1). A *log-ramp time setting* of 40–10 s means that a measurement interval of 40 s was used at the lowest shear rate of 0.1 s^{-1} and logarithmically reduced to 10 s at the highest shear rate of 1000 s^{-1}. At different time settings, the viscosity curves did not superimpose each other, especially at the onset of shear-thickening. Marked differences in terms of the onset of shear-thickening and maximum viscosity (η_{max}) were observed. These observed differences suggested that the steady-state viscosity was not achieved at short measurement intervals of 1, 10, and *log-ramp* 40–10 s. Data collection at 60 s *fixed time interval* and *no time setting* resulted in a very similar viscosity curves with both showing the highest maximum viscosity (η_{max}) as compared to that of those observed at other time settings of *log-ramp* 40–10 s and fixed intervals of 10, and 1 s. The lowest viscosity profile was observed at the shortest *fixed time interval* of 1 s and a delayed onset of shear-thickening occurring only at higher shear rates of ~100 s^{-1}. The results from different time settings indicated that the 120 °C DWPS exhibited time-dependency.

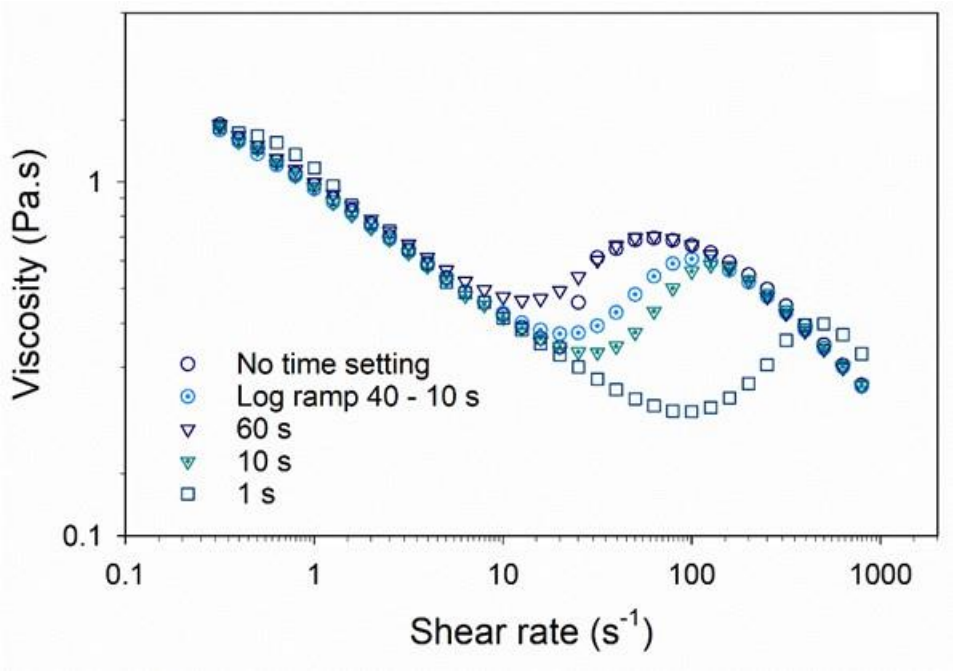

Figure B-1 Viscosity of 5% w/w 120 °C DWPS as a function of shear rate at different rheometer time setting. All measurements were done at 20 °C.

Appendix C: Effect of storage degradation on the rheological profile of DWPS

Despite showing signs of the polymer degradation (reduced M_w) due to storage over ~2.5 years (Table 4-1 and Table 6-1), the shear-induced rheological properties of DWPS were retained—shear-thickening for 120 °C DWPS and anti-thixotropy for both 120 and 140 °C DWPS (Figure C-1).

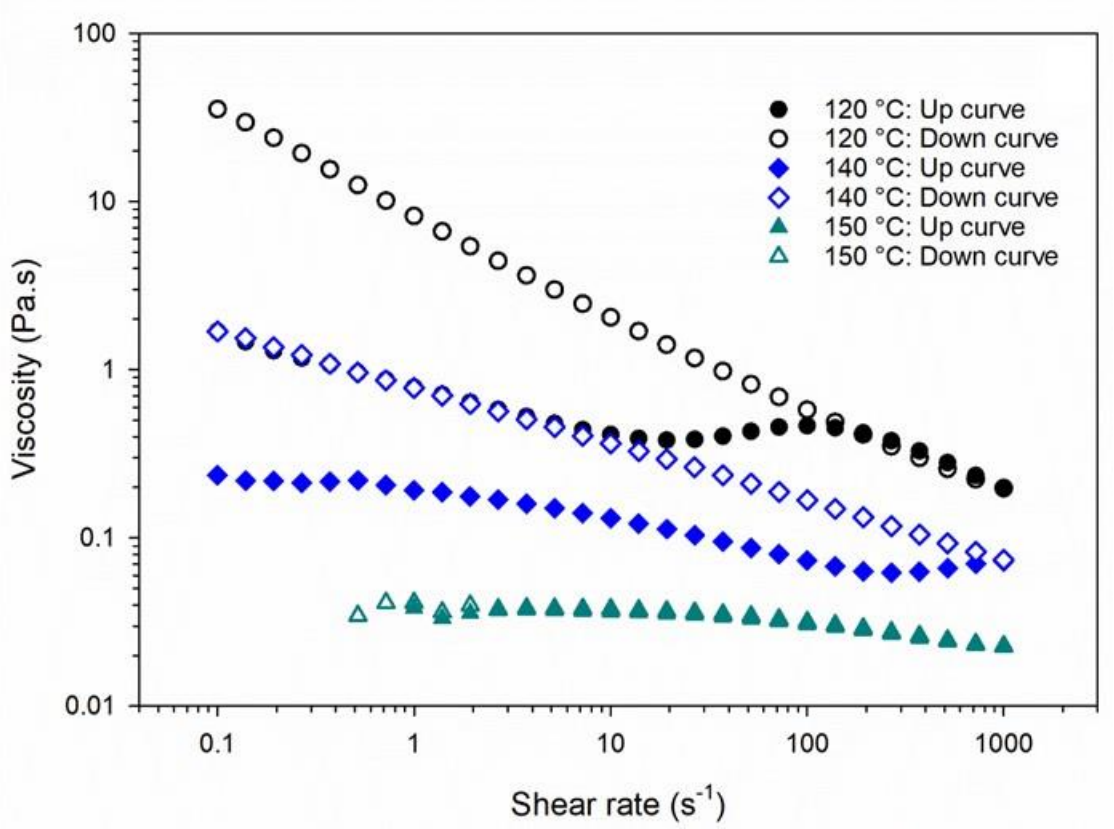

Figure C-1 Effect of shear on the viscosity of 5% w/w 120 °C DWPS at increasing (0.1 to 1000 s^{-1}) and decreasing (1000 to 0.1 s^{-1}) shear rate. Measurements taken at 20 °C.

Appendix D: Effect of dialysis on shear-thickening behaviour of 120 °C DWPS

The dialysis process for 48 h did not affect the shear-thickening behaviour of 2% w/w 120 °C DWPS (Figure D-1).

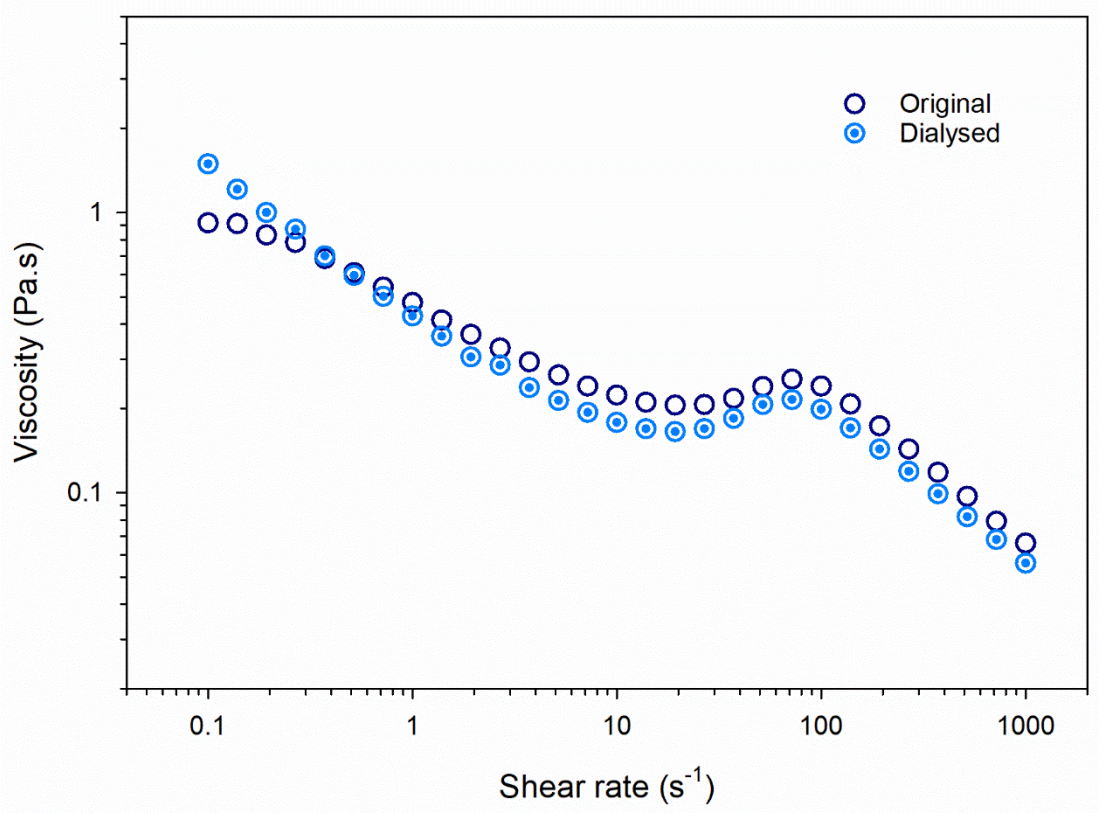

Figure D-1 Effect of dialysis (with Milli-Q for 48 h) on the viscosity of 2% w/w 120 ° C DWPS. Measurements were taken at 20 °C.

Appendix E: Effect of KCl on WPI + 140 °C DWPS composite gels

The effect of KCl was tested on 13% w/w WPI + 4% w/w 140 °C DWPS composite gels to confirm the monovalent effect of added NaCl (Section 8.3.3.1). The effect of KCl on the visual appearance and textural hardness was studied at KCl concentrations of 50, 100 and 500 mM. Similar gel textures (visual and hardness values) were noted at similar concentrations of NaCl and KCl (Figure E-5). Hence, the observations indicate that the manipulation of WPI + 140 °C DWPS gel texture with NaCl was contributed by the effect of a monovalent salt.

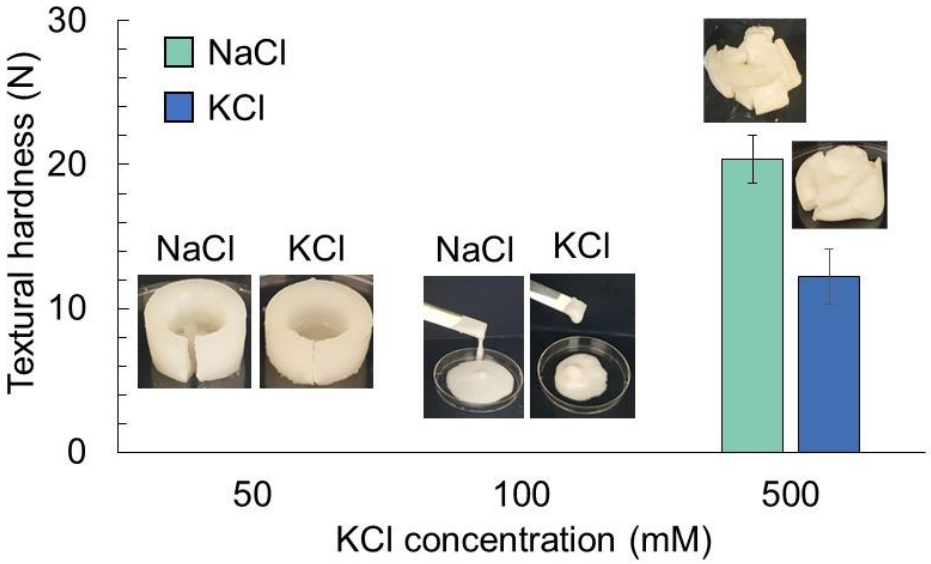

Figure E-1 Textual hardness of 13% w/w WPI + 4% w/w 140 °C DWPS gels at 500 mM NaCl or KCl concentrations, with inset showing the visual appearance of 13% w/w WPI + 4% w/w 140 °C DWPS gels at 50 (self-supporting gels with a liquid centre), 100 (paste-like weak gels) and 500 (deformed gels from compression test) mM KCl concentrations. Measurements was conducted on homogeneous gels at room temperature. Plotted values are presented as means ± standard error.

Appendix F: Enzymatically-modified waxy potato starch *

Contrasting to DWPS modified by purely physical methods in this thesis, waxy potato starch was also enzymatically-modified using α-amylase (EC 3.2.1.1, 30 U/mg, St. Louis, MO, USA) and pullulanase (Promozyme® D2, EC 3.2.1.41, ≥ 1000 NPUN/g, St. Louis, MO, USA) to check if DWPS is different from enzymatically-modified starch.

Viscosity curve of enzymatically-modified waxy potato starch

The viscosity curve of gelatinised starch (control sample), α-amylase-treated starch and pullulanase-treated starch at different treatment intervals is shown in Figure F-1. Starch samples treated with α-amylase and pullulanase are denoted with 'A' and 'P' respectively, followed by the number of treatment duration (in min). At increasing treatment duration, a decreasing trend was observed in both viscosity and particle size of α-amylase-treated and pullulanase-treated starch samples (Figure F-1). Starch samples treated with α-amylase for 20–40 min and pullulanase for 20–60 min exhibited shear-thinning behaviour, whereas starch treated with α-amylase for 180 min showed Newtonian behaviour. Unlike DWPS, none of the enzymatically-modified starch samples showed shear-thickening behaviour.

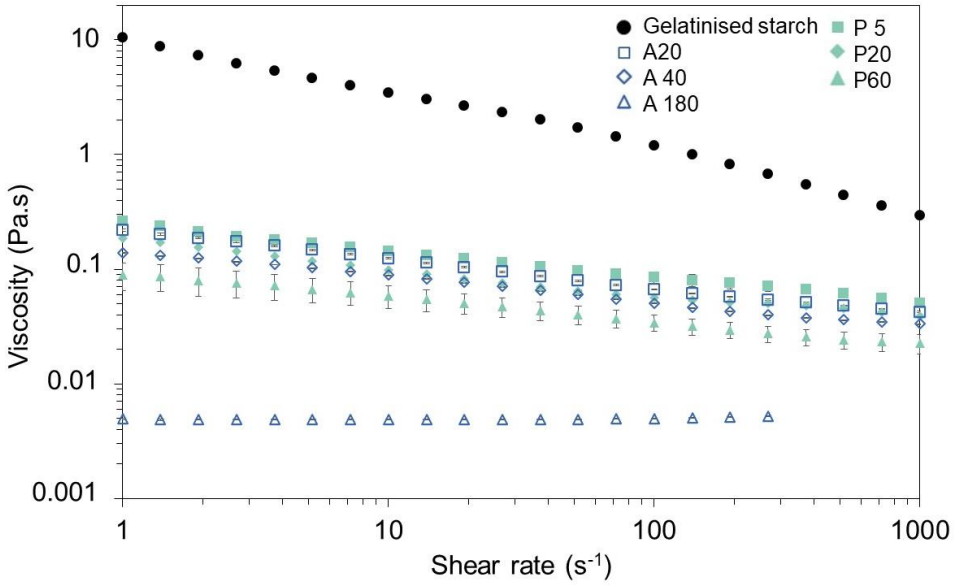

Figure F-1 Shear-dependent viscosity of gelatinised starch (95 °C for 30 min), α-amylase-treated starch samples at 20, 40 and 180 min of enzymatic treatment, and pullulanase-treated starch samples at 5, 20 and 60 min of enzymatic treatment. Plotted values of gelatinised starch and pullulanase-treated starch samples are presented as means of two replicate measurements ± standard error, whereas only one measurement was carried out for α-amylase-treated starch samples. Measurements were taken at 20 °C.

*Work contributed by Ian Marcus Yeow Sze Wei, under the supervision from Kelvin Kim Tha Goh, Lara Matia-Merino, and Cai Ling Ang

Effect of enzymatically modified starch on the textural hardness of WPI

The influence of these enzymatically-treated starches on WPI gels was also tested at 13% w/w WPI and 4% w/w starch concentrations. All the composite gel samples except gel containing A20 exhibited significantly lower gel hardness as compared to the control sample (WPI + gelatinised starch) (Figure F-2). A synergistic increase in gel hardness was observed in WPI + A20 composite gel, and this increase may be similar to that of WPI + 140 °C DWPS (Figure 7-2A). Further work is recommended to investigate the cause of the synergistic increase in the gel strength of WPI + A20.

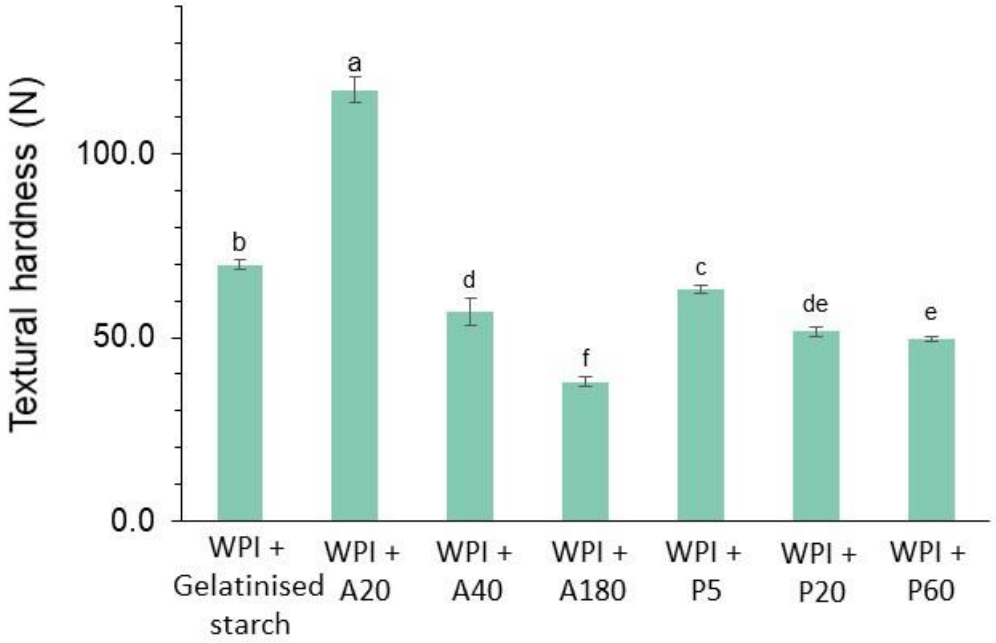

Figure F-2 Gel hardness of 13% w/w WPI + 4% w/w gelatinised starch (95 °C for 30 min) or A20 or A40 or A180 or P5 or P20 or P60. All plotted values are presented as means ± standard error. Values denoted the same superscript are not significantly different ($p \leq 0.05$).

Appendix G: Effect of DMSO on shear-induced behaviours of 120 °C DWPS

The effect of DMSO on shear-thickening behaviour of 120 °C DWPS was investigated using DMSO solutions at varied concentrations of 0, 5, 10, 25, 50 and 100 % DMSO. The 120 °C DWPS (5 % w/w) were first dispersed in Milli-Q/DMSO solutions and followed by heating in a boiling water-bath for 1 h. The mixing of the sample was done using a vortex to ensure sample homogeneity.

Effect of DMSO on shear-thickening and hysteresis behaviours of 120 °C DWPS

Samples prepared in 0–25% w/w DMSO exhibited both anti-thixotropy and shear-thickening behaviour in the shear curves, whereas samples prepared in 50 and 100% w/w DMSO exhibited thixotropy behaviour with no shear-thickening behaviour noted (Figure G-1A and B).

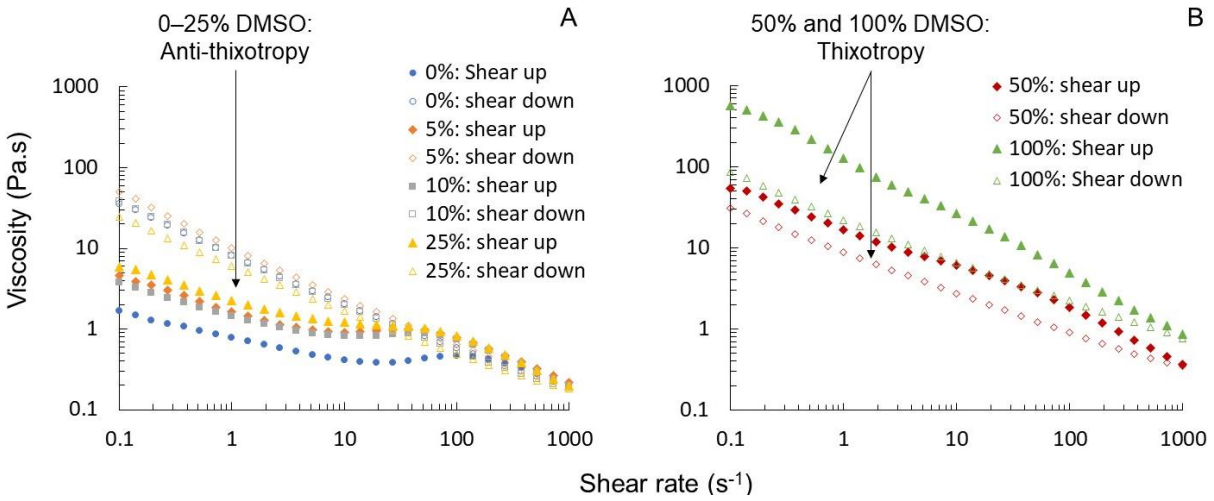

Figure G-1 Effect of DMSO on the hysteresis behaviours of 5% w/w 120 °C DWPS upon increasing and decreasing shear rate from 0.1 to 1000 s-1, for samples prepared in (A) 0–25% w/w DMSO and (b) 50 and 100% w/w DMSO. All plotted values are means of two replicate measurements taken at 20 °C.

Effect of DMSO on viscoelasticity of 120 °C DWPS

The viscoelasticity of these samples was also characterised before and after shear at 1000 s^{-1} for 5 min. The viscosity results agree with the viscoelastic moduli results, which are presented in Figure G-2A, where the samples prepared 0–25% w/w DMSO exhibited shear-induced gelation, shear-thickening and anti-thixotropy behaviours. In contrast, samples containing 50 and 100% w/w DMSO had gel-like behaviour ($G' > G''$) before shear. Upon shear, the sample containing 100% DMSO had a substantial drop in its viscosity, G' and G''. A self-supporting gel before heating was also noted in the sample prepared with 100% w/w DMSO, and such behaviour was not observed in other samples (Figure G-2B). These observations indicate that the 120 °C DWPS interacts differently with DMSO as compared to water molecules, leading to an alteration of its rheological properties.

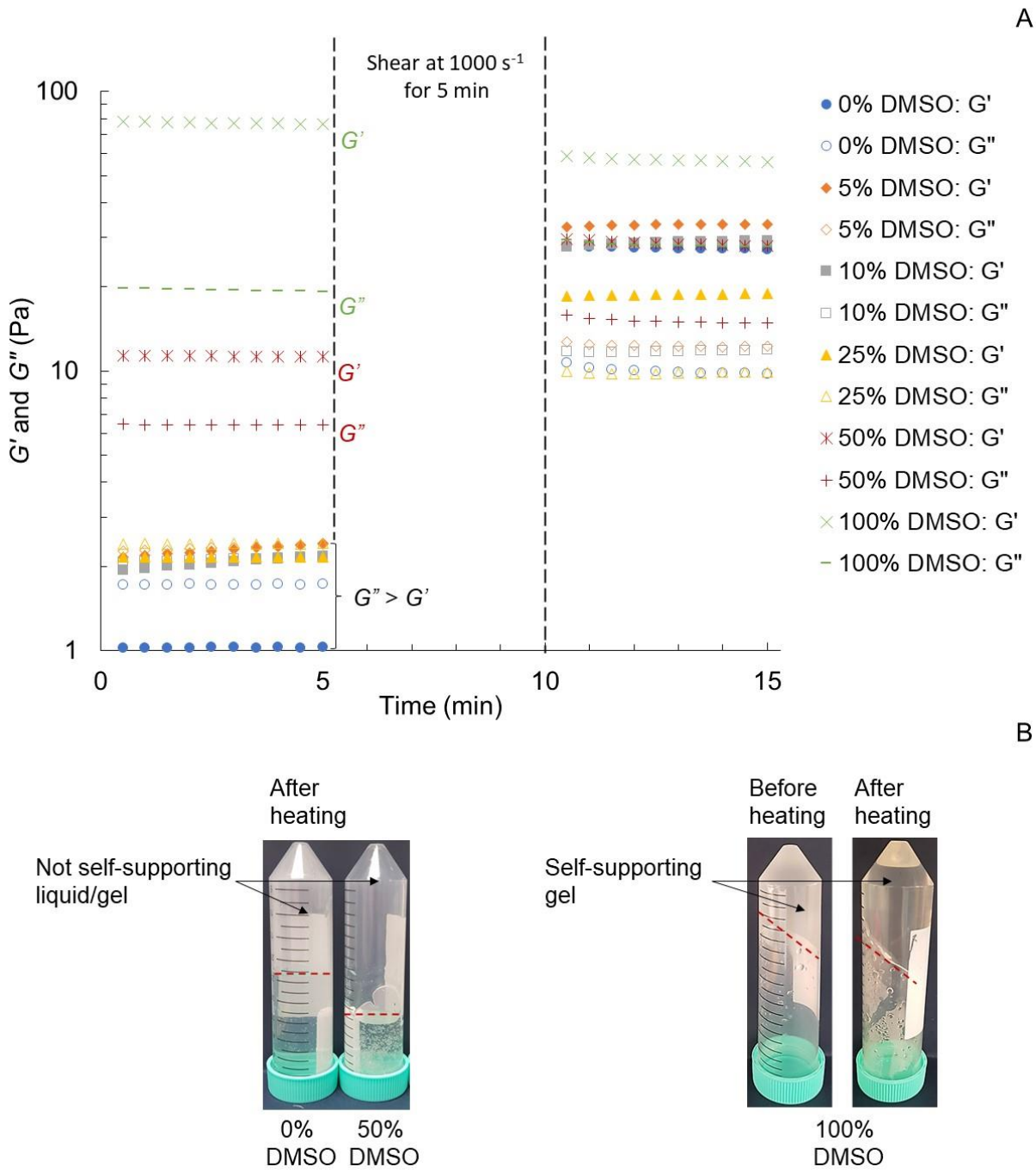

Figure G-2 Effect of DMSO on (A) *G'* and *G"* of 5% w/w 120 °C DWPS before and after shearing at 1000 s^{-1} for 5 min. All plotted values are means of two replicates with measurements taken at 20 °C. (B) Photographs showing 5% w/w 120 °C DWPS with 0 and 50% DMSO samples were not self-supporting after heating, and gels containing 100% DMSO were self-supporting before and after heating.

Effect of DMSO on the particle-size distribution of 120 °C DWPS

The particle-size distributions of unsheared- and sheared-120 °C DWPS at different DMSO concentrations were determined using LD. The results are presented Figure G-3. In Chapter 6, the shear-induced behaviour of DWPS was attributed to amylopectin chain associations and the physical interlocking of starch particles (producing particles ~2–20 µm), the obtained results here agree with the previous hypothesis in Chapter 6. An increase in particles within the size range of 2–20 µm was observed in samples prepared in 0–25% w/w DMSO (same samples that exhibited shear-thickening behaviour; Figure G-3). In contrast, minimal change in particle-size distribution was observed for samples containing 50 and 100% w/w DMSO.

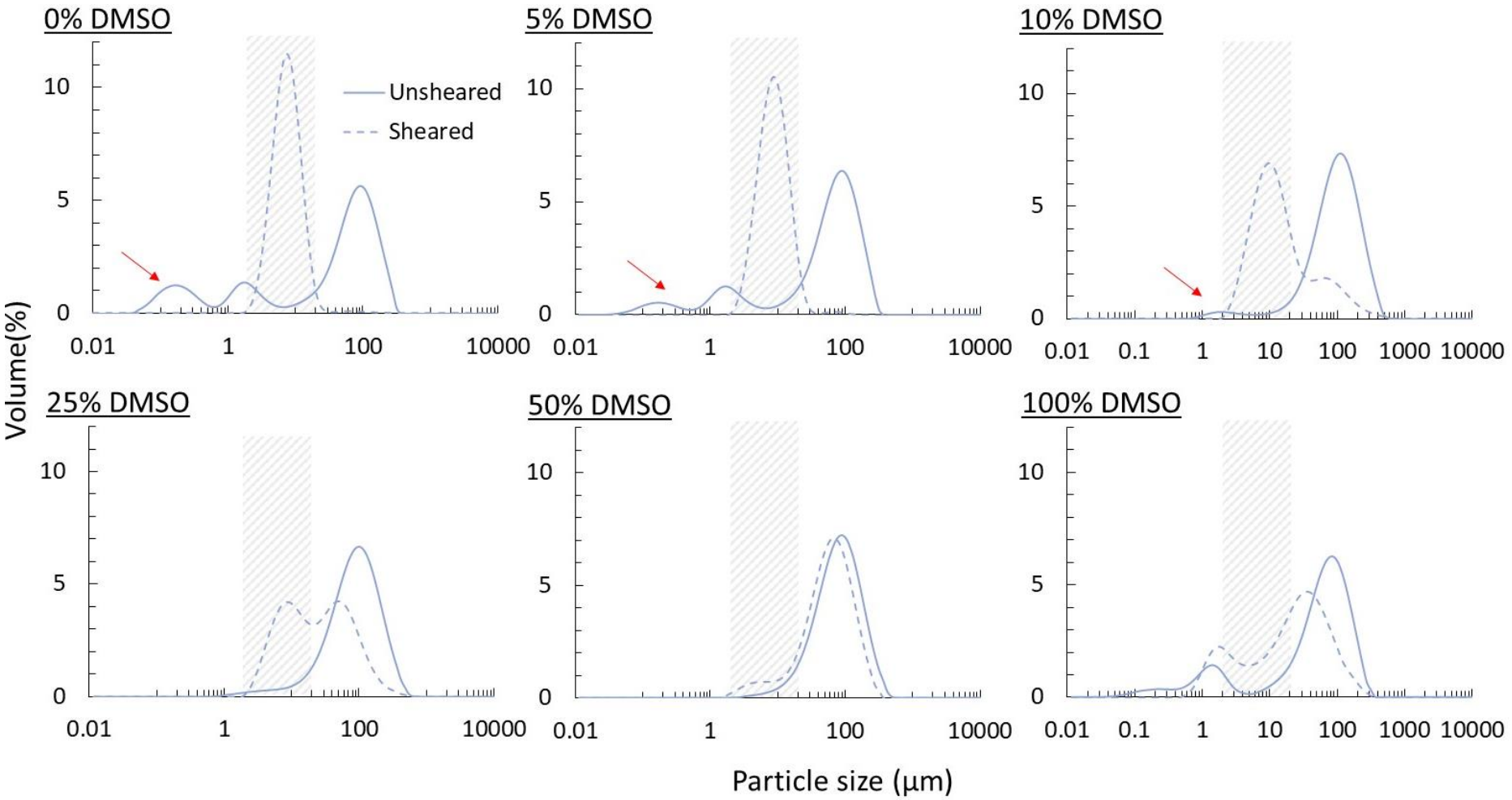

Figure G-3 Effect of DMSO on the particle-size distribution of unsheared and sheared 5% w/w 120 °C DWPS samples at DMSO concentrations of 0, 5, 10, 25, 50 and 100% determined using LD, with the region of interest (2–20 µm) shaded in grey. All plotted values are means of two replicate measurements.

Moreover, a new peak (3–8 µm) was observed in the DLS particle-size distribution of sample containing 50% w/w DMSO upon shear (Figure G-4). This additional peak could be used to explain the increase in *G'* (from ~10 to ~30 Pa) upon shear in the sample with 50 % w/w DMSO, which was contrasting to the reduced *G'* (from ~60 to ~80 Pa) observed in sample with 100% w/w DMSO upon shear (no new peak in the range of 2–20 µm; Figure G-4).

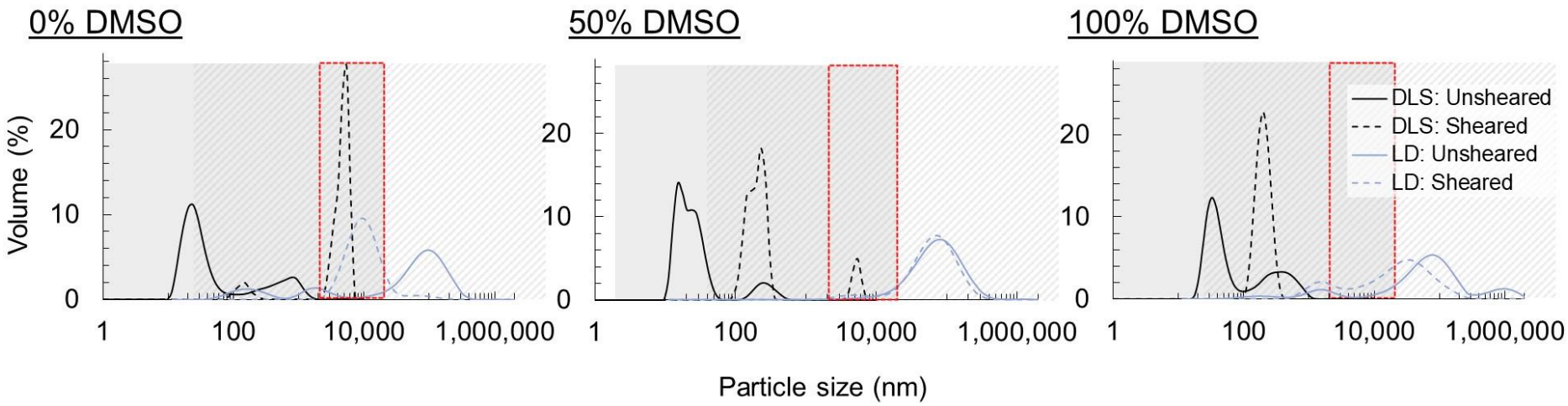

Figure G-4 Effect of DMSO on the particle-size distribution of unsheared and sheared 5% w/w 120 °C DWPS samples prepared in 0, 50 and 100% w/w DMSO determined using DLS (with measurable region coloured in grey) and LD (with measurable region shaded in grey), with the region of interest (2–20 µm) enclosed in a red dotted box. All plotted values are means of two replicate measurements.

Appendix H: Influence of DWPS on the mechanical properties and soaking stability of acidic WPI gels

Mechanical properties of acidic WPI + DWPS gels at pH 5

In addition to the study of neutral WPI + DWPS in Chapter 7, the influence of DWPS on the mechanical properties and water-immersion stability of acidic WPI (SureProtein^{TM} WPI 8855, Fonterra Co-operative Group Limited, Auckland, New Zealand) gels were also evaluated at same pH conditions (*i.e.*, pH 5 and 7). The mechanical properties of 13% w/w WPI and 4% w/w maltodextrin or gelatinised starch or DWPS at pH 5 and the appearance of deformed gels from the compression test are presented in Figure H-1. The *G'* and gel hardness of acidic WPI gels (both pure WPI and composite gels) followed similar trends as neutral WPI gels at pH 5. The pH of neutral and acidic WPI stock solutions was ~6.6–6.8 and ~3.7–4.0, respectively. During pH adjustment to pH 5, a higher amount of HCl was added to neutral WPI as compared to the amount of added NaOH to acidic WPI. The higher amount of HCl resulted in more sodium ions being introduced in the neutral WPI systems compared to acidic WPI systems. Thus, the ionic strength of the neutral systems was higher than those of the acidic systems. The higher ionic strength in turn resulted in higher *G'* and hardness values being observed in the acidic systems, which were consistent in gels with/without added carbohydrates.

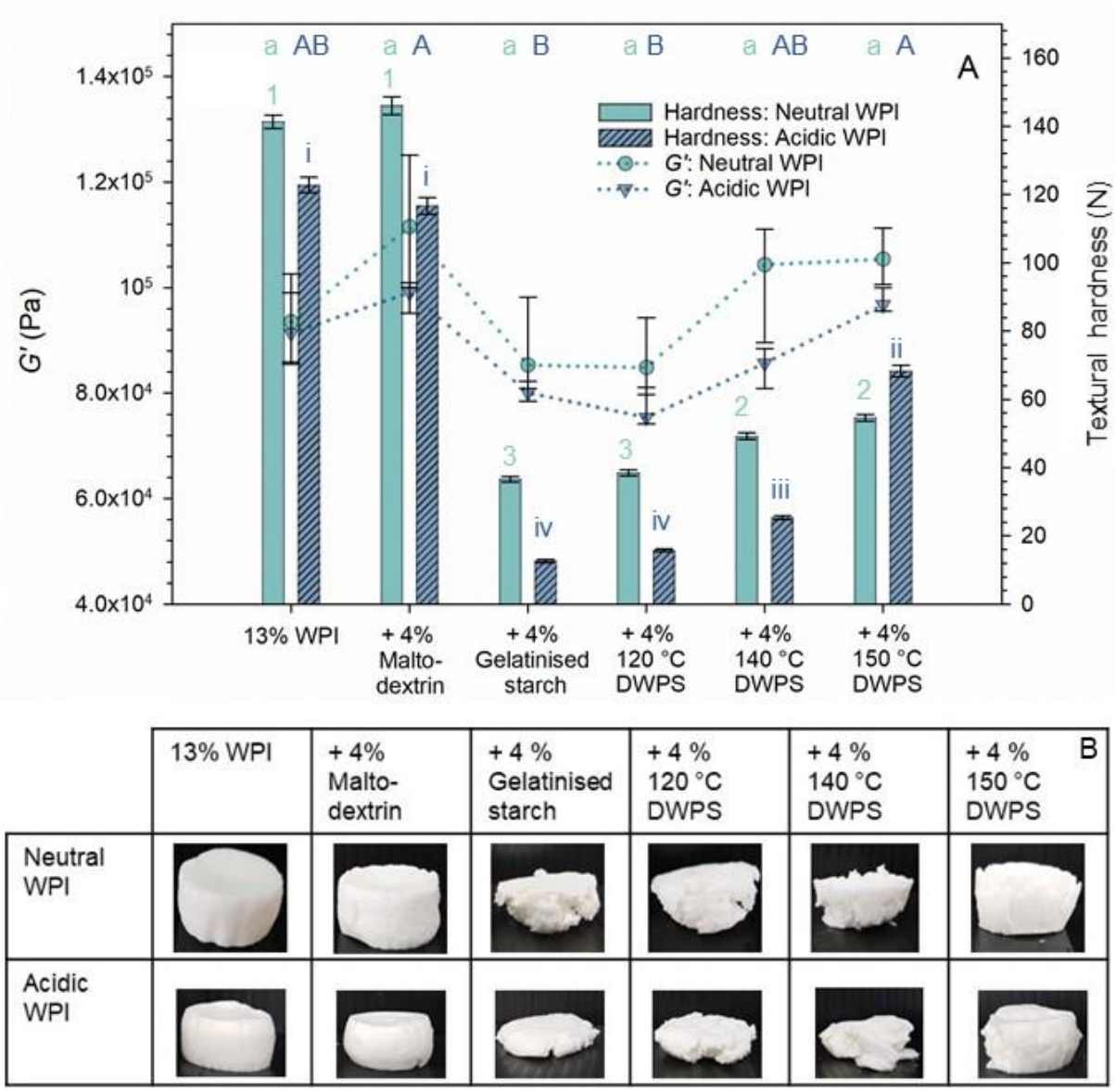

Figure H-1 Mechanical properties of 13 % WPI, 13% WPI + 4% maltodextrin or gelatinised starch or DWPS (120–150 °C): (A) *G'* from frequency sweep at 1 Hz and 1% strain at 20 °C and textural hardness at room temperature of made with neutral and acidic WPIs at pH 5 and (B) the appearance of deformed gels after compression test. All plotted values are presented as means ± standard error. Values denoted within the same series of data with the same superscript/number are not significantly different ($p \leq 0.05$).

Mechanical properties of acidic WPI + DWPS gels at pH 7

At pH 7, the gels made with acidic WPI had markedly higher *G'* and hardness values compared to that of gels made with neutral WPI with/without added carbohydrates (Figure H-2A). A higher amount of NaOH solutions was added to mixtures containing acidic WPI than that of those mixtures containing neutral WPI. Thus, this introduced more sodium ions in acidic WPI systems and led to higher *G'* and hardness values. In addition, the synergistic increase in gel hardness for WPI + 140 °C DWPS in a neutral WPI system was not seen in system with acidic WPI. Instead, gels containing gelatinised starch

or 120 °C DWPS showed the highest *G'* and hardness values in the acidic WPI system. Note that the disappearance of the synergistic increase in gel strength of WPI + 140 °C DWPS was also noted in a neutral WPI system at ≥ 12.5 mM NaCl concentration (Section 8.3.3.1). Thus, the disappearance of the synergistic increase is likely caused by the high amount of NaOH added.

As reported in Section 7.3.2.1, fine-stranded polymeric gels with transparent gels appearance were noted for systems containing neutral WPI. These gels were elastic, and no fracture were observed upon compression. In contrast, the gels containing acidic WPI were translucent or opaque and were more brittle (fractured WPI and WPI + maltodextrin or 150 °C upon compressed, seen in Figure H-2B) as compared to the neutral gels.

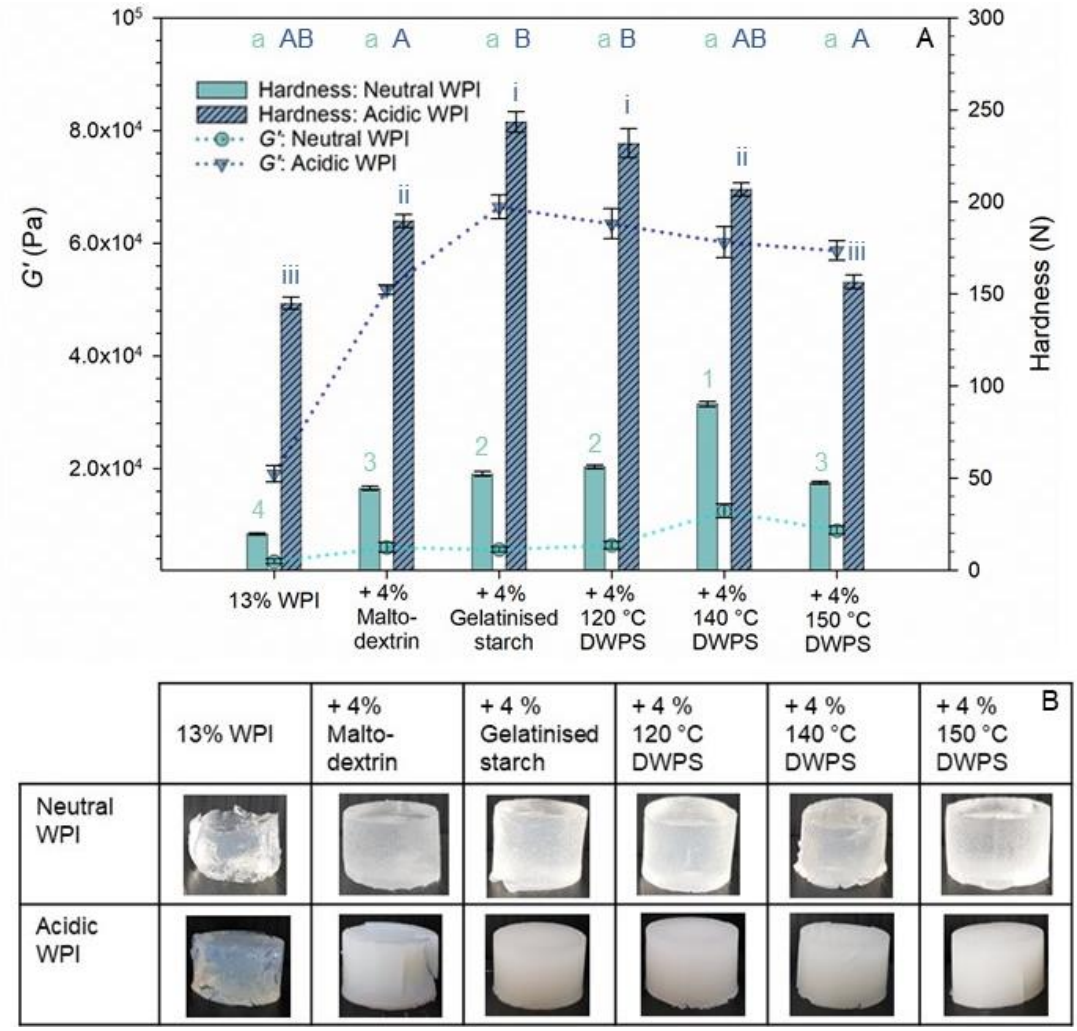

Figure H-2 Mechanical properties of 13 % WPI, 13% WPI + 4% maltodextrin or gelatinised starch or DWPS (120–150 °C): (A) *G'* from frequency sweep at 1 Hz and 1% strain at 20 °C and gel hardness at room temperature made with neutral and acidic WPIs at pH 7 and (B) the appearance of deformed gels. All plotted values are presented as means ± standard error. Values denoted within the same series of data with the same superscript/number are not significantly different ($p \leq 0.05$).

Water-immersion stability of acidic WPI + DWPS gels

At pH 7, gels that contained acidic WPI had markedly a lower water absorption capacity than those of neutral WPI systems (~21–29% w/w in acidic WPI systems versus ~305–589% in neutral WPI systems (Figure H-3A). At pH 5, both WPI systems exhibited a low water absorption (< 12% w/w) (Figure H-3B). Furthermore, contrasting to the swollen and fluid or disintegrated gels observed in pure neutral WPI and neutral WPI + maltodextrin upon water immersion at pH 7 (Figure 7-4B), intact gels were observed for the samples containing acidic WPI (Figure H-4). The intact gels are an indication that the gels containing acidic WPI had enhanced stability due to the low water uptake at pH 7.

A very low protein leaching (≤ 1.4% w/w) was also observed in all the gels made with acidic WPI at both pH 5 and 7 (Figure H-3B). As for carbohydrate leaching, at pH 7, ~15–40% w/w higher leaching was noted in gels containing acidic WPI than that of those containing neutral WPI (Figure H-3C). The higher leaching values could be explained by carbohydrate being trapped in a more open network of the acidic protein gel matrix as an inactive filler, which could be easily released into the immersion liquid. Such a claim is supported by similar carbohydrate leaching values of acidic WPI systems at pH 7, as compared to particulate WPI systems at pH 5. The data indicate that the gel matrix of acidic WPI systems at pH 7 is likely to be more similar to that of a particulate gel network (Figure H-3C).

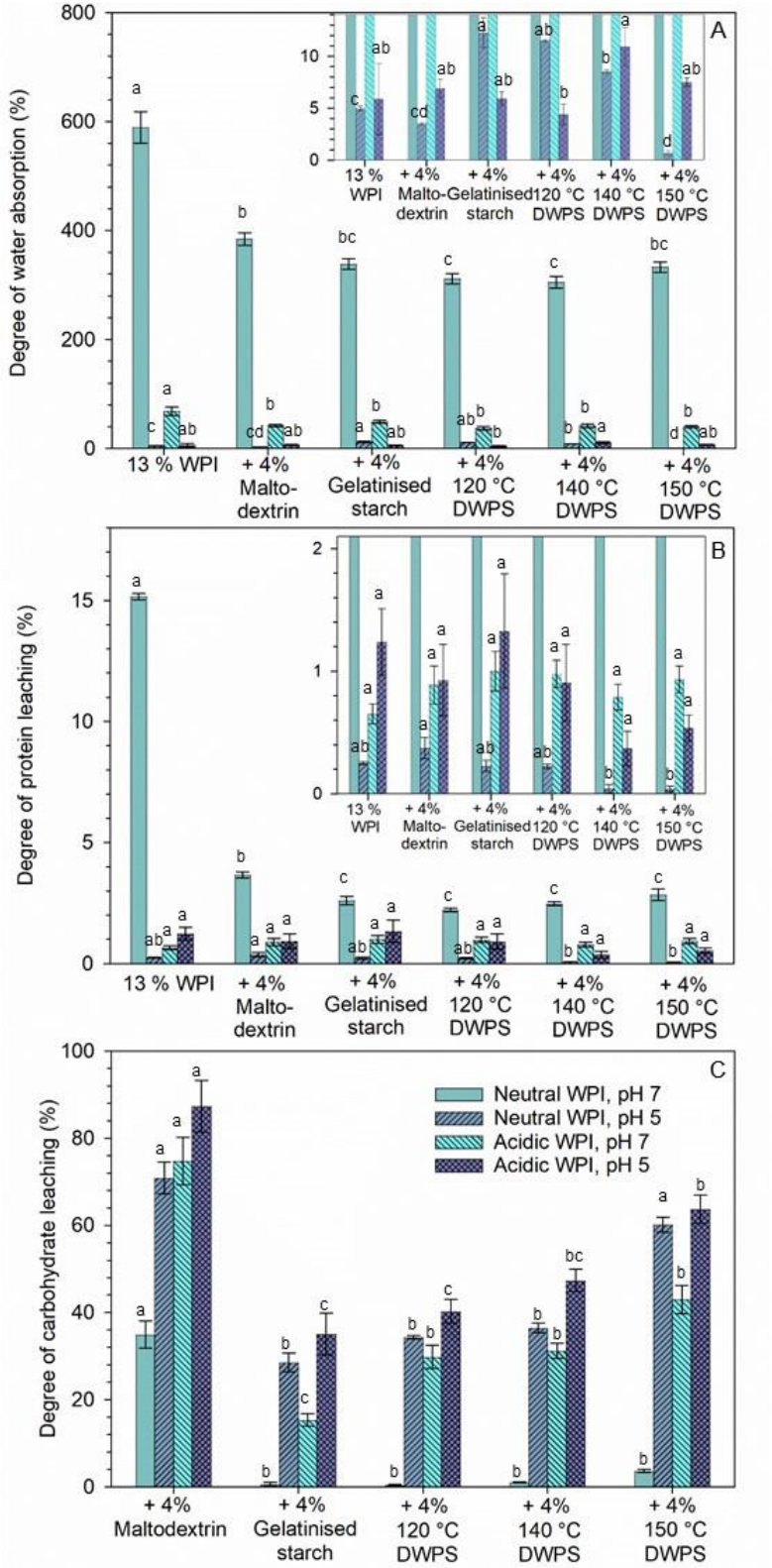

Figure H-3 Water-immersion stability of 13% w/w WPI and 13% WPI + 4% w/w maltodextrin or gelatinised starch or DWPS (120–150 °C) gels made with neutral and acidic WPIs at pH 5 and 7 after 40 h immersion in 0.02% sodium azide solution: (A) water absorption with an inset graph showing 0–14% w/w water absorption, (B) leached protein, with an inset graph showing 0–2.1% protein leaching, and (C) leached carbohydrate. All plotted values are presented as means ± standard error. Values denoted within the same series of data with the same superscript/number are not significantly different ($p \leq 0.05$).

	13% WPI	+ 4% Malto-dextrin	+ 4 % Gelatinised starch	+ 4 % 120 °C DWPS	+ 4 % 140 °C DWPS	+ 4 % 150 °C DWPS
pH 7	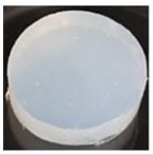		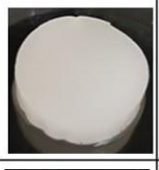	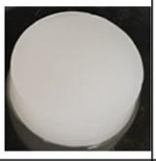	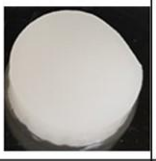	
pH 5						

Figure H-4 Appearance of drained gels containing 13% acidic WPI and 13% acidic WPI + 4% maltodextrin/gelatinised starch/ DWPS (120–150 °C) at pH 7 and pH 5 after 40 h of soaking.

Appendix I: Copyright permissions for figures and publications used in this thesis

Permission for Figure 2-2

ELSEVIER LICENSE
TERMS AND CONDITIONS

May 12, 2022

This Agreement between Massey University -- Cai Ling Ang ("You") and Elsevier ("Elsevier") consists of your license details and the terms and conditions provided by Elsevier and Copyright Clearance Center.

License Number	5302151420326
License date	May 04, 2022
Licensed Content Publisher	Elsevier
Licensed Content Publication	Elsevier Books
Licensed Content Title	Starch in Food
Licensed Content Author	Yongfeng Ai,Jay-lin Jane
Licensed Content Date	Jan 1, 2018
Licensed Content Pages	28
Start Page	151
End Page	178
Type of Use	reuse in a thesis/dissertation
Portion	figures/tables/illustrations

Number of figures/tables /illustrations	1
Format	both print and electronic
Are you the author of this Elsevier chapter?	No
Will you be translating?	No
Title	Characterisation of de-structured starch and its interactions in whey protein isolate gels
Institution name	Massey University
Expected presentation date	Dec 2022
Portions	Figure 3.2
Requestor Location	Massey University School of Food and Advanced Technology Riddet Road, Massey University Palmerston North, Manawatu-Wanganui 4410 New Zealand Attn: Cai Ling Ang
Publisher Tax ID	GB 494 6272 12
Total	0.00 USD
Terms and Conditions	

Permission for Figure 2-3

Reviews

The structural characteristics of starches and their functional properties

Características Estructurales de Almidones y sus Propiedades Funcionales

Yaeel Isbeth Cornejo-Ramírez, Oliviert Martínez-Cruz, Carmen Lizette Del Toro-Sánchez, Francisco Javier Wong-Corral, Jesús Borboa-Flores & **Francisco Javier Cinco-Moroyoqui**

Pages 1003-1017 | Received 18 Jun 2018, Accepted 24 Aug 2018, Published online: 24 Nov 2018

Download citation https://doi.org/10.1080/19476337.2018.1518343 Check for updates

Full Article Figures & data References Supplemental Citations Metrics Licensing Rep

Reprints and Permissions

Permission for Figure 2-4

ELSEVIER LICENSE
TERMS AND CONDITIONS

May 12, 2022

This Agreement between Massey University -- Cai Ling Ang ("You") and Elsevier ("Elsevier") consists of your license details and the terms and conditions provided by Elsevier and Copyright Clearance Center.

License Number	5306431054302
License date	May 12, 2022
Licensed Content Publisher	Elsevier
Licensed Content Publication	Journal of Cereal Science
Licensed Content Title	Starch—composition, fine structure and architecture
Licensed Content Author	Richard F. Tester,John Karkalas,Xin Qi
Licensed Content Date	Mar 1, 2004
Licensed Content Volume	39
Licensed Content Issue	2
Licensed Content Pages	15
Start Page	151
End Page	165

Permission for Figure 2-5

CCC Marketplace™

Order Number: 1218154
Order Date: 05 May 2022

Payment Information

Cai Ling Ang
c.ang@massey.ac.nz
Payment method: Invoice

Billing Address:
Ms. Cai Ling Ang
Massey University
School of Food and Advanced Technology
Riddet Road, Massey University
Palmerston North, Manawatu-Wanganui 4410
New Zealand

+64 2041852183
c.ang@massey.ac.nz

Customer Location:
Ms. Cai Ling Ang
Massey University
School of Food and Advanced Technology
Riddet Road, Massey University
Palmerston North, Manawatu-Wanganui 4410
New Zealand

Order Details

1. Food & function

Billing Status: Open

Article: Molecular disassembly of starch granules during gelatinization and its effect on starch digestibility: a review.

Order License ID	1218154-1	**Type of use**	Republish in a thesis/dissertation
Order detail status	Completed		
ISSN	2042-650X	**Publisher**	Royal Society of Chemistry
		Portion	Chart/graph/table /figure

0.00 USD
Republication Permission

LICENSED CONTENT

Publication Title	Food & function	**Publication Type**	e-Journal
Article Title	Molecular disassembly of starch granules during gelatinization and its effect on starch digestibility: a review.	**Start Page**	1564
		End Page	1580
		Issue	11
		Volume	4
Author/Editor	Royal Society of Chemistry (Great Britain)	**URL**	http://pubs.rsc.org/en/Journals/JournalIssues/FO
Date	01/01/2010		

Language	English
Country	United Kingdom of Great Britain and Northern Ireland
Rightsholder	Royal Society of Chemistry

REQUEST DETAILS

Portion Type	Chart/graph/table /figure	**Distribution**	Worldwide
		Translation	Original language of publication
Number of charts / graphs / tables / figures requested	1	**Copies for the disabled?**	No
Format (select all that apply)	Print,Electronic	**Minor editing privileges?**	No
Who will republish the content?	Academic institution	**Incidental promotional use?**	No
Duration of Use	Life of current edition	**Currency**	USD
Lifetime Unit Quantity	Up to 499		
Rights Requested	Main product		

NEW WORK DETAILS

Title	Characterisation of de-structured starch and its interactions in whey protein isolate gels	**Institution name**	Massey University
		Expected presentation date	2022-12-01
Instructor name	Cai Ling Ang		

ADDITIONAL DETAILS

The requesting person / organization to appear on the license	Cai Ling Ang

REUSE CONTENT DETAILS

Title, description or numeric reference of the portion(s)	Figure 2	**Title of the article/chapter the portion is from**	Molecular disassembly of starch granules during gelatinization and its effect on starch digestibility: a review.
Editor of portion(s)	Wang, Shujun; Copeland, Les		
Volume of serial or monograph	4	**Author of portion(s)**	Wang, Shujun; Copeland, Les
Page or page range of portion	1564-1580	**Issue, if republishing an article from a serial**	11
		Publication date of portion	2013-11-01

Total Items: 1

Subtotal: 0.00 USD

Order Total: 0.00 USD

Permission for Figure 2-6

ELSEVIER LICENSE
TERMS AND CONDITIONS

May 12, 2022

This Agreement between Massey University -- Cai Ling Ang ("You") and Elsevier ("Elsevier") consists of your license details and the terms and conditions provided by Elsevier and Copyright Clearance Center.

License Number	5302160745246
License date	May 04, 2022
Licensed Content Publisher	Elsevier
Licensed Content Publication	International Journal of Biological Macromolecules
Licensed Content Title	Analysis of the pasting profile in corn starch: Structural, morphological, and thermal transformations, Part I
Licensed Content Author	Natalia Rincón-Londoño,Lineth J. Vega-Rojas,Margarita Contreras-Padilla,A.A. Acosta-Osorio,Mario E. Rodríguez-García
Licensed Content Date	Oct 1, 2016
Licensed Content Volume	91
Licensed Content Issue	n/a
Licensed Content Pages	9
Start Page	106

End Page	114
Type of Use	reuse in a thesis/dissertation
Portion	figures/tables/illustrations
Number of figures/tables /illustrations	1
Format	both print and electronic
Are you the author of this Elsevier article?	No
Will you be translating?	No
Title	Characterisation of de-structured starch and its interactions in whey protein isolate gels
Institution name	Massey University
Expected presentation date	Dec 2022
Portions	Figure 3
Requestor Location	Massey University School of Food and Advanced Technology Riddet Road, Massey University Palmerston North, Manawatu-Wanganui 4410 New Zealand Attn: Cai Ling Ang
Publisher Tax ID	GB 494 6272 12
Total	0.00 USD

Permission for Figure 2-7

Food and Nutrition Sciences
Vol.5 No.3(2014), Article ID:42262,12 pages
DOI:10.4236/fns.2014.53035

• Abstract
• Full-Text PDF
• Full-Text HTML
• Full-Text XML
• Full-Text ePUB
• Linked References
• How to Cite this Article

The Principles of Starch Gelatinization and Retrogradation*

Masakuni Tako[1,2#], Yukihiro Tamaki[1], Takeshi Teruya[1], Yasuhito Takeda[3]

[1]Department of Subtropical Bioscience and Biotechnology, University of the Ryukyus, Nishihara, Japan; [2]Health and Longevity Research Laboratory, Integrated Innovation Research Center, University of the Ryukyus, Nishihara, Japan; [3]Department of Biochemical Science and Technology, Kagoshima University, Kagoshima, Japan.

Email: #tako@eve.u-ryukyu.ac.jp

Permission for Figure 2-8

ELSEVIER LICENSE
TERMS AND CONDITIONS

May 12, 2022

This Agreement between Massey University -- Cai Ling Ang ("You") and Elsevier ("Elsevier") consists of your license details and the terms and conditions provided by Elsevier and Copyright Clearance Center.

License Number	5302170677477
License date	May 04, 2022
Licensed Content Publisher	Elsevier
Licensed Content Publication	Current Opinion in Colloid & Interface Science
Licensed Content Title	Rheology of associative polymer solutions
Licensed Content Author	Christophe Chassenieux,Taco Nicolai,Lazhar Benyahia
Licensed Content Date	Feb 1, 2011
Licensed Content Volume	16
Licensed Content Issue	1
Licensed Content Pages	9
Start Page	18
End Page	26

Type of Use	reuse in a thesis/dissertation
Portion	figures/tables/illustrations
Number of figures/tables /illustrations	1
Format	both print and electronic
Are you the author of this Elsevier article?	No
Will you be translating?	No
Title	Characterisation of de-structured starch and its interactions in whey protein isolate gels
Institution name	Massey University
Expected presentation date	Dec 2022
Portions	Figure 1
Requestor Location	Massey University School of Food and Advanced Technology Riddet Road, Massey University Palmerston North, Manawatu-Wanganui 4410 New Zealand Attn: Cai Ling Ang
Publisher Tax ID	GB 494 6272 12
Total	0.00 USD
Terms and Conditions	

Permission for Figure 2-9

ELSEVIER LICENSE
TERMS AND CONDITIONS

May 12, 2022

This Agreement between Massey University -- Cai Ling Ang ("You") and Elsevier ("Elsevier") consists of your license details and the terms and conditions provided by Elsevier and Copyright Clearance Center.

License Number	5302170847902
License date	May 04, 2022
Licensed Content Publisher	Elsevier
Licensed Content Publication	Carbohydrate Polymers
Licensed Content Title	Probing hydrogen bond interactions in a shear thickening polysaccharide using nonlinear shear and extensional rheology
Licensed Content Author	Aditya Jaishankar,May Wee,Lara Matia-Merino,Kelvin K.T. Goh,Gareth H. McKinley
Licensed Content Date	Jun 5, 2015
Licensed Content Volume	123
Licensed Content Issue	n/a
Licensed Content Pages	10
Start Page	136

End Page	145
Type of Use	reuse in a thesis/dissertation
Portion	figures/tables/illustrations
Number of figures/tables /illustrations	1
Format	both print and electronic
Are you the author of this Elsevier article?	No
Will you be translating?	No
Title	Characterisation of de-structured starch and its interactions in whey protein isolate gels
Institution name	Massey University
Expected presentation date	Dec 2022
Portions	Figure 2
Requestor Location	Massey University School of Food and Advanced Technology Riddet Road, Massey University Palmerston North, Manawatu-Wanganui 4410 New Zealand Attn: Cai Ling Ang
Publisher Tax ID	GB 494 6272 12
Total	0.00 USD

Permission for Figure 2-10

Polymers (Basel). 2018 Jul; 10(7): 762.
Published online 2018 Jul 11. doi: 10.3390/polym10070762
PMCID: PMC6404037
PMID: 30960687

Structure-Related Gelling of Pectins and Linking with Other Natural Compounds: A Review

Diana Gawkowska, Justyna Cybulska,* and Artur Zdunek

Permission for Figure 2-12

ELSEVIER LICENSE
TERMS AND CONDITIONS

May 12, 2022

This Agreement between Massey University -- Cai Ling Ang ("You") and Elsevier ("Elsevier") consists of your license details and the terms and conditions provided by Elsevier and Copyright Clearance Center.

License Number	5302171393994
License date	May 04, 2022
Licensed Content Publisher	Elsevier
Licensed Content Publication	Elsevier Books
Licensed Content Title	Whey Proteins
Licensed Content Author	Heni B. Wijayanti,André Brodkorb,Sean A. Hogan,Eoin G. Murphy
Licensed Content Date	Jan 1, 2019
Licensed Content Pages	63
Start Page	185
End Page	247
Type of Use	reuse in a thesis/dissertation
Portion	figures/tables/illustrations

Number of figures/tables /illustrations	1
Format	both print and electronic
Are you the author of this Elsevier chapter?	No
Will you be translating?	No
Title	Characterisation of de-structured starch and its interactions in whey protein isolate gels
Institution name	Massey University
Expected presentation date	Dec 2022
Portions	Figure 1a
Requestor Location	Massey University School of Food and Advanced Technology Riddet Road, Massey University Palmerston North, Manawatu-Wanganui 4410 New Zealand Attn: Cai Ling Ang
Publisher Tax ID	GB 494 6272 12
Total	0.00 USD
Terms and Conditions	

Permission for Figure 2-14

ELSEVIER LICENSE
TERMS AND CONDITIONS

May 12, 2022

This Agreement between Massey University -- Cai Ling Ang ("You") and Elsevier ("Elsevier") consists of your license details and the terms and conditions provided by Elsevier and Copyright Clearance Center.

License Number	5302180044291
License date	May 04, 2022
Licensed Content Publisher	Elsevier
Licensed Content Publication	Carbohydrate Polymers
Licensed Content Title	Phase segregation of amylopectin and β-lactoglobulin in aqueous system
Licensed Content Author	Carmen Carla Quiroga,Björn Bergenståhl
Licensed Content Date	Apr 3, 2008
Licensed Content Volume	72
Licensed Content Issue	1
Licensed Content Pages	9
Start Page	151
End Page	159

Type of Use	reuse in a thesis/dissertation
Portion	figures/tables/illustrations
Number of figures/tables /illustrations	1
Format	both print and electronic
Are you the author of this Elsevier article?	No
Will you be translating?	No
Title	Characterisation of de-structured starch and its interactions in whey protein isolate gels
Institution name	Massey University
Expected presentation date	Dec 2022
Portions	Figure 5
Requestor Location	Massey University School of Food and Advanced Technology Riddet Road, Massey University Palmerston North, Manawatu-Wanganui 4410 New Zealand Attn: Cai Ling Ang
Publisher Tax ID	GB 494 6272 12
Total	0.00 USD
Terms and Conditions	

Permission for Figure 2-16

Cailing Ang

From: Mary Ellen Kuhn <mkuhn@ift.org>
Sent: Thursday, 12 May 2022 7:14 AM
To: Cailing Ang
Cc: Donna Morris
Subject: Permission Granted

Dear Cai Ling,

Re your query, we are happy to grant permission. Please just credit Food Technology, and the author.

We apologize for the confusion with Copyright Clearance Center (we do subscribe to some of their services, so we're looking into the issue there).

Best of luck with the doctoral thesis!--Mary Ellen

Hi there,

I am writing to ask for permission to use Figure 4 from the IFT Food Technology publications on November 2000, Volume 54, No. 11 (https://www.ift.org/news-and-publications/food-technology-magazine/issues/2000/november/features/microstructure-and-food-product-engineering) in my Doctoral thesis. Different from journal articles, this is an online magazine article does not have a hyperlink that redirects me for permission request.

I have previously written to IFT and they have directed me to Copyright Clearance Center to ask for permission.

Please advise.

Thank you.

Warmest regards, Cai Ling

Mary Ellen Kuhn
Executive Editor, *Food Technology* Magazine
Institute of Food Technologists®
525 W. Van Buren Street, Suite 1000
Chicago, IL 60607-3830 USA
331.826.9653 Mobile (Preferred)
+1.312.604.0216 Ph
mkuhn@ift.org
ift.org | @IFT

Permission for Figure 3-7

JOHN WILEY AND SONS LICENSE
TERMS AND CONDITIONS

May 12, 2022

This Agreement between Massey University -- Cai Ling Ang ("You") and John Wiley and Sons ("John Wiley and Sons") consists of your license details and the terms and conditions provided by John Wiley and Sons and Copyright Clearance Center.

License Number	5302150418544
License date	May 04, 2022
Licensed Content Publisher	John Wiley and Sons
Licensed Content Publication	Wiley Books
Licensed Content Title	Resolution
Licensed Content Date	Nov 24, 2009
Licensed Content Pages	24
Type of use	Dissertation/Thesis
Requestor type	University/Academic
Format	Print and electronic
Portion	Figure/table
Number of figures/tables	1

Will you be translating?	No
Title	Characterisation of de-structured starch and its interactions in whey protein isolate gels
Institution name	Massey University
Expected presentation date	Dec 2022
Portions	Figure 4.11
Requestor Location	Massey University School of Food and Advanced Technology Riddet Road, Massey University Palmerston North, Manawatu-Wanganui 4410 New Zealand Attn: Cai Ling Ang
Publisher Tax ID	EU826007151
Total	0.00 USD

Permission for Figure 3-8 and Figure 3-9

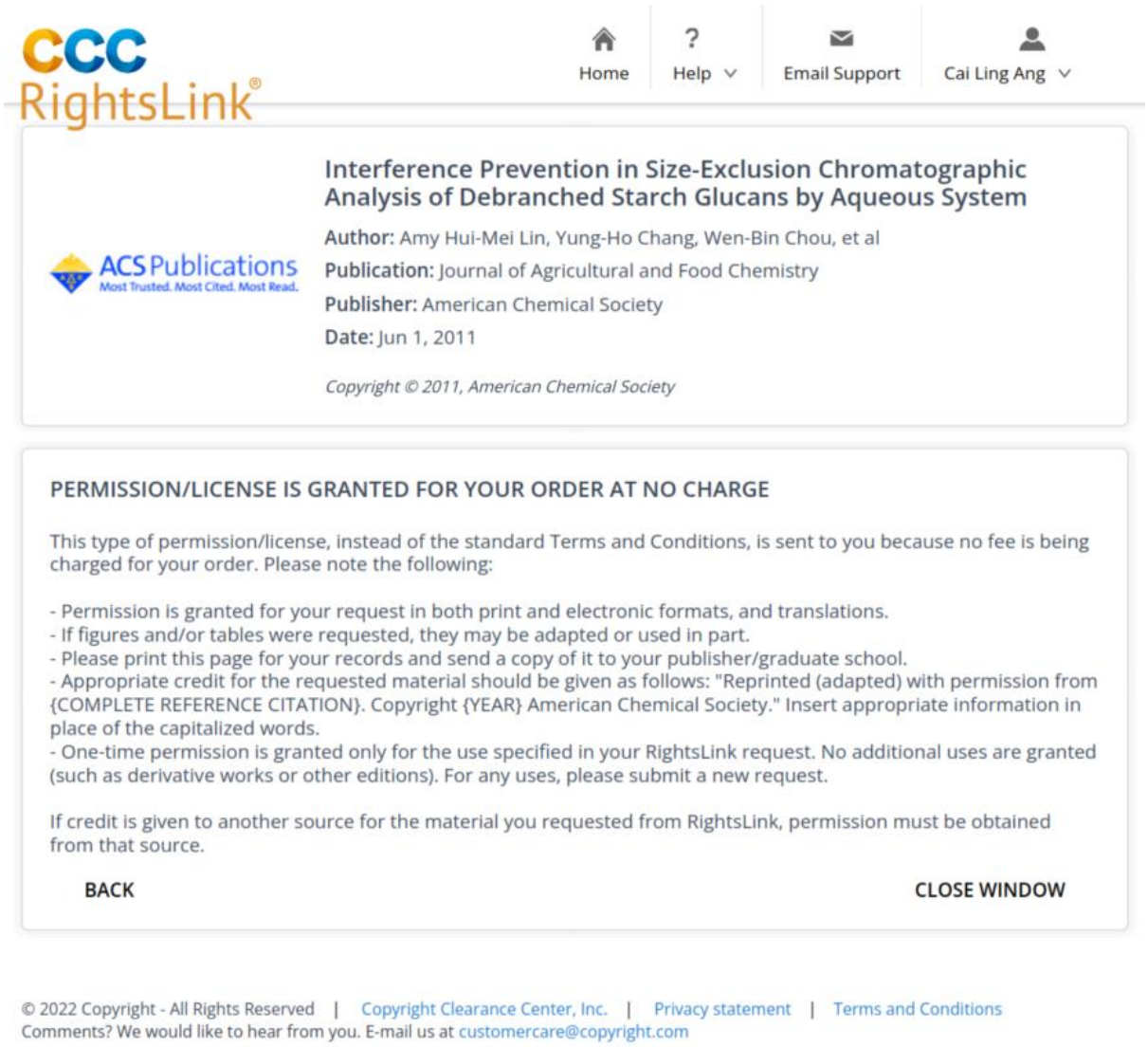

CCC RightsLink®

Home | Help | Email Support | Cai Ling Ang

ACS Publications
Most Trusted. Most Cited. Most Read.

Interference Prevention in Size-Exclusion Chromatographic Analysis of Debranched Starch Glucans by Aqueous System

Author: Amy Hui-Mei Lin, Yung-Ho Chang, Wen-Bin Chou, et al
Publication: Journal of Agricultural and Food Chemistry
Publisher: American Chemical Society
Date: Jun 1, 2011

Copyright © 2011, American Chemical Society

PERMISSION/LICENSE IS GRANTED FOR YOUR ORDER AT NO CHARGE

This type of permission/license, instead of the standard Terms and Conditions, is sent to you because no fee is being charged for your order. Please note the following:

- Permission is granted for your request in both print and electronic formats, and translations.
- If figures and/or tables were requested, they may be adapted or used in part.
- Please print this page for your records and send a copy of it to your publisher/graduate school.
- Appropriate credit for the requested material should be given as follows: "Reprinted (adapted) with permission from {COMPLETE REFERENCE CITATION}. Copyright {YEAR} American Chemical Society." Insert appropriate information in place of the capitalized words.
- One-time permission is granted only for the use specified in your RightsLink request. No additional uses are granted (such as derivative works or other editions). For any uses, please submit a new request.

If credit is given to another source for the material you requested from RightsLink, permission must be obtained from that source.

BACK CLOSE WINDOW

Permission for Figure 3-19

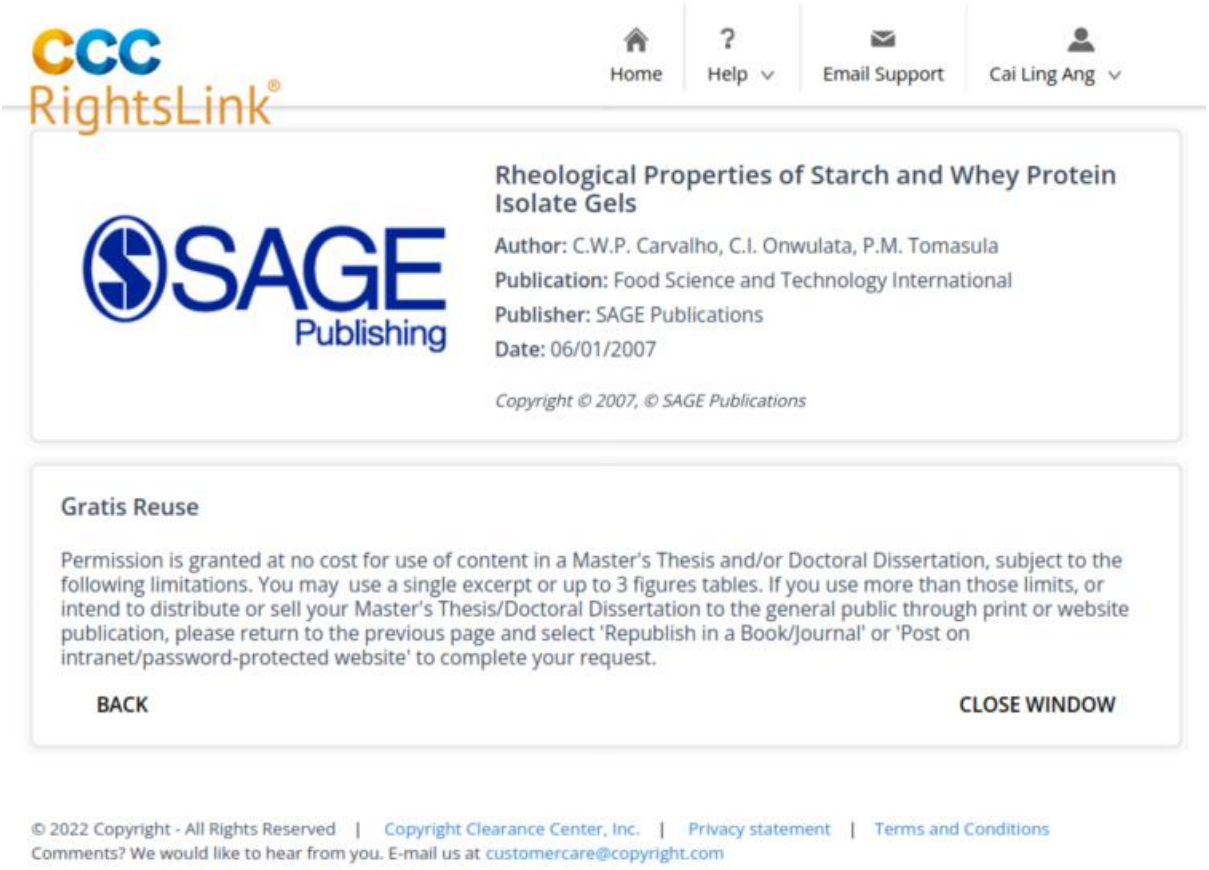

CCC RightsLink

Home | Help | Email Support | Cai Ling Ang

SAGE Publishing

Rheological Properties of Starch and Whey Protein Isolate Gels

Author: C.W.P. Carvalho, C.I. Onwulata, P.M. Tomasula

Publication: Food Science and Technology International

Publisher: SAGE Publications

Date: 06/01/2007

Copyright © 2007, © SAGE Publications

Gratis Reuse

Permission is granted at no cost for use of content in a Master's Thesis and/or Doctoral Dissertation, subject to the following limitations. You may use a single excerpt or up to 3 figures tables. If you use more than those limits, or intend to distribute or sell your Master's Thesis/Doctoral Dissertation to the general public through print or website publication, please return to the previous page and select 'Republish in a Book/Journal' or 'Post on intranet/password-protected website' to complete your request.

BACK CLOSE WINDOW

Permission for Figure 3-20

ELSEVIER LICENSE
TERMS AND CONDITIONS

May 12, 2022

This Agreement between Massey University -- Cai Ling Ang ("You") and Elsevier ("Elsevier") consists of your license details and the terms and conditions provided by Elsevier and Copyright Clearance Center.

License Number	5302131192517
License date	May 04, 2022
Licensed Content Publisher	Elsevier
Licensed Content Publication	Journal of Dairy Science
Licensed Content Title	Functionality of Extrusion—Texturized Whey Proteins 1
Licensed Content Author	C.I. Onwulata,R.P. Konstance,P.H. Cooke,H.M. Farrell
Licensed Content Date	Nov 1, 2003
Licensed Content Volume	86
Licensed Content Issue	11
Licensed Content Pages	8
Start Page	3775
End Page	3782

Type of Use	reuse in a thesis/dissertation
Portion	figures/tables/illustrations
Number of figures/tables /illustrations	1
Format	both print and electronic
Are you the author of this Elsevier article?	No
Will you be translating?	No
Title	Characterisation of de-structured starch and its interactions in whey protein isolate gels
Institution name	Massey University
Expected presentation date	Dec 2022
Portions	Figure 1
Requestor Location	Massey University School of Food and Advanced Technology Riddet Road, Massey University Palmerston North, Manawatu-Wanganui 4410 New Zealand Attn: Cai Ling Ang
Publisher Tax ID	GB 494 6272 12
Total	0.00 USD

Permission for Figure 3-22

ELSEVIER LICENSE
TERMS AND CONDITIONS

May 12, 2022

This Agreement between Massey University -- Cai Ling Ang ("You") and Elsevier ("Elsevier") consists of your license details and the terms and conditions provided by Elsevier and Copyright Clearance Center.

License Number	5302140444621
License date	May 04, 2022
Licensed Content Publisher	Elsevier
Licensed Content Publication	Food Hydrocolloids
Licensed Content Title	Combining protein micro-phase separation and protein–polysaccharide segregative phase separation to produce gel structures
Licensed Content Author	Esra Çakır,E. Allen Foegeding
Licensed Content Date	Aug 1, 2011
Licensed Content Volume	25
Licensed Content Issue	6
Licensed Content Pages	9
Start Page	1538

End Page	1546
Type of Use	reuse in a thesis/dissertation
Portion	figures/tables/illustrations
Number of figures/tables /illustrations	1
Format	both print and electronic
Are you the author of this Elsevier article?	No
Will you be translating?	No
Title	Characterisation of de-structured starch and its interactions in whey protein isolate gels
Institution name	Massey University
Expected presentation date	Dec 2022
Portions	Figure 1
Requestor Location	Massey University School of Food and Advanced Technology Riddet Road, Massey University Palmerston North, Manawatu-Wanganui 4410 New Zealand Attn: Cai Ling Ang
Publisher Tax ID	GB 494 6272 12
Total	0.00 USD

Permission to use author's own publications

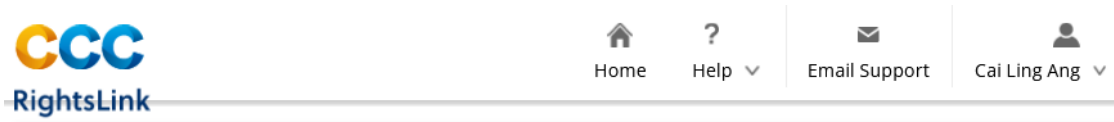

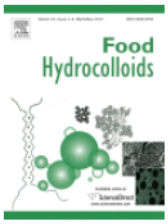

Molecular and physico-chemical characterization of de-structured waxy potato starch

Author: Cai Ling Ang,Lara Matia-Merino,Kaiyang Lim,Kelvin Kim Tha Goh

Publication: Food Hydrocolloids

Publisher: Elsevier

Date: August 2021

Journal Author Rights

Please note that, as the author of this Elsevier article, you retain the right to include it in a thesis or dissertation, provided it is not published commercially. Permission is not required, but please ensure that you reference the journal as the original source. For more information on this and on your other retained rights, please visit: https://www.elsevier.com/about/our-business/policies/copyright#Author-rights

BACK CLOSE WINDOW

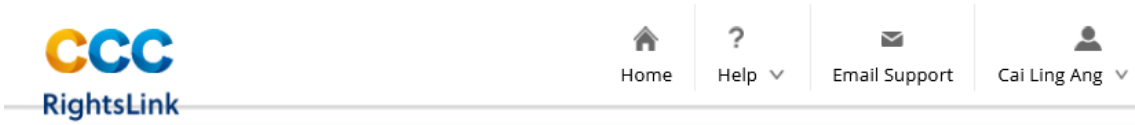

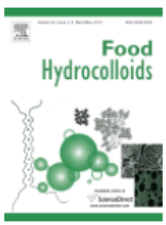

Rheological characterization of a physically-modified waxy potato starch: Investigation of its shear-thickening mechanism

Author: Cai Ling Ang,Kelvin Kim Tha Goh,Kaiyang Lim,Lara Matia-Merino

Publication: Food Hydrocolloids

Publisher: Elsevier

Date: November 2021

Journal Author Rights

Please note that, as the author of this Elsevier article, you retain the right to include it in a thesis or dissertation, provided it is not published commercially. Permission is not required, but please ensure that you reference the journal as the original source. For more information on this and on your other retained rights, please visit: https://www.elsevier.com/about/our-business/policies/copyright#Author-rights

BACK CLOSE WINDOW

MDPI Open Access Information and Policy

All articles published by MDPI are made immediately available worldwide under an open access license. This means:

- everyone has free and unlimited access to the full-text of *all* articles published in MDPI journals;
- everyone is free to re-use the published material if proper accreditation/citation of the original publication is given;
- open access publication is supported by the authors' institutes or research funding agencies by payment of a comparatively low Article Processing Charge (APC) for accepted articles.

Permissions

No special permission is required to reuse all or part of article published by MDPI, including figures and tables. For articles published under an open access Creative Common CC BY license, any part of the article may be reused without permission provided that the original article is clearly cited. Reuse of an article does not imply endorsement by the authors or MDPI.

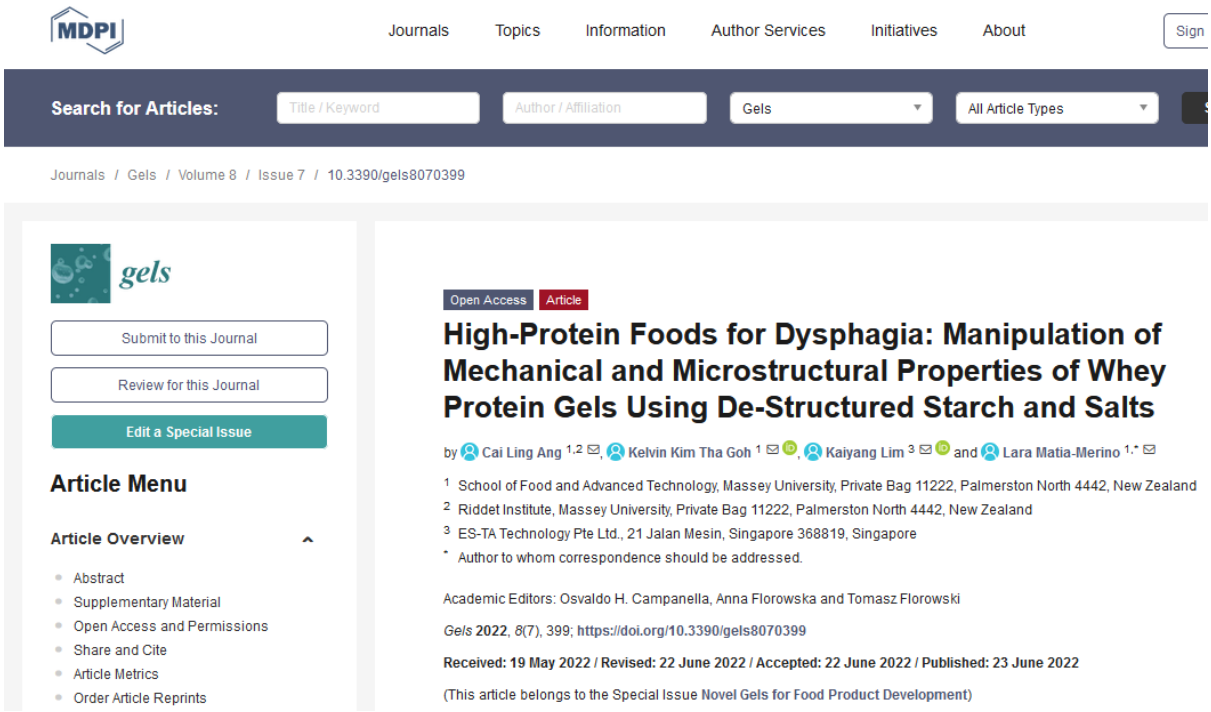

Appendix J: Statement of Contribution

DRC 16

MASSEY UNIVERSITY
TE KUNENGA KI PŪREHUROA
UNIVERSITY OF NEW ZEALAND

GRADUATE RESEARCH SCHOOL

STATEMENT OF CONTRIBUTION
DOCTORATE WITH PUBLICATIONS/MANUSCRIPTS

We, the candidate and the candidate's Primary Supervisor, certify that all co-authors have consented to their work being included in the thesis and they have accepted the candidate's contribution as indicated below in the *Statement of Originality*.

Name of candidate:	Cai Ling Ang
Name/title of Primary Supervisor:	Kelvin Kim Tha Goh/Associate Professor
In which chapter is the manuscript /published work:	Chapter 4 and 5

Please select one of the following three options:

(●) The manuscript/published work is published or in press

- Please provide the full reference of the Research Output:

Ang, C. L., Matia-Merino, L., Lim, K., & Goh, K. K. T. (2021). Molecular and physico-chemical characterisation of de-structured waxy potato starch. Food Hydrocolloids, 117, 106667.

( ) The manuscript is currently under review for publication – please indicate:

- The name of the journal:
- The percentage of the manuscript/published work that was contributed by the candidate:
- Describe the contribution that the candidate has made to the manuscript/published work:

( ) It is intended that the manuscript will be published, but it has not yet been submitted to a journal

Candidate's Signature:	Cai Ling Digitally signed by Cai Ling Date: 2022.07.03 14:02:24 +12'00'
Date:	03-Jul-2022
Primary Supervisor's Signature:	Kelvin Goh Digitally signed by Kelvin Goh Date: 2022.07.03 09:35:27 +08'00'
Date:	3-Jul-2022

This form should appear at the end of each thesis chapter/section/appendix submitted as a manuscript/ publication or collected as an appendix at the end of the thesis.

GRS Version 5 – 13 December 2019
DRC 19/09/10

DRC 16

MASSEY UNIVERSITY
TE KUNENGA KI PŪREHUROA
UNIVERSITY OF NEW ZEALAND

GRADUATE RESEARCH SCHOOL

STATEMENT OF CONTRIBUTION
DOCTORATE WITH PUBLICATIONS/MANUSCRIPTS

We, the candidate and the candidate's Primary Supervisor, certify that all co-authors have consented to their work being included in the thesis and they have accepted the candidate's contribution as indicated below in the *Statement of Originality*.

Name of candidate:	Cai Ling Ang
Name/title of Primary Supervisor:	Kelvin Kim Tha Goh/Associate Professor
In which chapter is the manuscript /published work:	Chapter 4, 5 and 6

Please select one of the following three options:

(●) The manuscript/published work is published or in press

- Please provide the full reference of the Research Output:

Ang, C. L., Matia-Merino, L., Sims, I. M., Sargison, L., Edwards, P. J. B., Lim, K., & Goh, K. K. T. (2022). Characterisation of de-structured starch and its shear-thickening mechanism. Food Hydrocolloids, 132, 107864.

( ) The manuscript is currently under review for publication – please indicate:

- The name of the journal:
- The percentage of the manuscript/published work that was contributed by the candidate:
- Describe the contribution that the candidate has made to the manuscript/published work:

( ) It is intended that the manuscript will be published, but it has not yet been submitted to a journal

Candidate's Signature:	Cai Ling Digitally signed by Cai Ling Date: 2022.07.03 14:00:37 +12'00'
Date:	03-Jul-2022
Primary Supervisor's Signature:	Kelvin Goh Digitally signed by Kelvin Goh Date: 2022.07.03 09:36:23 +08'00'
Date:	3-Jul-2022

This form should appear at the end of each thesis chapter/section/appendix submitted as a manuscript/ publication or collected as an appendix at the end of the thesis.

GRS Version 5 – 13 December 2019
DRC 19/09/10

DRC 16

MASSEY UNIVERSITY
TE KUNENGA KI PŪREHUROA
UNIVERSITY OF NEW ZEALAND

GRADUATE RESEARCH SCHOOL

STATEMENT OF CONTRIBUTION
DOCTORATE WITH PUBLICATIONS/MANUSCRIPTS

We, the candidate and the candidate's Primary Supervisor, certify that all co-authors have consented to their work being included in the thesis and they have accepted the candidate's contribution as indicated below in the *Statement of Originality*.

Name of candidate:	Cai Ling Ang
Name/title of Primary Supervisor:	Kelvin Kim Tha Goh/Associate Professor
In which chapter is the manuscript /published work:	Chapter 5 and 6

Please select one of the following three options:

(●) The manuscript/published work is published or in press

- Please provide the full reference of the Research Output:

Ang, C. L., Goh, K. K. T., Lim, K., & Matia-Merino, L. (2021). Rheological characterisation of a physically-modified waxy potato starch: Investigation of its shear-thickening mechanism. Food Hydrocolloids, 120, 106908.

( ) The manuscript is currently under review for publication – please indicate:

- The name of the journal:
- The percentage of the manuscript/published work that was contributed by the candidate:
- Describe the contribution that the candidate has made to the manuscript/published work:

( ) It is intended that the manuscript will be published, but it has not yet been submitted to a journal

Candidate's Signature:	Cai Ling Digitally signed by Cai Ling Date: 2022.07.03 13:57:16 +12'00'
Date:	03-Jul-2022
Primary Supervisor's Signature:	Kelvin Goh Digitally signed by Kelvin Goh Date: 2022.07.03 08:56:06 +08'00'
Date:	3-Jul-2022

This form should appear at the end of each thesis chapter/section/appendix submitted as a manuscript/ publication or collected as an appendix at the end of the thesis.

GRS Version 5 – 13 December 2019
DRC 19/09/10

DRC 16

MASSEY UNIVERSITY
TE KUNENGA KI PŪREHUROA
UNIVERSITY OF NEW ZEALAND

GRADUATE RESEARCH SCHOOL

STATEMENT OF CONTRIBUTION
DOCTORATE WITH PUBLICATIONS/MANUSCRIPTS

We, the candidate and the candidate's Primary Supervisor, certify that all co-authors have consented to their work being included in the thesis and they have accepted the candidate's contribution as indicated below in the *Statement of Originality*.

Name of candidate:	Cai Ling Ang
Name/title of Primary Supervisor:	Kelvin Kim Tha Goh/Associate Professor
In which chapter is the manuscript /published work:	Chapter 7

Please select one of the following three options:

(●) The manuscript/published work is published or in press

- Please provide the full reference of the Research Output:

Ang, C. L., Matia-Merino, L., Lim, K., & Goh, K. K. T. (2023). Influence of de-structured starch on fine-stranded polymeric and coarse-stranded particulate whey protein gels. Food Hydrocolloids, 135, 108201.

( ) The manuscript is currently under review for publication – please indicate:

- The name of the journal:
- The percentage of the manuscript/published work that was contributed by the candidate:
- Describe the contribution that the candidate has made to the manuscript/published work:

( ) It is intended that the manuscript will be published, but it has not yet been submitted to a journal

Candidate's Signature:	Sign Here: Ling
Date:	03-Jul-2022
Primary Supervisor's Signature:	Kelvin Goh Digitally signed by Kelvin Goh Date: 2022.07.03 09:33:11 +08'00'
Date:	3-Jul-2022

This form should appear at the end of each thesis chapter/section/appendix submitted as a manuscript/ publication or collected as an appendix at the end of the thesis.

GRS Version 5 – 13 December 2019
DRC 19/09/10

DRC 16

MASSEY UNIVERSITY TE KUNENGA KI PŪREHUROA UNIVERSITY OF NEW ZEALAND | GRADUATE RESEARCH SCHOOL

STATEMENT OF CONTRIBUTION
DOCTORATE WITH PUBLICATIONS/MANUSCRIPTS

We, the candidate and the candidate's Primary Supervisor, certify that all co-authors have consented to their work being included in the thesis and they have accepted the candidate's contribution as indicated below in the *Statement of Originality*.

Name of candidate:	Cai Ling Ang
Name/title of Primary Supervisor:	Kelvin Kim Tha Goh/Associate Professor
In which chapter is the manuscript /published work:	Chapter 8

Please select one of the following three options:

(●) The manuscript/published work is published or in press

- Please provide the full reference of the Research Output:

Ang, C. L., Goh, K. K. T., Lim, K., & Matia-Merino, L. (2022). High-protein foods for dysphagia: Manipulation of mechanical and microstructural properties of whey protein gels using de-structured starch and salts. Gels, 8(7), 399.

( ) The manuscript is currently under review for publication – please indicate:

- The name of the journal:
- The percentage of the manuscript/published work that was contributed by the candidate:
- Describe the contribution that the candidate has made to the manuscript/published work:

( ) It is intended that the manuscript will be published, but it has not yet been submitted to a journal

Candidate's Signature:	Cai Ling — Digitally signed by Cai Ling Date: 2022.07.03 13:59:16 +12'00'
Date:	03-Jul-2022
Primary Supervisor's Signature:	Kelvin Goh — Digitally signed by Kelvin Goh Date: 2022.07.03 09:34:00 +08'00'
Date:	3-Jul-2022

This form should appear at the end of each thesis chapter/section/appendix submitted as a manuscript/ publication or collected as an appendix at the end of the thesis.

GRS Version 5 – 13 December 2019
DRC 19/09/10